DISSERTATION

FATE OF SNOWMELT IN COMPLEX SUBALPINE TERRAIN

Submitted by

Ryan W. Webb

Department of Civil and Environmental Engineering

In partial fulfillment of the requirements

For the Degree of Doctor of Philosophy

Colorado State University

Fort Collins, Colorado

Summer 2016

Doctoral Committee:

Advisor: Michael Gooseff

Steven Fassnacht
Jorge Ramirez
Jeffrey Niemann

ABSTRACT

FATE OF SNOWMELT IN COMPLEX SUBALPINE TERRAIN

Snow is important to human communities and natural ecosystems around the world that rely on snowmelt runoff for as much as 80% or more of streamflow. In addition to streamflow, snowmelt can drive hydrological processes such as groundwater recharge, soil moisture dynamics, forest ecosystem dynamics, and potentially cause high damage flooding. Multiple environmental controls will cause snow to vary in depth, density, and snow crystal metamorphism causing a complex three dimensional matrix of ice, air, water vapor, and liquid water (during melt) that is non-uniform across a landscape and varies in time at the daily and even hourly scale. Because of the non-uniform dynamics of snow and snowmelt processes, multi-dimensional studies are necessary to determine hydrological flow paths during spring snowmelt. The goal of this dissertation is to investigate the physical processes that control the fate of snowmelt during spring runoff in complex subalpine terrain. These processes were investigated through 1) observing the diurnal pattern of snowmelt in Colorado's Front Range, 2) testing the diversion potential of hydraulic barriers within a layered snowpack through numerical modeling, 3) collecting field data to investigate the spatio-temporal patterns of water distribution during spring snowmelt, and 4) analyzing a network of soil moisture sensors in California's Southern Sierra Nevada to determine the variability of infiltration in a headwater catchment.

Observations of the diurnal temporal pattern of snowmelt resulted in a relatively simple method to capture the outflow from a snowpack using hourly snow water equivalent data. The resulting temporal pattern is comparable to design rainfall distribution types specifically for snowmelt that can be important for flood risk analysis or design of channels in previously unmonitored headwater systems. The observed temporal patterns were also used to inform

numerical simulations in the modeling package TOUGH2 that utilized additional data from NASA CLPX datasets to simulate meltwater percolation through a melting snowpack. Results of this component of the dissertation displays the potential for hydraulic barriers to form on south, flat, and north aspect hillslopes and potentially divert downward flowing water at similar scales as the topographic or land cover variability. Hydraulic barriers in simulations were permeability barriers only on the south and flat aspect slopes and capillary barriers only on the north aspect slopes. The dynamic nature of a snowpack in the presence of water implies that the capillary barriers are likely short-lived relative to permeability barriers and thus capillary barriers may be important at the day or week timescale and permeability barriers may be more influential at the monthly or seasonal time scale.

Field observations near Steamboat Springs, Colorado were made for above normal, relatively normal, and below normal snow seasons including measurements of bulk snow water equivalent and soil moisture on varying slope, aspect, soil parameters, and canopy conditions with results displaying the variability from these influences. Evidence was present of meltwater flowing above the soil surface and through the snowpack. At the base of the north aspect slope the water table rose above the soil surface and the snowpack added storage capacity to the vadose zone. The variability of snowmelt and resulting soil moisture and infiltration dynamics was supported by the analysis of a network of soil moisture sensors in California's Southern Sierra Nevada. This component of the dissertations displayed the high variability of wetting and drying dynamics beneath a snowpack at the sub-hillslope and watershed scale. Results of this dissertation display that the snowpack acts as an extension of the vadose zone during spring snowmelt and that one-dimensional assumptions are not appropriate in headwater catchments during this time. Consideration of the snowpack and soil together will improve modeling, remote sensing, and water balance calculations for hydrologic studies during spring snowmelt and improvements upon allocation of streamflow, groundwater recharge, and evapotranspiration.

ACKNOWLEDGEMENTS

There have been many influential people that I have met during my time at Colorado State University. I will certainly not be able to mention all of them, but here is an attempt to summarize important influences and contributions to this dissertation. I would like to first acknowledge the guidance and mentorship of my advisor Michael Gooseff and committee member Steven Fassnacht who both have freely offered their experience and time towards my development. I would also like to acknowledge individuals that have helped with various aspects of this dissertation, these include: Domenico Bau, Stefan Finsterle, Antonio Rinaldi, Sarah Schmeer, and Stephen Webb. Groups of people that I would like to additionally recognize include the WR 575 classes, various fieldwork volunteers, the CSU snow hydrology lab group, the Gooseff hydroecology lab group, the Critical Zone Observatory investigators, and anyone I may be forgetting.

I would like to further acknowledge financial assistance that I have received to pursue my degree from the CSU Borland Scholarship, Colorado Ground Water Association Harlan Erker Scholarship, teaching assistantships in both civil engineering and watershed science, and the flexibility of Smith Geotechnical Engineering Consultants while I worked there in addition to similar flexibility of Canyon Ridge Consulting.

TABLE OF CONTENTS

CHAPTER 1: INTRODUCTION

Snow is a major component of the hydrologic cycle in many geographic regions around the world. Many human communities and natural ecosystems rely on snowmelt runoff for vital water resources. In areas such as the western United States and Canada, snow can contribute more than 80% of streamflow to downstream water users [*Daly et al., 2000; Gray and Landine, 1988; Rice et al., 2011; Seyfried et al., 2009*]. In addition to direct consumptive water use from streamflow snowmelt is important for groundwater recharge [*Flint et al., 2008; Clilverd et al., 2011; Cao et al., 2013*], soil moisture dynamics [*McNamara et al., 2005; Jencso and McGlynn, 2011; Harpold et al., 2015*], forest ecosystem dynamics [*Williams et al., 2009a; Smith et al., 2011; Harpold et al., 2014*], and can cause high damage flooding [*Graybeal and Leathers, 2006; Zhao et al., 2009; Fang et al., 2013*]. With variable past and projected changes to snowpack accumulation and melt rates [*Adam et al., 2009; Clow, 2010; Harpold et al., 2012; Fassnacht and Hultstrand, 2015; Fassnacht et al., 2016*] it is important to accurately represent a melting snowpack to properly relate it to processes that may be affected.

Snowmelt driven streamflow is important in regions such as the western U.S. for agricultural, municipal, and ecosystem purposes [*e.g. Harr, 1981; Fassnacht et al., 2001; Liu et al., 2004; Litaor et al., 2008; Pelto, 2008; Williams et al., 2009b; Fassnacht et al., 2014*]. Many of the current storage systems are highly stressed during times of drought and current management practices are insufficient to handle projected changes in snowmelt dominated hydrographs [*Adam et al., 2009*]. For example, more than 75% of agricultural water in California has been historically provided by snowmelt [*Rosenthal and Dozier, 1996*] until recent severe drought has increased groundwater pumping in an unsustainable manner [*Howitt et al., 2015*]. Similar reliance on snowmelt for agricultural, municipal, ecosystems, and sometimes hydroelectrical power is not a localized issue and can be seen around the world. Projected population increases will place increased demands for water use and accurate knowledge of

water availability from snowmelt runoff will need to be quantified for future management purposes [*Harshburger et al., 2012; Painter et al., 2012; Skiles et al., 2012; Bryant et al., 2013*]. These quantifications of available water from snowmelt will need to include streamflow, groundwater recharge, soil moisture storage, and plant production.

The majority of snowmelt during spring will infiltrate into the soil with a noticeable signal in the state of soil moisture prior to recharging ground water storage, producing streamflow, or contributing to evapotranspiration [*Bales et al., 2011; Ebel et al., 2012; Hunsaker et al., 2012; Hinckley et al., 2014; Kampf et al., 2015*]. The state of soil moisture, or level of saturation in the vadose zone, controls the stream connectivity and release of water and nutrients from subsurface storage [*McNamara et al., 2005; Seyfried et al., 2009; Williams et al., 2009a; Geroy et al., 2011*]. Soil moisture during spring is often driven by snowmelt that can impact water availability for plant production [*Molotch et al., 2009; Harpold et al., 2015*] as well as the ionic signature of soil moisture and stream flow [*Bales et al., 1993; Harrington et al., 1996; Harrington and Bales, 1998*]. For these reasons the connections between snowmelt and soil moisture are critical in understanding the hydrologic cycle in snow dominated headwater systems [*Jencso et al., 2009; Sanadhya et al., 2014*], particularly in the face of a changing climate that will likely alter the snowmelt season and resulting responses [*Adam et al., 2009; Clow, 2010; Clilverd et al., 2011; Harpold et al., 2012; Rasmussen et al., 2014; Fassnacht and Hultstrand, 2015; Fassnacht et al., 2016*].

Spring snowmelt is projected to change in future climate scenarios. This will alter the energy and mass exchanges between the land and atmosphere that is influenced by the spatial variability of snow accumulation and ablation processes [*Cess et al., 1991; Liston, 1995; Essery, 1997; Liston, 1999*]. Climate studies using remotely sensed snow and ice observations need to account for the variability of snow, ice, and liquid water content throughout the snowpack to accurately simulate snowmelt processes [*Shi and Dozier, 1995; Tedesco et al., 2013*]. These parameters can vary due to the stratigraphy of the snow and enhancing their

accuracy of representation has been shown to improve remote sensing analyses that estimate radiative feedback from ice sheets [*Flanner et al., 2011; Pistone et al., 2014*], a process that is of known significance to global climate change [*Cao et al., 2015*]. This importance of appropriately representing snow in climate modeling has recently been further highlighted in a workshop designed specifically for this exact purpose [*Perovich et al., 2015*]. However, current efforts to model these processes during snowmelt generally represent the snowmelt as a one-dimensional process that is known to be inaccurate, particularly when considering sloping terrain [*Flint et al., 2008; Eiriksson et al., 2013; Förster et al., 2014; Kormos et al., 2014; Heilig et al., 2015*]. Snow accumulation and ablation is known be non-uniform and will have strong influences on the radiative and turbulent heat fluxes between the land and atmosphere [*Cess et al., 1991; Liston, 1995; Essery, 1997*] that results in further non-uniform nature of snow affecting the magnitude and timing of streamflow [*Blöschl, 1999; Lundquist and Dettinger, 2005*].

The diurnal cycle of streamflow in a headwater river is often controlled by snowmelt [*Caine, 1992; Laudon et al., 2004; Liu et al., 2004; Lundquist and Dettinger, 2005; Lundquist et al., 2005; Jencso and McGlynn, 2011; Mutzner et al., 2015*]. Streamflow can fluctuate as much as 10% on a regular basis from snowmelt input [*Lundquist and Cayan, 2002*] and even larger during high melt or rain on snow events [*Jennings and Jones, 2015*]. Hydrological models often use a simple degree-day snowmelt algorithm [*Frankenberger et al., 1999; Hock, 1999; Jost et al., 2012; Tobin et al., 2013*] or more computationally intensive mass and energy balances [*Brooks et al., 2007; Bittelli et al., 2010*]. For flood design, modeling efforts generally take a simple degree-day approach that has been adapted to include time varying melt at the hourly temporal scale, imposing a half-sinusoidal variation in melt centered about solar noon [*Hock, 1999*]. Further improvements have utilized available solar radiation data and minimum and maximum temperatures [*Jost et al., 2012; Tobin et al., 2013*]. Though these methods do show improvement for hydrological modeling, they do not account for other components in the energy balance such as long-wave radiation from tree canopies or ground heat flux that may be

important on days producing large amounts of melt that result in a higher risk of floods. All of these above-referenced studies, however, do highlight the importance of snowmelt variability on the resulting hydrology of a headwater basin.

Multiple environmental controls cause snow processes to vary at multiple scales of interest [*Clark et al., 2011*]. From a basin scale perspective, elevation has been shown to influence the depth and persistence of a snowpack [*Elder et al.*, *1991; Blöschl and Kirnbauer, 1992; Richer et al., 2013; Molotch and Meromy, 2014; Sexstone and Fassnacht, 2014*], while at finer resolutions the spatial variability of both accumulation and melt may be controlled by aspect [*Williams et al.*, *2009a; López-Moreno et al., 2013; Hinckley et al., 2014*], and snow in forested areas can be affected by interception during accumulation, shortwave radiation shading, and longwave radiation from vegetative influences prior to and during melt [*Storck et al.*, *2002; Musselman et al., 2008; Molotch et al., 2009; Adams et al., 2011*]. Furthermore, redistribution and increased sublimation losses of snow due to wind effects can occur across a landscape and has been shown to cause a large portion of variability in many environments [*Luce et al.*, *1998; Anderton et al., 2004; Liston and Elder, 2006; Lehning et al., 2008*]. Observations made at the experimental plot scale show additional variability and implications for using single point measurements of snow [*López-Moreno et al.*, *2011*]. With such variable and dynamic controls on the accumulation and melt rates across a landscape that lead to a range of melt inputs across the soil surface [*Harms and Chanasyk*, *1998; Kormos et al., 2014*] it is essential to understand the nature of the snowpack itself in a snowmelt dominated catchment.

A snowpack forms a complex three-dimensional matrix of ice, air, water vapor, impurities such as dust or other constituents, and liquid water (during melt or rain events) that varies over time. Snow crystal metamorphism has been studied for decades [*Yosida*, *1955*] with the primary driving mechanism often a temperature gradient between layers inducing sublimation, diffusion, and re-sublimation of water vapor that removes and deposits water particles [*Colbeck and Anderson*, *1982; Staron et al., 2014*]. When temperature gradients are low, compression and

friction can also drive metamorphism and in the spring metamorphism becomes rapid with the presence of liquid water [*Marsh*, *1987*]. Snow crystal metamorphism is an ongoing process different for each new layer [*Colbeck*, *1987; Colbeck, 1991*] and because it is a function of time, temperature gradients, and water vapor gradients, all of which vary among layers of a snowpack, each layer will develop its own characteristics as a porous medium.

As a snowpack evolves over the season each layer will develop different hydraulic properties based on grain size and snow density [*Colbeck*, *1975; 1979; 1991; Colbeck and Anderson, 1982*]. *Yamaguchi et al.* [*2010*] determined, through laboratory experiments, the *van Genuchten* [*1980*] parameters for snow samples. The *van Genuchten* [*1980*] equation describes the ability of porous media to retain moisture at a given suction/tension through the following equation:

$$\theta = \theta_r + (\theta_s - \theta_r)[1 + (\propto |h|)^n]^{-m} \quad \text{(Eq. 1.1)}$$

where θ is the volumetric water content (m^3m^{-3}), θ_r is the residual water content (m^3m^{-3}), θ_s is the saturated water content (m^3m^{-3}), α is a fit coefficient that is related to the pore size of the medium and approximately the inverse of the air entry pressure for soils, h is the suction (m), n and m are additional curve fitting parameters where m is commonly taken to be 1-(1/n).

Yamaguchi et al. [*2010*] estimated that for snow:

$$\alpha = 7.3(2r) + 1.9 \quad \text{(Eq. 1.2)}$$

where r is the mean radius of the snow grains (mm) and *Hirashima et al*. [*2010*] expanded on this work to improve an equation for n to be:

$$n = 15.68e^{(-0.46(2r))} + 1 \quad \text{(Eq. 1.3)}$$

This improvement increased the range of the grain size from 2 mm to an upper limit of 5 mm. The value for θ_r is commonly estimated near 0.02 and θ_s is estimated from a volumetric calculation of pore space from density measurements. For estimation of hydraulic conductivity

of snow, *Calonne et al*. [*2012*] used microscale 3D imaging to compute the intrinsic permeability (*K*) to be:

$$K = (3.0 \pm 0.3) r_{es}{}^2 \exp\left((-0.0130 \pm 0.0003)\rho_s\right) \quad \text{(Eq. 1.4)}$$

where r_{es} is the equivalent sphere radius (mm) estimated from grain specific surface area and ρ_s is the density of the snow (kg m^{-3}). Intrinsic permeability is easily converted to hydraulic conductivity using the viscosity and density of water at the temperature of interest.

Yamaguchi et al. [*2010*] conducted gravity drainage column experiments with a column diameter of 50 mm, snow grain sizes ranging from 0.5 to 3.1 mm, and all densities near 550 kg m^{-3} to develop the above equations for hydraulic properties of samples. *Hirashima et al.* [*2010*] used these results for implementation of the equations into the model package SNOWPACK [*Bartelt and Lehning*, *2002*]. *Calonne et al*. [*2012*] tested a higher range of snow densities between 100 and 550 kg/m^3 and specific surface areas from 3.8 to 56 m^2kg^{-1} for computing permeability from 3-D tomographic images. This study's primary limitation was that the maximum size of samples was only 4 mm. The primary limitation of *Yamaguchi et al*. [*2010*] and *Hirashima et al*. [*2010*] is the few densities and grain sizes tested. However, the equations developed have been successfully applied towards one-dimensional water flow through a natural layered snowpack [*Wever et al.*, *2014*] using Richard's equation [*Richards*, *1931*] in a mixed form that could be discretized in a finite difference approximation to ensure mass balance based on *Celia et al.* [*1990*]:

$$\frac{\partial \theta}{\partial t} - \frac{\partial}{\partial z}\left(K(\theta)\left(\frac{\partial h}{\partial z} + \cos\gamma\right)\right) + s = 0 \quad \text{(Eq. 1.5)}$$

where z is the vertical coordinate (m), γ is the slope angle, and s is a source/sink term (m^3 m^{-3} s^{-1}).

Though these studies have successfully implemented laboratory scale results towards simulating water flow through a natural layered snowpack in one dimension, snow environments

in mountainous terrain will require movement beyond one dimension to include the spatial variability and lateral connection across complex landscape.

The development and/or deposition of layers will often be controlled by energy fluxes that are largely influenced by topographic and land cover scale variability [*Adams et al.*, *2011*]. When these layers begin to melt, the increased liquid water content will speed up the process of metamorphism [*Colbeck*, *1987*; *Marsh*, *1987*] creating areas with larger grain sizes and higher hydraulic conductivities [*Yamaguchi et al.*, *2010*; *Katsushima et al.*, *2013*]. These areas have been shown to have correlation lengths, in alpine environments, of five to seven meters between areas of large grains during snowmelt due to preferential melt pattern investigations by *Sommerfeld et al*. [*1994*] and *Williams et al*. [*1999*]. These complex melt processes create a snowpack with zones of higher and lower water contents [*Techel and Pielmeier*, *2011*] that forms the complex matrix of ice, water, and air that changes non-uniformly through time and space resulting from and potentially further producing preferential flow paths.

Preferential flow paths for vertically infiltrating water will develop from the natural heterogeneity of a layered snowpack that is often influenced by ice lenses [*Colbeck*, *1979; 1991; Marsh and Woo, 1985; Harrington and Bales, 1998; Williams et al., 2010*] that redistribute water across layer interfaces prior to breakthrough [*Kattelmann and Dozier*, *1999; Liu et al., 2004; Eiriksson et al., 2013*]. These preferential flow paths and melt patterns are important for consideration of solute concentrations of snow runoff [*Marsh and Pomeroy*, *1993; Harrington et al., 1996; Harrington and Bales, 1998; Williams et al., 2009b*], soil moisture patterns important for vegetation diversity of an alpine landscape [*Litaor et al.*, *2008*] and wet slab avalanches [*Mitterer et al.*, *2011*]. The development of flow paths has been observed at the centimeter to meter scale [*Williams et al.*, *2010*], at the meters to tens of meters scale from a rain on snow events [*Eiriksson et al.*, *2013*], and even mostly bypassing soil interaction to produce streamflow in deep snow packs on sloping terrain [*Laudon et al.*, *2004; Liu et al., 2004*]. Identifying specific flow paths has been observed in the form of ice columns connected by ice ribs by *Williams et al.*

[*2000*] in an alpine environment regardless of aspect. These preferential flow paths that develop at multiple scales will likely have impacts on the soil moisture at similar scales within a headwater catchment when flow is directed laterally above the soil-snow-interface.

Preferential flow paths causing lateral flow above the soil-snow-interface occurs in the form of capillary and/or permeability barriers at interfaces between layers. At the interface between layers, if capillary pressures in the upper layer are large enough relative to the capillary pressures in the lower layer, water will be held above the interface and transported downslope (if a slope exists); this is a capillary barrier. A permeability barrier occurs when water is percolating through the upper layer at a higher rate than the permeability of the bottom layer; the differences in permeability allow water to flow more readily through the upper layer resulting in lateral flow. These types of barriers promote flow through snow that often has hydraulic conductivities orders of magnitude greater than those of typical soils [*Calonne et al.*, *2012; Domine et al., 2013*] suggesting meltwater likely flows downhill at a greater rate within a snowpack than soil, as taking a one-dimensional approach assumes. Therefore, the lateral connectivity and formation of hydraulic barriers within a snowpack is of key importance to the distribution of snowmelt water across a landscape [*Colbeck*, *1979; Marsh and Woo, 1985; Williams et al., 1999; 2009; Williams et al., 2009a*] and a key component of the hydrologic cycle in a headwater basin.

Goals and Objectives

The goal of this dissertation is to investigate the physical processes that control the fate of snowmelt during spring runoff. The physical processes described above will create environments in snow-dominated regions that distribute snowmelt water across a landscape based on a number of different factors. Variable meteorological forcing of melt in complex terrain will cause snowmelt to be non-uniform across a landscape. At varying rates of snowmelt different hydraulic barriers in a layered snowpack will act differently and range in effectiveness of diverting vertically infiltrating meltwater on a hillslope. Similarly, soil parameters when

considered with the bottom-most layer of snow will also have the potential to create a hydraulic barrier to vertically percolating meltwater. These physical processes will likely vary in complex mountainous terrain depending on slope angle, slope aspect, land cover, and meteorology during melt (Fig. 1.1). These factors are investigated in the following chapters of this dissertation through: 1) observing the diurnal pattern of snowmelt for flood design and other hydrological modeling purposes, 2) testing the diversion potential of hydraulic barriers in a layered snowpack through numerical modeling, 3) collecting field data to investigate the spatio-temporal patterns of water distribution during spring snowmelt, and 4) analyzing a network of soil moisture sensors to determine the variability of snowmelt infiltration and groundwater recharge and water balance implications within a headwater catchment.

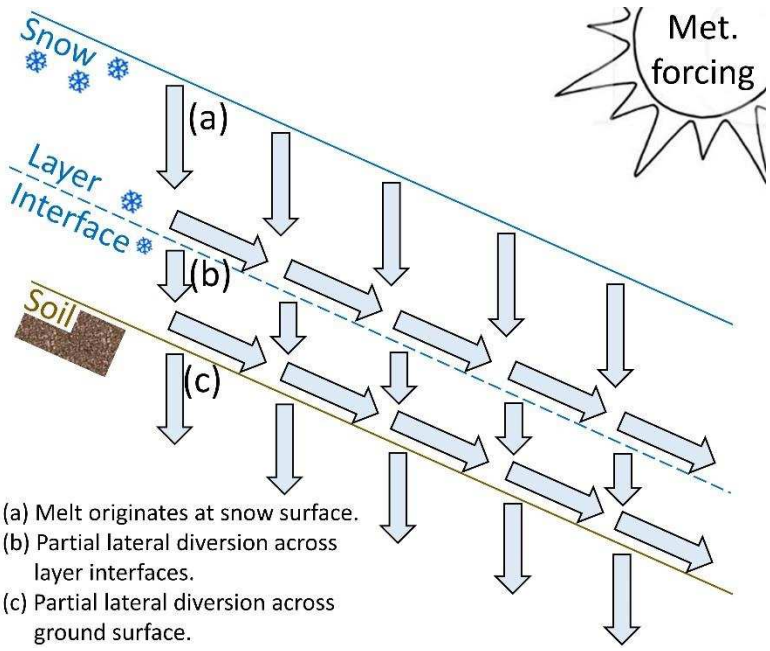

Figure 1.1: Conceptual model of potential flow paths for snowmelt water. The controls shown are: meteorological forcing, slope angle, snow stratigraphy, and soil. Controls not shown in the figure are slope aspect and land cover.

The diurnal pattern of snowmelt is observed using multiple snow telemetry (SNOTEL) stations along the Front Range of the Colorado Rocky Mountains. Snow water equivalent (SWE) data are processed and analyzed to determine a diurnal pattern of snowmelt outflow for a snowpack in this region and a function is fit to the observed data. The timing of the snowmelt

outflow function is then tested against soil moisture sensors installed at the SNOTEL sites to confirm the timing of peak outflow from the snowpack. This chapter of the dissertation determines the diurnal pattern of snowmelt that may be used for “design runoff” events during spring snowmelt that may pose a flood risk or for design of open channel hydraulic systems in previously unmonitored headwater basins. The observations additionally provide information concerning the expected range of normal snowmelt rates of a mountain snowpack in the Colorado Rocky Mountains.

The snowmelt rates are used to inform simulations of water flow through a two-dimensional snowpack in the next chapter of this dissertation to test the diversion capacity of hydraulic barriers that form in a layered snowpack. This chapter of the dissertation utilizes publically available data from the National Aeronautics and Space Administration (NASA) Cold Land Process Experiment (CLPX) dataset [*Elder et al*., 2009]. Data for this study are from the Spring Creek intensive study area near Steamboat Springs, CO collected on March 30, 2003. Stratigraphy from three snow pits of varying aspect (north, south, and flat) are used to estimate the hydraulic properties of snowpack layers using equations (1.2) through (1.4) listed above and similarly applies Richard’s equation (1.5) to a two-dimensional snowpack. This chapter uses the numerical model TOUGH2 equation of state module EOS9 [*Finsterle*, *2007*]. TOUGH2 is a numerical code that has been used in a number of previous studies of hydraulic barriers in soils [e.g. *Ho and Webb*, *1998; Webb, 1997*]. The simulations investigate steady state infiltration rates in order to test the potential of layered snowpacks to divert vertically infiltrating snowmelt water.

The snowmelt season is then observed and analyzed for patterns of water distribution at the Dry Lake study site near Steamboat Springs, CO. The goal of this chapter is to gain understanding of the spatio-temporal variability of physical hydrological processes that occur during spring snowmelt in a small headwater catchment with a deep seasonally persistent snowpack. Intensive surveys were conducted during spring snowmelt to investigate the

variability of both SWE and near surface soil moisture on north, south, and flat aspect slopes as well as at the bases of each hillslope. The snowmelt season was observed for three years, 2013, 2014, and 2015, providing a variety of accumulation and ablation patterns from different meteorological forcing of melt during each spring. This chapter analyzes patterns of snowmelt water distribution in the field during spring snowmelt that are indicative of hydrological flow paths that drive hydraulic gradients important for generation of streamflow, groundwater recharge, and soil moisture storage.

Soil moisture sensors were analyzed as a fourth component of this dissertation using data from the Southern Sierra Critical Zone Observatory (CZO) in California. The sensor network at this CZO chosen for analysis is the Providence Creek study area that includes a total of 97 soil moisture sensors at depths of 10, 30, 60, and 90 cm across 27 locations within the headwater basin. Sensor locations include north, south, and flat aspects for under tree canopy, at tree canopy drip edges, and in open canopy conditions. The purpose of this chapter in the dissertation was to determine the variability of infiltration of snowmelt within a headwater catchment in the top meter of soil for implications towards the generation of streamflow, groundwater recharge, and soil moisture storage.

All of the above mentioned chapters of this dissertation investigate different physical processes that occur during snowmelt in headwater systems. When viewed together, they offer insight towards the flow paths that develop during this time of year and the manner that snowmelt water distributes across complex terrain. This can be important for improving estimates of the water balance for water management and assessment of ecosystem dynamics in headwater regions.

REFERENCES

Adam, J. C., A. F. Hamlet, and D. P. Lettenmaier (2009), Implications of global climate change for snowmelt hydrology in the twenty-first century, Hydrological Processes, 23(7), 962-972, doi: 10.1002/hyp.7201.

Adams, E., A. Slaughter, L. McKittrick, and D. Miller (2011), Local terrain-topography and thermal-properties influence on energy and mass balance of a snow cover, Annals of Glaciology, 52(58), 169-175.

Anderton, S., S. White, and B. Alvera (2004), Evaluation of spatial variability in snow water equivalent for a high mountain catchment, Hydrological Processes, 18(3), 435-453, doi: 10.1002/hyp.1319.

Bales, R. C., R. E. Davis, and M. W. Williams (1993), Tracer Release in Melting Snow - Diurnal and Seasonal Patterns, Hydrological Processes, 7(4), 389-401, doi: 10.1002/hyp.3360070405.

Bales, R. C., J. W. Hopmans, A. T. O'Geen, M. Meadows, P. C. Hartsough, P. Kirchner, C. T. Hunsaker, and D. Beaudette (2011), Soil Moisture Response to Snowmelt and Rainfall in a Sierra Nevada Mixed-Conifer Forest, Vadose Zone Journal, 10(3), 786, doi: 10.2136/vzj2011.0001.

Bartelt, P., and M. Lehning (2002), A physical SNOWPACK model for the Swiss avalanche warning Part I: numerical model, Cold Regions Science and Technology, 35(3), 123-145, doi: 10.1016/S0165-232X(02)00074-5.

Bittelli, M., F. Tomei, A. Pistocchi, M. Flury, J. Boll, E. S. Brooks, and G. Antolini (2010), Development and testing of a physically based, three-dimensional model of surface and subsurface hydrology, Advances in Water Resources, 33(1), 106-122, doi: 10.1016/j.advwatres.2009.10.013.

Blöschl, G., and R. Kirnbauer (1992), An Analysis of Snow Cover Patterns in a Small Alpine Catchment, Hydrological Processes, 6(1), 99-109.

Blöschl, G. (1999), Scaling issues in snow hydrology, Hydrological Processes, 13(14-15), 2149-2175, doi: 10.1002/(SICI)1099-1085(199910)13:14/15<2149::AID-HYP847>3.0.CO;2-8.

Brooks, E. S., J. Boll, and P. A. McDaniel (2007), Distributed and integrated response of a geographic information system-based hydrologic model in the eastern Palouse region, Idaho, Hydrological Processes, 21(1), 110-122, doi: 10.1002/hyp.6230.

Bryant, A. C., T. H. Painter, J. S. Deems, and S. M. Bender (2013), Impact of dust radiative forcing in snow on accuracy of operational runoff prediction in the Upper Colorado River Basin, Geophysical Research Letters, 40(15), 3945-3949, doi: 10.1002/grl.50773.

Caine, N. (1992), Modulation of the diurnal streamflow response by the seasonal snowcover of an alpine basin, Journal of Hydrology, 137, 245-260.

Calonne, N., C. Geindreau, F. Flin, S. Morin, B. Lesaffre, S. Rolland du Roscoat, and P. Charrier (2012), 3-D image-based numerical computations of snow permeability: links to specific surface area, density, and microstructural anisotropy, The Cryosphere, 6(5), 939-951, doi: 10.5194/tc-6-939-2012.

Cao, J., C. Liu, and W. Zhang (2013), Response of rock-fissure seepage to snowmelt in Mount Taihang slope-catchment, North China, Water Sci Technol, 67(1), 124-130, doi: 10.2166/wst.2012.542.

Cao, Y., S. Liang, X. Chen, and T. He (2015), Assessment of Sea Ice Albedo Radiative Forcing and Feedback over the Northern Hemisphere from 1982 to 2009 Using Satellite and Reanalysis Data, Journal of Climate, 28(3), 1248-1259, doi: 10.1175/JCLI-D-14-00389.1.

Celia, MA, E. Bouloutas, and R. Zarba (1990), A General Mass-Conservative Numerical-Solution for the Unsaturated Flow Equation, Water Resources Research, 26(7), 1483-1496, doi: 10.1029/90WR00196.

Cess, R. D., et al. (1991), Interpretation of snow-climate feedback as produced by 17 general-circulation models, Science, 253(5022), 888-892, doi: 10.1126/science.253.5022.888.

Clark, M., J. Hendrikx, A. Slater, D. Kavetski, B. Anderson, N. Cullen, T. Kerr, E. Hreinsson, and R. Woods (2011), Representing spatial variability of snow water equivalent in hydrologic and land-surface models: A review, Water Resources Research, 47, doi: 10.1029/2011WR010745.

Clilverd, H. M., D. M. White, A. C. Tidwell, and M. A. Rawlins (2011), Sensitivity of Northern Groundwater Recharge to Climate Change: A Case Study in Northwest Alaska, Journal of the American Water Resources Association, 47(6), 1228-1240, doi: 10.1111/j.1752-1688.2011.00569.x.

Clow, D. W. (2010), Changes in the Timing of Snowmelt and Streamflow in Colorado: A Response to Recent Warming, Journal of Climate, 23(9), 2293-2306, doi: 10.1175/2009jcli2951.1.

Colbeck, S. (1975), A theory for water flow through a layered snowpack, Water Resources Research, 11(2), 261-266.

Colbeck, S. (1979), Water-flow through heterogeneous snow, Cold Regions Science and Technology, 1(1), 37-45, doi: 10.1016/0165-232X(79)90017-X.

Colbeck, S. C., and E. A. Anderson (1982), The permeability of a melting snow cover, Water Resources Research, 18(4), 904-908.

Colbeck, S. C. (1987), Theory of particle coarsening with a log-normal distribution, Acta Metallurgica, 35(7), 1583-1588, doi: 10.1016/0001-6160(87)90105-2.

Colbeck, S. C. (1991), The layered character of snow covers, Reviews of Geophysics, 29(1), 81-96.

Daly, S. F., R. Davis, E. Ochs, and T. Pangburn (2000), An approach to spatially distributed snow modelling of the Sacramento and San Joaquin basins, California, Hydrological

Processes, 14(18), 3257-3271, doi: 10.1002/1099-1085(20001230)14:18<3257::aid-hyp199>3.3.co;2-q.

Domine, F., S. Morin, E. Brun, M. Lafaysse, and C. M. Carmagnola (2013), Seasonal evolution of snow permeability under equi-temperature and temperature-gradient conditions, The Cryosphere, 7(6), 1915-1929, doi: 10.5194/tc-7-1915-2013.

Ebel, B. A., E. S. Hinckley, and D. A. Martin (2012), Soil-water dynamics and unsaturated storage during snowmelt following wildfire, Hydrology and Earth System Sciences, 16(5), 1401-1417, doi: 10.5194/hess-16-1401-2012.

Eiriksson, D., M. Whitson, C. H. Luce, H. P. Marshall, J. Bradford, S. G. Benner, T. Black, H. Hetrick, and J. P. McNamara (2013), An evaluation of the hydrologic relevance of lateral flow in snow at hillslope and catchment scales, Hydrological Processes, 27(5), 640-654, doi: 10.1002/hyp.9666.

Elder, K., J. Dozier, and J. Michaelsen (1991), Snow Accumulation and Distribution in an Alpine Watershed, Water Resources Research, 27(7), 1541-1552.

Elder, K., D. Cline, G. E. Liston, and R. Armstrong (2009), NASA Cold Land Processes Experiment (CLPX 2002/03): Field Measurements of Snowpack Properties and Soil Moisture, Journal of Hydrometeorology, 10(1), 320-329, doi: 10.1175/2008jhm877.1.

Essery, R. (1997), Modelling fluxes of momentum, sensible heat and latent heat over heterogeneous snow cover, Quarterly Journal of the Royal Meteorological Society, 123(543), 1867-1883, doi: 10.1002/qj.49712354305.

Fang, S., L. Xu, Y. Zhu, Y. Liu, Z. Liu, H. Pei, J. Yan, and H. Zhang (2013), An integrated information system for snowmelt flood early-warning based on internet of things, Information Systems Frontiers, 17(2), 321-335, doi: 10.1007/s10796-013-9466-1.

Fassnacht, S. R., S. R. Helfrich, D. J. Lampkin, K. A. Dressler, R. C. Bales, E. B. Halper, D. Reigle, and B. Imam (2001), Snowpack modelling of the Salt Basin with water management implications, in Proceedings of the Western Snow Conference, 69th Annual Meeting, edited by K. Elder, pp. 65-76, Western Snow Conference, Portland.

Fassnacht, S. R., D. C. Deitemeyer, and N. B. H. Venable (2014), Capitalizing on the daily time step of snow telemetry data to model the snowmelt components of the hydrograph for small watersheds, Hydrological Processes, 28(16), 4654-4668, doi: 10.1002/hyp.10260.

Fassnacht, S. R., and M. Hultstrand (2015), Snowpack variability and trends at long-term stations in northern Colorado, USA, International Association of Hydrological Sciences, 92, 1-6, doi: 10.5194/piahs-92-1-2015.

Fassnacht, S. R., M. L. Cherry, N. B. H. Venable, and F. Saavedra (2016), Snow and albedo climate change impacts across the United States Northern Great Plains, The Cryosphere, 10, 329-339, doi: 10.5194/tc-10-329-2016.

Finsterle, S. (2007), iTOUGH2 user's guide, edited, Earth Sciences Division, Lawrence Berkeley National Laboratory, University of Berkely, Berkeley, California.

Flanner, M., K. Shell, M. Barlage, D. Perovich, and M. Tschudi (2011), Radiative forcing and albedo feedback from the Northern Hemisphere cryosphere between 1979 and 2008, Nature Geoscience, 4(3), 151-155, doi: 10.1038/ngeo1062|10.1038/NGEO1062.

Flint, A. L., L. E. Flint, and M. D. Dettinger (2008), Modeling Soil Moisture Processes and Recharge under a Melting Snowpack, Vadose Zone Journal, 7(1), 350, doi: 10.2136/vzj2006.0135.

Frankenberger, J., E. Brooks, M. Walter, M. Walter, and T. Steenhuis (1999), A GIS-based variable source area hydrology model, Hydrological Processes, 13(6), 805-822, doi: 10.1002/(SICI)1099-1085(19990430)13:6<805::AID-HYP754>3.0.CO;2-M.

Förster, K., G. Meon, and U. Strasser (2014), Modelling of snow processes in catchment hydrology by means of downscaled WRF meteorological data fields, Hydrology and Earth System Sciences Discussions, 11(4), 4063-4102, doi: 10.5194/hessd-11-4063-2014.

Geroy, I. J., M. M. Gribb, H. P. Marshall, D. G. Chandler, S. G. Benner, and J. P. McNamara (2011), Aspect influences on soil water retention and storage, Hydrological Processes, 25, 3836-3842, doi: 10.1002/hyp.8281.

Gray, D. M., and P. G. Landine (1988), An Energy-Budget Snowmelt Model for the Canadian Prairies, Can. J. Earth Sci., 25(8), 1292-1303, doi: 10.1139/e88-124.

Graybeal, D., and D. Leathers (2006), Snowmelt-related flood risk in Appalachia: First estimates from a historical snow climatology, Journal of Applied Meteorology and Climatology, 45(1), 178-193, doi: 10.1175/JAM2330.1.

Harms, T. E., and D. S. Chanasyk (1998), Variability of Snowmelt Runoff and Soil Moisture Recharge, Nordic Hydrology, 29, 179-198.

Harpold, A., P. Brooks, S. Rajagopal, I. Heidbuchel, A. Jardine, and C. Stielstra (2012), Changes in snowpack accumulation and ablation in the intermountain west, Water Resources Research, 48(11), n/a-n/a, doi: 10.1029/2012wr011949.

Harpold, A. A., J. A. Biederman, K. Condon, M. Merino, Y. Korgaonkar, T. Nan, L. L. Sloat, M. Ross, and P. D. Brooks (2014), Changes in snow accumulation and ablation following the Las Conchas Forest Fire, New Mexico, USA, Ecohydrology, 7(2), 440-452, doi: 10.1002/eco.1363.

Harpold, A. A., N. P. Molotch, K. N. Musselman, R. C. Bales, P. B. Kirchner, M. Litvak, and P. D. Brooks (2015), Soil moisture response to snowmelt timing in mixed-conifer subalpine forests, Hydrological Processes, 29(12), 2782-2798, doi: 10.1002/hyp.10400.

Harr, R. D. (1981), Some Characteristics and Consequences of Snowmelt During Rainfall in western Oregon, Journal of Hydrology, 53(3-4), 277-304, doi: 10.1016/0022-1694(81)90006-8.

Harrington, R. F., R. C. Bales, and P. Wagnon (1996), Variability of meltwater and solute fluxes from homogeneous melting snow at the laboratory scale, Hydrological Processes, 10(7), 945-953, doi: 10.1002/(sici)1099-1085(199607)10:7<945::aid-hyp349>3.0.co;2-s.

Harrington, R., and R. C. Bales (1998), Interannual, seasonal, and spatial patterns of meltwater and solute fluxes in a seasonal snowpack, Water Resources Research, 34(4), 823-831, doi: 10.1029/97wr03469.

Harshburger, B. J., V. P. Walden, K. S. Humes, B. C. Moore, T. R. Blandford, and A. Rango (2012), Generation of Ensemble Streamflow Forecasts Using an Enhanced Version of the Snowmelt Runoff Model, Journal of the American Water Resources Association, 48(4), 643-655, doi: 10.1111/j.1752-1688.2012.00642.x.

Heilig, A., C. Mitterer, L. Schmid, N. Wever, J. Schweizer, H. P. Marshall, and O. Eisen (2015), Seasonal and diurnal cycles of liquid water in snow-Measurements and modeling, Journal of Geophysical Research: Earth Surface, 120, doi: 10.1002/2015JF003593.

Hinckley, E.-L. S., B. A. Ebel, R. T. Barnes, R. S. Anderson, M. W. Williams, and S. P. Anderson (2014), Aspect control of water movement on hillslopes near the rain-snow transition of the Colorado Front Range, Hydrological Processes, 28(1), 74-85, doi: 10.1002/hyp.9549.

Hirashima, H., S. Yamaguchi, A. Sato, and M. Lehning (2010), Numerical modeling of liquid water movement through layered snow based on new measurements of the water retention curve, Cold Regions Science and Technologh, 64, 94-103, doi: 10.1016/j.coldregions.2010.09.003.

Ho, C. K., and S. W. Webb (1998), Capillary barrier performance in heterogeneous porous media, Water Resources Research, 34(4), 603-609, doi: 10.1029/98wr00217.

Hock, R. (1999), A distributed temperature-index ice- and snowmelt model including potential direct solar radiation, Journal of Glaciology, 45(149), 101-111.

Howitt, R. E., D. MacEwan, J. Medellin-Azuara, J. R. Lund, and D. A. Summer (2015), Economic Analysis of the 2015 Drought for California Agriculture*Rep.*, 16 pp, University of California-Davis, Davis, CA.

Hunsaker, C. T., T. W. Whitaker, and R. C. Bales (2012), Snowmelt Runoff and Water Yield Along Elevation and Temperature Gradients in California's Southern Sierra Nevada1, JAWRA Journal of the American Water Resources Association, 48(4), 667-678, doi: 10.1111/j.1752-1688.2012.00641.x.

Jencso, K., B. McGlynn, M. Gooseff, S. Wondzell, K. Bencala, and L. Marshall (2009), Hydrologic connectivity between landscapes and streams: Transferring reach-and plot-scale understanding to the catchment scale, Water Resources Research, 45, doi: 10.1029/2008WR007225.

Jencso, K. G., and B. L. McGlynn (2011), Hierarchical controls on runoff generation: Topographically driven hydrologic connectivity, geology, and vegetation, Water Resources Research, 47(11), n/a-n/a, doi: 10.1029/2011wr010666.

Jennings, K., and J. Jones (2015), Precipitation-snowmelt timing and snowmelt augmentation of large peak flow events, western Cascades, Oregon, Water Resources Research, 51(9), 7649-7661, doi: 10.1002/2014WR016877.

Jost, G., R. Moore, R. Smith, and D. Gluns (2012), Distributed temperature-index snowmelt modelling for forested catchments, Journal of Hydrology, 420, 87-101, doi: 10.1016/j.jhydrol.2011.11.045.

Kampf, S., J. Markus, J. Heath, and C. Moore (2015), Snowmelt runoff and soil moisture dynamics on steep subalpine hillslopes, Hydrological Processes, 29(5), 712-723, doi: 10.1002/hyp.10179.

Katsushima, T., S. Yamaguchi, T. Kumakura, and A. Sato (2013), Experimental analysis of preferential flow in dry snowpack, Cold Regions Science and Technology, 85, 206-216, doi: 10.1016/j.coldregions.2012.09.012.

Kattelmann, R., and J. Dozier (1999), Observations of snowpack ripening in the Sierra Nevada, California, USA, Journal of Glaciology, 45(151), 409-416.

Kormos, P., D. Marks, J. McNamara, H. Marshall, A. Winstral, and A. Flores (2014), Snow distribution, melt and surface water inputs to the soil in the mountain rain-snow transition zone, Journal of Hydrology, 519, 190-204, doi: 10.1016/j.jhydrol.2014.06.051.

Laudon, H., J. Seibert, S. Kohler, and K. Bishop (2004), Hydrological flow paths during snowmelt: Congruence between hydrometric measurements and oxygen 18 in meltwater, soil water, and runoff, Water Resources Research, 40(3), doi: 10.1029/2003WR002455.

Lehning, M., H. Lowe, M. Ryser, and N. Raderschall (2008), Inhomogeneous precipitation distribution and snow transport in steep terrain, Water Resources Research, 44(7), doi: 10.1029/2007WR006545.

Liston, G. E. (1995), Local advection of momentum, heat, and moisture during the melt of patchy snow covers, Journal of Applied Meteorology, 34(7), 1705-1715, doi: 10.1175/1520-0450-34.7.1705.

Liston, G. (1999), Interrelationships among snow distribution, snowmelt, and snow cover depletion: Implications for atmospheric, hydrologic, and ecologic modeling, Journal of Applied Meteorology, 38(10), 1474-1487, doi: 10.1175/1520-0450(1999)038<1474:IASDSA>2.0.CO;2.

Liston, G. E., and K. Elder (2006), A distributed snow-evolution modeling system (SnowModel), Journal of Hydrometeorology, 7, 1259-1276.

Litaor, M. I., M. Williams, and T. R. Seastedt (2008), Topographic controls on snow distribution, soil moisture, and species diversity of herbaceous alpine vegetation, Niwot Ridge, Colorado, Journal of Geophysical Research, 113(G2), doi: 10.1029/2007jg000419.

Liu, F., M. W. Williams, and N. Caine (2004), Source waters and flow paths in an alpine catchment, Colorado Front Range, United States, Water Resources Research, 40(9), n/a-n/a, doi: 10.1029/2004wr003076.

Luce, C., D. Tarboton, and R. Cooley (1998), The influence of the spatial distribution of snow on basin-averaged snowmelt, Hydrological Processes, 12(10-11), 1671-1683, doi: 10.1002/(SICI)1099-1085(199808/09)12:10/11<1671::AID-HYP688>3.0.CO;2-N.

Lundquist, J., and D. Cayan (2002), Seasonal and spatial patterns in diurnal cycles in streamflow in the western United States, Journal of Hydrometeorology, 3(5), 591-603, doi: 10.1175/1525-7541(2002)003<0591:SASPID>2.0.CO;2.

Lundquist, J., and M. Dettinger (2005), How snowpack heterogeneity affects diurnal streamflow timing, Water Resources Research, 41(5), doi: 10.1029/2004WR003649.

Lundquist, J., M. Dettinger, and D. Cayan (2005), Snow-fed streamflow timing at different basin scales: Case study of the Tuolumne River above Hetch Hetchy, Yosemite, California, Water Resources Research, 41(7), doi: 10.1029/2004WR003933.

López-Moreno, J. I., S. R. Fassnacht, S. Beguería, and J. B. P. Latron (2011), Variability of snow depth at the plot scale: implications for mean depth estimation and sampling strategies, The Cryosphere, 5(3), 617-629, doi: 10.5194/tc-5-617-2011.

López-Moreno, J. I., J. Revuelto, M. Gilaberte, E. Morán-Tejeda, M. Pons, E. Jover, P. Esteban, C. García, and J. W. Pomeroy (2013), The effect of slope aspect on the response of snowpack to climate warming in the Pyrenees, Theoretical and Applied Climatology, 117(1-2), 207-219, doi: 10.1007/s00704-013-0991-0.

Marsh, P., and M.-K. Woo (1985), Meltwater movement in natural heterogeneous snow covers, Water Resources Research, 21(11), 1710-1716.

Marsh, P. (1987), Grain growth in a wet arctic snow cover, Cold Regions Science and Technology, 14, 23-31.

Marsh, P., and J. W. Pomeroy (1993), The Impact of heterogeneous flow paths on snowmelt runoff chemistry, in *Eastern Snow Conference*, edited, pp. 231-238, Quebec City.

McNamara, J. P., D. Chandler, M. Seyfried, and S. Achet (2005), Soil moisture states, lateral flow, and streamflow generation in a semi-arid, snowmelt-driven catchment, Hydrological Processes, 19(20), 4023-4038, doi: 10.1002/hyp.5869.

Mitterer, C., H. Hirashima, and J. Schweizer (2011), Wet-snow instabilities: comparison of measured and modelled liquid water content and snow stratigraphy, Annals of Glaciology, 52(58), 201-208.

Molotch, N. P., P. D. Brooks, S. P. Burns, M. Litvak, R. K. Monson, J. R. McConnell, and K. Musselman (2009), Ecohydrological controls on snowmelt partitioning in mixed-conifer sub-alpine forests, Ecohydrology, 2(2), 129-142, doi: 10.1002/eco.48.

Molotch, N. P., and L. Meromy (2014), Physiographic and climatic controls on snow cover persistence in the Sierra Nevada Mountains, Hydrological Processes, 28(16), 4573-4586, doi: 10.1002/hyp.10254.

Musselman, K. N., N. P. Molotch, and P. D. Brooks (2008), Effects of vegetation on snow accumulation and ablation in a mid-latitude sub-alpine forest, Hydrological Processes, 22(15), 2767-2776, doi: 10.1002/hyp.7050.

Mutzner, R., S. Weijs, P. Tarolli, M. Calaf, H. Oldroyd, and M. Parlange (2015), Controls on the diurnal streamflow cycles in two subbasins of an alpine headwater catchment, Water Resources Research, 51(5), 3403-3418, doi: 10.1002/2014WR016581.

Painter, T. H., S. M. Skiles, J. S. Deems, A. C. Bryant, and C. C. Landry (2012), Dust radiative forcing in snow of the Upper Colorado River Basin: 1. A 6 year record of energy balance, radiation, and dust concentrations, Water Resources Research, 48(7), n/a-n/a, doi: 10.1029/2012wr011985.

Pelto, M. S. (2008), Impact of climate change on north cascade alpine glaciers, and alpine runoff, Northwest Sci., 82(1), 65-75.

Perovich, D., M. Holland, and E. Hunke (2015), Improving representation of snow on sea ice in climate models, Eos, 96, doi: 10.1029/2015EO039419.

Pistone, K., I. Eisenman, and V. Ramanathan (2014), Observational determination of albedo decrease caused by vanishing Arctic sea ice, Proceedings of the National Academy of Sciences of the United States of America, 111(9), 3322-3326, doi: 10.1073/pnas.1318201111.

Rasmussen, R., et al. (2014), Climate Change Impacts on the Water Balance of the Colorado Headwaters: High-Resolution Regional Climate Model Simulations, Journal of Hydrometeorology, 15(3), 1091-1116, doi: 10.1175/jhm-d-13-0118.1.

Rice, R., R. C. Bales, T. H. Painter, and J. Dozier (2011), Snow water equivalent along elevation gradients in the Merced and Tuolumne River basins of the Sierra Nevada, Water Resources Research, 47, 11, doi: 10.1029/2010wr009278.

Richards, L. A. (1931), Capillary conduction of liquids through porous mediums, Physics, 1, 318-333.

Richer, E. E., S. K. Kampf, S. R. Fassnacht, and C. C. Moore (2013), Spatiotemporal index for analyzing controls on snow climatology: application in the Colorado Front Range, Physical Geography, 34(2), 85-107.

Rosenthal, W., and J. Dozier (1996), Automated mapping of montane snow cover at subpixel resolution from the Landsat Thematic Mapper, Water Resources Research, 32(1), 115-130, doi: 10.1029/95wr02718.

Sanadhya, P., J. Gironás, and M. Arabi (2014), Global sensitivity analysis of hydrologic processes in major snow-dominated mountainous river basins in Colorado, Hydrological Processes, 28(9), 3404-3418, doi: 10.1002/hyp.9896.

Sexstone, G. A., and S. R. Fassnacht (2014), What drives basin scale spatial variability of snowpack properties in northern Colorado?, The Cryosphere, 8(2), 329-344, doi: 10.5194/tc-8-329-2014.

Seyfried, M. S., L. E. Grant, D. Marks, A. Winstral, and J. McNamara (2009), Simulated soil water storage effects on streamflow generation in a mountainous snowmelt environment, Idaho, USA, Hydrological Processes, 23(6), 858-873, doi: 10.1002/hyp.7211.

Shi, J., and J. Dozier (1995), Inferring snow wetness using C-band data from SIR-C's polarimetric synthetic aperture radar (vol 33, pg 905, 1995), Ieee Transactions on Geoscience and Remote Sensing, 33(6), 1340-1340.

Skiles, S. M., T. H. Painter, J. S. Deems, A. C. Bryant, and C. C. Landry (2012), Dust radiative forcing in snow of the Upper Colorado River Basin: 2. Interannual variability in radiative forcing and snowmelt rates, Water Resources Research, 48(7), n/a-n/a, doi: 10.1029/2012wr011986.

Smith, T. J., J. P. McNamara, A. N. Flores, M. M. Gribb, P. S. Aishlin, and S. G. Benner (2011), Small soil storage capacity limits benefit of winter snowpack to upland vegetation, Hydrological Processes, 25(25), 3858-3865, doi: 10.1002/hyp.8340.

Sommerfeld, R. A., R. C. Bales, and A. Mast (1994), Spatial Statistics of Snowmelt Flow - Data from Lysimeters and Aerial Photos, Geophysical Research Letters, 21(25), 2821-2824, doi: 10.1029/94gl02493.

Staron, P., E. Adams, and D. Miller (2014), Nonequilibrium thermodynamics of kinetic metamorphism in snow, Cold Regions Science and Technology, 97, 60-71, doi: 10.1016/j.coldregions.2013.10.007.

Storck, P., D. P. Lettenmaier, and S. M. Bolton (2002), Measurement of snow interception and canopy effects on snow accumulation and melt in a mountainous maritime climate, Oregon, United States, Water Resources Research, 38(11), 5-1-5-16, doi: 10.1029/2002wr001281.

Techel, F., and C. Pielmeier (2011), Point observations of liquid water content in wet snow - investigating methodical, spatial and temporal aspects, The Cryosphere, 5(2), 405-418, doi: 10.5194/tc-5-405-2011.

Tedesco, M., X. Fettweis, T. Mote, J. Wahr, P. Alexander, J. Box, and B. Wouters (2013), Evidence and analysis of 2012 Greenland records from spaceborne observations, a regional climate model and reanalysis data, Cryosphere, 7(2), 615-630, doi: 10.5194/tc-7-615-2013.

Tobin, C., B. Schaefli, L. Nicotina, S. Simoni, G. Barrenetxea, R. Smith, M. Parlange, and A. Rinaldo (2013), Improving the degree-day method for sub-daily melt simulations with physically-based diurnal variations, Advances in Water Resources, 55, 149-164, doi: 10.1016/j.advwatres.2012.08.008.

Van Genuchten, M. T. (1980), A closed-form equation for predicting the hydraulic conductivity of unsaturated soils, Soil Science Society of America Journal, 44, 892-898.

Webb, R. W., S. R. Fassnacht, and M. N. Gooseff (2015), Wetting and Drying Variability of the Shallow Subsurface Beneath a Snowpack in California's Southern Sierra Nevada, Vadose Zone Journal, 14(8), 0, doi: 10.2136/vzj2014.12.0182.

Webb, S. W. (1997), Generalization of Ross' tilted capillary barrier diversion formula for different two-phase characteristic curves, Water Resources Research, 33(8), 1855-1859, doi: 10.1029/97wr01231.

Wever, N., C. Fierz, C. Mitterer, H. Hirashima, and M. Lehning (2014), Solving Richards Equation for snow improves snowpack meltwater runoff estimations in detailed multi-layer snowpack model, The Cryosphere, 8(1), 257-274, doi: 10.5194/tc-8-257-2014.

Williams, C. J., J. P. McNamara, and D. G. Chandler (2009a), Controls on the temporal and spatial variability of soil moisture in a mountainous landscape: the signature of snow and complex terrain, Hydrology and Earth System Sciences, 13, 1325-1336.

Williams, M. W., R. Sommerfeld, S. Massman, and M. Rikkers (1999), Correlation lengths of meltwater flow through ripe snowpacks, Colorado Front Range, USA, Hydrological Processes, 13(1807-1826).

Williams, M. W., M. Rikkers, and W. T. Pfeffer (2000), Ice columns and frozen rills in a warm snowpack, Green Lakes Valley, Colorado, USA, Nordic Hydrology, 31(3), 169-186.

Williams, M. W., C. Seibold, and K. Chowanski (2009b), Storage and release of solutes from a subalpine seasonal snowpack: soil and stream water response, Niwot Ridge, Colorado, Biogeochemistry, 95(1), 77-94, doi: 10.1007/s10533-009-9288-x.

Williams, M. W., T. A. Erickson, and J. L. Petrzelka (2010), Visualizing meltwater flow through snow at the centimetre-to-metre scale using a snow guillotine, Hydrological Processes, n/a-n/a, doi: 10.1002/hyp.7630.

Yamaguchi, S., T. Katsushima, A. Sato, and T. Kumakura (2010), Water retention curve of snow with different grain sizes, Cold Regions Science and Technology, 64(2), 87-93, doi: 10.1016/j.coldregions.2010.05.008.

Yosida, Z. (1955), Physical studies of deposited snow, 1. Thermal properties, in Thermal properties, edited, pp. 19-74, Institute of Low Temperature Science Hokkaido University.

Zhao, Q., Z. Liu, B. Ye, Y. Qin, Z. Wei, and S. Fang (2009), A snowmelt runoff forecasting model coupling WRF and DHSVM, Hydrology and Earth System Sciences, 13(10), 1897-1906.

CHAPTER 2: DIURNAL PATTERN OF SNOWMELT

Introduction

The hydrologic cycle of many mountainous regions worldwide is dominated by snow accumulation and ablation processes. Changes to snowpack accumulation and melt processes due to warming trends will affect an estimated one-sixth of the global population [*Barnett et al.*, *2005*]. Snowmelt can be linked to vital water resources such as groundwater [*Flint et al.*, *2008; Clilverd et al., 2011; Cao et al., 2013*], streamflow connectivity [*McNamara et al.*, *2005; Hunsaker et al., 2012; Kampf et al., 2015*], soil moisture dynamics [*Harpold et al.*, *2015*] and forest ecosystem dynamics [*Williams et al.*, *2009; Smith et al., 2011; Harpold et al., 2014*]. With past and projected changes to snowpack accumulation and melt rates [*Adam et al.*, *2009; Clow, 2010; Harpold et al., 2012; Fassnacht and Hultstrand, 2015*], it is important to accurately represent a snowmelt to properly relate it to the hydrological processes that will be impacted.

In addition to its importance to water resources and ecosystem dynamics, snowmelt can cause high-damage flooding [*Graybeal and Leathers*, *2006; Zhao et al., 2009*] that has motivated countries such as China to invest in snowmelt specific flood warning systems [*Fang et al.*, *2013*]. The United States standard used for flood modeling and design includes frequency estimates for rainfall but often lacks snowmelt estimates for regions such as the southern Rocky Mountains [*Perica et al., 2013*]. This region, though, has shown a 10 year 24 hour snowmelt event can be as much as 45% greater than a 10 year 24 hour rain event [*Fassnacht and Records*, *2015*]. It is also important to note that the majority of a 24 hour snowmelt event will likely occur over a shorter duration relative to a rain event and with different antecedent soil moisture conditions resulting in different runoff processes. The general temporal pattern occurring at the sub-daily time scale has been shown using snow lysimeters in multiple North American locations, all displaying similar shapes in outflow [*Dunne et al.*, *1976; Colbeck, 1979; Marsh and Woo, 1985; Harrington et al., 1996; Fox and Williams, 1999*].

The temporal pattern of meltwater outflow from a snowpack is driven by unsaturated flow. As snow begins to melt early in the day, the liquid water content of the snowpack will be relatively low resulting in a lower hydraulic conductivity and the downward percolation of water to occur slowly. As melt increases throughout the day meltwater percolation will begin to increase in downward velocity. The later faster moving meltwater will meet the initial slower moving wetting front prior to water release from the snowpack causing a rapid increase in water outflow from a snowpack during initial release followed by a long decline after peak outflow for the day [U.S. Army Corps of Engineers, *1956; Dunne et al., 1976; Colbeck, 1979; Marsh and Woo, 1985; Harrington et al., 1996*]. Unsaturated flow follows physical laws that have been long-understood in soil sciences [*van Genuchten*, *1980; Ross, 1990*], successfully applied to snow science modeling [*Wever et al.*, *2014; Heilig et al., 2015*] and supported by observations in field studies [*Jordan*, *1983; Marsh and Woo, 1985; Kattelmann and Dozier, 1999; Laudon et al., 2004; Techel and Pielmeier, 2011; Eiriksson et al., 2013*]. Multiple dye tracer experiments have displayed flow paths or flow fingers that form as meltwater breaks through capillary forces across snow layer interfaces [*McGurk and Marsh*, *1995; Schneebeli, 1995; Eiriksson et al., 2013; Katsushima et al., 2013; Williams et al., 2010*] supporting the above described physical process causing the temporal pattern of meltwater outflow from a snowpack.

The timing of water being released from a snowpack is important for the diurnal cycle of streamflow in headwater rivers [*Caine*, *1992; Laudon et al., 2004; Lundquist and Dettinger, 2005; Lundquist et al., 2005; Jencso and McGlynn, 2011; Mutzner et al., 2015*]. Streamflow can fluctuate as much as 10% on a regular basis from snowmelt input [*Lundquist and Cayan*, *2002*] and even larger during high melt or rain on snow events [*Jennings and Jones*, *2015*]. Hydrological models often use a simple degree-day snowmelt algorithm [*Frankenberger et al.*, *1999; Hock, 1999; Jost et al., 2012; Tobin et al., 2013*] or a more computationally intensive mass and energy balance [*Brooks et al.*, *2007; Bittelli et al., 2010*]. For flood design, modeling efforts generally take a simple degree-day approach. This method has been adapted to include

time varying melt at the hourly temporal scale, often imposing a half-sinusoidal variation in melt centered about solar noon [*Hock*, *1999*]. Further improvements to *Hock* [*1999*] have utilized available solar radiation data and minimum and maximum temperatures [*Jost et al.*, *2012; Tobin et al., 2013*]. However, measurements of these variables have shown large errors, particularly for temperature over snow with a high albedo [*Huwald et al.*, *2009*], and solar radiation sensors can be obscured by the accumulation of snowfall on the sensor. These studies improving degree-day modeling approaches have highlighted the importance of the diurnal pattern of snowmelt for streamflow generation.

Modeling large floods in previously unmonitored streams in the United States often uses only rainfall estimates for large storms such as 10 year or 100 year recurrence interval events [e.g. *Yochum*, *2012*]. Many of these modeling efforts implement the Soil Conservation Service (SCS) standardized rainfall distribution [*USDA*, *1986*]. This may be appropriate for lower elevations, but for higher elevations where snowmelt can dominate the flood risk, a more computationally intensive method such as a mass and energy balance is currently necessary due to the lack of a standardized snowmelt model. Such efforts often require new instrumentation to collect data for calibration that can be costly both monetarily and temporally.

The goal of this paper is to develop a diurnal snowmelt curve for the improvement of hydrograph predictions for large snowmelt events using readily available public data sources. This function is developed using the following objectives: (1) fit a function to observed hourly changes in SWE, (2) use soil moisture data to assess the timing of meltwater outflow, and (3) test the function to changes in SWE with other sites in the same region.

Methods

Data

Across the mountains of the western United States, the Natural Resource Conservation Service (NRCS) operates the snow telemetry (SNOTEL) network with over 800 stations that provide public domain daily and hourly snow data. SNOTEL stations have snow pillows to

measure snow water equivalent (SWE) that provide data that have been used for decades for flow forecasts and resource management [*Beaumont*, *1965; Robertson, 1967; Archer and Stewart, 1995; Penton et al., 2010; Palmer, 2015*]. Some SNOTEL sites also provide volumetric soil moisture data, and although the sensors are not calibrated to the site-specific soils or for the known influence of temperature [*Seyfried and Grant*, *2007*], they still provide useful information of the changes in soil moisture beneath a melting snowpack. Furthermore, the addition of soil moisture sensors allows estimates of snowmelt outflow in the absence of less common instrumentation, such as snow lysimeters, by comparing changes in snow pillow SWE and soil moisture data.

The data used in this study were from eight SNOTEL stations located in the Southern Rocky Mountains of northern Colorado (Table 2.1 and Fig. 2.1). The five calibration stations include soil volumetric water content (VWC) data and were used to develop a function for the diurnal pattern of snowmelt; the three testing stations did not measure VWC. Data acquired from these sites were daily and hourly SWE, daily precipitation, and hourly soil VWC (where available) at 5 cm depth. For this study only days with no recorded daily precipitation and a daily loss of SWE greater than 10 mm were used for analysis.

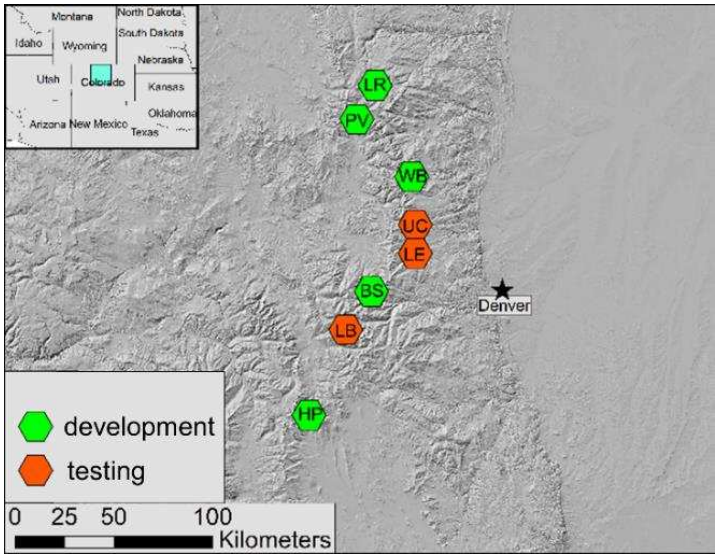

Figure 2.1: Map of SNOTEL stations listed in Table 2.1 used to calibrate and test the function.

Table 2.1: Summary of daily SNOTEL data for Berthoud Summit (BS), Hoosier Pass (HP), Long Draw Reservoir (LR), Phantom Valley (PV), Wild Basin (WB), Loveland Basin (LB), University Camp (UC), and Lake Eldora (LE) showing the date and amount of peak snow water equivalent (SWE), days from peak SWE to 100% melt, as well as the percent of 30 year median for April and May 1st. (note: LR and WB do not have a long enough period of record to calculate long-term median)

	STATION	HP	BS	LR	WB	PV	LB	UC	LE
	Latitude	39.37	39.80	40.52	40.20	40.40	39.67	40.03	39.93
	Longitude	-106.07	-105.78	-105.77	-105.60	-105.85	-105.90	-105.58	-105.57
	Elevation (m)	3475	3444	3042	2914	2752	3475	3140	2957
	Median peak SWE (mm)	406	554	----	----	236	588	483	310
2012	Peak SWE (mm)	259	330	277	361	185	----	----	----
2012	date of Peak	25-Mar	6-Mar	28-Mar	9-Apr	6-Mar	----	----	----
2012	days to 100% melt	51	60	39	35	27	----	----	----
2012	Apr 1st % median	68	52	----	----	2	----	----	----
2012	May 1st % median	33	14	----	----	0	----	----	----
2013	Peak SWE (mm)	427	582	447	422	264	----	----	----
2013	date of Peak	10-May	10-May	9-May	25-Apr	24-Apr	----	----	----
2013	days to 100% melt	28	32	30	36	30	----	----	----
2013	Apr 1st % median	75	83	----	----	77	----	----	----
2013	May 1st % median	93	91	----	----	195	----	----	----
2014	Peak SWE (mm)	549	678	597	594	338	724	721	485
2014	date of Peak	21-Apr	17-May	22-Apr	18-Apr	9-Apr	26-May	17-May	8-Apr
2014	days to 100% melt	56	27	53	46	47	27	45	47
2014	Apr 1st % median	134	133	----	----	134	130	157	159
2014	May 1st % median	142	119	----	----	195	120	145	183

The stations range in elevation from 2750 m to 3450 m with long term median peak SWE values from 230 mm to over 580 mm. The five calibration stations offer a range of elevations and snowpack accumulation and seasonal melt patterns for the three water years analyzed for developing the function (2012, 2013, and 2014) (Table 2.1). The 2012 water year was a low snow year for all stations with a range of peak SWE values from 185 mm (PV) to 361 mm (WB) and the melt season from peak to no SWE lasting from 27 days (PV) to 60 days (BS). The 2013 water year was relatively normal with peak SWE ranging from 264 (PV) to 582 (BS) and melt ranging from 28 (HP) to 36 (WB) days. Lastly, 2014 was a high snowpack year with peak SWE ranging from 338 (PV) to 678 (BS) and melt lasting from 27 (BS) to 56 (HP) days (Table 2.1). Long term median values were not available at the LR and WB SNOTEL stations, as they were installed in 2009 and 2002, respectively.

The stations utilized for testing the developed function in this study were only tested in 2014, a relatively large snow year (Table 2.1). These stations were chosen because of their locations within the region of interest to develop the methods described below and having similar range of elevations as the stations used for development. LB, the highest elevation site for testing also had the highest peak SWE at 724 mm occurring the latest in the season on May 26, 2014 whereas the lowest elevation site, LE, had a peak SWE of 485 mm occurring on April 8, 2014. All of these stations had above 100% median SWE values on April 1 and May 1 of the 2014 spring snowmelt season (Table 2.1).

Data Processing & Analysis

Daily SWE data are quality assessed by the NRCS prior to online publication whereas hourly data are not. Hourly SWE data were processed in this study using multiple steps. First a threshold approach was applied using the quality assessed daily data for minimum and maximum thresholds, removing large outliers from the dataset [see *Avanzi et al*., *2014*]. Next the hourly loss of SWE was calculated by subtracting hourly SWE recordings from the previous hour's recording. Days that produced 100% of daily SWE loss in one hour were removed from analyses. NRCS hourly SWE measurements published at 00:00 is the daily quality controlled value for the previous day that causing erroneous SWE loss estimates at 0:00 and 01:00 and thus calculated losses at these times were removed. Obvious sensor noise, defined as two adjacent time steps of equal and opposite values, was next removed and such SWE loss was set to a value of zero. The final processing step of hourly SWE data was the conversion of hourly SWE losses to fraction of daily melt (FDM) by dividing each hourly SWE loss by the cumulative daily SWE loss.

For the five calibration stations, 194 days of hourly FDM were available to develop the diurnal function of snowmelt; a total of 57 days of hourly FDM were used to test the function for the three stations. For function development, the data from the five stations were combined and the mean and median values for each hourly time step of the day were calculated. Visual

observation revealed noise in the morning that has been shown in snow pillow data for many years (Fig. 2.2) [*Penton and Robertson*, *1967*]. Snow lysimeter studies have shown no such early increase in release of meltwater but rather a continued gradual decrease and these early morning fluctuations in snow pillow data have largely been attributed to temperature fluctuations causing battery voltage fluctuations during rapid changes as the sun

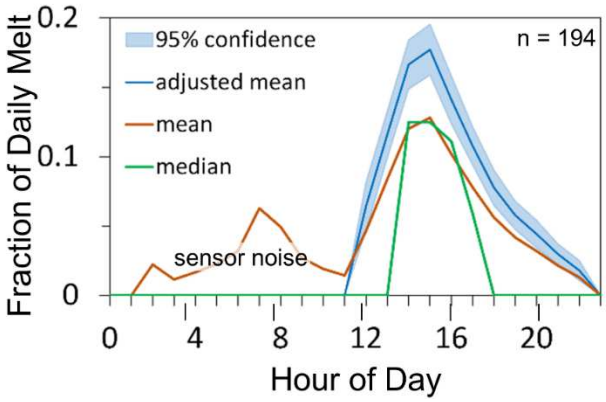

Figure 2.2: Fraction of daily melt (FDM) data compiled from all five SNOTEL stations. The mean and adjusted mean values are shown in addition to the 95% confidence band for the adjusted mean.

rises creating apparent SWE fluctuations. For this reason, the mean hourly FDM data was adjusted to remove values occurring at or before 11:00 hr and recalculated such that the sum of the adjusted mean FDM equaled 1.0. A 95% confidence interval was then calculated for the adjusted mean values assuming a normal distribution of data at each time step and a function was fit to the adjusted mean FDM data. Focus in this study was the total time of the meltwater release cycle and the timing and magnitude of peak FDM.

The function used to fit observed SWE data in this study is the two-parameter gamma distribution function, modified for purposes herein. A simplified version of the two-parameter gamma distribution function has been widely used for synthetic unit hydrographs [*e.g. Bhunya et al., 2003*] as well as deriving a synthetic sediment graph [*Singh et al., 2013*]. Though there are similarities to the version of the gamma distribution function applied in Bhunya *et al*. (2003), we have utilized the expression with modifications in the form of:

$$FDM(t) = \frac{1}{\beta^{\alpha}\Gamma(\alpha)} \cdot (t - t_0)^{\alpha-1} \cdot e^{-(t+t_0)/\beta} + c \quad (2.1)$$

where α and β are fitting parameters, $\Gamma(\alpha)$ is the gamma mathematical function, t is the time of day in hours, t_0 is a time shifting factor to adjust for the time of day that snowmelt begins, and c is a constant applied only after curve fitting to ensure conservation of mass (*i.e*. $\Sigma FDM = 1.0$). For this study, when t_0 is greater than t the function is set to FDM = 0.

The resulting function for FDM was qualitatively compared with the hourly FDM from each of the five SNOTEL stations individual FDM and VWC data. Mean and median values of VWC and FDM at individual SNOTEL stations were calculated as well as an adjusted mean FDM as described above through visual observation of early morning noise for each station individually and adjusted mean 95% confidence intervals calculated with an assumed normal distribution. The adjusted mean and median diurnal fluctuations of VWC and FDM data were used qualitatively to assess the timing of the start and peak of diurnal snowmelt outflow at individual stations. This allows determination of the influence each station's FDM had on the function and if a single location has a snowmelt pattern that is not represented well in the mean of all five stations.

Soil moisture sensors installed are time domain reflectometers that need to be calibrated for each site specific soil and for the effects of temperature [*Seyfried and Grant, 2007*]. SNOTEL soil moisture sensors were not calibrated at these sites and for this reason caution was used when interpreting the SNOTEL VWC data. No attempt was made to calibrate or manipulate the data. Frozen soil was determined through the shape of hourly data over time and removed from analyses using VWC data; frozen soil will display a relatively low VWC value with an asymptotic increase in VWC during the thawing period.

Testing of the developed gamma function FDM was conducted using three SNOTEL sites during the 2014 water year. These sites (LE, UC, and LB) do not have VWC data available and so were only used to test the function against SWE data used to determine FDM. The

developed FDM function was tested to the three stations FDM for fit using root mean squared error (RMSE) as well as visually assessing the duration of melt and the timing and magnitude of peak FDM.

Results

The mean FDM for all five stations used for function development from the 194 days analyzed produced a clear diurnal cycle of snowmelt runoff from the snowpack (Fig. 2.2). VWC data produced 130 days for analysis after removal of 64 days with frozen soils. The 2014 water year SWE data at LR and PV was excluded from analysis due to instrumentation error. The data processing described above did not remove all errors from the hourly data and negative SWE losses (increases in SWE) were still observed during days with no precipitation. Similar noise in the positive direction is likely balancing out the mean data. The gamma FDM function that was found to best fit the adjusted mean FDM for all five stations has parameter values for equation (2.1) of: $\alpha = 3.8$, $\beta = 1.3$, $t_0 = 11{:}00$, and $c = 8.5 \times 10^{-4}$ with a resulting RMSE value is 0.01 (Fig. 2.3). This equation results in an approximate peak FDM of 0.177 occurring at 16:00 hours that is the same magnitude and timing as the adjusted mean FDM from the data (Fig. 2.3).

Comparison with FDM mean and median of individual stations to the gamma FDM function shows reasonable agreement for all stations (Fig. 2.4). Some of the SNOTEL stations contributed a greater number of data points towards the early morning noise and less obvious sensor noise resulted in a more reasonable agreement between the hourly FDM data and developed function is observed (Fig. 2.4). In general, the timing of the peak FDM and beginning of melt matched well for all stations, particularly the median values of the data. All five stations had a clear diurnal pattern that was similar to the mean of all five stations.

When observing the diurnal cycle of the mean and median values of the VWC data a clear pattern is present (Fig. 2.5). All of the VWC sensors display a sharp increase to peak daily values at around the same time for each station followed by a more gradual decrease. This corresponds well with the shape of the FDM function (Fig. 2.5). The median values tend to

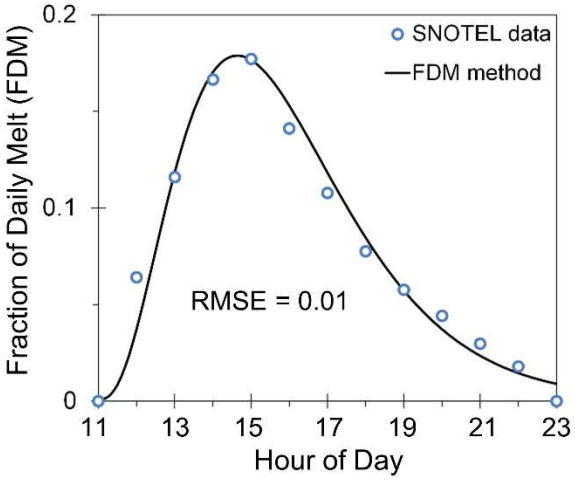

Figure 2.3: Gamma function Fraction of Daily Melt (FDM) method fit to the SNOTEL data FDM with root mean squared error value shown.

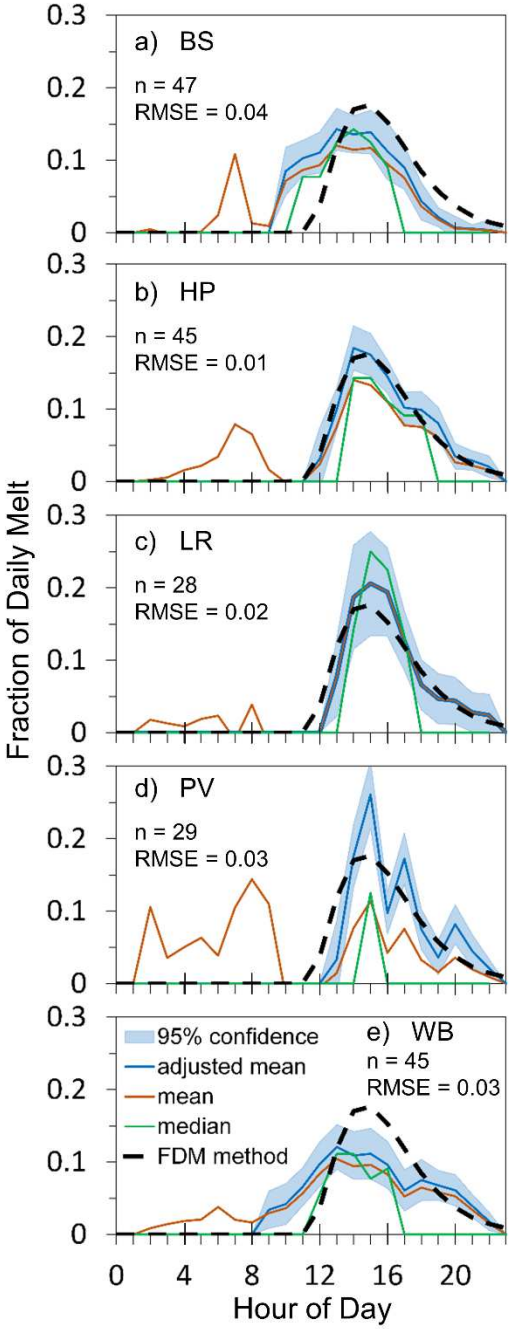

Figure 2.4: Fraction of daily melt (FDM) data compiled for each of the SNOTEL stations: a) Berthoud Summit (BS), b) Hoosier Pass (HP), c) Long Draw Reservoir (LR), d) Phantom Valley (PV), and e) Wild Basin (WB). The mean and adjusted mean values are shown in addition to the 95% confidence band for the adjusted mean and the gamma function FDM method fit to the adjusted mean using all stations combined. The number of data points used to calculate the values (n) and root mean squared error (RMSE) are shown.

display this sharp increase better compared to the mean values. The PV location displays two different timings in outflow shown in the mean values but this is not observed in the calculated median (Fig. 2.5d). This is likely a result of only 14 days of VWC data for this location causing stronger influence of a small number of days with earlier or later melt (from different observed years) to influence the mean rather than two meltwater outflow events each day (Fig. 2.5). The LR, PV and WB sites display slightly earlier but overall similar timing of outflow when comparing the FDM function to VWC whereas BS and HP show earlier outflow may be occurring and not captured well in the snow pillow data (maximum lag of three hours). The large initial outflow followed by decreasing rates are apparent in all VWC data. The stations that have the earliest outflow observed in the VWC data, BS and HP, are also the sites at the highest elevations at 3444 m and 3475 m, respectively (Table 2.1). The next highest site is LR at 3042 m. The higher elevation sites also generally have a later date of peak SWE (Table 2.1) indicating that solar radiation may be influencing the energy balance earlier and other energy balance components such as sensible heat and longwave radiation may influence the timing of melt differently. The FDM function does not take this into account, however the normal years produced a FDM occurring over a shorter duration that may be considered conservative for design purposes.

Testing the FDM function to the other three SNOTEL station FDMs for the 2014 water year shows that the function did not performed as well at these individual sites with no adjustment, but error was greatly improved by shift the timing of the FDM (Fig. 2.6). These locations showed melt to begin and peak earlier in the day relative to the FDM function developed in this study. These stations also tended to reach peak SWE later in the year than normal (Table 2.2). The LB site was the location at the highest elevation (Table 2.2) and showed the earliest peak FDM (Fig. 2.6b). The UC location shows the influence of possible noise in the data when using a single year for analysis, though the magnitude of peak FDM was slightly lower than the fit function and the length of daily melt slightly longer (Fig. 2.6c). The lowest elevation site of the three (LE) also had the most days for analysis and the FDM function

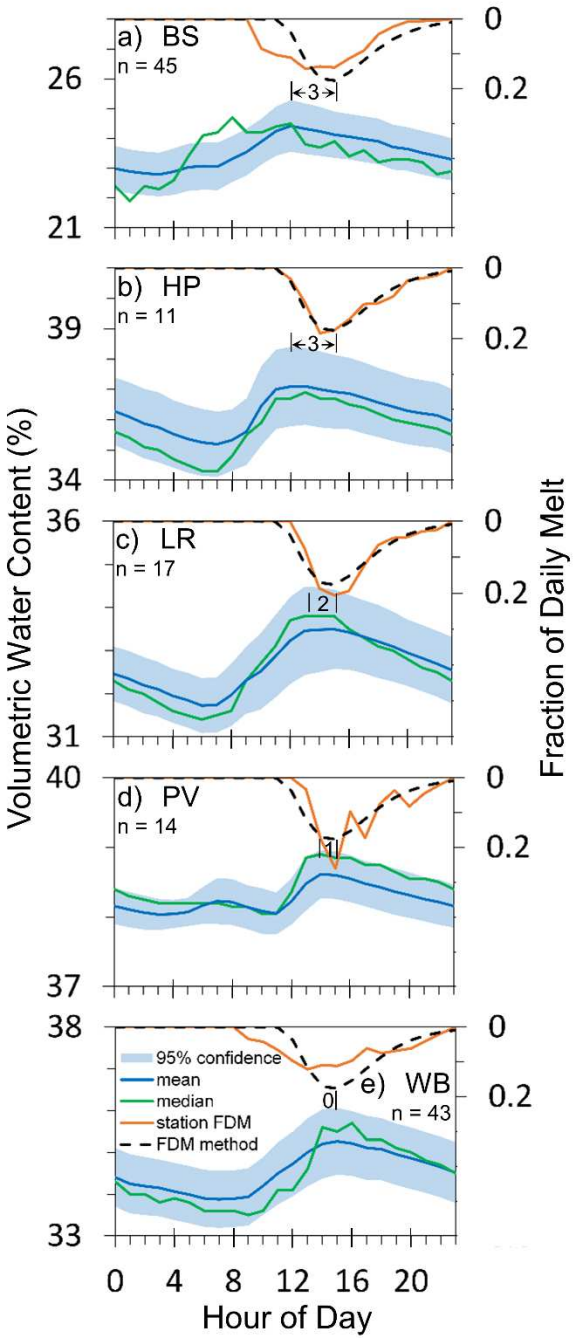

Figure 2.5: Volumetric water content (VWC) data for each SNOTEL station: a) Berthoud Summit (BS), b) Hoosier Pass (HP), c) Longdraw Reservoir (LR), d) Phantom Valley (PV), and e) Wild Basin (WB). The mean, median values, and the 95% confidence band, gamma function fraction of daily melt (FDM) method shown above, number of data points (n), and time difference between peak VWC and peak gamma function FDM are all shown.

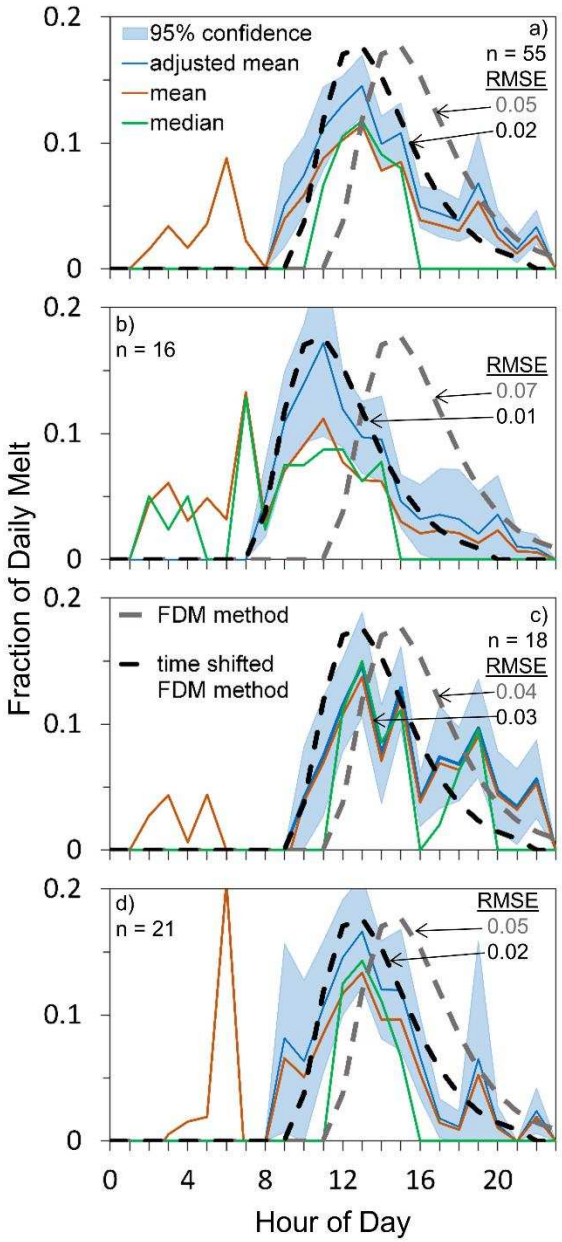

Figure 2.6: Testing of the gamma function fit fraction of daily melt (FDM) to a) all three additional SNOTEL locations and each one individually: b) Loveland Basin (LB), c) University Camp (UC), and d) Lake Eldora (LE).

match the timing and magnitude of peak FDM well, though the length of melt was observed to be longer with possible influence of sensor noise later in the evening hours (Fig. 2.6.d). When observing all three sites combined (Fig. 2.6a) the FDM function appears to occur over a shorter duration and with a higher peak, though this may be useful as a conservative estimate for design purposes. RMSE values are shown for the FDM function compared to the 2014 FDM of each individual station used for testing both for the original timing of the FDM function as well as shifting it earlier in the day to match timing of peak FDM for each of the stations. LB Station resulted in the lowest RMSE value of 0.01 for the shifted FDM function and UC had the highest of 0.03. All RMSE values were improved by shifting the timing of the FDM function to match the time of day of peak FDM (adjusting the t_0 parameter).

Discussion

The diurnal pattern of snowmelt outflow in Colorado's Front Range was observed and fit with a modified gamma distribution function. The shape of the FDM function developed in this study is similar to previous observations using snow lysimeters in multiple locations (Fig. 2.7) [*Dunne et al.*, *1976; Colbeck, 1979; Colbeck and Anderson, 1982; Harrington and Bales, 1998; Wever et al., 2014*] as well as runoff hydrographs during snowmelt [*Caine*, *1992; Lundquist and Cayan, 2002; Lundquist and Dettinger, 2005; Kampf et al., 2015; Mutzner et al., 2015*]. Hourly SWE data from SNOTEL stations can be noisy and difficult to use (Fig. 2.2). Some known errors with the hourly snow water equivalent (SWE) data from snow pillows include sensor noise in the early morning, general noise throughout the day, and lag times from actual SWE changes to recorded changes [*Archer and Stewart*, *1995; Beaumont, 1965; Penton and Robertson, 1967; Johnson and Schaefer, 2002; Johnson and Marks, 2004*]. However, the methodology presented in this study shows a diurnal pattern based on multiple days and years of hourly data. The noise that is observed in the online (published) hourly data can be a fluctuation between values, but much of such noise is removed using the methods presented here; the remaining noise did not display any noticeable positive or negative bias.

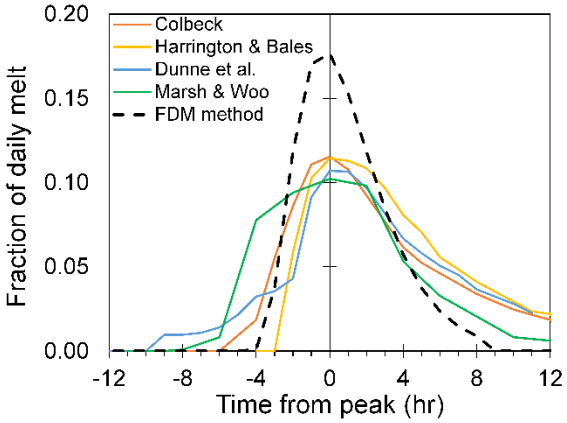

Figure 2.7: Comparison of individual days of snow lysimeter data from California's Sierra Nevada [*Colbeck, 1979; Harrington and Bales, 1998*], a boreal forest [*Dunne et al., 1976*], the high arctic [*Marsh and Woo, 1985*], and the gamma function FDM developed in this study for Colorado's continental Rocky Mountains.

When testing the fit FDM function to a single year of data (Fig. 2.6), the general shape of the diurnal pattern of melt was noticeable at the stations, though timing was variable and the influence of noise as well as possible conditions unique to individual years can vary such as timing and magnitude of peak SWE. The primary occurrence of sensor noise was early in the morning as discussed earlier and known to occur near sunrise [*Penton and Robertson*, *1967*]; all other noise was random in both timing and direction. There were also no noticeable differences in the diurnal pattern of FDM between low, normal, and high peak SWE years other than the time of day that melt occurred (Fig. 2.6). The results of this study show that the diurnal pattern of melt at a SNOTEL station may be determined using as few as three years of data. The spatial and temporal extent of SNOTEL sites could allow testing of the presented method to investigate if the diurnal pattern changes through time seasonally. Though this is outside the scope of this paper, as the melt season extends later into spring and summer the duration of melt each day will become longer as the days become longer and air temperatures warm [*U.S. Army Corps of Engineers, 1956; Weber, 2016*].

The timing of snowmelt outflow is determined by multiple factors in the energy balance that will vary both temporally and spatially. SNOTEL stations in close proximity may have

different climatologies, usually for varying elevations [*Fassnacht and Derry, 2010*]. Such information could help categorize melt patterns as well. Shortwave radiation is one major factor that contributes to melt and will be controlled by the timing of sunrise and sunset. Higher elevation sites generally melt later in the water year and as a result will begin melting earlier in the day due to earlier exposure to shortwave radiation and continue for a longer period of time from longer days. The earlier snowmelt outflow was displayed in this study at BS, HP, and LB, the three highest elevation sites used. This is less apparent in the hourly SWE data (Fig. 2.4) but clear in the VWC measurements (Fig. 2.5) for BS and HP and apparent in SWE data for LB (Fig. 2.6b). Even though the timing of outflow may occur earlier in the day at these higher elevation sites the melt duration did not appear to be greatly lengthened and the shape of the diurnal FDM is still apparent and follows the fit function (Fig. 2.4). Latitude will also have an influence on the diurnal FDM pattern similar to elevation (Fig. 2.7). Locations at higher latitudes will have different climates and timing of year that the melt season occurs. Additionally, latitude will determine the angle of incidence for solar radiation and the resulting energy balance of the snowpack. Future investigations of the application and expansion of the presented methods should consider latitude for defining appropriate regions with different diurnal FDM patterns.

The aspect of a slope can also influence the rate and duration that a snowpack melts [*Sextone and Fassnacht, 2014; Molotch and Meromy, 2014*]. For example, in the northern hemisphere where the SNOTEL stations analyzed are located, a more southerly aspect will have higher solar radiation exposure and melt for a longer duration throughout each day and have more total melt with respect to a SNOTEL station on a relatively flat aspect. Conversely, a northern aspect slope will receive less solar radiation and melt for shorter durations each day in the spring and less total melt. This is an important consideration when applying a FDM function to a single basin that is more southerly or northerly facing.

The timing of the FDM function was shown to occur later in the day than what is observed in soil moisture sensors, though the shape of the function developed using snow

pillow data was further supported by the soil moisture data in the absence of snow lysimeters (Fig. 2.5). The diurnal fluctuation in soil moisture is what is expected in unsaturated soils with a temporally varying flux as the FDM function. Soil moisture data peaks earlier in the day relative to the peak FDM displaying a lag time between datasets. Snow pillows are known to have a time delay in recording SWE losses [*Beaumont*, *1965; Penton and Robertson, 1967; Archer and Stewart, 1995*]. The snow pillow itself can create a thermal barrier between the ground and snow layer that is not representative of the surrounding soil-snow-interface, resulting in snow on the pillow melting at a different rate than the surrounding snow yielding a lag in the snow pillow data compared to the actual loss in SWE, particularly early in the melt season [*Johnson and Schaefer*, *2002; Johnson and Marks, 2004*]. Snow pillows are also impermeable and any meltwater outflow will have to runoff of the surface of the pillow prior to being recorded as a loss. These errors in timing of errors are usually in the hourly to daily time scale [*Beaumont, 1965; Johnson and Schaefer, 2002*]. However, a lag time between actual and recorded losses is simple to correct in hydrological modeling or flood design at this scale (Fig. 2.6). Provided the shape of the diurnal cycle of snowmelt outflow is accurate, equation (2.1) may be easily adjusted for this with the t_0 parameter (Fig. 2.6). The shape of the FDM function presented in this study, even with consideration of the known errors in snow pillow data, fits well with known diurnal patterns of snowmelt [*Dunne et al., 1976; Colbeck, 1979; Marsh and Woo, 1985; Harrington and Bales, 1998; Mutzner et al., 2015*].

The diurnal pattern of outflow can be easily defined using equation (2.1) and can then be used for design purposes of previously unmonitored streams where snowmelt is important. In scenarios that a specific recurrence interval storm event is needed for channel or bridge design, it may be necessary to investigate both rainfall and snowmelt. The presented method may be used to determine the shape of a design snowmelt event for a determined recurrence interval of total melt, similar to SCS type rainstorm events. Comparison of the two show differences in water input to the system that may be important (Fig. 2.8). Furthermore, during snowmelt the

soil is likely more saturated in comparison to a summer rain event and thus runoff processes will be different [*Bales et al.*, *2011; Kampf et al., 2015*]. The developed FDM function may be used in a hydrological model parameterized with wetter soils and compared to a rain event with relatively dry soils for determining potential outflow hydrographs of previously unmonitored streams.

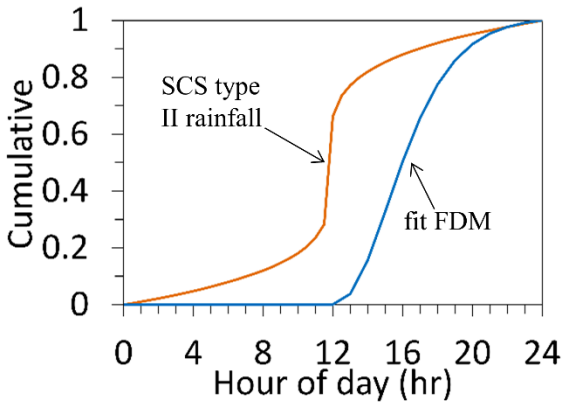

Figure 2.8: Comparison of the resulting fraction of daily melt (FDM) using the gamma function method presented in this study to the SCS type II rainfall distribution displayed as the cumulative fraction of water input over a 24 hour time period.

With considerations to other climate regions and snowpack types, the FDM function developed in this study can also be compared to snow lysimeter data for individual days in the Sierra Nevada of California [*Colbeck, 1979; Harrington and Bales, 1998*], high arctic [*Marsh and Woo, 1985*], and boreal forest [*Dunne et al., 1976*] adjusted to display FDM and time centered around peak snowmelt outflow (Fig. 2.7). Comparing these FDM data, it is clear that the general shape of sharp increase and gradual decrease of meltwater release is present. However, the duration of melt will change based on different meteorological conditions forcing melting at the four locations that are quite different than the continental Rocky Mountains. It should also be noted that these snow lysimeter data are for individual days and may not be representative of a normal melt for the region. These data were collected for specific scientific questions different from those of this study. This does, however, confirm the general shape of the FDM function

and the potential for applications to other regions with adjustments for meteorological conditions.

Limitations of the methods presented in this study are similar to those of design rain storms and synthetic unit hydrographs. These limitations include application to small and medium size watersheds [*Bhunya et al., 2003*]. These limitations are due to the spatial variability and extent of precipitation as well as changes in topography and geology. Similar limitations to the presented methods will occur due to the spatial variability of snowpacks over these extents that will alter the snowpack type and layer characteristics, as well as the varying meteorological forcing of melt [*Fassnacht and Derry, 2010*]. Thus, the presented method should be applied to small to medium sized watersheds when used for design purposes.

The parameters α and β will need to be adjusted when fitting equation (2.1) to a new location, after processing SWE data from instrumentation such as SNOTEL sites. Increases in both parameters will generally lower and delay the peak outflow represented in the FDM function (Fig. 2.9). The β parameter is more sensitive to small changes in values. These parameters may be adjusted to allow a 24 hour melt cycle for locations that outflow is always occurring above some minimum “baseflow” value. The c parameter is designed to make sure that the cumulative value of the FDM is equal to 1.0 for conservation of mass. For the presented study, c was only calculated and applied after α and β were adjusted to the best fit FDM function for the SNOTEL data.

The shown diurnal pattern of FDM could additionally be used to smooth noisy SNOTEL data or temporal downscaling estimates of remote intermittent measurements. In combination with manual observations on a weekly or bi-weekly basis and simple temperature index modeling for daily melt estimates, sub-daily SWE estimates could be calculated using the

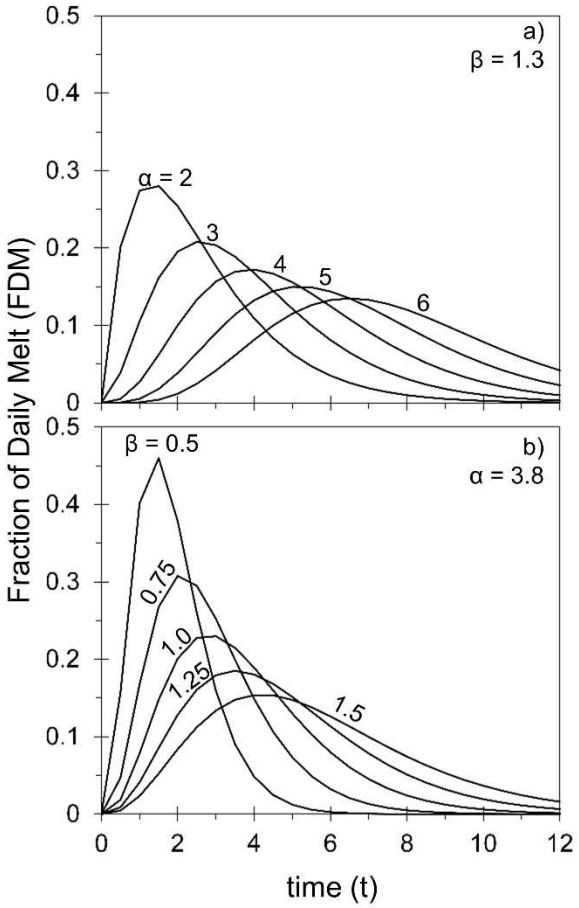

Figure 2.9: Parameter sensitivity in equation (2.1) with a) β remaining constant at 1.3 as α varies and b) α remaining constant at 3.8 as β varies. Parameters c and t_0 are kept constant at zero for all calculations in this figure.

shown FDM function. This would be beneficial for study areas that require such temporal estimates of SWE or SWE outflow without new expensive instrumentation such as a snow pillow. This application could be used for investigating processes such as groundwater or soil moisture recharge that snowmelt can be an important component [*Flint et al.*, *2008; Clilverd et al., 2011; Cao et al., 2013*]. Groundwater models can be computationally expensive by themselves without the addition of energy balance modeling of snowmelt. A simple but relatively accurate representation of snowmelt fluxes across the soil-snow interface is beneficial for appropriately representing sub-surface gradients and this study provides a function for the front range of Colorado and a method to determine the FDM elsewhere for representation of diurnal

fluctuation of snowmelt release from the snowpack with a relatively simple and computationally inexpensive method.

Hydrological models that use temperature index modeling could also be improved by incorporating the shown FDM. Modified temperature index models such as *Jost et al.* [*2012*] and *Tobin et al.* [*2013*] require additional data and further calibration. With the shown diurnal pattern of snowmelt outflow from a snowpack, sub-daily time varying melt factors could be modified from a sinusoidal curve to the gamma FDM function in this study. This would allow hydrological models to input estimated snowmelt outflow directly at the base of the snowpack rather than modeling the percolation through the snowpack that is known to not occur in the assumed uniform manner [*Harrington et al.*, *1996; McGurk and Marsh, 1995; Williams et al., 2010*]. However, further comparisons between methods are necessary to determine the benefit for using the FDM function displayed in this study.

Conclusions

A relatively simple method is presented in this paper to capture the diurnal cycle of snowmelt outflow from a snowpack in the Colorado Front Range. The FDM function for all five SNOTEL sites used in this study resulted in parameters for equation (2.1) of: $\alpha = 3.8$, $\beta = 1.3$, $t_0 = 11{:}00$, and $c = 8.5 \times 10^{-4}$ with a resulting RMSE value is 0.01 (Fig. 2.3). The diurnal cycle showed a clear pattern that can be determined using as little as three years of hourly SWE data. Hourly SWE data has some inherent errors that are unavoidable when using snow pillows, however the additional use of soil moisture data is shown to be beneficial in confirming the pattern observed from SWE data and correcting for the timing of snowmelt outflow from a snowpack. Care should also be taken when attempting to apply a fit FDM function to another location, even in the same region as shown in this study with the testing of the function. The presented methods can be used to parameterize a design snowmelt event that is comparable to the SCS rainfall distribution curve, though each show a clear difference in shape and would be applied to different antecedent soil moisture conditions of systems providing unique runoff

processes that are important for design purposes in previously unmonitored streams in mountainous regions. The method presented here can also be used to provide a computationally less expensive method to represent snowmelt outflow for groundwater recharge or general hydrological modeling, though further testing is necessary. Future investigations of snowmelt and runoff processes may benefit from application of the methods presented here.

REFERENCES

Adam, J. C., A. F. Hamlet, and D. P. Lettenmaier (2009), Implications of global climate change for snowmelt hydrology in the twenty-first century, Hydrological Processes, 23(7), 962-972, doi: 10.1002/hyp.7201.

Archer, D., and D. Stewart (1995), The Installation and Use of a Snow Pillow to Monitor Snow Water Equivalent, Journal of the Chartered Institution of Water and Environmental Management, 9(3), 221-230.

Avanzi, F., C.D. Michele, A. Ghezzi, C. Jommi, M. Pepe (2014), A processing-modeling routine to use SNOTEL hourly data in snowpack dynamic models, *Advances in Water Resources* 73: 16-29.

Bales, R. C., J. W. Hopmans, A. T. O'Geen, M. Meadows, P. C. Hartsough, P. Kirchner, C. T. Hunsaker, and D. Beaudette (2011), Soil Moisture Response to Snowmelt and Rainfall in a Sierra Nevada Mixed-Conifer Forest, Vadose Zone Journal, 10(3), 786, doi: 10.2136/vzj2011.0001.

Barnett, T. P., J. C. Adam, and D. P. Lettenmaier (2005), Potential impacts of a warming climate on water availability in snow-dominated regions, Nature, 438(7066), 303-309, doi: 10.1038/nature04141.

Beaumont, R. T. (1965), Mt. Hood Pressure Pillow Snow Gage, Journal of Applied Meteorology, 4, 626-631.

Bhunya, P. K., S. K. Mishra, and R. Berndtsson (2003), Simplified two-parameter gamma distribution for derivation of synthetic unit hydrograph, *Journal of Hydrologic Engineering*, 8(4), 226, doi: 10.1061/(ASCE)1084-0699(2003)8:4(226).

Bittelli, M., F. Tomei, A. Pistocchi, M. Flury, J. Boll, E. S. Brooks, and G. Antolini (2010), Development and testing of a physically based, three-dimensional model of surface and subsurface hydrology, Advances in Water Resources, 33(1), 106-122, doi: 10.1016/j.advwatres.2009.10.013.

Brooks, E. S., J. Boll, and P. A. McDaniel (2007), Distributed and integrated response of a geographic information system-based hydrologic model in the eastern Palouse region, Idaho, Hydrological Processes, 21(1), 110-122, doi: 10.1002/hyp.6230.

Caine, N. (1992), Modulation of the diurnal streamflow response by the seasonal snowcover of an alpine basin, Journal of Hydrology, 137, 245-260.

Cao, J., C. Liu, and W. Zhang (2013), Response of rock-fissure seepage to snowmelt in Mount Taihang slope-catchment, North China, Water Sci Technol, 67(1), 124-130, doi: 10.2166/wst.2012.542.

Clilverd, H. M., D. M. White, A. C. Tidwell, and M. A. Rawlins (2011), Sensitivity of Northern Groundwater Recharge to Climate Change: A Case Study in Northwest Alaska, Journal of the American Water Resources Association, 47(6), 1228-1240, doi: 10.1111/j.1752-1688.2011.00569.x.

Clow, D. W. (2010), Changes in the Timing of Snowmelt and Streamflow in Colorado: A Response to Recent Warming, Journal of Climate, 23(9), 2293-2306, doi: 10.1175/2009jcli2951.1.

Colbeck, S. (1979), Water-flow through heterogeneous snow, Cold Regions Science and Technology, 1(1), 37-45, doi: 10.1016/0165-232X(79)90017-X.

Colbeck, S. C., and E. A. Anderson (1982), The permeability of a melting snow cover, Water Resources Research, 18(4), 904-908.

Dunne, T., A. Price, and S. Colbeck (1976), Generation of Runof from Subarctic Snowpacks, Water Resources Research, 12(4), 677-685, doi: 10.1029/WR012i004p00677.

Eiriksson, D., M. Whitson, C. H. Luce, H. P. Marshall, J. Bradford, S. G. Benner, T. Black, H. Hetrick, and J. P. McNamara (2013), An evaluation of the hydrologic relevance of lateral flow in snow at hillslope and catchment scales, Hydrological Processes, 27(5), 640-654, doi: 10.1002/hyp.9666.

Fang, S., L. Xu, Y. Zhu, Y. Liu, Z. Liu, H. Pei, J. Yan, and H. Zhang (2013), An integrated information system for snowmelt flood early-warning based on internet of things, Information Systems Frontiers, 17(2), 321-335, doi: 10.1007/s10796-013-9466-1.

Fassnacht, S.R., and J.E. Derry (2010), Defining similar regions of snow in the Colorado River Basin using self-organizing maps, Water Resour. Res., 46, W04507, doi:10.1029/2009WR007835.

Fassnacht, S. R., and M. Hultstrand (2015), Snowpack variability and trends at long-term stations in northern Colorado, USA, International Association of Hydrological Sciences, 92, 1-6, doi: 10.5194/piahs-92-1-2015.

Fassnacht, S. R., and R. M. Records (2015), Large snowmelt versus rainfall events in the mountains, Journal of Geophysical Research: Atmospheres, 120(6), 2375-2381, doi: 10.1002/2014jd022753.

Flint, A. L., L. E. Flint, and M. D. Dettinger (2008), Modeling Soil Moisture Processes and Recharge under a Melting Snowpack, Vadose Zone Journal, 7(1), 350, doi: 10.2136/vzj2006.0135.

Fox, A. M., and M. W. Williams (1999), Equivalent permeability of a continental, alpine snowpack, in *Western Snow Conference*, edited, pp. 114-124, Tahoe, California USA.

Frankenberger, J., E. Brooks, M. Walter, M. Walter, and T. Steenhuis (1999), A GIS-based variable source area hydrology model, Hydrological Processes, 13(6), 805-822, doi: 10.1002/(SICI)1099-1085(19990430)13:6<805::AID-HYP754>3.0.CO;2-M.

Graybeal, D., and D. Leathers (2006), Snowmelt-related flood risk in Appalachia: First estimates from a historical snow climatology, Journal of Applied Meteorology and Climatology, 45(1), 178-193, doi: 10.1175/JAM2330.1.

Harpold, A., P. Brooks, S. Rajagopal, I. Heidbuchel, A. Jardine, and C. Stielstra (2012), Changes in snowpack accumulation and ablation in the intermountain west, Water Resources Research, 48(11), n/a-n/a, doi: 10.1029/2012wr011949.

Harpold, A. A., J. A. Biederman, K. Condon, M. Merino, Y. Korgaonkar, T. Nan, L. L. Sloat, M. Ross, and P. D. Brooks (2014), Changes in snow accumulation and ablation following the Las Conchas Forest Fire, New Mexico, USA, Ecohydrology, 7(2), 440-452, doi: 10.1002/eco.1363.

Harpold, A. A., N. P. Molotch, K. N. Musselman, R. C. Bales, P. B. Kirchner, M. Litvak, and P. D. Brooks (2015), Soil moisture response to snowmelt timing in mixed-conifer subalpine forests, Hydrological Processes, 29(12), 2782-2798, doi: 10.1002/hyp.10400.

Harrington, R. F., R. C. Bales, and P. Wagnon (1996), Variability of meltwater and solute fluxes from homogeneous melting snow at the laboratory scale, Hydrological Processes, 10(7), 945-953, doi: 10.1002/(sici)1099-1085(199607)10:7<945::aid-hyp349>3.0.co;2-s.

Harrington, R., and R. C. Bales (1998), Interannual, seasonal, and spatial patterns of meltwater and solute fluxes in a seasonal snowpack, Water Resources Research, 34(4), 823-831, doi: 10.1029/97wr03469.

Heilig, A., C. Mitterer, L. Schmid, N. Wever, J. Schweizer, H. P. Marshall, and O. Eisen (2015), Seasonal and diurnal cycles of liquid water in snow-Measurements and modeling, Journal of Geophysical Research: Earth Surface, 120, doi: 10.1002/2015JF003593.

Hock, R. (1999), A distributed temperature-index ice- and snowmelt model including potential direct solar radiation, Journal of Glaciology, 45(149), 101-111.

Hunsaker, C. T., T. W. Whitaker, and R. C. Bales (2012), Snowmelt Runoff and Water Yield Along Elevation and Temperature Gradients in California's Southern Sierra Nevada1, JAWRA Journal of the American Water Resources Association, 48(4), 667-678, doi: 10.1111/j.1752-1688.2012.00641.x.

Huwald, H., C. Higgins, M. Boldi, E. Bou-Zeid, M. Lehning, and M. Parlange (2009), Albedo effect on radiative errors in air temperature measurements, Water Resources Research, 45, doi: 10.1029/2008WR007600.

Jencso, K. G., and B. L. McGlynn (2011), Hierarchical controls on runoff generation: Topographically driven hydrologic connectivity, geology, and vegetation, Water Resources Research, 47(11), n/a-n/a, doi: 10.1029/2011wr010666.

Jennings, K., and J. Jones (2015), Precipitation-snowmelt timing and snowmelt augmentation of large peak flow events, western Cascades, Oregon, Water Resources Research, 51(9), 7649-7661, doi: 10.1002/2014WR016877.

Johnson, J. B., and G. L. Schaefer (2002), The influence of thermal, hydrologic, and snow deformation mechanisms on snow water equivalent pressure sensor accuracy, Hydrological Processes, 16(18), 3529-3542, doi: 10.1002/hyp.1236.

Johnson, J., and D. Marks (2004), The detection and correction of snow water equivalent pressure sensor errors, Hydrological Processes, 18(18), 3513-3525, doi: 10.1002/hyp.5795.

Jordan, P. (1983), Meltwater Movement in a Deep Snowpack. 1. Field Observations, Water Resources Research, 19(4), 971-978, doi: 10.1029/WR019i004p00971.

Jost, G., R. Moore, R. Smith, and D. Gluns (2012), Distributed temperature-index snowmelt modelling for forested catchments, Journal of Hydrology, 420, 87-101, doi: 10.1016/j.jhydrol.2011.11.045.

Kampf, S., J. Markus, J. Heath, and C. Moore (2015), Snowmelt runoff and soil moisture dynamics on steep subalpine hillslopes, Hydrological Processes, 29(5), 712-723, doi: 10.1002/hyp.10179.

Katsushima, T., S. Yamaguchi, T. Kumakura, and A. Sato (2013), Experimental analysis of preferential flow in dry snowpack, Cold Regions Science and Technology, 85, 206-216, doi: 10.1016/j.coldregions.2012.09.012.

Kattelmann, R., and J. Dozier (1999), Observations of snowpack ripening in the Sierra Nevada, California, USA, Journal of Glaciology, 45(151), 409-416.

Laudon, H., J. Seibert, S. Kohler, and K. Bishop (2004), Hydrological flow paths during snowmelt: Congruence between hydrometric measurements and oxygen 18 in meltwater, soil water, and runoff, Water Resources Research, 40(3), doi: 10.1029/2003WR002455.

Lundquist, J., and D. Cayan (2002), Seasonal and spatial patterns in diurnal cycles in streamflow in the western United States, Journal of Hydrometeorology, 3(5), 591-603, doi: 10.1175/1525-7541(2002)003<0591:SASPID>2.0.CO;2.

Lundquist, J., and M. Dettinger (2005), How snowpack heterogeneity affects diurnal streamflow timing, Water Resources Research, 41(5), doi: 10.1029/2004WR003649.

Lundquist, J., M. Dettinger, and D. Cayan (2005), Snow-fed streamflow timing at different basin scales: Case study of the Tuolumne River above Hetch Hetchy, Yosemite, California, Water Resources Research, 41(7), doi: 10.1029/2004WR003933.

Marsh, P., and M.-K. Woo (1985), Meltwater movement in natural heterogeneous snow covers, Water Resources Research, 21(11), 1710-1716.

McGurk, B. J., and P. Marsh (1995), Flow-finger continuity in serial thick-sections in melting Sierran snowpack, paper presented at Biogeochemistry of Seasonally Snow-Covered Catchments, IAHS, Boulder, CO.

McNamara, J. P., D. Chandler, M. Seyfried, and S. Achet (2005), Soil moisture states, lateral flow, and streamflow generation in a semi-arid, snowmelt-driven catchment, Hydrological Processes, 19(20), 4023-4038, doi: 10.1002/hyp.5869.

Molotch, N. P., and L. Meromy (2014), Physiographic and climatic controls on snow cover persistence in the Sierra Nevada Mountains, Hydrological Processes, 28(16), 4573-4586, doi: 10.1002/hyp.10254.

Mutzner, R., S. Weijs, P. Tarolli, M. Calaf, H. Oldroyd, and M. Parlange (2015), Controls on the diurnal streamflow cycles in two subbasins of an alpine headwater catchment, Water Resources Research, 51(5), 3403-3418, doi: 10.1002/2014WR016581.

Palmer, P. L. (2015), Estimating snow course water equivalent from SNOTEL pillow telemetry: an analysis of accuracy, paper presented at Western Snow Conference, Phoenix, Arizona.

Penton, V., and A. Robertson (1967), Experience with Pressure Pillow as a Snow Measuring Device, Water Resources Research, 3(2), 405-&, doi: 10.1029/WR003i002p00405.

Perica, S., D. Martin, S. Pavlovic, I. Roy, M. St. Laurent, C. Trypaluk, D. Unruh, M. Yekta, and G. Bonnin (2013), Precipitation-Frequency Atlas of the United States, NOAA Atlas 14, vol. 8, edited by N. O. a. A. A. U.S. Department of Commerce, National Weather Service, Silver Spring, MD.

Rice, R., and R. C. Bales (2010), Embedded-sensor network design for snow cover measurements around snow pillow and snow course sites in the Sierra Nevada of California, Water Resources Research, 46(3), n/a-n/a, doi: 10.1029/2008wr007318.

Ross, B. (1990), The Diversion Capacity of Capillary Barriers, Water Resources Research, 26(10), 2625-2629, doi: 10.1029/WR026i010p02625.

Sexstone, G. A., and S. R. Fassnacht (2014), What drives basin scale spatial variability of snowpack properties in northern Colorado?, The Cryosphere, 8(2), 329-344, doi: 10.5194/tc-8-329-2014.

Schneebeli, M. (1995), Development and stability of preferential flow paths in a layered snowpack, paper presented at Biogeochemistry of Seasonally Snow-Covered Catchments, IAHS, Boulder, CO.

Seyfried, M., and L. Grant (2007), Temperature effects on soil dielectric properties measured at 50 MHz, Vadose Zone Journal, 6(4), 759-765, doi: 10.2136/vzj2006.0188.

Singh, P. K., M. K. Jain, S. K. Mishra (2013), Fitting a simplified two-parameter gamma distribution function for synthetic sediment graph derivation from ungauged catchments, *Arab J. Geosci*, 6, 1835-1841, doi: 10.1007/s12517-011-0473-6.

Smith, T. J., J. P. McNamara, A. N. Flores, M. M. Gribb, P. S. Aishlin, and S. G. Benner (2011), Small soil storage capacity limits benefit of winter snowpack to upland vegetation, Hydrological Processes, 25(25), 3858-3865, doi: 10.1002/hyp.8340.

Techel, F., and C. Pielmeier (2011), Point observations of liquid water content in wet snow - investigating methodical, spatial and temporal aspects, The Cryosphere, 5(2), 405-418, doi: 10.5194/tc-5-405-2011.

Tobin, C., B. Schaefli, L. Nicotina, S. Simoni, G. Barrenetxea, R. Smith, M. Parlange, and A. Rinaldo (2013), Improving the degree-day method for sub-daily melt simulations with physically-based diurnal variations, Advances in Water Resources, 55, 149-164, doi: 10.1016/j.advwatres.2012.08.008.

U.S. Army Corps of Engineers (1956), Summary Report of the Snow Investigations: Snow Hydrology*Rep.*, 437 pp, U.S. Army Corps of Engineers - North Pacific Division, Portlan, Oregon.

U.S. Department of Agriculture (1986), Technical Release 55: Urban hydrology for small watersheds*Rep.*, United States Department of Agriculture, Natural Resource Conservation Service, Conservation Engineering Division, Washington, D.C.

Van Genuchten, M. T. (1980), A closed-form equation for predicting the hydraulic conductivity of unsaturated soils, Soil Science Society of America Journal, 44, 892-898.

Weber, A.N., 2016. Spatial patterns of snowmelt across the Southern Rocky Mountains. Unpublished B.S. thesis, watershed science, Colorado State Univerisity.

Wever, N., C. Fierz, C. Mitterer, H. Hirashima, and M. Lehning (2014), Solving Richards Equation for snow improves snowpack meltwater runoff estimations in detailed multi-layer snowpack model, The Cryosphere, 8(1), 257-274, doi: 10.5194/tc-8-257-2014.

Williams, C. J., J. P. McNamara, and D. G. Chandler (2009), Controls on the temporal and spatial variability of soil moisture in a mountainous landscape: the signature of snow and complex terrain, Hydrology and Earth System Sciences, 13, 1325-1336.

Williams, M. W., T. A. Erickson, and J. L. Petrzelka (2010), Visualizing meltwater flow through snow at the centimetre-to-metre scale using a snow guillotine, Hydrological Processes, n/a-n/a, doi: 10.1002/hyp.7630.

Yochum, S. E. (2012), High Park Fire: Increased Flood Potential Analysis*Rep.*, United States Department of Agriculture Natural Resources Conservation Service, Colorado State Office, Denver, CO.

Zhao, Q., Z. Liu, B. Ye, Y. Qin, Z. Wei, and S. Fang (2009), A snowmelt runoff forecasting model coupling WRF and DHSVM, Hydrology and Earth System Sciences, 13(10), 1897-1906.

CHAPTER 3: SIMULATING WATER FLOW THROUGH A LAYERED SNOWPACK[1]

Introduction

Snow is a major component of the hydrologic cycle in many geographic regions around the world and is important to both human communities and natural ecosystems. In areas such as the western United States and Canada, snow can contribute more than 80% of streamflow to downstream water users [*Daly et al., 2000; Gray and Landine, 1988; Rice et al., 2011; Seyfried et al., 2009*]. In addition to direct consumptive water use from streamflow, snowmelt is important for groundwater recharge [*Flint et al., 2008; Clilverd et al., 2011; Cao et al., 2013*], soil moisture dynamics [*McNamara et al., 2005; Jencso and McGlynn, 2011; Harpold et al., 2015; Webb et al., 2015*], forest ecosystem dynamics [*Williams et al., 2009a; Smith et al., 2011; Harpold et al., 2014*], and can cause high-damage flooding [*Graybeal and Leathers, 2006; Zhao et al., 2009; Fang et al., 2013*]. With variable changes to snowpack accumulation and melt rates projected in the future [*Caine, 1992; Bales et al., 2006; Adam et al., 2009; Clow, 2010; Harpold et al., 2012; Fassnacht and Hultstrand, 2015; Fassnacht et al., 2016*] it is important to properly understand and represent processes that occur during melt.

Snow processes vary as a result of many environmental controls at multiple scales of interest [*Clark et al., 2011*]. From a basin scale perspective, elevation has been shown to influence the depth and persistence of a snowpack [*Elder et al.*, *1991; Blöschl and Kirnbauer, 1992; Richer et al., 2013; Molotch and Meromy, 2014; Sexstone and Fassnacht, 2014*], while at finer resolutions the spatial variability of both accumulation and melt may be controlled by aspect [*Williams et al.*, *2009a; López-Moreno et al., 2013; Hinckley et al., 2014*], and snow in forested areas will be affected by interception during accumulation, shortwave radiation shading, and longwave radiation from vegetative influences prior to and during melt [*Storck et*

[1]Parts of this chapter appear in Webb, R.W., and S.W. Webb (2015), Simulated water flow through a layered snowpack, in TOUGH Symposium 2015, edited, Berkeley, CA.

al., *2002; Musselman et al., 2008; Molotch et al., 2009; Adams et al., 2011*]. Furthermore, redistribution and increased sublimation losses of snow due to wind effects can occur across a landscape and has been shown to cause a large portion of variability in many environments [*Luce et al.*, *1998; Anderton et al., 2004; Liston and Elder, 2006; Lehning et al., 2008*]. With such variable and dynamic controls on the accumulation and melt rates across a landscape that lead to a range of melt inputs across the soil surface [*Harms and Chanasyk*, *1998; Kormos et al., 2014; Webb et al., 2015*], it is essential to understand the movement of water as a function of snowpack properties.

Snowpacks are layered, dynamic porous media that result variably saturated flow during melt experiencing flow mechanisms such as capillary barriers, permeability barriers, and flow fingers. However, the understanding of water flow through a snowpack has been limited, in part, due to the destructive nature of observations constraining results to discrete temporal resolution rather than continuous datasets [*Williams et al, 2010, Kattelmann & Dozier, 1999*] and the rapidly changing intrinsic properties over time [*Colbeck, 1987; Marsh, 1987; Colbeck, 1991*].

A snowpack forms a complex three-dimensional matrix of ice, air, water vapor, impurities such as dust or other constituents, and liquid water (during melt or rain events) that will vary with time. Snow crystal metamorphism has been studied for decades [*Yosida*, *1955*] with the primary driving mechanism known to be a vapor gradient resulting from vapor pressure gradients driven by either temperature gradients between layers or vapor gradients driven by concave and convex shape of grain structure inducing sublimation, diffusion, and re-sublimation of water vapor [*Colbeck and Anderson*, *1982; Staron et al., 2014*]. When temperature and vapor pressure gradients are low, compression and friction can also drive metamorphism while in the spring liquid water increases the rate of metamorphism [*Marsh*, *1987*]. Snow grain metamorphism is an ongoing process different for each new layer [*Colbeck*, *1987; Colbeck, 1991*] and because it is a function of time, temperature, and water vapor gradients, all of which

vary among layers of a snowpack, each layer will develop its own characteristics as a porous medium.

The formation of each layer within a snowpack occurs throughout the winter season. Each snow storm produces a new layer that immediately begins metamorphism dependent upon the subsequent atmospheric and lower boundary conditions unique to each layer [*Colbeck, 1991*]. As winter transitions to spring and the snowpack warms and melts, each layer will have a range of grain sizes and densities that can be used to estimate hydraulic properties. *Yamaguchi et al.* [*2010*] determined, through laboratory experiments, parameters to represent the moisture retention parameters at a given suction/tension for use with the *van Genuchten* [*1980*] equation:

$$\theta = \theta_r + (\theta_s - \theta_r)[1 + (\propto |h|)^n]^{-m} \quad \text{(Eq. 3.1)}$$

where θ is the volumetric water content (m^3m^{-3}), θ_r is the residual water content (m^3m^{-3}), θ_s is the saturated water content (m^3m^{-3}), α is a fit coefficient that is related to the pore size of the medium and approximately the inverse of the air entry pressure for soils, h is the suction (m), n and m are additional curve fitting parameters where m is commonly taken to be 1-(1/n). *Yamaguchi et al.* [*2010*] estimated that for snow:

$$\alpha = 7.3(2r) + 1.9 \quad \text{(Eq. 3.2)}$$

where r is the mean radius of the snow grains (mm). *Hirashima et al*. [*2010*] expanded on this work to improve an equation for n to be:

$$n = 15.68e^{(-0.46(2r))} + 1 \quad \text{(Eq. 3.3).}$$

This improvement increased the range of the grain size to an upper limit of 5 mm. The value for θ_r is commonly estimated near 0.02 and θ_s is estimated from a volumetric calculation of pore space using density measurements assuming an ice density of 917 kg/m3 for snow grains. For estimations of hydraulic conductivity for snow, *Calonne et al*. [*2012*] used microscale 3D imaging to compute the intrinsic permeability (*K*) to be:

$$K = (3.0 \pm 0.3) {r_{es}}^2 \exp\big((-0.0130 \pm 0.0003)\rho_s\big) \quad \text{(Eq. 3.4)}$$

where r_{es} is the equivalent sphere radius (mm) estimated from grain specific surface area and ρ_s is the density of the snow (kg m^{-3}). Intrinsic permeability is then converted to hydraulic conductivity using the viscosity and density of water at the temperature of interest, often 0° C for snowmelt studies.

Recently, the above equations have been successfully applied to a layered snowpack by *Wever et al*. [*2014*] using Richard's equation [*Richards*, *1931*] in a mixed form that could be discretized in a finite difference approximation to ensure mass balance based on *Celia et al.* [*1990*]:

$$\frac{\partial \theta}{\partial t} - \frac{\partial}{\partial z}\left(K(\theta)\left(\frac{\partial h}{\partial z} + \cos\gamma\right)\right) + s = 0 \quad \text{(Eq. 3.5)}$$

where z is the vertical coordinate (m), γ is the slope angle, and s is a source/sink term ($m^3\ m^{-3}\ s^{-1}$).. This study resulted in improved estimations of snowmelt runoff in a one-dimensional (vertical) setting. Other studies have qualitatively shown retention of percolating meltwater above layer interfaces as well as the transmission of meltwater downslope through the use of dye tracers as a means to visualize flow paths [*Williams et al., 2010; Walter et al., 2013; Eirikkson et al., 2013*].

Water flow through layered porous media such as soils and the physics of hydraulic barriers have long been studied and successfully modeled [*Oldenburg & Pruess, 1993; Stormont, 1995; Webb, 1997; Ho & Webb, 1998*]. For isolated capillary barriers on a sloped interface, a diversion length approximation has been derived to estimate the distance water will flow downslope prior to breaking through the barrier. The diversion length (L) can be estimated (in meters) through the following equation [*Ross* ,*1990*]; *Webb*, *1997*]:

$$L = \frac{K_s \tan\gamma \int K_r d\psi}{q} \quad \text{(Eq. 3.6)}$$

where K_s is the saturated hydraulic conductivity (m/s), K_r is the relative permeability, ψ is the moisture potential (m), and q is the infiltration rate. The boundary conditions of the integration are the moisture potential of the top layer far away from the barrier interface and the moisture potential of the bottom layer at the interface after breakthrough occurs. It is important to note that this approximation assumes an isolated capillary barrier without any influence from other porous media or water table near the interface.

Flow paths in a snowpack that cause lateral flow will occur in the form of capillary and/or permeability barriers at interfaces between layers. Permeability barriers form in the case that the upper layer has a permeability greater than the lower layer such that if water is infiltrating at a higher rate than the infiltration capacity of the lower layer then lateral flow will occur as is seen in these results. Capillary barriers form when capillary forces are large enough in the top layer relative to the bottom to hold water within the pore space and allow flow diversion downslope. The primary difference between permeability barriers and capillary barriers is that permeability barriers allow partial flux of percolating water across the interface whereas capillary barriers will divert all of the flow for a specific diversion length. These barriers will promote flow downslope through snow that often has hydraulic conductivities orders of magnitude greater than those of typical soils [*Calonne et al.*, *2012; Domine et al., 2013*] suggesting meltwater likely flows downhill at a greater rate within a snowpack than it would through soil. Therefore, the lateral connectivity and formation of hydraulic barriers within a snowpack is of key importance to the distribution of snowmelt water across a landscape [*Colbeck*, *1979; Marsh and Woo, 1985; Williams et al., 1999a; 2009; Williams et al., 2009a*] and a key component of the hydrologic cycle in a headwater basin with a snowmelt dominated hydrograph.

This paper investigates the potential diversion lengths of hydraulic barriers within layered snowpacks for a range of observed densities and grain sizes through the following objectives: 1) simulating two-dimensional water flow through snow layers in complex terrain and estimate diversion lengths across layer interfaces as a result of capillary and/or permeability barriers and

2) utilize the above equations to approximate potential diversion lengths of isolated capillary barriers for varying densities and grain sizes of snow layers.

Methods

Snowpack stratigraphy data for this study were collected from the National Aeronautics and Space Administration (NASA) Cold Land Process Experiment (CLPX) dataset [*Elder et al., 2003; Cline et al., 2002*]. Data used in this study are from the Spring Creek intensive study area collected on March 30, 2003, part of the Rabbit Ears mesoscale study area in northern Colorado (Fig. 3.1) (for more information on NASA CLPX data collection see *Elder et al., 2009*). Three snow pits were chosen for simulations from the NASA CLPX dataset based on slope and aspect (Fig. 3.1). Aspects chosen for simulations were flat, south, and north. The flat aspect has a slope of 5° whereas both the south and north snow pits were on slopes of approximately 20 °. Slopes and aspects were determined from airborne Light Detection and Ranging data collected for the intensive study area [*Miller, 2004*]. Grain sizes of all three pits ranged in mean diameter from 0.2 mm to 1.5 mm and density ranged from 48.5 kg/m^3 for a layer of fresh snow to 461.0 kg/m^3 for older snow (Fig. 3.2). Hydraulic properties of snowpack layers were estimated from equations (3.2) through (3.4) based on mean grain size and snow density to estimate saturated hydraulic conductivity and *van Genuchten* [*1980*] unsaturated properties (Fig. 3.3).

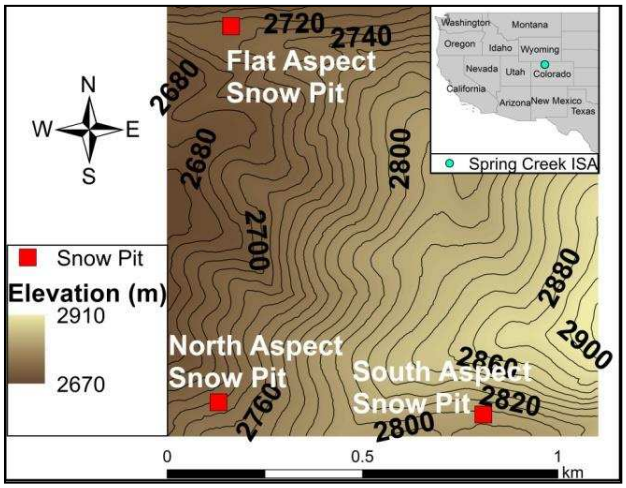

Figure 3.1: Map of Spring Creek Intensive Study Area showing snow pit locations for data used in this study and 10 meter contours.

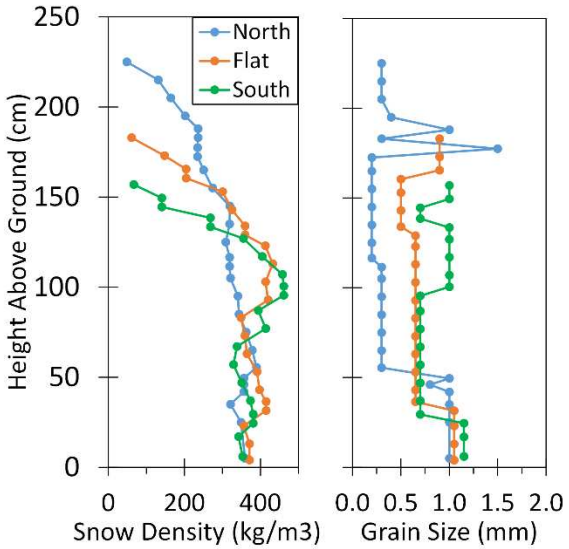

Figure 3.2: Stratigraphy data displaying grain size and layer density of the three snow pits (north aspect, flat aspect, and south aspect) chosen for TOUGH2 EOS9 simulations.

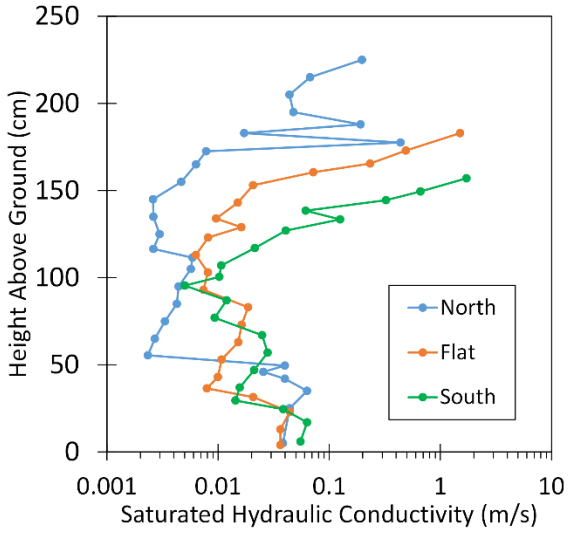

Figure 3.3: Estimated values of saturated hydraulic conductivity based on *Yamaguchi et al*. [*2010*].

The numerical code TOUGH2 was utilized for simulating water in the unsaturated conditions of this study [*Pruess, 1999*]. TOUGH2 has been used in previous studies concerning effects of capillary barriers [*Webb, 1997, Ho & Webb, 1998*] and is capable of simulating multiphase transport of air, water, and heat in porous media. The transport of liquid water was investigated using the TOUGH2 equation of state module EOS9 that uses Richards' equation [*Richards, 1931*] that has been successfully applied to simulate water flowing through snow in a one-dimensional setting [*Wever et al., 2014*]. The unsaturated hydraulic properties at element connections was chosen as upstream weighting, or using the properties of the element that water is flowing out of, as has been shown to accurately describe the behavior of capillary barriers [*Webb, 1997*].

A rectilinear grid was used to constrain the simulations to 25 m long hill slopes at 0.5 m horizontal resolution with a seepage face at the downslope end. Minimum vertical element separation at interfaces was 5×10^{-4} m with a growth rate factor of 1.4 away from all layer interfaces. Snowpack profiles had total depths of 1.9 m for the flat aspect, 1.6 m for the south, and 2.3 m for the north. The north aspect slope had the most layers at 27, resulting largely from

the resolution of the data collection [*Elder et al., 2009*]. Each modeled snow pit was used to simulated steady state melt rates of 0.1, 1.0, and 5.0 mm/hr generated in the uppermost row in the grid of the model. These melt rates are within the range of normal melt rates expected in Colorado as determined in chapter 2 and lysimeter data from an alpine site [*Williams et al., 1999b*]. The rate of 5 mm/hr is representative of the peak FDM for a day with total snowmelt of approximately 28 mm. In cases of total diversion of meltwater across the entire 25 m domain, melt was restarted below the barrier causing the total diversion.

Diversion length potential for isolated capillary barriers as a result of snow layer density and grain size were estimated using equation (3.6). For purposes of isolating the effects of grain size and density, a slope of 20 degrees was assumed for calculations and an infiltration rate equal to 1.0 mm/hr for reasonable representation of an expected melt rate in Colorado [*Williams et al., 1999b*]. Snow layers above and below an isolated capillary barrier were adjusted with densities ranging from 200 kg/m^3 to 400 kg/m^3 and grain sizes ranging from 0.2 mm to 2.0 mm.

Additional calculations were conducted to isolate the effect of slope and make direct comparisons with TOUGH2 simulation results. For this comparison an identified capillary barrier from the simulations is used to quantify top and bottom layer parameters. For these additional calculations the slope angle is varied between five degrees and 50 degrees for all three percolation rates simulated (0.1, 1.0, and 5.0 mm/hr). The diversion lengths at the 20 degree slope are used to compare the isolated capillary barrier estimates using equation (3.6) and the results of the TOUGH2 simulations of a capillary barrier occurring within a layered snowpack.

Results

Results from TOUGH2 simulations display distinct hydraulic barriers forming in all three snowpack profiles (Fig. 3.4). Multiple lateral diversions of vertically infiltrating water by capillary and permeability barriers can be seen in each simulation, displaying how a “stair step” flow path develops as water flows through the snow, similar to that suggested by *Colbeck* [*1975*]

concerning ice lenses (Fig. 3.4). Simulations resulted in permeability barriers in the flat and south aspect slopes with capillary barriers on the north aspect slope.

The flat aspect stratigraphy resulted in two distinct permeability barriers at heights of 130 cm and 35 cm above the soil-snow-interface (58 and 153 cm below the snow surface, respectively) diverting water at all three infiltration rates (Fig. 3.4a). No capillary barriers were observed in simulation results for the flat aspect stratigraphy. The interface 130 cm above the SSI resulted from two layers with similar density, 360 kg/m^3, and the lower layer having a grain diameter 0.2 mm larger than the top (0.5 mm above 0.7 mm). The interface 35 cm above the SSI also resulted from two layers of similar density, 415 kg/m^3, and a grain size 0.4 mm larger in the layer below the interface (0.7 mm above 1.1 mm). The maximum diversion length for each of these barriers occurred at a melt rate of 0.1 mm/hr and lengths of 3.0 m at 130 cm above the SSI and 6.5 m at 35 cm above the SSI (Table 3.1). Diversion lengths for permeability barriers were considered to be the distance from the lateral boundary that infiltration rate above the interface is equal to the flux across the interface, though a larger flux continues laterally as simulation results show (Fig. 3.4).

The south aspect stratigraphy also resulted in two distinct permeability barrier effects at heights of 135 cm and 27 cm above the SSI (27 cm and 135 cm below the snow surface, respectively) (Fig. 3.4b). No capillary barrier effects were observed in the south aspect stratigraphy simulations. Both permeability barriers diverted water percolating at all three melt rates. The interface at 135 cm above the SSI resulted from two layers with similar density, 269 kg/m^3, and the lower layer having a grain diameter 0.3 mm larger (0.7 mm above 1.0 mm). The interface 27 cm above the SSI resulted from two layers of similar density, 381 kg/m^3, and a grain size 0.5 mm larger in the layer below the interface (0.7 mm above 1.2 mm). The maximum diversion length for each of these barriers occurred at a melt rate of 0.1 mm/hr and lengths of 5.5 m at 135 cm above the SSI and 9.0 m at 27 cm above the SSI (Table 3.1).

The north aspect stratigraphy displayed a more stratified snowpack with five identified capillary barriers (Fig. 4c). Full diversion lengths of 25 m were simulated between layers at two interfaces, 220 cm and 190 cm above the SSI (10 cm and 40 cm below the snow surface) (Table 1). Therefore, melt was restarted again at 205 cm and 170 cm above the SSI (25 cm and 60 cm below the snow surface). The other capillary barriers that were simulated occurred at 200 cm, 113 cm, and 51 cm above the SSI (30 cm, 117 cm, and 179 cm below the snow surface, respectively). From the topmost capillary barrier downward the difference in grain sizes were: 0.0 cm, 0.1 cm (0.3 mm above 0.4 mm), 0.6 cm (0.4 mm above 1.0 mm), 0.1 cm (0.2 mm above 0.3 mm), and 0.7 mm (0.3 mm above 1.0 mm). The differences in densities are (respectively): 82 kg/m^3 (49 kg/m^3 above 131 kg/m^3), 38 kg/m^3 (164 kg/m^3 above 202 kg/m^3), 34 kg/m^3 (202 kg/m^3 above 236 kg/m^3), 0.0 kg/m^3 (319 kg/m^3), and 33 kg/m^3 (390 kg/m^3 above 357 kg/m^3). With the exception of the two barriers closest to the ground surface all layers below the barrier interfaces were of higher density.

The minimum difference in crystal grain diameter creating either type of hydraulic barrier was 0.1 mm occurring twice within the north aspect stratigraphy (crystal diameters of 0.3 mm above 0.4 mm and 0.2 mm above 0.3 mm at 200 cm and 113 cm above SSI, respectively) resulting in the lower diversion lengths simulated for capillary barriers (Table 3.1). Two capillary barriers had the longest diversion lengths and diverted meltwater beyond the domain for all three melt rates (Table 3.1), the first of these was the topmost capillary barrier on the north aspect slope and the only difference between layers was the density whereas the other barrier that completely diverted meltwater showed one of the largest differences in grain size and also a difference in density. All capillary and permeability barriers in this study resulted from larger grain diameters in the layer below the barrier interface and only one barrier resulted from a higher density in the layer above the interface.

Using equation (3.6) to estimate the potential diversion lengths for isolated capillary barriers in snow resulted in a range of diversion lengths from less than one meter to up to nearly

1300 m (Fig. 3.5). Calculations show that when the top layer of a capillary barrier in snow is less dense than the bottom layer, greater diversion lengths occur. As the density of the top layer changes, the magnitude of diversion lengths is greatly affected. A top layer density of 200 kg/m^{3}resulted in maximum diversion lengths near 1300 m (Fig. 3.5i), a density of 300 kg/m^3 only 350 m (Fig. 3.5ii), and 400 kg/m^3 resulted in diversion lengths less than 100 m (Fig. 3.5iii). Also, the top layer grain size is shown to be controlling whether or not a capillary barrier exists with a diameter necessary to produce a capillary barrier being 1.0 mm or less and many density combinations resulting in a threshold of 0.5 mm or less. The bottom layer grain size shows a less dramatic effect on diversion length, though maximum diversion occurred at grain sizes from 1.0 mm to 1.5 mm (Fig. 3.5).

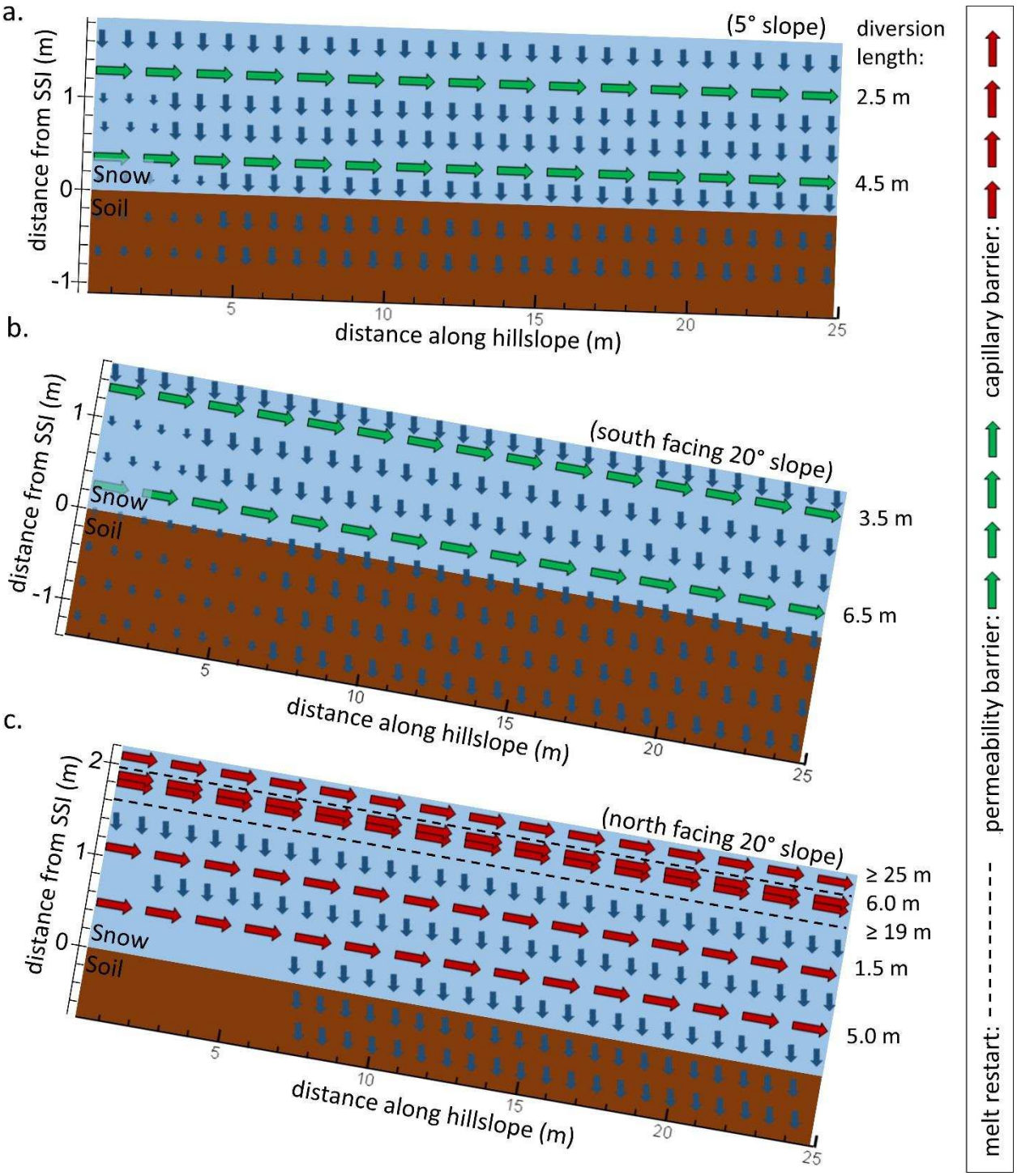

Figure 3.4: Simulation results from TOUGH2 EOS9 for a) flat aspect, b) south aspect, and c) north aspect stratigraphy. Results display flow path directions for melt rates of 1.0 mm/hr. (note: arrows are not vectors and sizes are not quantitatively representative of flux rates but rather qualitatively representative).

Table 3.1: Summary of permeability and capillary barriers for the flat (F), south (S), and north (N) aspect locations showing the diversion lengths simulated for 0.1 mm/hr melt, 1.0 mm/hr melt, and 5.0 mm/hr melt. Barriers are identified by aspect and height above the soil-snow-interface (SSI).

Aspect	Height Above SSI (cm)	Diversion Length at 0.1 mm/hr melt (m)	Diversion Length at 1.0 mm/hr melt (m)	Diversion Length at 5.0 mm/hr melt (m)
F	130	3.5	2.5	2.5
	35	6.5	4.5	4.0
S	135	5.5	3.5	3.5
	27	9.5	6.5	6.5
N	220	≥ 25	≥ 25	≥ 25
	190	16.5	6.0	1.0
	180	≥ 8.5	≥ 19	≥ 24
	113	4.5	1.5	0.0
	51	≥ 25	5.0	1.0

The diversion length will also increase as slope increases according to equation (3.6). To show how sensitive the diversion length is to slope, the capillary barrier occurring at 113 cm above the SSI on the north aspect slope is used as an example for further calculations. Estimates of diversion length at varying slope angles were made using the *Ross* [*1990*] and *Webb* [*1997*] approximation for an isolated capillary barrier without any influence from other porous media or water table near the interface. The effect of slope is non-linear with a clear difference between the approximated diversion length of an isolated capillary barrier and a capillary barrier within a complex layered snowpack (Fig.3.6). In the selected capillary barrier, the 0.1 mm/hr melt rate produced a larger diversion length than what is predicted for an isolated barrier whereas the other two simulated melt rates resulted in lesser diversion lengths relative to an isolated barrier (Fig. 3.6). These comparisons show how different diversion lengths can be in layered porous media relative to isolated capillary barriers. Equation (3.6), therefore, may not result in accurate approximations of diversion lengths for snow layers but rather offer insight to which interfaces will produce larger capillary diversion lengths relative to other layer interfaces.

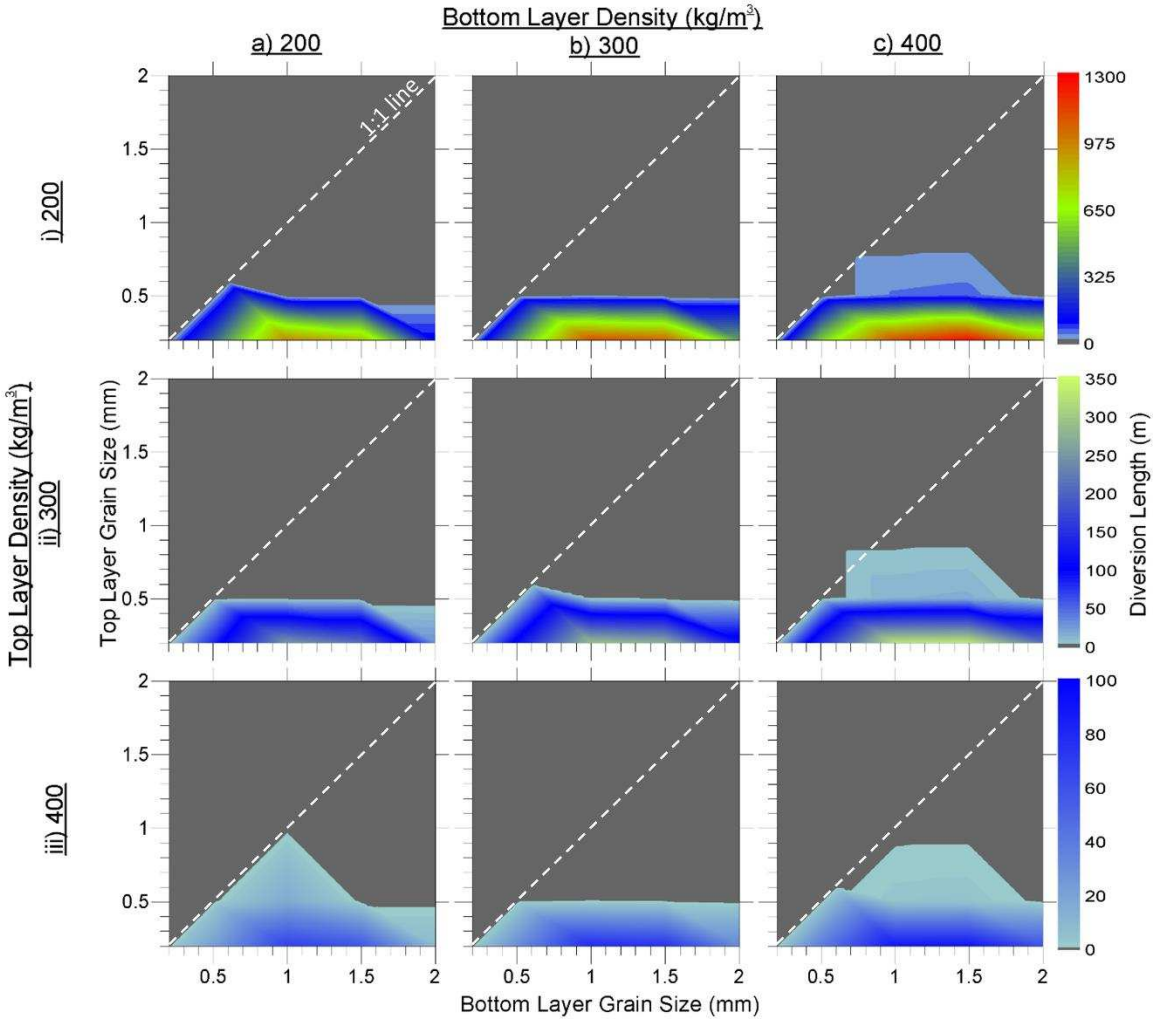

Figure 3.5: Diversion lengths for isolated capillary barriers using equation (3.6) for a constant slope of 20° and a percolation rate of 1.0 mm/hr. Bottom layer densities shown are a) 200 kg/m^3, b) 300 kg/m^3, and c) 400 kg/m^3 and top layers are i) 200 kg/m^3, ii) 300 kg/m^3, and iii) 400 kg/m^3 with grain sizes ranging from 0.2 mm to 2.0 mm for all density combinations. For each row of varying top layer density the color scale is magnified for the range of results for that row.

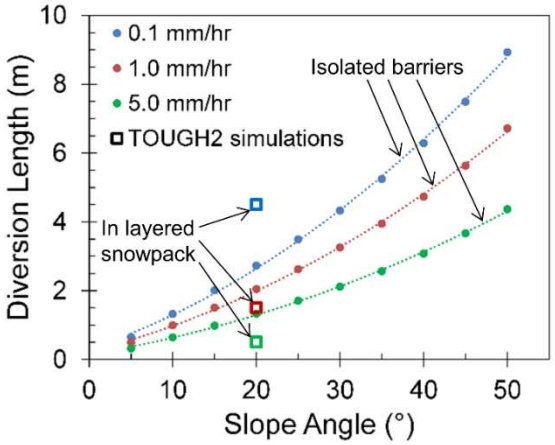

Figure 3.6: Effect of slope on diversion lengths using the equation (3.6) for isolated capillary barriers compared to the TOUGH2 simulations of a capillary barrier 113 cm above the soil-snow-interface in the north aspect snow pit, each for the three simulated melt rates.

Discussion

Highly stratified snowpacks such as the north aspect location in this study add complexity to the modeling process, making it difficult to represent in a 25 m wide domain because of the complex unsaturated flow that results and the high computational expense. The simulations resulted in the diversion of vertically infiltrating melt water from permeability barriers on the south and flat aspects as well as from capillary barriers on the north aspect. The topmost capillary barrier observed in the north aspect stratigraphy may be an unrealistic result of calculating hydraulic properties from the equations developed by *Yamaguchi et al*. [*2010*] and *Hirashima et al*. [*2010*]. *Yamaguchi et al*. [*2010*] tested samples with all densities approximately 550 kg/m^3 whereas the topmost layer in the north aspect stratigraphy simulated in this study has a density of 49 kg/m^3. Some of the layer interfaces will also cause diversions less than the resolution of these simulations or smaller scale heterogeneity that will produce flow fingering of the infiltrating water as shown in field studies [*Williams et al., 2010, Eiriksson et al., 2013*]. However, it has been shown in previous studies that the homogenous layer approach is a reasonable approximation of the mean diversion length of heterogeneous realizations [*Ho and Webb, 1998*]. Ultimately, these simulations display the potential for diversion lengths at the

meter scale of percolating water flowing through a porous snowpack as a result of multiple permeability and/or capillary barriers within each snow profile tested.

Diversion lengths of the magnitude shown in this study are approaching the upper limits for the terrain from which the snow pit stratigraphy data were collected. In complex mountainous subalpine terrain such as the Spring Creek Intensive Study Area, it is unlikely that snowpack layers will remain continuous and homogenous for the entirety of the larger diversion lengths. The scale of the spatial variability in snowpack layers will be controlled by the scale of the topographic and land cover variability causing a range of temperature and radiation gradients [*Colbeck, 1991; Blöschl, 1999*]. In the case of subalpine mountainous terrain this variability can range from meters to tens of meters [*Musselman et al., 2008, Sextone & Fassnacht, 2014*] to the millimeter to meter scale [*Fassnacht et al., 2009*]. In complex terrain such as the Rocky Mountains of Colorado, slope can vary widely and can be steeper than those tested in this study resulting in larger diversion lengths than those observed in simulations of this study on a 20 degree slope (Fig. 3.6).

Density did not vary as often as grain size between layers in this study though this may be a result of the sampling method [*Elder et al., 2009*]. Density measurements were conducted using a 1 L wedge cutter representing vertical increments of 0.1 m resolution yielding averaged density measurements over this interval and not identifying individual layers. Further field data collection measure the density of individual layers to match the grain size measurements, and model testing should quantify the impact of the 0.1 m density measurements on the simulation results. It should also be noted that some of these simulated barriers occurred at locations that were observed to have melt-freeze crusts or ice layers present that were only accounted for in the model through density and grain size. Such layers occurred at the south aspect stratigraphy at 135 cm above the SSI and on the north aspect at 51 cm, 180 cm, and 190 cm above the SSI. The flat aspect simulations did not produce any barriers at depths of observed crusts or ice layers. These melt-freeze crusts are further evidence of capillary and/or permeability barriers

occurring at these interfaces and holding percolating meltwater as the snowpack cools in the evening and re-freezing occurs. As these barriers hold water crystal growth is accelerated in the presence of liquid water [*Colbeck, 1987, Marsh, 1987*] and therefore, the capillary barriers shown in this study to exist in a snowpack will be short lived and only applicable over a short temporal scale. Wet snow metamorphism has been shown at the day [*Kattelmann & Dozier, 1999*] and hour timescale in laboratory settings [*Walter et al., 2013*] and thus capillary barriers with smaller differences in grain size only will disappear from snow metamorphism. As water is diverted, the crystal growth will reduce the diversion length during the day that the melt is occurring.

The presence of permeability barriers rather than capillary barriers in the south and flat aspect snowpacks are evidence of the further progressed seasonal metamorphism observed in grain types being rounded throughout with new snow at the snow surface and mixed grains at the ground surface. The north aspect slope had a combination of grain types being rounded and mixed grains throughout the pack and facets turning to rounds at the ground surface [*Cline et al., 2004*]. This can be attributed to increased solar radiation on the flat and south aspect locations (Fig. 3.7). Earlier in the winter these layer interfaces were likely capillary barriers that metamorphosed into permeability barriers and/or melt-freeze layers while others do not. This will occur from the above described process of a capillary barrier that holds water and turns into a melt-freeze crust. More investigations are necessary towards what variables may control this process and determine which barriers become permeability barriers and which do not. However, these processes result in permeability barriers within a layered snowpack being more persistent in time and thus more important to water movement at the seasonal or monthly time scale where capillary barriers will be important at the daily or weekly time scale.

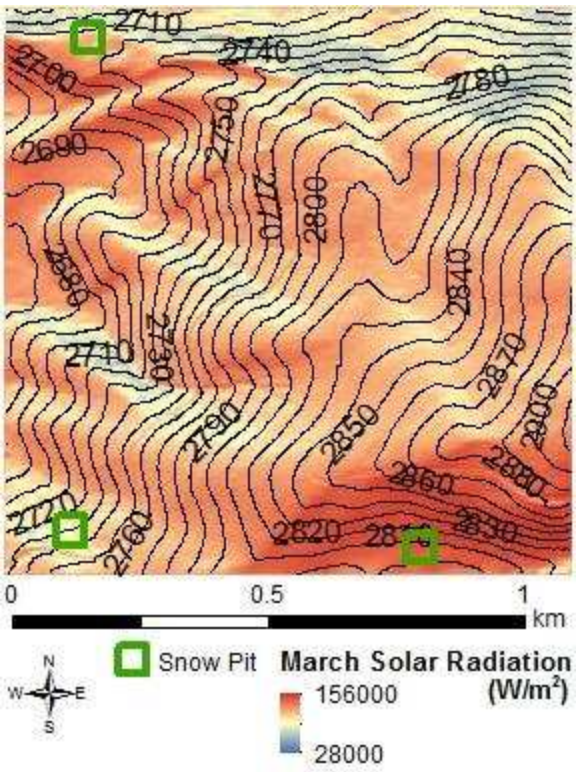

Figure 3.7: Calculated solar radiation accumulated during the month of March, 2003 for the Spring Creek Intensive Study Area with 10 m contours shown.

This study has implications to the distribution of water within a snowpack early in the melt season. During the transition from winter to spring as the snowpack ripens, meltwater will be diverted laterally as a result of capillary and/or permeability barriers, particularly as the snowpack is ripening and low melt rates are occurring. As shown in this study, diversion lengths are greatest during lower melt rates and small melt events during the ripening transition of a snowpack from winter to spring are important for re-distribution of water across a landscape. In complex subalpine mountainous environments such as the site for this study, meltwater may be diverted across multiple capillary and/or permeability barriers within the snowpack at lengths similar to those of the topographic and land cover variability. This will result in more water reaching the SSI at locations of topographic depressions or transition zones from open to under canopy conditions (for two examples) as has been shown in previous studies of the shallow

subsurface [*Williams et al., 2009, Webb et al., 2015*]. Additionally, this will cause variable release rates of water from the snowpack at the SSI.

The results of the potential diversion lengths of capillary barriers in snow layers show that less dense top layers will have greater diversion lengths relative to higher density layers (Fig. 3.5). Additionally, crystal diameters of the top layer need to be smaller than 1.0 mm to have the possibility to produce a capillary barrier and smaller than 0.5 mm above a larger grain size to definitely produce a capillary barrier (Fig. 3.5). More recently deposited snow layers will likely have smaller grain sizes and lesser densities as evidenced by the fresh snow layer in this study having grain diameters of 0.3 mm and a density of 49 kg/m^3 at the north aspect location. These lesser densities and smaller grain sizes occurring in the younger layers indicate the increased likelihood for capillary barriers to occur closer to the snow surface rather than near the SSI. In the north aspect snow profile, three of the five capillary barriers (60%) occurred in the top 0.4 m (less than 20% of total snow depth) (Table 3.1). This can be especially important for spring snowstorms that occur after spring melt has begun as this indicates the snowpack has become or is approaching isothermal conditions and grain sizes have been enlarging. New snow during this time will often be less dense and have small grain sizes. Even though the snow may fall relatively evenly across the landscape, meltwater from this storm layer as the temperatures warm again can be redistributed across the interface between the new snow layer and the old snow surface with slopes as low as five degrees. This can also be an important process for wet snowfall during this time that has liquid water content attached to fresh snow crystals that may move within the fresh layer depending on snow grain sizes, air temperature, and snowpack temperature during and after the event. This has the potential for meltwater from spring snowstorms to runoff directly into streams through the snowpack similar to rain-on-snow events [*Eiriksson et al., 2013*]. With the movement of water within the snowpack snow surveys that follow will have bias estimates of SWE if a single location is used for snow density where meltwater collected in or drained from the snowpack.

Hydrologic modeling of processes such as groundwater recharge and streamflow generation from a melting snowpack can be improved through a better representation of the snowpack as a porous media. As we have shown in this study, multiple hydraulic barriers occur within a layered snowpack in complex subalpine terrain, redistributing meltwater across a landscape prior to interactions with the SSI. Vadose zone hydrologic studies will benefit from conceptualizing the snowpack as an extension of the unsaturated zone to consider snowmelt as a variable process above the ground surface resulting in a range of melt inputs across the SSI.

Conclusions

We were able to represent water flowing through a layered snowpack using the EOS9 module of TOUGH2 and show the formation of hydraulic barriers in all snowpacks simulated. Highly stratified snowpacks as observed in the north aspect snow pit data used for this study form the most hydraulic barriers to vertically infiltrating meltwater in the form of capillary barriers. Capillary barriers formed only on the north aspect slope with diversion lengths ranging from 1.0 m to ≥25 m. Permeability barriers were observed in the south and flat aspect snowpack simulations with diversion lengths from 2.5 m to 9.5 m. The simulations in this study display the large potential for percolating water to move laterally within a snowpack. Highly stratified snowpacks such as the north aspect snow pit in this study produce higher potential for lateral diversion of percolating melt water, though these capillary barriers are less persistent temporally and only important at the daily or weekly time scale. Permeability barriers between snowpack layers are more persistent through the melt season and thus important at the monthly or seasonal melt timescale.

Utilizing previously developed equations for soil physics allowed analysis of the potential for capillary barriers in a layered snowpack. Snow above a layer interface needs to have grain size diameters of 1.0 mm or less to present the possibility of forming a capillary barrier with larger diversion lengths as grain size decreases. Top layers with grain sizes 0.5 mm or less above larger grains consistently produce capillary barriers according to estimates using

equation (3.6). As the density of the top layer decreases the magnitude of diversion lengths increase from below 100 m at a density of 400 kg/m^3 up to almost 1300 m at a density of 200 kg/m^3 though these diversion lengths usually exceed the distance a snow interfaces will be continuous and these calculations are assuming isolated capillary barriers that do not occur within a layered snowpack. Equation (3.6) is for isolated barriers and will not predict an accurate diversion length within a layered snowpack but will assist in determining which layer interfaces will divert water for greater lengths relative to other layer interfaces in the snowpack. TOUGH2 simulations show lesser magnitude diversion lengths within a layered snowpack for melt rates of 1.0 and 5.0 mm/hr and larger diversion lengths at a melt rate of 0.1 mm/hr. These results also show that more recently deposited snow layers have the potential for larger diversion lengths and thus these larger diversions will occur closer to the snow surface.

Future investigations of the movement of water during spring snowmelt will benefit from conceptualizing the snowpack as an extension of the unsaturated zone rather than separate from. This will allow for consideration of variable meltwater input to the soil surface. Additionally, future simulation studies will benefit from incorporating temporally varying hydraulic properties of snow layers to investigate these processes. These results have strong implications on the distribution of water within a layered snowpack during the transition period from winter to spring, though further studies are necessary to verify large capillary diversion in layered snowpacks in the field. Incorporating the variable input of snowmelt water to the ground surface will improve modeling for groundwater recharge, streamflow generation, and plant production quantifications.

REFERENCES

Adam, J. C., A. F. Hamlet, and D. P. Lettenmaier (2009), Implications of global climate change for snowmelt hydrology in the twenty-first century, Hydrological Processes, 23(7), 962-972, doi: 10.1002/hyp.7201.

Adams, E., A. Slaughter, L. McKittrick, and D. Miller (2011), Local terrain-topography and thermal-properties influence on energy and mass balance of a snow cover, Annals of Glaciology, 52(58), 169-175.

Anderton, S., S. White, and B. Alvera (2004), Evaluation of spatial variability in snow water equivalent for a high mountain catchment, Hydrological Processes, 18(3), 435-453, doi: 10.1002/hyp.1319.

Bales, R. C., J. W. Hopmans, A. T. O'Geen, M. Meadows, P. C. Hartsough, P. Kirchner, C. T. Hunsaker, and D. Beaudette (2011), Soil Moisture Response to Snowmelt and Rainfall in a Sierra Nevada Mixed-Conifer Forest, Vadose Zone Journal, 10(3), 786, doi: 10.2136/vzj2011.0001.

Bales, R.C., N.P. Molotch, T.H. Painter, M.D. Dettinger, R. Rice, and J. Dozer (2006), Mountain hydrology of the western United States, Water Resour. Res*.,* 42(8), W08432, doi: 10.1029/2005WR004387.

Blöschl, G., and R. Kirnbauer (1992), An Analysis of Snow Cover Patterns in a Small Alpine Catchment, Hydrological Processes, 6(1), 99-109.

Blöschl, G. (1999), Scaling issues in snow hydrology, Hydrological Processes, 13(14-15), 2149-2175, doi: 10.1002/(SICI)1099-1085(199910)13:14/15<2149::AID-HYP847>3.0.CO;2-8.

Caine, N. (1992), Modulation of the diurnal streamflow response by the seasonal snowcover of an alpine basin, Journal of Hydrology, 137, 245-260.

Calonne, N., C. Geindreau, F. Flin, S. Morin, B. Lesaffre, S. Rolland du Roscoat, and P. Charrier (2012), 3-D image-based numerical computations of snow permeability: links to specific surface area, density, and microstructural anisotropy, The Cryosphere, 6(5), 939-951, doi: 10.5194/tc-6-939-2012.

Cao, J., C. Liu, and W. Zhang (2013), Response of rock-fissure seepage to snowmelt in Mount Taihang slope-catchment, North China, Water Sci Technol, 67(1), 124-130, doi: 10.2166/wst.2012.542.

Celia, MA, E. Bouloutas, and R. Zarba (1990), A General Mass-Conservative Numerical-Solution for the Unsaturated Flow Equation, Water Resources Research, 26(7), 1483-1496, doi: 10.1029/90WR00196.

Clark, M., J. Hendrikx, A. Slater, D. Kavetski, B. Anderson, N. Cullen, T. Kerr, E. Hreinsson, and R. Woods (2011), Representing spatial variability of snow water equivalent in hydrologic and land-surface models: A review, Water Resources Research, 47, doi: 10.1029/2011WR010745.

Clilverd, H. M., D. M. White, A. C. Tidwell, and M. A. Rawlins (2011), Sensitivity of Northern Groundwater Recharge to Climate Change: A Case Study in Northwest Alaska, Journal of the American Water Resources Association, 47(6), 1228-1240, doi: 10.1111/j.1752-1688.2011.00569.x.

Cline, D., R. Armstrong, R. Davis, K. Elder, and G. Liston (2002 updated 2004), CLPX: ISA Snow Pit Measurements, Edited by M. Parsons and M.J. Brodzik, Boulder, CO: National Snow and Ice Data Center.

Clow, D. W. (2010), Changes in the Timing of Snowmelt and Streamflow in Colorado: A Response to Recent Warming, Journal of Climate, 23(9), 2293-2306, doi: 10.1175/2009jcli2951.1.

Colbeck, S. (1975), A theory for water flow through a layered snowpack, Water Resources Research, 11(2), 261-266.

Colbeck, S. (1979), Water-flow through heterogeneous snow, Cold Regions Science and Technology, 1(1), 37-45, doi: 10.1016/0165-232X(79)90017-X.

Colbeck, S. C., and E. A. Anderson (1982), The permeability of a melting snow cover, Water Resources Research, 18(4), 904-908.

Colbeck, S. C. (1987), Theory of particle coarsening with a log-normal distribution, Acta Metallurgica, 35(7), 1583-1588, doi: 10.1016/0001-6160(87)90105-2.

Colbeck, S. C. (1991), The layered character of snow covers, Reviews of Geophysics, 29(1), 81-96.

Daly, S. F., R. Davis, E. Ochs, and T. Pangburn (2000), An approach to spatially distributed snow modelling of the Sacramento and San Joaquin basins, California, Hydrological Processes, 14(18), 3257-3271, doi: 10.1002/1099-1085(20001230)14:18<3257::aid-hyp199>3.3.co;2-q.

Domine, F., S. Morin, E. Brun, M. Lafaysse, and C. M. Carmagnola (2013), Seasonal evolution of snow permeability under equi-temperature and temperature-gradient conditions, The Cryosphere, 7(6), 1915-1929, doi: 10.5194/tc-7-1915-2013.

Eiriksson, D., M. Whitson, C. H. Luce, H. P. Marshall, J. Bradford, S. G. Benner, T. Black, H. Hetrick, and J. P. McNamara (2013), An evaluation of the hydrologic relevance of lateral flow in snow at hillslope and catchment scales, Hydrological Processes, 27(5), 640-654, doi: 10.1002/hyp.9666.

Elder, K., J. Dozier, and J. Michaelsen (1991), Snow Accumulation and Distribution in an Alpine Watershed, Water Resources Research, 27(7), 1541-1552.

Elder, K. and D. Cline, edited by M. Parsons and M. Brodzik (2003), CLPX-Ground: ISA snow pit measurements, version 2 [Spring Creek ISA], Boulder, Colorado USA: NASA National Snow and Ice Data Center Distributed Active Archive Center, http://dx.doi.org/10.5060/D4H41PBP.

Elder, K., D. Cline, G. E. Liston, and R. Armstrong (2009), NASA Cold Land Processes Experiment (CLPX 2002/03): Field Measurements of Snowpack Properties and Soil Moisture, Journal of Hydrometeorology, 10(1), 320-329, doi: 10.1175/2008jhm877.1.

Fang, S., L. Xu, Y. Zhu, Y. Liu, Z. Liu, H. Pei, J. Yan, and H. Zhang (2013), An integrated information system for snowmelt flood early-warning based on internet of things, Information Systems Frontiers, 17(2), 321-335, doi: 10.1007/s10796-013-9466-1.

Fassnacht, S. R., and M. Hultstrand (2015), Snowpack variability and trends at long-term stations in northern Colorado, USA, International Association of Hydrological Sciences, 92, 1-6, doi: 10.5194/piahs-92-1-2015.

Fassnacht, S. R., M. L. Cherry, N. B. H. Venable, and F. Saavedra (2016), Snow and albedo climate change impacts across the United States Northern Great Plains, The Cryosphere, 10, 329-339, doi: 10.5194/tc-10-329-2016.

Flint, A. L., L. E. Flint, and M. D. Dettinger (2008), Modeling Soil Moisture Processes and Recharge under a Melting Snowpack, Vadose Zone Journal, 7(1), 350, doi: 10.2136/vzj2006.0135.

Gray, D. M., and P. G. Landine (1988), An Energy-Budget Snowmelt Model for the Canadian Prairies, Can. J. Earth Sci., 25(8), 1292-1303, doi: 10.1139/e88-124.

Graybeal, D., and D. Leathers (2006), Snowmelt-related flood risk in Appalachia: First estimates from a historical snow climatology, Journal of Applied Meteorology and Climatology, 45(1), 178-193, doi: 10.1175/JAM2330.1.

Harms, T. E., and D. S. Chanasyk (1998), Variability of Snowmelt Runoff and Soil Moisture Recharge, Nordic Hydrology, 29, 179-198.

Harpold, A., P. Brooks, S. Rajagopal, I. Heidbuchel, A. Jardine, and C. Stielstra (2012), Changes in snowpack accumulation and ablation in the intermountain west, Water Resources Research, 48(11), n/a-n/a, doi: 10.1029/2012wr011949.

Harpold, A. A., J. A. Biederman, K. Condon, M. Merino, Y. Korgaonkar, T. Nan, L. L. Sloat, M. Ross, and P. D. Brooks (2014), Changes in snow accumulation and ablation following the Las Conchas Forest Fire, New Mexico, USA, Ecohydrology, 7(2), 440-452, doi: 10.1002/eco.1363.

Harpold, A. A., N. P. Molotch, K. N. Musselman, R. C. Bales, P. B. Kirchner, M. Litvak, and P. D. Brooks (2015), Soil moisture response to snowmelt timing in mixed-conifer subalpine forests, Hydrological Processes, 29(12), 2782-2798, doi: 10.1002/hyp.10400.

Hinckley, E.-L. S., B. A. Ebel, R. T. Barnes, R. S. Anderson, M. W. Williams, and S. P. Anderson (2014), Aspect control of water movement on hillslopes near the rain-snow transition of the Colorado Front Range, Hydrological Processes, 28(1), 74-85, doi: 10.1002/hyp.9549.

Hirashima, H., S. Yamaguchi, A. Sato, and M. Lehning (2010), Numerical modeling of liquid water movement through layered snow based on new measurements of the water retention curve, Cold Regions Science and Technologh, 64, 94-103, doi: 10.1016/j.coldregions.2010.09.003.

Ho, C. K., and S. W. Webb (1998), Capillary barrier performance in heterogeneous porous media, Water Resources Research, 34(4), 603-609, doi: 10.1029/98wr00217.

Jencso, K. G., and B. L. McGlynn (2011), Hierarchical controls on runoff generation: Topographically driven hydrologic connectivity, geology, and vegetation, Water Resources Research, 47(11), n/a-n/a, doi: 10.1029/2011wr010666.

Kattelmann, R., and J. Dozier (1999), Observations of snowpack ripening in the Sierra Nevada, California, USA, Journal of Glaciology, 45(151), 409-416.

Kormos, P., D. Marks, J. McNamara, H. Marshall, A. Winstral, and A. Flores (2014), Snow distribution, melt and surface water inputs to the soil in the mountain rain-snow transition zone, Journal of Hydrology, 519, 190-204, doi: 10.1016/j.jhydrol.2014.06.051.

Lehning, M., H. Lowe, M. Ryser, and N. Raderschall (2008), Inhomogeneous precipitation distribution and snow transport in steep terrain, Water Resources Research, 44(7), doi: 10.1029/2007WR006545.

Liston, G. E., and K. Elder (2006), A distributed snow-evolution modeling system (SnowModel), Journal of Hydrometeorology, 7, 1259-1276.

López-Moreno, J. I., J. Revuelto, M. Gilaberte, E. Morán-Tejeda, M. Pons, E. Jover, P. Esteban, C. García, and J. W. Pomeroy (2013), The effect of slope aspect on the response of snowpack to climate warming in the Pyrenees, Theoretical and Applied Climatology, 117(1-2), 207-219, doi: 10.1007/s00704-013-0991-0.

Luce, C., D. Tarboton, and R. Cooley (1998), The influence of the spatial distribution of snow on basin-averaged snowmelt, Hydrological Processes, 12(10-11), 1671-1683, doi: 10.1002/(SICI)1099-1085(199808/09)12:10/11<1671::AID-HYP688>3.0.CO;2-N.

Marsh, P., and M.-K. Woo (1985), Meltwater movement in natural heterogeneous snow covers, Water Resources Research, 21(11), 1710-1716.

Marsh, P. (1987), Grain growth in a wet arctic snow cover, Cold Regions Science and Technology, 14, 23-31.

McNamara, J. P., D. Chandler, M. Seyfried, and S. Achet (2005), Soil moisture states, lateral flow, and streamflow generation in a semi-arid, snowmelt-driven catchment, Hydrological Processes, 19(20), 4023-4038, doi: 10.1002/hyp.5869

Miller, S. (2004), CLPX-Airborne: infrared orthophotography and lidar topographic mapping, [Spring Creek ISA], Boulder, Colorado USA: NASA National Snow and Ice Data Center Distributed Active Archive Center. http://dx.doi.org/10.5067/KRWSPR2J1N2N.

Molotch, N. P., P. D. Brooks, S. P. Burns, M. Litvak, R. K. Monson, J. R. McConnell, and K. Musselman (2009), Ecohydrological controls on snowmelt partitioning in mixed-conifer sub-alpine forests, Ecohydrology, 2(2), 129-142, doi: 10.1002/eco.48.

Molotch, N. P., and L. Meromy (2014), Physiographic and climatic controls on snow cover persistence in the Sierra Nevada Mountains, Hydrological Processes, 28(16), 4573-4586, doi: 10.1002/hyp.10254.

Musselman, K. N., N. P. Molotch, and P. D. Brooks (2008), Effects of vegetation on snow accumulation and ablation in a mid-latitude sub-alpine forest, Hydrological Processes, 22(15), 2767-2776, doi: 10.1002/hyp.7050.

Oldenburg, C.M., and K. Pruess (1993), On numerical modeling of capillary barriers. Water Resour. Res., 29, 4: 1045-1056.

Pruess, K., C. Oldenburg, and G. Moridis (1999), *TOUGH2 User's Guide, Version 2.0*, Report LBNL-43134, Lawrence Berkeley National Laboratory, Berkeley, Calif..

Rice, R., R. C. Bales, T. H. Painter, and J. Dozier (2011), Snow water equivalent along elevation gradients in the Merced and Tuolumne River basins of the Sierra Nevada, Water Resources Research, 47, 11, doi: 10.1029/2010wr009278.

Richards, L. A. (1931), Capillary conduction of liquids through porous mediums, Physics, 1, 318-333.

Richer, E. E., S. K. Kampf, S. R. Fassnacht, and C. C. Moore (2013), Spatiotemporal index for analyzing controls on snow climatology: application in the Colorado Front Range, Physical Geography, 34(2), 85-107.

Ross, B. (1990), The diversion capacity of capillary barriers, Water Resour. Res., 26(10), 2625-2629.

Sexstone, G. A., and S. R. Fassnacht (2014), What drives basin scale spatial variability of snowpack properties in northern Colorado?, The Cryosphere, 8(2), 329-344, doi: 10.5194/tc-8-329-2014.

Seyfried, M. S., L. E. Grant, D. Marks, A. Winstral, and J. McNamara (2009), Simulated soil water storage effects on streamflow generation in a mountainous snowmelt environment, Idaho, USA, Hydrological Processes, 23(6), 858-873, doi: 10.1002/hyp.7211.

Smith, T. J., J. P. McNamara, A. N. Flores, M. M. Gribb, P. S. Aishlin, and S. G. Benner (2011), Small soil storage capacity limits benefit of winter snowpack to upland vegetation, Hydrological Processes, 25(25), 3858-3865, doi: 10.1002/hyp.8340.

Staron, P., E. Adams, and D. Miller (2014), Nonequilibrium thermodynamics of kinetic metamorphism in snow, Cold Regions Science and Technology, 97, 60-71, doi: 10.1016/j.coldregions.2013.10.007.

Storck, P., D. P. Lettenmaier, and S. M. Bolton (2002), Measurement of snow interception and canopy effects on snow accumulation and melt in a mountainous maritime climate, Oregon, United States, Water Resources Research, 38(11), 5-1-5-16, doi: 10.1029/2002wr001281.

Stormont, J.C. (1995), The effect of constant anisotropy on capillary barrier performance, Water Resour. Res., 31(3), 783-785.

Van Genuchten, M. T. (1980), A closed-form equation for predicting the hydraulic conductivity of unsaturated soils, Soil Science Society of America Journal, 44, 892-898.

Waldner, P.A., M. Schneebeli, U. Schultze-Zimmermann, and H. Flühler (2004), Effect of snow structure on water flow and solute transport, *Hydrol. Process*., 18, 1271-1290, doi: 10.1002/hyp.1401.

Walter, B., S. Horender, C. Gromke, and M. Lehning (2013), Measurements of the pore-scale water flow through snow using fluorescent particle tracking velocimetry, *Water Resour. Res*., 49, 7448-7456, doi: 10.1002/2013WR013960.

Webb, R. W., S. R. Fassnacht, and M. N. Gooseff (2015), Wetting and Drying Variability of the Shallow Subsurface Beneath a Snowpack in California's Southern Sierra Nevada, Vadose Zone Journal, 14(8), 0, doi: 10.2136/vzj2014.12.0182.

Webb, S. W. (1997), Generalization of Ross' tilted capillary barrier diversion formula for different two-phase characteristic curves, Water Resources Research, 33(8), 1855-1859, doi: 10.1029/97wr01231.

Wever, N., C. Fierz, C. Mitterer, H. Hirashima, and M. Lehning (2014), Solving Richards Equation for snow improves snowpack meltwater runoff estimations in detailed multi-layer snowpack model, The Cryosphere, 8(1), 257-274, doi: 10.5194/tc-8-257-2014.

Williams, C. J., J. P. McNamara, and D. G. Chandler (2009a), Controls on the temporal and spatial variability of soil moisture in a mountainous landscape: the signature of snow and complex terrain, Hydrology and Earth System Sciences, 13, 1325-1336.

Williams, M. W., R. Sommerfeld, S. Massman, and M. Rikkers (1999a), Correlation lengths of meltwater flow through ripe snowpacks, Colorado Front Range, USA, Hydrological Processes, 13(1807-1826).

Williams, M. W., D. Cline, M. Hartman, and T. Bardsley (1999b), Data for snowmelt model development, calibration, and verification at an alpine site, Colorado Front Range, Water Resources Research, 35(10), 3205-3209.

Williams, M. W., C. Seibold, and K. Chowanski (2009b), Storage and release of solutes from a subalpine seasonal snowpack: soil and stream water response, Niwot Ridge, Colorado, Biogeochemistry, 95(1), 77-94, doi: 10.1007/s10533-009-9288-x.

Williams, M. W., T. A. Erickson, and J. L. Petrzelka (2010), Visualizing meltwater flow through snow at the centimetre-to-metre scale using a snow guillotine, Hydrological Processes, n/a-n/a, doi: 10.1002/hyp.7630.

Yamaguchi, S., T. Katsushima, A. Sato, and T. Kumakura (2010), Water retention curve of snow with different grain sizes, Cold Regions Science and Technology, 64(2), 87-93, doi: 10.1016/j.coldregions.2010.05.008.

Yosida, Z. (1955), Physical studies of deposited snow, 1. Thermal properties, in Thermal properties, edited, pp. 19-74, Institute of Low Temperature Science Hokkaido University.

Zhao, Q., Z. Liu, B. Ye, Y. Qin, Z. Wei, and S. Fang (2009), A snowmelt runoff forecasting model coupling WRF and DHSVM, Hydrology and Earth System Sciences, 13(10), 1897-1906.

CHAPTER 4: PATTERN ANALYSIS AT DRY LAKE FIELD SITE

Introduction

In many mountainous headwater catchments snow and soil moisture are key components of the hydrologic cycle, providing valuable information pertaining to the dynamic processes that occur during spring runoff. This has justified large data collection efforts to further understand the distribution of snow and soil moisture across landscapes during the winter and spring seasons [*Elder et al.*, *2009*]. The majority of snowmelt during spring will infiltrate into the soil with a noticeable signal in the state of soil moisture prior to recharging groundwater storage, producing streamflow, or contributing to evapotranspiration [*Bales et al.*, *2011; Kampf et al., 2015*]. The state of soil moisture, or level of saturation in the vadose zone, controls the stream connectivity and release of water and nutrients from subsurface storage [*McNamara et al., 2005; Williams et al., 2009*]. Soil moisture during this time is driven by snowmelt that can impact the water availability for plant production [*Molotch et al.*, *2009; Harpold et al., 2015*] as well as the ionic signature of the soil moisture and stream flow [*Harrington and Bales*, *1998*]. For these reasons the connections between snowmelt and soil moisture are critical in understanding the hydrologic cycle in snow dominated headwater systems [*Jencso et al.*, *2009*], particularly in the face of a changing climate that will alter the snowmelt season and resulting dynamics [*Adam et al.*, *2009; Clow, 2010; Clilverd et al., 2011; Harpold et al., 2012; Rasmussen et al., 2014; Fassnacht et al., 2016*].

The dynamic snowmelt period of a catchment is important to the state of soil moisture and resulting streamflow [*McNamara et al.*, *2005; Williams et al., 2009; Bales et al., 2011; Hunsaker et al., 2012*]. The hydrologic connectivity a stream has to the surrounding landscape through different soil moisture states generally follows seasonal trends with highest connectivity during spring snowmelt [*McNamara et al.*, *2005*]. Topography has been shown by *Jencso et al*. [*2009*] and *Jencso and McGlynn* [*2011*] as most influential for water distribution and stream

connectivity during snowmelt but flow path lengths and gradients, vegetation, and geology also have importance. The aspect of a hillslope can additionally increase soil water storage and retention on north aspect slopes [*Geroy et al.*, *2011*].

Snow accumulation, redistribution, and ablation will affect the soil moisture state at varying scales. The timing of soil moisture drying after snowmelt was shown by *Bales et al*. [*2011*] to vary up to four weeks at the same elevation within a catchment due to the heterogeneity of snowmelt processes. Snow distribution near the rain snow transition zone directly impacts the spatial and temporal patterns of soil moisture [*Williams et al.*, *2009*] with snowmelt often having the largest influence in the top 10 cm of soil [*Blankinship et al.*, *2014*] and pulses of water that reach further depths varying widely at both the hillslope and catchment scale [*Webb et al.*, *2015*]. At the plot scale, saturation variability in the vadose zone during snowmelt can produce preferential flow paths than add further complexity to the processes [*French and Binley*, *2004; Hinckley et al., 2014*]. With soil moisture being shown to vary widely during the spring melt season it is important to investigate these processes across multiple elevation, ecological, and climate environments for a better understanding of environmental controls.

Multiple environmental controls cause snow processes to vary at multiple scales of interest. From a basin scale perspective, elevation has been shown to influence the depth and persistence of a snowpack [*Richer et al.*, *2013; Molotch and Meromy, 2014; Sexstone and Fassnacht, 2014*] while at finer resolutions the spatial variability of both accumulation and melt may be controlled by aspect [*Williams et al.*, *2009; López-Moreno et al., 2013; Hinckley et al., 2014*] and snow in forested areas can be affected by interception during accumulation, shortwave radiation shading, and longwave radiation influences prior to and during melt [*Storck et al.*, *2002; Musselman et al., 2008; Molotch et al., 2009; Adams et al., 2011*]. Furthermore, redistribution and increased sublimation losses of snow due to wind effects can occur across a landscape [*Liston and Elder*, *2006*]. Observations made at the experimental plot scale show

additional variability and implications for using single point measurements of snow [*López-Moreno et al.*, *2011*]. With such variable and dynamic controls on the accumulation and melt rates across a landscape that lead to a range of melt inputs across the soil surface [*Kormos et al.*, *2014*] it is essential to understand the nature of the snowpack itself for any investigation of soil moisture in a snowmelt dominated catchment once melt begins.

As a snowpack evolves over the season the layers undergo metamorphism leading to different permeabilities based on grain size and snow density [*Yamaguchi et al.*, *2010; Domine et al., 2013*]. The development and/or deposition of layers will often be controlled by energy fluxes that are largely influenced by landscape scale variability [*Adams et al.*, *2011*]. When these layers begin to melt, the increased liquid water content will speed up the process of metamorphism [*Marsh*, *1987*] creating areas with larger grain sizes and higher hydraulic conductivities [*Yamaguchi et al.*, *2010; Katsushima et al., 2013*]. Snowpacks have been shown to have correlation lengths of five to seven meters between areas of large grains during snowmelt due to preferential melt patterns by *Sommerfeld et al*. [*1994*] and *Williams et al*. [*1999*]. These complex melt processes create a snowpack with zones of higher and lower water contents [*Techel and Pielmeier*, *2011*] that forms a matrix of ice, water, and air that changes non-uniformly through time and space resulting from and potentially further producing preferential flow paths.

Preferential flow paths for vertically infiltrating water will develop from the natural heterogeneity of a layered snowpack that is often influenced by ice lenses [*Colbeck*, *1979; Marsh and Woo, 1985; Harrington and Bales, 1998; Williams et al., 2010*] that redistribute water downslope across layer interfaces [*Kattelmann and Dozier*, *1999; Liu et al., 2004; Eiriksson et al., 2013; Chapter 3*]. These preferential flow paths and melt patterns are important for consideration of solute concentrations of snow runoff [*Marsh and Pomeroy*, *1993; Harrington et al., 1996; Harrington and Bales, 1998; Williams et al., 2009*], biodiversity of an alpine landscape [*Litaor et al.*, *2008*] and wet slab avalanches [*Mitterer et al.*, *2011b*]. The development of flow

paths at the centimeter to meter scale across interfaces has been observed [*Williams et al.*, *2010*], at the meters to tens of meters scale from a rain on snow events [*Eiriksson et al.*, *2013*], and even directly bypassing soil interaction to produce streamflow in deep snow packs [*Laudon et al.*, *2004; Liu et al., 2004*]. Identifying specific flow paths has been observed in the form of ice columns connected by ice ribs by *Williams et al*. [*2000b*] in an alpine environment regardless of aspect and were found consistently. These preferential flow paths that develop at multiple scales will have impacts on the soil moisture at similar scales within a headwater catchment.

The ability to observe soil moisture states throughout the water year has seen recent technological advances to allow instrumentation of watersheds to capture higher resolution data both spatially and temporally [*e.g. Bales et al., 2011*] in addition to the liquid water content of a snowpack [*Mitterer et al.*, *2011a; Techel and Pielmeier, 2011; Koch et al., 2014; Heilig et al., 2015*]. These types of data collections are essential for gaining further understanding of hydrologic systems and the dynamic processes that may be vulnerable to a changing climate [*Bales et al.*, *2006*]. Remote sensing opportunities have enabled extensive spatial availability of data for assessment of the physical controls on parameters such as snow depth and snow persistence [*Richer et al., 2013; Molotch and Meromy, 2014*]. However, the state of soil moisture beneath a measureable snowpack has been limited to an array of discreet points at locations of instrument installations. Few studies have investigated soil moisture during spring snowmelt at a similar scale as the snow above it. One study in Norway by *French and Binley* [*2004*] showed microtopography controls preferential infiltration of snowmelt across the snow-soil-interface (SSI) in a relatively flat experimental plot. Near the rain-snow transition zone in Idaho, *Williams et al*. [*2009*] measured soil moisture beneath a snowpack concluding that points tend to remain either wetter or drier relative to the mean and that static properties such as slope, aspect, and soil depth that control the snow have a similar effect on the resulting soil moisture. A similar study in an alpine environment of Colorado conducted by *Litaor et al.* [*2008*] at a larger scale showed similar topographic influence on soil moisture from wind shielding and

snow accumulation though there was less association of these parameters in low snow years. These studies suggest that topographic influences on soil moisture are strong but more investigations towards these influences during varying snow accumulation and melt dynamics are important, particularly with variable regional and environmental snowpack responses to climate variability [*Harpold et al.*, *2012*]. To our knowledge there has not been a similar study investigating snow and soil moisture interactions in a sub-alpine environment beneath a deep (2 m) seasonally persistent snowpack.

The goal of this study is to gain understanding in flow path development in a snowmelt dominated subalpine headwater catchment through analysis of the static and dynamic controls of spatial and temporal variability of near surface soil moisture during snowmelt. This was undertaken at a subalpine forested setting across varying slope, aspect, canopy cover and beneath a deep seasonally persistent snowpack through: 1) observing the snow water equivalent (SWE) and the near surface soil moisture variability between north, south, and flat aspects and 2) observing how SWE and near surface soil moisture vary at the bases of hillslopes compared to flat and sloped areas.

Methods

Study Site

The study site is Dry Lake study (DL) area that is approximately 6.5 km northeast of Steamboat Springs, Colorado located in in Routt National Forest; most of the data collection was within a primary area of interest over 0.2 km^2 (Fig. 4.1). The elevation at DL ranges from 2500 m to 2600 m with slope angles from 1°to 30°as determined from a 1 0 m digital elevation model (DEM) [*The National Map*, *2015*]. The site has a mix of deciduous and evergreen forest with a majority of the vegetation growing near the small stream and large areas of open canopy conditions on each of the two predominant hillslopes (one south-southeast facing, and one north-northwest facing).

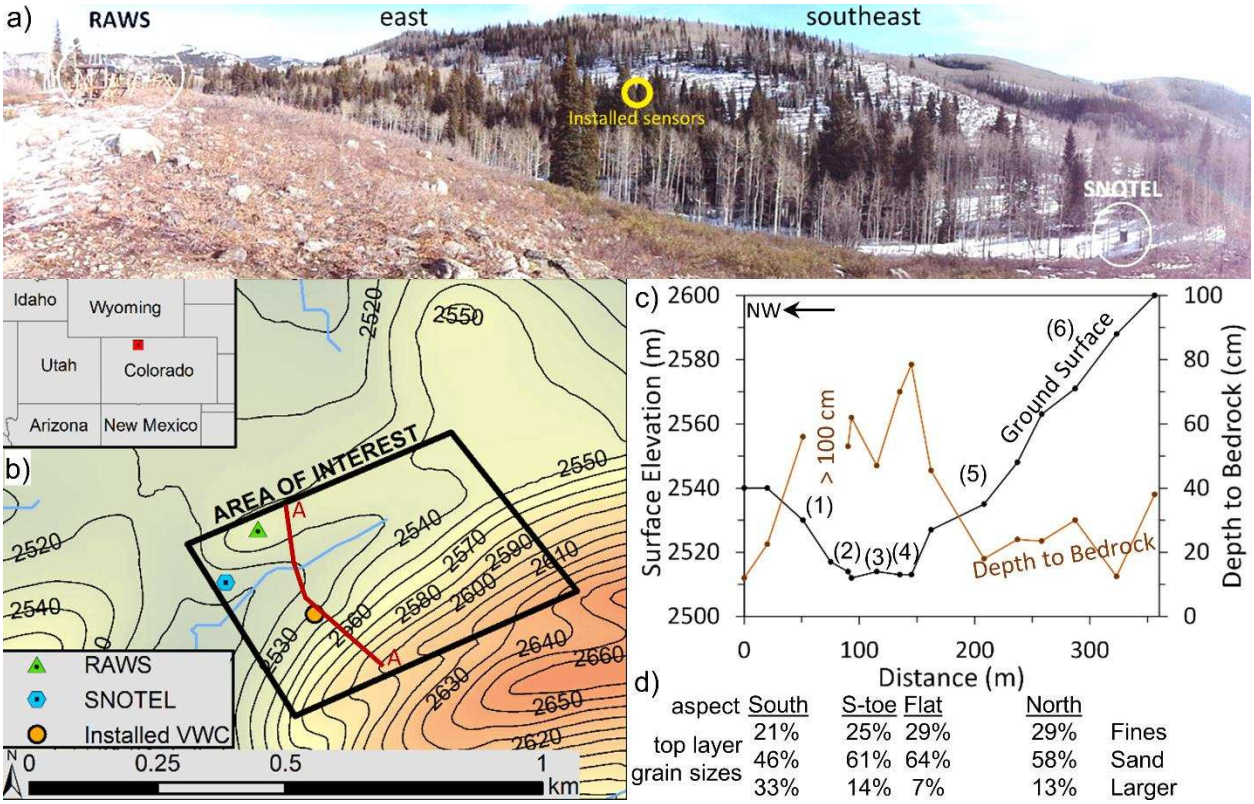

Figure 4.1: a) Panoramic picture of the Dry Lake study area facing east to southeast. Locations of the Remote Automated Weather Station (RAWS), SNOTEL station, and installed soil moisture sensors are circled and labeled. b) Map of the Dry Lake study site and the primary area of interest in this investigation. 10 m contours are shown. c) Cross section A-A from panel (b) showing the elevation of the ground surface and depth to bedrock using a 100 cm long hand auger. Areas of interest are identified as (1) south aspect hillslope, (2) toe of the south aspect hill, (3) flat aspect, (4) toe of the north aspect, (5) low on the north aspect, and (6) high on the north aspect hillslope. d) Percent of grain sizes by mass determined from sieve analysis of samples collected using a ~200 cm^3 sample.

The soil types located within DL are primarily loams with very cobbly loam dominating the south aspect slope, cobbly sandy loam on the north aspect, and loam on the flatter aspects with observations of highly organic soils in the flat northeastern section of the area at the base of the north aspect hillslope. Depth to bedrock was estimated using a one meter long hand auger at 16 locations within the study site, resulting in soil depths ranging from 12 cm to greater than one meter at one location. Soil depths tend to decrease with increasing elevation with a mean depth to bedrock of 40 cm and a median of 38 cm was calculated for the 15 depths less than one meter (Fig. 4.1c). Sieve analyses were also conducted on six different volumetric samples of approximately 200 cm^3 for the top soil layers (Fig. 4.1d).

Time Series Data

At approximately 2540 m elevation along an exposed ridge at the top of the south aspect slope is a Remote Automated Weather Station (RAWS) operated since 1985 by the United States Forest Service (Fig. 4.1). Hourly data are available from this station including solar radiation, wind speed and direction, air temperature, relative humidity, dewpoint temperature, wet bulb temperature, and precipitation. Additionally, the Dry Lake Snow Telemetry (SNOTEL) station is located approximately 120 m to the south-southwest of the RAWS at a lower elevation of 2510 m with light canopy shading (Fig. 4.1a). Data from this enhanced SNOTEL station include daily and hourly observations of air temperature, precipitation, relative humidity, snow depth, SWE, soil moisture and temperature at three depths (5, 20, and 50 cm), solar radiation, and wind speed and direction. All data are available from 2003 to present, with SWE and precipitation being collected since 1979. The SNOTEL data show peak SWE occurs on average April 5 with a 35 year median peak of 570 mm and a mean of 590 mm (Fig. 4.2). The RAWS and SNOTEL data provide meteorological data at two elevations and different canopy conditions within the relatively small area of interest for this study.

Additional soil moisture and temperature instruments were installed at a single location on the north aspect slope on December 27, 2013 at depths of 5, 12.5, and 20 cm. Instruments installed were Decagon Devices, Inc. 5TM temperature and moisture sensors connected to a Decagon Em50 data logger. Sensor data prior to March 15 was not included in analysis to allow the snowpack and soil moisture to return to near undisturbed conditions after installation. The soil moisture sensors and data logger were calibrated prior to installation using approximately 1500 cm^3 of soil collected from DL tampered around the sensor to a density of 1.0 g cm^{-3}, similar to measured conditions in the field. The calibration occurred at a temperature maintained near 0.5℃ and additions of seven to ten percent volumetric water content (VW C) every three to four days. The container mass was recorded to confirm mass of soil, sensor, and water as well

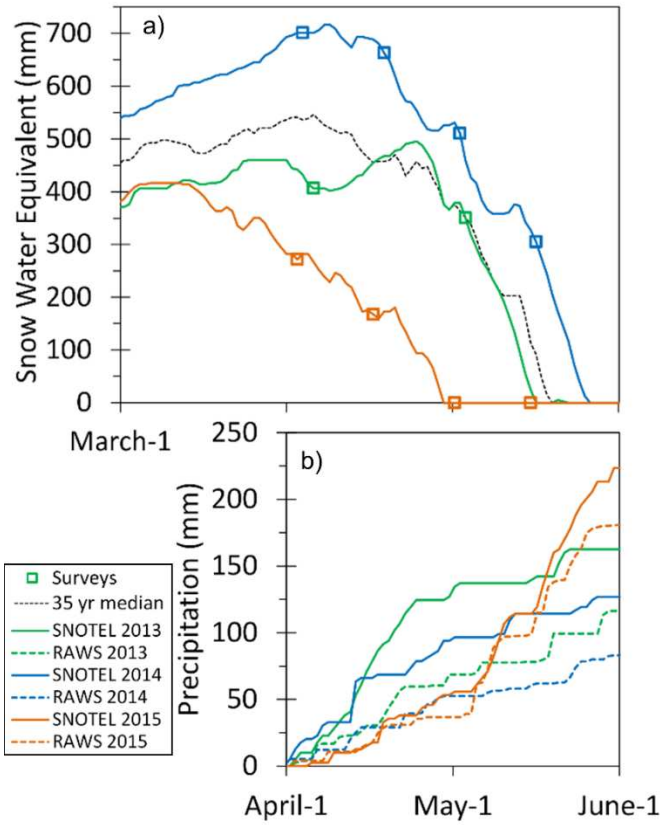

Figure 4.2: a) Daily Snow Water Equivalent (SWE) measured at the SNOTEL station each spring of the study period and the 35 year median of the station measurements and b) accumulated precipitation occurring during the spring survey study periods of April and May as measured at the SNOTEL station (solid lines) and the RAWS site (dashed lines) for each of the survey years.

as the sensor reading of temperature and VWC prior to the addition of water each time. All mass recordings were at a precision of 1.0 g and VWC recordings to 0.1%.

Spatial Data Collection

Spatial surveys were conducted in the spring of 2013, 2014, and 2015. In 2013 two surveys were conducted four weeks apart whereas in 2014 and 2015 four surveys were conducted at two week intervals. All survey periods began during the first week of April each year (April 6, 2013; April 4, 2014; April 3, 2015). Surveys consisted of a series of snow pits for collecting data for soil moisture and bulk SWE. At each snow pit, the first measurements taken were soil moisture using a handheld time domain reflectometer (TDR) (FieldScout TDR 100;

Spectrum Technologies, Inc.) to measure the volumetric water content (VWC) of the soil using seven centimeter long prongs inserted vertically into the soil. A total of five TDR measurements were averaged across the bottom of each snow pit (approximately one meter across, measurements ~20 cm apart). Volumetric soil samples (~40 cm^3) were collected at three of the same point locations as TDR measurements in each snow pit for laboratory confirmation of VWC during spatial surveys in 2013 and 2014. SWE measurements were collected using a plastic tube with an inner diameter of 68 mm and a length of 1.8 m. A core was collected for the full depth of the snowpack when possible, and in no more than two segments when the depth of the snowpack was greater than the length of the coring tube. Snow cores were placed in a plastic bucket and mass measured using a digital scale with 10 g precision. At least two cores per snow pit were collected with more if the first two showed greater than 10 percent mass difference. SWE and depth from the snow cores were averaged for each snow pit location. When pit locations were returned to a new pit was dug within one to two meters with care to avoid previously disturbed snow.

On April 6, 2013, a total of 15 snow pits were dug within DL at random with six of these locations returned to and measured again on May 4, 2013. The 2014 and 2015 surveys collected data along approximate north-to-south transects perpendicular to topographic contours. In 2014 a total of 25 snow pits were dug on April 4 and nine of these locations were returned to in two week intervals through May 17; eight of the nine pits were measured on April 19. The 2015 surveys made observations at 47 locations within DL on April 3 and 23 of these locations were returned to on two week intervals through May 16.

Correlation of VWC to SWE was investigated to test the influence of snow on soil moisture using Pearson's correlation coefficient, r, and a level of significance determined at a p-values of 0.05 and 0.01. VWC was compared to the SWE at the same location on the date of observation, SWE on the first survey date (representative of peak SWE), the change in SWE between survey dates prior to measurement, VWC on the first survey date, as well as

topographic aspect, slope, and elevation as calculated from the 10 m DEM. These analyses were then used to gain insight towards the flow path development and movement of water during the snowmelt period.

Results

Time Series Snow and Meteorological Data

The three spring snowmelt seasons studied represent varying conditions with peak SWE that averaged 540 mm on April 3, as observed at the SNOTEL station (Fig. 4.2). Peak SWE values recorded here were 495, 715, and 415 mm for 2013, 2014 and 2015, respectively, representing 90%, 125%, and 75% of the 35 year median. The earliest peak SWE of the three years occurred in 2015 on March 9 preceding the first spatial survey by nearly one month. The highest peak SWE of the study period, in 2014, occurred on April 8 only four days after the first survey and in 2013 peak SWE occurred on April 25, 19 days after the first survey and 9 days prior to the second survey of that year. Snowmelt at the SNOTEL station for all three years was complete by the end of May (Fig. 4.2). The number of days from peak SWE to zero snow on the SNOTEL snow pillow ranged from 22 days in 2013 to 52 days in 2015, and 2014 taking 49 days. The years observed melted faster than the 35 year median number of melt days of 71 days and a mean of 70 (including the observed years). Each year observed had varying degrees of incremental snowfall during the melt period as well, causing a pause in decline as SWE increased (Fig. 4.2). In 2013 melt had begun prior to the first survey and before a large accumulation period that increased and delayed the date of peak SWE; this is the only year that observed a large loss of SWE prior to peak. Spatial surveys conducted during melt in 2013 and 2014 occurred while a measureable snowpack was still observed at the SNOTEL station for all survey dates whereas in 2015 the SNOTEL station measured zero snow for the final two of the four surveys. However, even though the SNOTEL station measured zero snow there were still locations of measurable snow for all surveys of 2015 (discussed below). The snowmelt

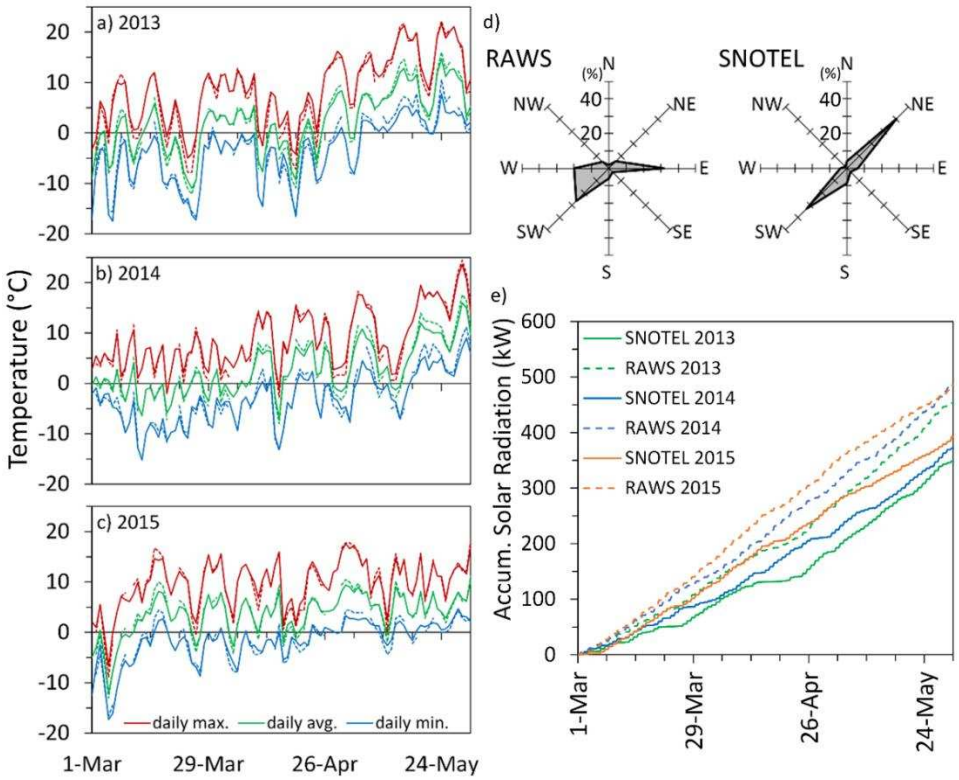

Figure 4.3: Daily temperatures recorded at the Dry Lake study site during March, April, and May as measured at the SNOTEL station (solid lines) and the RAWS site (dashed lines) for each of the survey years (a) 2013, (b) 2014, and (c) 2015. d) Average wind roses at the Dry Lake study site for the survey years 2013, 2014, and 2015 during March, April, and May as measured at the RAWS site and the SNOTEL station. e) Accumulated solar radiation recorded at the Dry Lake study site from March 1as measured at the SNOTEL station (solid lines) and the RAWS site (dashed lines) for each of the survey years 2013, 2014, and 2015.

dynamics that occurred during the three years of this study captured three different snow environments during the spring snowmelt seasons.

Meteorological conditions displayed variable forcing conditions for the melt season each year surveyed during March, April, and May (Fig. 4.3). Hourly temperature from the SNOTEL station shows air temperature during these months in 2013, 2014, and 2015 above freezing 62%, 64%, and 77% of the time, respectively (Fig. 4.3). The RAWS recorded air temperature during March, April, and May being above freezing for 58%, 60%, and 74% of the time in 2013, 2014, and 2015, respectively, displaying the variability between the two locations. Solar radiation shows a similar pattern where the total radiation accumulated over the three months in

2013, 2014, and 2015 at the SNOTEL station was 355 kW, 380 kW, and 400 kW and the RAWS location measured 460 kW, 491 kW, and 493 kW, respectively (Fig. 4.3). The greater amount of time temperature was above freezing and higher accumulated solar radiation during the spring in 2015 likely had a compounding effect on the lower and earlier occurring peak accumulation. The relatively similar accumulated solar radiation and percentage of time above freezing in 2013 and 2014 show similar melting conditions that resulted in average melt rates during the month of May being 23 and 20 mm d^{-1}, respectively (Fig. 4.2). 2015 also varied more when considering precipitation relative to the other two years with nearly 100 mm more (Fig. 4.2). Recorded precipitation at the SNOTEL station was 135 mm for both 2013 and 2014 in March, April, and May whereas 2015 accumulated 230 mm during this period with most of it falling in late April and May (Fig. 4.2). Precipitation was observed for every period between surveys. The RAWS location measured higher March, April, and May accumulated precipitation with 172 mm, 161 mm, and 244 mm in 2013, 2014, and 2015, respectively. The precipitation that fell during the melt period in 2015 likely included a number of rain on snow events due to the regular above freezing temperatures and lack of snow accumulation on the snow pillow in late April and May. The combination of temperature, solar radiation, and precipitation variability observed during the three years of investigation offer multiple melt dynamics for our observations.

Wind directions remained consistent each year for the spring months. Wind recorded at the RAWS location shows wind direction generally coming from the west, southwest, and east alternating diurnally between the westerly and east directions. The SNOTEL station data show a similar diurnal change in direction, but with directions being more concentrated in the southwest and northeast directions due to the effects of topography and vegetative cover around the station. All three years were similar with little interannual variability in wind roses and thus the average is displayed for each of the two stations (Fig. 4.3).

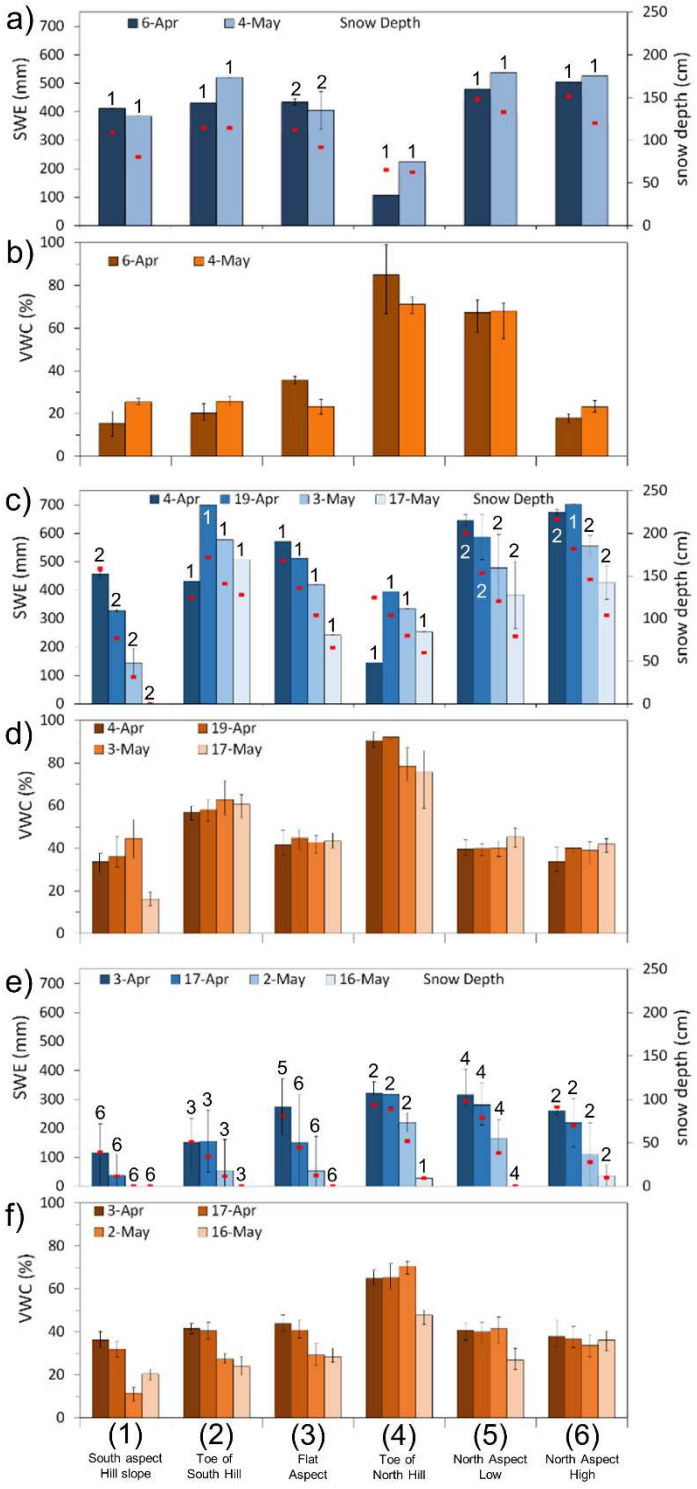

Figure 4.4: Snow water equivalent (SWE) and snow depth measured in a) 2013, c) 2014, and e) 2015; and soil volumetric water content (VWC) in b) 2013, d) 2014, and f) 2015 as measured at the Dry Lake study site in 2014 in regions indicated in Figure 1. Numbers above SWE bars indicate number of snow pit locations averaged and error bars indicate total range of measurements.

Spatial Surveys

The spatial surveys resulted in varying changes in SWE and VWC for locations measured each year. In 2013 all but flat aspect and south aspect locations increased in SWE between surveys though all locations decreased in depth to varying degrees (Fig. 4.4a). This general increase in SWE can be attributed to the nearly 130 mm of precipitation that fell during the four weeks between surveys. The largest increase in SWE was at the base of the north aspect slope with an increase of 160 mm and the next highest was low on the south aspect slope with an increase of 90 mm. The soil moisture during the two surveys of 2013 varied from mean values of 15% to 85% VWC. The maximum soil moisture consistently occurred at the toe of the north aspect hillslope (Fig. 4.4) in the highly organic soil.

In 2014 three locations resulted in an increase in SWE between the first two surveys, occurring at the base of each hillslope and once high on the north aspect slope (Fig. 4.4b). At the toe of the south aspect slope this increase in SWE is accompanied by a similar increase in snow depth that is not shown at the locations of other SWE increases. This increase in SWE at the toe of the south aspect slope can likely be attributed to the local variability of snow. The other increases in SWE were accompanied with a decrease in depth similar to all other observation locations that did not show an increase in SWE. One of the high north locations was not observed on April 19, 2014 due to limited number of surveyors for that day. The increase in SWE at the base of the north aspect slope is the largest observed increase from 125 mm to 396 mm (Fig. 4.4b). The VWC below this snow pit was also supersaturated. It was observed at the toe of the north aspect slope on April 4, 2014 that the water table was approximately 20 cm below the surface and on April 19, 2014 it was at the surface and likely above the soil surface and within the snowpack as indicated by the large increase in SWE. This was the only location that a depth to the water table was estimated. All locations show a clear melting trend after April 19 with both SWE and depth decreasing each survey date. The VWC during 2014 showed variable observations of increasing and decreasing soil moisture beneath a melting snowpack

(Fig. 4.4). However, soil moisture clearly dries rapidly after snow disappearance as was observed at the south aspect locations. VWC mean values generally remained similar to previous observations at each location while snow was present with the exception of a south aspect location that increased each survey and at the base of the north aspect that decreased immediately following the observation of super saturation. The locations that displayed larger differences in mean observations from survey to survey relative to other locations also displayed larger variability in VWC individual readings (Fig. 4.4).

In 2015 four locations showed an increase in SWE from April 3 to April 17 (Fig. 4.4c). However, two of these locations also resulted in an increase in depth and these changes can likely be attributed to local variability. The other locations that experienced an increase in SWE and accompanied by a decrease in depth were located at the base of the south aspect slope and high on the north aspect slope. VWC at these locations did not measure as super saturated (Fig. 4.4). Also in 2015, only two locations had a measurable snowpack for all four surveys. As with previous observations, soil moisture decreased noticeably after the disappearance of snow for all locations. Many of the increases in VWC after the disappearance of snow in 2015 are the result of rain events that occurred frequent relative to other years (Fig. 4.4).

Also observed during manual surveys in 2013 and 2014 were the presence of frozen ice “veins” immediately above the snow-soil-interface (SSI) (Fig. 4.5). These were observed on the north

Figure 4.5: Picture of frozen “ice vein” observed at the snow-soil-interface (SSI) with foot shown for scale.

aspect and on the flat aspect near the base of the north aspect only and appeared to be continuous. The occurrence of this phenomena was in the direction of the hillslope fall line, even with a small slope on the flat aspect, and on ground that was not super saturated. These ice “veins” were not observed in 2015. Also qualitatively observed was the relative density of snow in each pit in 2014. On the north aspect slope, snow density tended to decrease as height above the SSI increased. Additionally the thickness of the higher density snow at the bottom of each snow pit increased downslope. The higher density snow closer to the SSI was qualitatively observed to also have higher liquid water content. These qualitative observations were primarily in 2014 and occurred during the second, third, and fourth surveys of the year.

Pattern Analysis

Static parameters of elevation, slope, and aspect showed mostly low correlations to VWC during observations and little significance at the 0.05 level (Table 4.1). The only static parameters that resulted in a pearson’s r value of magnitudes above 0.5 were slope and aspect, all of which occurred later in the observation period for each year and the only one that showed any significance was aspect on May 16, 2015. It is important to recognize that these results considered significant occur during the last three surveys of 2015 when soil had been exposed to the atmosphere from complete loss of snow for 31% of measurement locations on April 17, 62% of locations on May 2, and 93% of locations on May 17. This contrast in correlation of soil moisture to static parameters in 2015 relative to other observation years can also be seen in the dynamic parameters tested (Table 4.1).

The dynamic parameters tested for correlation to VWC included SWE, Δ SWE, first measured SWE, and first measured VWC. These dynamic parameters showed, in general, higher correlations and more occurrences of significance at the 0.05 and 0.01 level relative to the static parameters (Table 4.1). The highest pearson’s r values of all parameters, static and dynamic, was the VWC measured during the first survey that are positive and all but one

Table 4.1. Pattern analysis of soil moisture measurements based on elevation, slope angle, slope aspect, Snow Water Equvalent (SWE), change in SWE, SWE on first survey of the year, and soil moisture (VWC) on first survey of the year. Significance is shown with table cell shading and **bold text** representing a p-value less than 0.05 and **<u>underlined text</u>** a p-value less than 0.01.

		slope	aspect	elev.	SWE	Δ SWE	1st SWE	1st VWC
2013	6-Apr	0.19	0.36	0.02	**0.52**	----	----	----
	4-May	0.12	0.51	0.12	-0.25	-0.68	-0.57	**<u>0.92</u>**
2014	4-Apr	-0.21	0.24	-0.12	-0.36	----	----	----
	19-Apr	-0.40	0.33	0.03	-0.08	**-0.82**	**-0.83**	**<u>0.99</u>**
	3-May	-0.63	0.15	-0.02	0.30	-0.38	**<u>-0.89</u>**	**<u>0.95</u>**
	17-May	0.57	0.62	-0.40	0.62	-0.48	-0.39	**<u>0.82</u>**
2015	3-Apr	-0.18	0.14	-0.22	0.12	----	----	----
	17-Apr	-0.08	**0.40**	-0.01	**<u>0.56</u>**	-0.09	**0.47**	**<u>0.95</u>**
	2-May	0.11	**0.45**	0.26	**<u>0.87</u>**	0.36	**<u>0.56</u>**	**<u>0.80</u>**
	16-May	0.06	**<u>0.52</u>**	0.26	**0.46**	**0.50**	0.15	**0.48**

correlation being significant at the 0.01 level. Pearson's r values tend to decrease in magnitude for this parameter as time from the first survey increases (Table 4.1, Fig. 4.6). The correlation of SWE to VWC was observed to be inconsistent in strength, direction, and significance with a lot of variability each survey (2014 as an example, Fig. 4.6). Δ SWE and first measured SWE show similar negative correlations in 2013 and 2014 but positive correlations in 2015 (Table 4.1). The only significant correlations between SWE and VWC are positive and mostly occurred in 2015 when much of the survey area was snow free and the correlation is likely influenced by the presence of snow versus no snow; However, a significant positive correlation is also observed on April 6, 2013 when the entire study area was snow covered. The negative correlations for VWC to Δ SWE indicate that in 2013 and 2014 locations that had lesser changes in SWE were locations where higher VWC was measured, though this was significant at the 0.05 level on April 19, 2014 only. It is important to note that this includes locations that observed an increase in SWE rather than a loss as most locations. In 2015, VWC shows a weak to no positive correlation to Δ SWE and is significant at the 0.05 level only on May 16. This is the date that 93% of the locations had no snow and 62% of the locations had no snow during the previous

survey, thus many locations observed a Δ SWE value of zero and the correlation is likely controlled by higher VWC at locations that had snow during the previous survey. The similar correlation direction and magnitudes of VWC to first measured SWE show that in 2013 and 2014 areas that had less SWE during the first survey tended to have higher measured VWC, significant at the 0.05 level on April 19, 2014, and at the 0.01 level on May 3, 2014 (Table 4.1, Fig. 4.6). The opposite occurs in 2015 when the higher amount of soil moisture again generally occurs where there is still snow on April 3 and this lasts through the survey period, as the snow melts out creating a smaller snow covered area. The locations that continue to have snow later into the period were those with higher initial SWE and have higher VWC due to lack of direct exposure to the atmosphere, this is shown in the increasing positive correlation and significance from April 17 to May 2 in 2015 and then again decreasing correlation strength and lack of significance on May 16 when 93% of the study area is snow free.

VWC Time Series Data

Soil moisture sensors clearly showed the diurnal fluctuation of VWC from snowmelt infiltration across the SSI and the fluctuation in temperature (Fig. 4.7). The VWC sensors at both the SNOTEL site and on the north aspect slope show the relatively quick drying after snow disappearance. One noticeable difference from the SNOTEL sensors and the north aspect hillslope sensors is the difference in values between 5 cm and 20 cm VWC at the north aspect slope and the similarity in values between these depths at the SNOTEL site. At the SNOTEL site, a flat aspect, the 5 cm and 20 cm VWC follow a similar trend remaining within 5% of each other the entire time. On the north aspect hillslope there is a greater difference between the 5 cm and 20 cm deep VWC readings, showing a difference of approximately 15-20% throughout the entire time beneath a snowpack. The 12.5 cm deep sensors on the north aspect slope display a more similar VWC value to the 20 cm sensor relative to the 5 cm sensor as well (Fig. 4.7). These trends are less noticeable during the spring of 2014, though this may be influenced by the mid-winter installation of the sensors. Soil temperature at 5 cm remains between 0^0C and

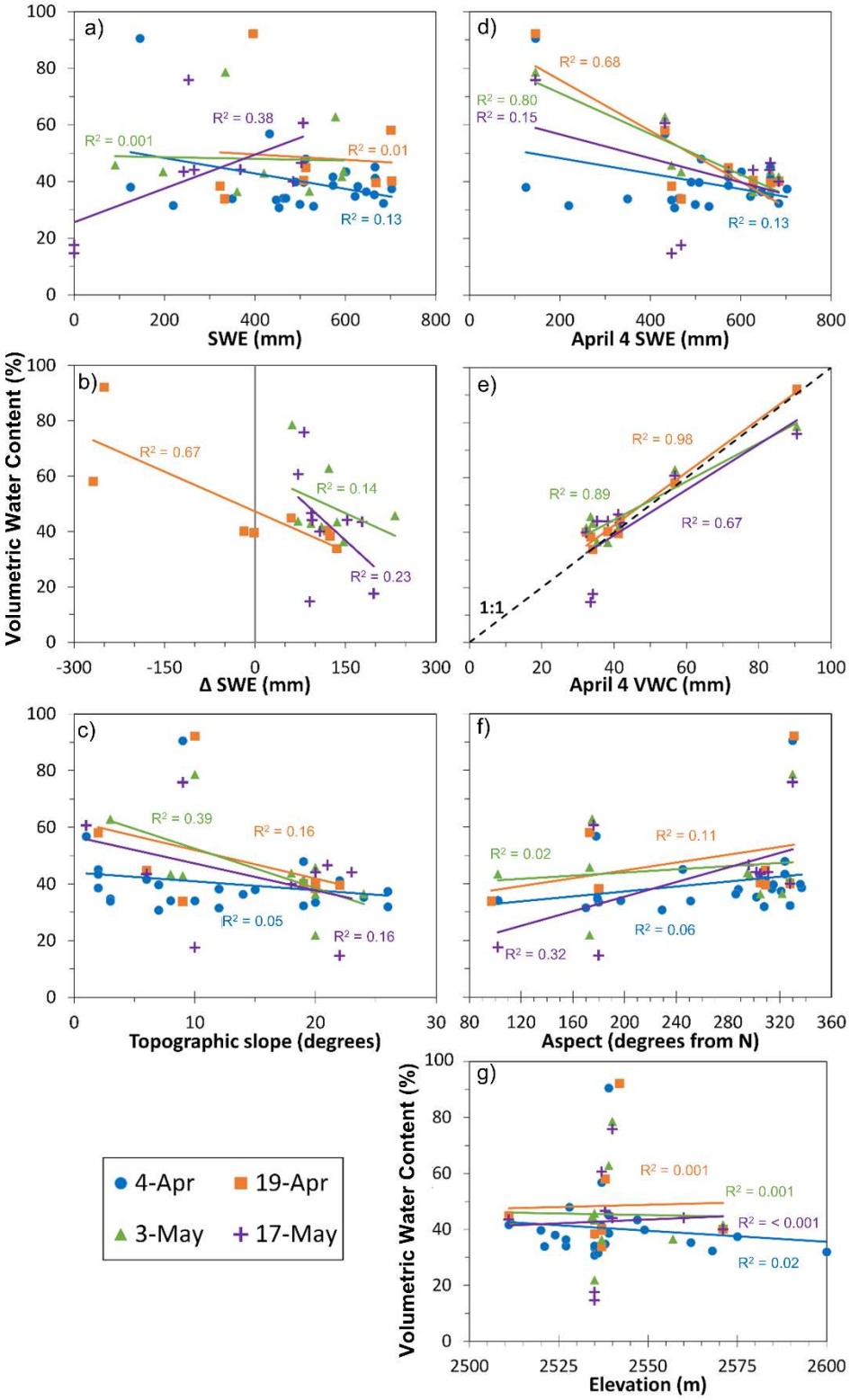

Figure 4.6: Pattern analysis of the 2014 volumetric water content (VWC) surveys with R^2 (squared pearson r values from table 4.1) values shown for dynamic controls of a) snow water equivalent (SWE), b) change in SWE between surveys, c) topographic slope, d) April 4, 2014 SWE value, and e) April 4, 2014 VWC value, f) aspect, and g) elevation.

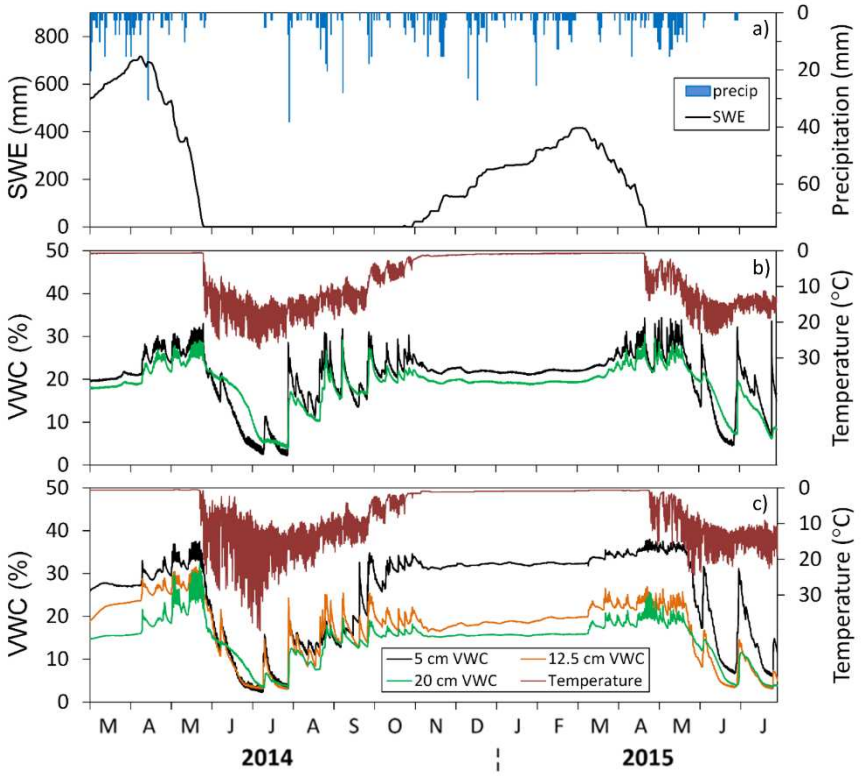

Figure 4.7: (a) Daily snow water equivalent (SWE) and precipitation recorded and (b) the hourly soil volumetric water content (VWC) at the relatively flat SNOTEL site as well as (c) the hourly VWC recorded using the installed sensors on the north aspect slope.

1^0C (Fig. 4.7). Temperatures begin to fluctuate in the soil at the SNOTEL station at about the same time of snow disappearance. This same trend appears to occur on the north aspect slope in 2014, but not in 2015 when soil temperatures appear to fluctuate prior to the disappearance of snow on the north aspect slope but corresponds more closely with the disappearance of snow at the SNOTEL site. During spring snowmelt, the 5 cm VWC sensor always recorded greater values on the north aspect slope relative to the SNOTEL site and the majority of measurements at 20 cm deep were greater at the SNOTEL site (Fig. 4.7).

Discussion

In this study we observed the spatio-temporal variability of bulk SWE and near surface VWC at the DL study site during the 2013, 2014, and 2015 spring snowmelt seasons. Peak SWE at the SNOTEL station occurred at different times relative to the survey period each year, though the snowmelt period was still captured each year and insights may be gained from the

data collected. The 2013, 2014, and 2015 years surveyed represent 90%, 125%, and 75% peak SWE, respectively (Fig. 4.2), offering observations for a variety of conditions. The 2015 observations included the addition of multiple rain on snow events for added variety of snowmelt conditions. The multiple years of observation at a subalpine location with a deep seasonally persistent snowpack offers analysis of SWE and VWC patterns that have previously been limited to lower elevations near the rain-snow transition zone [*Williams et al., 2009*] and an alpine environment [*Litaor et al., 2008*].

At DL, the only static control that displayed any significance at the 0.05 level was hillslope aspect and this appeared to increase in significance and strength with time indicating that it is likely more related to the presence or absence of snow and perhaps influences from rain (Table 4.1). The soils on the south aspect slope are generally coarser than the north or flat aspects, suggesting that soil water retention is higher on north aspects similar to observations in Idaho [*Geroy et al.*, *2011*]. This was reflected with the north aspect soils generally having higher water contents than south aspect soils, both with and without the presence of a snowpack during the survey periods (Figs 4.4). Near surface soil moisture approached a relative equilibrium soil moisture state with a persistent snowpack rather than varying through time on the north and flat aspects whereas the south aspect hillslope generally increased throughout the melt season beneath a snowpack. As the snowpack melts the shallow soil moisture has a diurnal fluctuation, but returns to the equilibrium soil moisture state each night on the north and flat aspects. This is shown both with the strong significant correlation between VWC and the first measured VWC (Table 4.1), in the soil moisture sensors installed on the north aspect slope, and the soil moisture sensors at the SNOTEL site (Fig. 4.7). The locations within DL that were wet relative to the other locations during the first survey remained as such for all following surveys when snow persistently covered the study area. This result compares well to the study by *Williams et al.* [*2009*] that showed similar observations at a smaller scale beneath a shallower snowpack at a lower elevation. Variability in soil parameters will influence the level of saturation

that a location establishes beneath a snowpack as well as influencing the infiltration or lateral flow of meltwater across the SSI when on a slope.

The movement of water across layer interfaces has been shown within a snowpack [*Williams et al.*, *2000a; Liu et al., 2004; Williams et al., 2010; Eiriksson et al., 2013*] and occurs at the SSI as well as shown in this study. This will depend upon the parameters of the soil, the parameters of the snow layers, the slope angle, and the rate that meltwater is percolating through the snowpack [*Chapter 3*]. The increases in SWE at locations, the frozen "ice veins" observed in this study (Fig. 4.5) and the qualitative observations of snow density with depth in each snow pit are results from meltwater flowing laterally above the SSI on the north aspect hillslope and on the flat aspect near the base of the north aspect slope. This phenomena was not observed on the south aspect slope. The south aspect hillslope has coarser soil and different meteorological forcing of snowmelt that increases the rate of water percolation from higher exposure to solar radiation (Fig. 4.3). This increased exposure to solar radiation will also increase the rate of snow metamorphism causing the snowpack to be less stratified relative to the snowpack on the flat or north aspect. Layers within a snowpack have been shown through numerical simulations to act as permeability barriers, similar to soil drains, and capillary barriers in Chapter 3. Results of this study suggest that meltwater is flowing above the SSI and downslope through the snowpack on the north aspect hillslope, similar to a soil drain that is caused by a permeability barrier at the SSI and likely at other layer interfaces within the snowpack as well.

The lateral flow of water through the snowpack on the north aspect hillslope is supported by the bulk SWE measurements. The increase of SWE between surveys occurred consistently on the north aspect slope, especially at the base of the slope (Figs. 4.4). In 2013 the increase in SWE was 30 mm greater than the amount of precipitation that was recorded. Wind is not likely causing increased deposition on any particular hillslope in DL due to the slope aspects and wind directions generally running perpendicular (Fig. 4.3), though snow drifts may still occur from

vegetative influences and also cause undercatch of precipitation recordings during snow events. However, care was taken during measurements to avoid any areas that were noticeable wind drifts and the SWE measurements at the SNOTEL pillow show accumulated increases in daily SWE to be less than the 130 mm of precipitation recorded suggesting it is unlikely that a high amount of undercatch occurred in the recorded precipitation data relative to the snow deposited in the study area during the spring survey period. The large increase in SWE at the base of the north aspect slope in 2014 is from the lateral flow of water in snow and also the rising of the water table above the soil surface (Fig. 4.4). Some locations on the north aspect slope in 2014 remained consistent in bulk SWE values while depth decreased and other locations on the hillslope decreased in SWE. This is a result from preferential flow paths within the snowpack causing locations on the hillslope to increase or remain consistent in SWE during active melting from upslope contributions while other locations are losing SWE as water is not flowing through the snowpack uniformly across the hillslope. These preferential flow paths begin to disperse as the topographic gradient is lost near the bottom of the hillslope and increases in SWE may have a correlation length similar to what has been shown in preferential melt patterns in alpine environments [*Sommerfeld et al.*, *1994; Williams et al., 1999*], though further investigation into this is necessary. 2015 shows similar increases in SWE values between surveys that may be the result of rain on snow events occurring that are known to produce lateral flow within snowpacks [*Eiriksson et al.*, *2013*]. It is also difficult to determine if this is isolated to the north aspect hillslope in 2015 due to the lack of snow on the south facing slope during the survey period. The snow pit at the base of the south aspect slope did increase in SWE between surveys, however it is difficult to separate this from local SWE variability due to the relative location of the slope to the stream and floodplain causing a lot of local topographic variability of the ground surface at the measurement location.

The 2014 increase in SWE at the base of the north aspect slope is a result of water flowing down the north aspect slope faster than it can travel through the flat aspect soil to

achieve stream connectivity. There was a lateral wetting front moving towards the stream in April 2014 that once stream connectivity was established the soil VWC and SWE both decreased as water was drained by the stream. This process of stream connectivity and soil moisture status are conditions described by *McNamara* [*2005*] as the winter wet, low flux period and the spring wet, high flux period. During these periods, the observations of this study show that the snowpack increases the storage capacity of an area. At the DL study site in 2014, 270 mm of water was added to and stored in the snowpack at the base of the north aspect hillslope (Fig. 4.4) whereas it likely would have runoff directly over the soil surface without the additional storage provided by the snowpack. This occurs at a location that has a highly organic soil that also has a relatively high storage capacity. The additional storage provided by the snowpack may be important for flood wave attenuation during high rates of snowmelt, rain on snow events, or in the case of organic soil losses due to wildfire.

Results of this study indicate that the north aspect slope of DL study area has flow paths during snowmelt that are similar to an alpine catchment [*Williams et al.*, *2000a; Liu et al., 2004*] and during rain on snow events at lower elevation sites [*Eiriksson et al.*, *2013*]. These flow paths are through the snowpack above the SSI and occur as preferential flow. The parameters of the soil, snow, topography, and rate of snowmelt create an environment on the north aspect slope that produces a permeability barrier to vertically percolating meltwater, causing flow to travel laterally across the interface and downslope, though some water still infiltrates across the interface as it is not a complete barrier to flow like a capillary barrier (Fig. 4.8). The south aspect slope has different parameters of soil, snow, and rates of snowmelt due to the variable meteorological forcing conditions that produce less observed flow laterally across the SSI and more infiltration into the soil (Fig. 4.8). The coarseness of the soil will have an impact on the formation of a permeability barrier at the bottom of a snowpack, where a finer soil will likely produce more diversion of meltwater due to the lower hydraulic conductivity. It is also possible that a soil is coarse enough that a capillary barrier is formed that diverts all vertically percolating

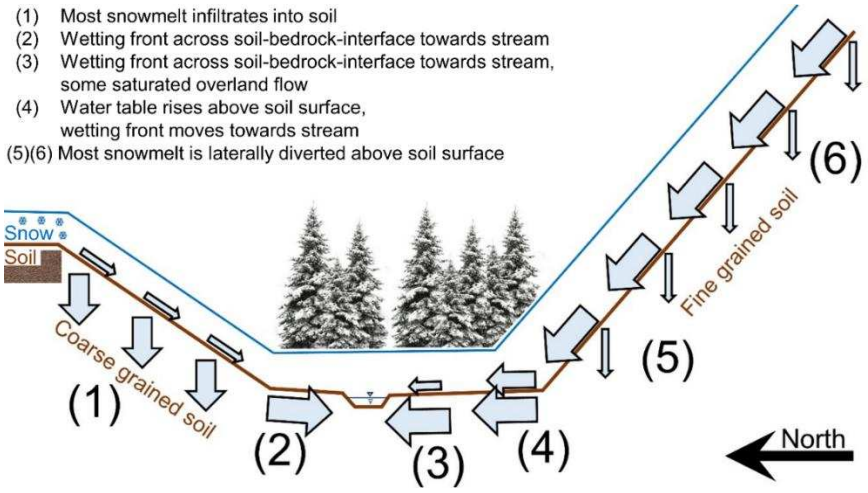

Figure 4.8: Conceptual model of flow paths observed at the Dry Lake study site at the locations defined in Figure 1 as (1) south aspect hillslope, (2) toe of south aspect slope, (3) flat aspect, (4) toe of north aspect slope, (5) low on the north aspect hillslope, and (6) high on the north aspect hillslope.

water for a length downslope as observed by *Eirikkson et al.* [*2015*], though this was not observed at the DL study site. The slope of the hill will affect this phenomena [*Chapter 3*], in DL the north aspect slope is steeper on average (Fig. 4.1), though further testing at multiple slope angles is necessary to investigate this. However, the slope of the south aspect and north aspect slopes in DL are both steep enough to divert meltwater by means of hydraulic barriers.

As permeability barriers form and promote flow paths to develop within the snowpack such as on the north aspect slope, the timing of runoff at the hillslope scale can change dramatically. Snow has been shown to have a higher hydraulic conductivity relative to common soils [*Yamaguchi et al.*, *2010; Domine et al., 2013*]. This is important for hydrologic modeling purposes and flood prediction from snowmelt runoff. Furthermore, any water balance calculations will need to take into account the variable infiltration across the SSI that will occur as a result. From a groundwater recharge perspective, much of the hydraulic gradients driving subsurface flow will be occurring at the base of the north aspect hillslope in situations similar to the DL study area due to the lateral flow of water through the snowpack and soil moisture sensors will only account for a fraction of the total meltwater on hillslopes. Also, at the base of the hillslope the snowpack can add storage up to 270 mm and will have a larger static head

than possible when only considering the soil porosity. However, in the DL study area the south aspect hillslope may act in a more classical conceptual model of snowmelt infiltration somewhat uniformly and travelling across the soil-bedrock interface to recharge groundwater resources and generate streamflow (Fig. 4.8). When considering dynamic hydrologic processes that occur during spring snowmelt in subalpine headwater catchments, it is important to consider the variable flow paths that develop based on factors such as slope, aspect, soil parameters, and snow parameters to move beyond single point measurements and one-dimensional assumptions. Additionally, the bases of hillslopes are an important locations to observe and estimate the amount of hillslope runoff occurring above the SSI relative to flow through the soil in future investigations. Future studies will benefit from consideration of the snow as an extension of the vadose zone during spring snowmelt due to the variably saturated flow that occurs through snow as shown in this study.

Conclusions

The observations of this study occurred during above normal, relatively normal, and below normal snow seasons. We observed the bulk SWE and soil VWC variability in space and time during spring snowmelt with varying meteorological forcing conditions including rain-on-snow events in 2015. Evidence was present of meltwater flowing above the SSI on the north aspect hillslope and to a lesser extent at the base of the north aspect hillslope on a relatively flat aspect. The base of the north aspect hillslope resulted in the convergence of flow paths, both above and below the SSI, causing the water table to rise above the soil surface and into the snowpack in 2014. This event displays the potential for a snowpack in a catchment to increase the water storage capacity of a location by as much as 270 mm of water that would directly runoff otherwise. The south aspect hillslope did not display evidence of water flow through the snowpack above the SSI. The differences in flow path development on the two opposite facing hillslopes is likely due to differences in parameters of the soil, snow, , slope, and snowmelt rates

as a result of meteorological forcing variability producing a permeability barrier on the north aspect hillslope at the SSI.

The formation of a permeability barrier at the SSI will be dependent upon both the snow and soil. Results from this study show that the snow acts as an extension of the vadose zone during spring snowmelt and future investigations will benefit from studying both the snow and soil rather than one or the other as is the case in many current approaches. It will also be important to consider the changing climate of subalpine headwater catchments that will alter the meteorological forcing conditions and thus change the stratigraphy and melt rate of snow. Results from this investigation can help improve hydrologic modeling of processes such as groundwater recharge, streamflow generation, and floods from high rates of snowmelt.

REFERENCES

Adam, J. C., A. F. Hamlet, and D. P. Lettenmaier (2009), Implications of global climate change for snowmelt hydrology in the twenty-first century, Hydrological Processes, 23(7), 962-972, doi: 10.1002/hyp.7201.

Adams, E., A. Slaughter, L. McKittrick, and D. Miller (2011), Local terrain-topography and thermal-properties influence on energy and mass balance of a snow cover, Annals of Glaciology, 52(58), 169-175.

Bales, R. C., N. P. Molotch, T. H. Painter, M. D. Dettinger, R. Rice, and J. Dozier (2006), Mountain hydrology of the western United States, Water Resources Research, 42(8), n/a-n/a, doi: 10.1029/2005wr004387.

Bales, R. C., J. W. Hopmans, A. T. O'Geen, M. Meadows, P. C. Hartsough, P. Kirchner, C. T. Hunsaker, and D. Beaudette (2011), Soil Moisture Response to Snowmelt and Rainfall in a Sierra Nevada Mixed-Conifer Forest, Vadose Zone Journal, 10(3), 786, doi: 10.2136/vzj2011.0001.

Blankinship, J. C., M. W. Meadows, R. G. Lucas, and S. C. Hart (2014), Snowmelt timing alters shallow but not deep soil moisture in the Sierra Nevada, Water Resources Research, 50(2), 1448-1456, doi: 10.1002/2013wr014541.

Clilverd, H. M., D. M. White, A. C. Tidwell, and M. A. Rawlins (2011), Sensitivity of Northern Groundwater Recharge to Climate Change: A Case Study in Northwest Alaska, Journal of the American Water Resources Association, 47(6), 1228-1240, doi: 10.1111/j.1752-1688.2011.00569.x.

Clow, D. W. (2010), Changes in the Timing of Snowmelt and Streamflow in Colorado: A Response to Recent Warming, Journal of Climate, 23(9), 2293-2306, doi: 10.1175/2009jcli2951.1.

Colbeck, S. (1979), Water-flow through heterogeneous snow, Cold Regions Science and Technology, 1(1), 37-45, doi: 10.1016/0165-232X(79)90017-X.

Domine, F., S. Morin, E. Brun, M. Lafaysse, and C. M. Carmagnola (2013), Seasonal evolution of snow permeability under equi-temperature and temperature-gradient conditions, The Cryosphere, 7(6), 1915-1929, doi: 10.5194/tc-7-1915-2013.

Eiriksson, D., M. Whitson, C. H. Luce, H. P. Marshall, J. Bradford, S. G. Benner, T. Black, H. Hetrick, and J. P. McNamara (2013), An evaluation of the hydrologic relevance of lateral flow in snow at hillslope and catchment scales, Hydrological Processes, 27(5), 640-654, doi: 10.1002/hyp.9666.

Elder, K., D. Cline, G. E. Liston, and R. Armstrong (2009), NASA Cold Land Processes Experiment (CLPX 2002/03): Field Measurements of Snowpack Properties and Soil Moisture, Journal of Hydrometeorology, 10(1), 320-329, doi: 10.1175/2008jhm877.1.

Fassnacht, S. R., M. L. Cherry, N. B. H. Venable, and F. Saavedra (2016), Snow and albedo climate change impacts across the United States Northern Great Plains, The Cryosphere, 10, 329-339, doi: 10.5194/tc-10-329-2016.

French, H., and A. Binley (2004), Snowmelt infiltration: monitoring temporal and spatial variability using time-lapse electrical resistivity, Journal of Hydrology, 297(1-4), 174-186, doi: 10.1016/j.jhydrol.2004.04.005.

Geroy, I. J., M. M. Gribb, H. P. Marshall, D. G. Chandler, S. G. Benner, and J. P. McNamara (2011), Aspect influences on soil water retention and storage, Hydrological Processes, 25, 3836-3842, doi: 10.1002/hyp.8281.

Harpold, A., P. Brooks, S. Rajagopal, I. Heidbuchel, A. Jardine, and C. Stielstra (2012), Changes in snowpack accumulation and ablation in the intermountain west, Water Resources Research, 48(11), n/a-n/a, doi: 10.1029/2012wr011949.

Harpold, A. A., N. P. Molotch, K. N. Musselman, R. C. Bales, P. B. Kirchner, M. Litvak, and P. D. Brooks (2015), Soil moisture response to snowmelt timing in mixed-conifer subalpine forests, Hydrological Processes, 29(12), 2782-2798, doi: 10.1002/hyp.10400.

Harrington, R. F., R. C. Bales, and P. Wagnon (1996), Variability of meltwater and solute fluxes from homogeneous melting snow at the laboratory scale, Hydrological Processes, 10(7), 945-953, doi: 10.1002/(sici)1099-1085(199607)10:7<945::aid-hyp349>3.0.co;2-s.

Harrington, R., and R. C. Bales (1998), Interannual, seasonal, and spatial patterns of meltwater and solute fluxes in a seasonal snowpack, Water Resources Research, 34(4), 823-831, doi: 10.1029/97wr03469.

Heilig, A., C. Mitterer, L. Schmid, N. Wever, J. Schweizer, H. P. Marshall, and O. Eisen (2015), Seasonal and diurnal cycles of liquid water in snow-Measurements and modeling, Journal of Geophysical Research: Earth Surface, 120, doi: 10.1002/2015JF003593.

Hinckley, E.-L. S., B. A. Ebel, R. T. Barnes, R. S. Anderson, M. W. Williams, and S. P. Anderson (2014), Aspect control of water movement on hillslopes near the rain-snow transition of the Colorado Front Range, Hydrological Processes, 28(1), 74-85, doi: 10.1002/hyp.9549.

Hunsaker, C. T., T. W. Whitaker, and R. C. Bales (2012), Snowmelt Runoff and Water Yield Along Elevation and Temperature Gradients in California's Southern Sierra Nevada1, JAWRA Journal of the American Water Resources Association, 48(4), 667-678, doi: 10.1111/j.1752-1688.2012.00641.x.

Jencso, K., B. McGlynn, M. Gooseff, S. Wondzell, K. Bencala, and L. Marshall (2009), Hydrologic connectivity between landscapes and streams: Transferring reach-and plot-scale understanding to the catchment scale, Water Resources Research, 45, doi: 10.1029/2008WR007225.

Jencso, K. G., and B. L. McGlynn (2011), Hierarchical controls on runoff generation: Topographically driven hydrologic connectivity, geology, and vegetation, Water Resources Research, 47(11), n/a-n/a, doi: 10.1029/2011wr010666.

Kampf, S., J. Markus, J. Heath, and C. Moore (2015), Snowmelt runoff and soil moisture dynamics on steep subalpine hillslopes, Hydrological Processes, 29(5), 712-723, doi: 10.1002/hyp.10179.

Katsushima, T., S. Yamaguchi, T. Kumakura, and A. Sato (2013), Experimental analysis of preferential flow in dry snowpack, Cold Regions Science and Technology, 85, 206-216, doi: 10.1016/j.coldregions.2012.09.012.

Kattelmann, R., and J. Dozier (1999), Observations of snowpack ripening in the Sierra Nevada, California, USA, Journal of Glaciology, 45(151), 409-416.

Koch, F., M. Prasch, L. Schmid, J. Schweizer, and W. Mauser (2014), Measuring Snow Liquid Water Content with Low-Cost GPS Receivers, Sensors, 14(11), 20975-20999, doi: 10.3390/s141120975.

Kormos, P., D. Marks, J. McNamara, H. Marshall, A. Winstral, and A. Flores (2014), Snow distribution, melt and surface water inputs to the soil in the mountain rain-snow transition zone, Journal of Hydrology, 519, 190-204, doi: 10.1016/j.jhydrol.2014.06.051.

Laudon, H., J. Seibert, S. Kohler, and K. Bishop (2004), Hydrological flow paths during snowmelt: Congruence between hydrometric measurements and oxygen 18 in meltwater, soil water, and runoff, Water Resources Research, 40(3), doi: 10.1029/2003WR002455.

Liston, G. E., and K. Elder (2006), A distributed snow-evolution modeling system (SnowModel), Journal of Hydrometeorology, 7, 1259-1276.

Litaor, M. I., M. Williams, and T. R. Seastedt (2008), Topographic controls on snow distribution, soil moisture, and species diversity of herbaceous alpine vegetation, Niwot Ridge, Colorado, Journal of Geophysical Research, 113(G2), doi: 10.1029/2007jg000419.

Liu, F., M. W. Williams, and N. Caine (2004), Source waters and flow paths in an alpine catchment, Colorado Front Range, United States, Water Resources Research, 40(9), n/a-n/a, doi: 10.1029/2004wr003076.

López-Moreno, J. I., S. R. Fassnacht, S. Beguería, and J. B. P. Latron (2011), Variability of snow depth at the plot scale: implications for mean depth estimation and sampling strategies, The Cryosphere, 5(3), 617-629, doi: 10.5194/tc-5-617-2011.

López-Moreno, J. I., J. Revuelto, M. Gilaberte, E. Morán-Tejeda, M. Pons, E. Jover, P. Esteban, C. García, and J. W. Pomeroy (2013), The effect of slope aspect on the response of snowpack to climate warming in the Pyrenees, Theoretical and Applied Climatology, 117(1-2), 207-219, doi: 10.1007/s00704-013-0991-0.

Marsh, P., and M.-K. Woo (1985), Meltwater movement in natural heterogeneous snow covers, Water Resources Research, 21(11), 1710-1716.

Marsh, P. (1987), Grain growth in a wet arctic snow cover, Cold Regions Science and Technology, 14, 23-31.

Marsh, P., and J. W. Pomeroy (1993), The Impact of heterogeneous flow paths on snowmelt runoff chemistry, in *Eastern Snow Conference*, edited, pp. 231-238, Quebec City.

McNamara, J. P., D. Chandler, M. Seyfried, and S. Achet (2005), Soil moisture states, lateral flow, and streamflow generation in a semi-arid, snowmelt-driven catchment, Hydrological Processes, 19(20), 4023-4038, doi: 10.1002/hyp.5869.

Mitterer, C., A. Heilig, J. Sweizer, and O. Eisen (2011a), Upward-looking ground-penetrating radar for measuring wet-snow properties, Cold Regions Science and Technology, 69, 129-138, doi: 10.1016/j.coldregions.2011.06.003.

Mitterer, C., H. Hirashima, and J. Schweizer (2011b), Wet-snow instabilities: comparison of measured and modelled liquid water content and snow stratigraphy, Annals of Glaciology, 52(58), 201-208.

Molotch, N. P., P. D. Brooks, S. P. Burns, M. Litvak, R. K. Monson, J. R. McConnell, and K. Musselman (2009), Ecohydrological controls on snowmelt partitioning in mixed-conifer sub-alpine forests, Ecohydrology, 2(2), 129-142, doi: 10.1002/eco.48.

Molotch, N. P., and L. Meromy (2014), Physiographic and climatic controls on snow cover persistence in the Sierra Nevada Mountains, Hydrological Processes, 28(16), 4573-4586, doi: 10.1002/hyp.10254.

Musselman, K. N., N. P. Molotch, and P. D. Brooks (2008), Effects of vegetation on snow accumulation and ablation in a mid-latitude sub-alpine forest, Hydrological Processes, 22(15), 2767-2776, doi: 10.1002/hyp.7050.

Rasmussen, R., et al. (2014), Climate Change Impacts on the Water Balance of the Colorado Headwaters: High-Resolution Regional Climate Model Simulations, Journal of Hydrometeorology, 15(3), 1091-1116, doi: 10.1175/jhm-d-13-0118.1.

Richer, E. E., S. K. Kampf, S. R. Fassnacht, and C. C. Moore (2013), Spatiotemporal index for analyzing controls on snow climatology: application in the Colorado Front Range, Physical Geography, 34(2), 85-107.

Sexstone, G. A., and S. R. Fassnacht (2014), What drives basin scale spatial variability of snowpack properties in northern Colorado?, The Cryosphere, 8(2), 329-344, doi: 10.5194/tc-8-329-2014.

Sommerfeld, R., R. Bales, and A. Mast (1994), Spatial statistics of snowmelt flow – Data from lysimeters and aerial photos, Geophysical Research Letters, 21(25), 2821-2824, doi: 10.1029/94GL02493.

Storck, P., D. P. Lettenmaier, and S. M. Bolton (2002), Measurement of snow interception and canopy effects on snow accumulation and melt in a mountainous maritime climate, Oregon, United States, Water Resources Research, 38(11), 5-1-5-16, doi: 10.1029/2002wr001281.

Techel, F., and C. Pielmeier (2011), Point observations of liquid water content in wet snow - investigating methodical, spatial and temporal aspects, The Cryosphere, 5(2), 405-418, doi: 10.5194/tc-5-405-2011.

The National Map, U. S. G. S. (2015), 3DEP products and services: The national Map, 3D Elevation Program Web page, accessed [November, 2015], edited, http://nationalmap.gov/3dep_prodserv.html.

Williams, C. J., J. P. McNamara, and D. G. Chandler (2009), Controls on the temporal and spatial variability of soil moisture in a mountainous landscape: the signature of snow and complex terrain, Hydrology and Earth System Sciences, 13, 1325-1336.

Williams, M. W., R. Sommerfeld, S. Massman, and M. Rikkers (1999), Correlation lengths of meltwater flow through ripe snowpacks, Colorado Front Range, USA, Hydrological Processes, 13(1807-1826).

Williams, M. W., M. Rikkers, and W. T. Pfeffer (2000a), Ice columns and frozen rills in a warm snowpack, Green Lakes Valley, Colorado, USA, Nordic Hydrology, 31(3), 169-186.

Williams, M. W., M. Rikkers, and W. T. Pfeffer (2000b), Ice columns and frozen rills in a warm snowpack, Green Lakes Valley, Colorado, USA, Nordic Hydrolocy, 31(3), 169-186.

Williams, M. W., C. Seibold, and K. Chowanski (2009), Storage and release of solutes from a subalpine seasonal snowpack: soil and stream water response, Niwot Ridge, Colorado, Biogeochemistry, 95(1), 77-94, doi: 10.1007/s10533-009-9288-x.

Williams, M. W., T. A. Erickson, and J. L. Petrzelka (2010), Visualizing meltwater flow through snow at the centimetre-to-metre scale using a snow guillotine, Hydrological Processes, n/a-n/a, doi: 10.1002/hyp.7630.

Yamaguchi, S., T. Katsushima, A. Sato, and T. Kumakura (2010), Water retention curve of snow with different grain sizes, Cold Regions Science and Technology, 64(2), 87-93, doi: 10.1016/j.coldregions.2010.05.008.

CHAPTER 5: WETTING AND DRYING VARIABILITY OF THE SHALLOW SUBSURFACE BENEATH A SNOWPACK IN CALIFORNIA'S SOUTHERN SIERRA NEVADA[2]

Introduction

In recent years, studies have implicated changing snow conditions and soil moisture in the mountainous regions of the western United States [*Adams et al., 2009, Harpold et al., 2014*]. Hydrologic predictions may be improved through advances in understanding of the connections between snowmelt and soil moisture at the catchment scale [*Bales et al., 2006*]. A number of studies have also shown the importance of sub-surface flow contributions to snowmelt driven streamflow [e.g. *Winter, 2007; Ghasemizade and Schirmer, 2013*] in addition to slope and aspect controls on a hill-slope scale [*Hinckley et al., 2014; Kampf et al., 2014*]. Many studies, however, do not account for the soil moisture variability that may develop at the sub-hillslope scale during snowmelt processes. With the projected impacts that global climate change may have on a snowmelt environment [*Adams et al., 2009*], it is important to better understand the sub-surface dynamics that occur. With a better understanding of these processes, snowmelt water availability could be appropriately allocated between surface runoff, groundwater recharge, and evapotranspiration.

Spatial variability of snowpack properties such as depth, density, and thus snow water equivalent (SWE) are known to exist from the fine (meters) scale [*Fassnacht et al., 2009*] to the coarse (10s to 100s of meters) scale [*Fassnacht et al., 2008; Sexstone and Fassnacht, 2014*]. Additionally, sub-alpine forests at mid-latitudes are known to have greater ablation rates of the snowpack in open areas [*Musselman et al., 2008*]. Such heterogeneity in the snowpack and ablation processes may create variability in the wetting and drying dynamics of the shallow sub-surface from the catchment to the sub-hillslope scale. In addition, potential exists for lateral flow

[2]Webb, R.W., S.R. Fassnacht, and M.N. Gooseff (2015), Wetting and Drying Variability of the Shallow Subsurface beneath a Snowpack in California's Southern Sierra Nevada, Vadose Zone Journal, 14(8), 0, doi: 10.2136/vzj2015.12.0182.

along soil-bedrock interfaces [*Flint et al., 2008*], which would be controlled by the permeability of the bedrock and the flux rates of the infiltrating snow melt, thus adding complexity to the prediction of soil wetting and drying.

Most studies investigating the infiltration and movement of sub-surface water derived from snowmelt take a uniform one-dimensional (vertical) approach at the catchment, hillslope, or plot scale [*e.g. Flint et al., 2008; Blankinship et al., 2014*]. *Flint et al*. [*2008*] measured snow depth at a location 10 m from soil moisture sensors and observed snow depth measurements of zero while snow persisted above the soil moisture sensors. *Iwata et al*. [*2011*] investigated snowmelt infiltration into frozen and non-frozen ground at the plot scale using a one-dimensional approach, concluding that this did not capture completely the observed dynamics. Observations made in these studies show that consideration of spatio-temporal variability in the snowpack accumulation and ablation is important to understanding soil moisture distribution during snow accumulation and melt.

The goal of this study is to gain understanding of soil moisture wetting and drying dynamics that occur beneath a seasonally persistent snowpack in non-frozen soil through the following objectives: 1) determine the number of wetting and drying events that occur at depth in one dimensional profiles of soil moisture sensors during snow accumulation and melt; and 2) use instrumentation under tree canopies, at drip edges, and in openings to identify the wetting and drying variability between locations and depths within the top one meter of soil in a mixed-conifer forest.

Study Site & Instrumentation

Data for this study are from the Providence Creek headwaters, part of the Southern Sierra Critical Zone Observatory (CZO) in California, USA (37.068°N, 119.191°W) (see *Bales et al., 2011 and Hunsaker et al., 2012* for more information on this CZO study site). The CZO is predominately a mixed-conifer forest (76-99%) with small amounts of mixed chaparral and barren land cover. The soils are derived from decomposed granite and their properties change

with elevation. Soils do not freeze during the winter and remain wet beneath a snowpack relative to summer months. Soil moisture increases have been determined to be dominated by snowmelt events, with spring and summer rainfall mainly affecting sites in the open [*Bales et al., 2011*].

The measurements used for this study are from instruments installed near a lower (1753 m) and an upper (1981 m) meteorological station (Fig. 5.1). The meteorological stations have been operated by the U.S. Forest Service's Pacific Southwest Region as part of the Kings River Experimental Watersheds system [*Hunsaker et al., 2012*] monitoring air temperature, relative humidity, wind speed, wind direction, radiation, snow depth, snow water equivalent (upper station only, by means of a snow pillow), and rainfall intensity [since 2001, *Hunsaker, 2011*]. Additional sensors to measure snow depth, soil moisture, and temperature were installed in 2007 near the meteorological stations as part of the CZO [*Bales et al., 2011*].

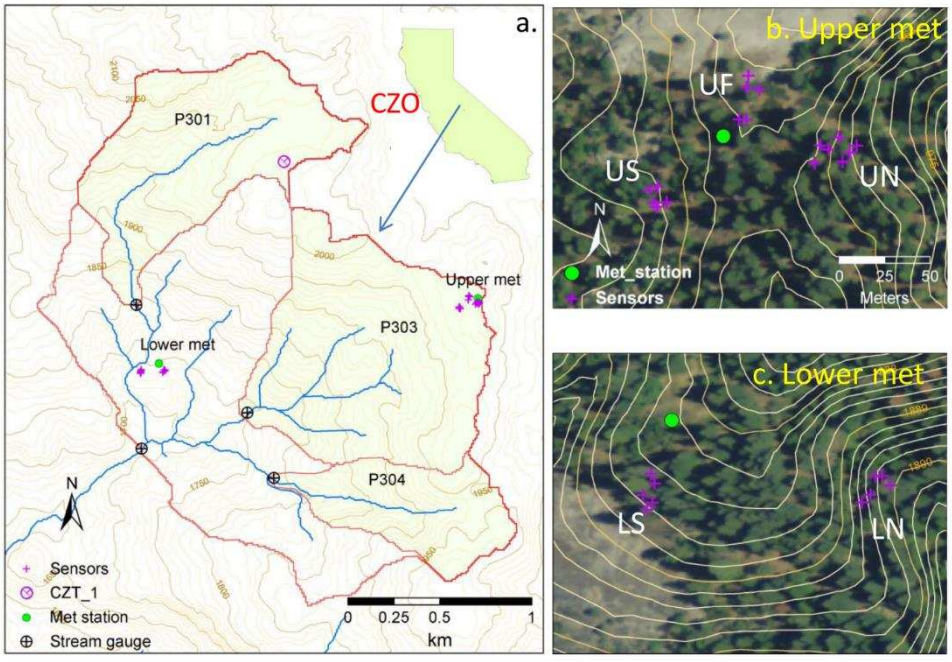

Figure 5.1: Critical Zone Observatory (CZO) map displaying a) location, CZO catchments, and instrument and sensor clusters with 10 m elevation contours, b) upper meteorological station, and c) lower meteorological station sensor locations with 2 m elevation contours. Background of b) and c) is from aerial photography. [*Bales et al., 2011*]

Table 5.1: Summary of locations for sensors used in this study showing elevation (1980 m for upper, 1750 m for lower), aspect, vegetation type, and canopy cover for drip edge (de), under canopy (uc) and open canopy. Check marks indicate a sensor was installed whereas shaded boxes indicate no sensor installed.

		Tree Species and Canopy Cover										
Elevation Aspect	**depth (cm)**	***Abies Concolor***		***Calocedrus decurrens***		***Pinus lambertiana***		***Pinus ponderosa***		***Quercus kelloggii***		
		de	**uc**	**de**	**uc**	**de**	**uc**	**de**	**uc**	**de**	**uc**	**open**
Upper North	**10**	✓	✓	✓	✓	✓	✓					✓
	30	✓	✓	✓	✓	✓	✓					✓
	60	✓	✓	✓	✓	✓	✓					✓
	90	✓	✓	✓	✓	✓	✓					✓
Upper Flat	**10**	✓	✓					✓	✓			✓
	30	✓	✓					✓	✓			✓
	60	✓	✓					✓	✓			✓
	90	✓	✓					✓				
Upper South	**10**	✓	✓							✓	✓	✓
	30	✓	✓							✓	✓	✓
	60	✓	✓							✓	✓	✓
	90										✓	
Lower North	**10**	✓	✓	✓	✓							✓
	30	✓	✓	✓	✓							✓
	60	✓	✓	✓	✓							✓
	90	✓		✓	✓							✓
Lower South	**10**			✓	✓			✓	✓			✓
	30			✓	✓			✓	✓			✓
	60			✓	✓			✓	✓			✓
	85											✓

The CZO sensors measure snow depth, soil moisture, and temperature for varying aspects (north and south-facing), elevations (upper-1980 m and lower-1750 m), and canopy conditions (open, drip edge, and under canopy) (Table 5.1) [*Bales et al., 2013*]. Additional data are collected on a flat aspect for the upper elevation sensor cluster. The five elevation and aspect locations are on slopes ranging from 7 to 18 degrees. Sensors were installed with an open canopy, under the canopy, and at the drip edges of 11 different mature trees, with at least two trees at each elevation and aspect. Mature trees were considered to be those ~40 m in height with canopies extending two to four m from the trunk. Open canopy sensors were placed

approximately one to five meters from the drip edge sensors with the under canopy and drip edge sensors typically two to four meters apart. The five tree species included in this study are white fir (*Abies concolor*, ac), ponderosa pine (*Pinus ponderosa*, pp), black oak (*Quercus kelloggii*, qk) sugar pine (*Pinus lambertiana*, pl), and incense cedar (*Calocedrus decurrens*, cd). Locations of sensors hereafter will be abbreviated as a sequence of letters to denote elevation as upper (U) or lower (L), aspect as north (N), south (S), or flat (F), tree species by Latin abbreviation, and with canopy as under canopy (uc), drip edge (de), or open canopy (open). For example the sensors at upper elevation (U) with flat aspect (F) located at the ponderosa pine (pp) drip edge (de) will be abbreviated as UF_ppde. Table 5.1 summarizes the 27 sensor locations, showing elevation, aspect, tree species, canopy association, and depths of soil moisture sensors.

An ultrasonic snow depth sensor (Judd Communications, Salt Lake City, UT) was installed at each measurement location 3 m above ground on a steel arm about 75 cm from a vertical steel pipe driven into the ground. Soil pits were excavated to a depth of 1 m with a 30 cm diameter directly below each snow depth sensor. Within each of these soil pits a soil temperature and volumetric water content (VWC) sensors (Decagon ECH$_2$O-TM, Decagon, Pullman, WA) were installed at depths of 10, 30, 60, and 90 cm. All depths were measured from the ground surface and include litter layers, where applicable. Only the top three sets of soil sensors were installed at some sensor locations (UF, US, LN, and LS) due to the presence of boulders or bedrock shallower than 90 cm, yielding a total of 97 sensors across 27 locations [*Bales et al., 2013*].

Methods

Three water years (2009, 2010, and 2011) of data were analyzed. Daily averages of snow depth and meteorological conditions were used to determine the approximate timing of snow accumulation and the end of ablation, while soil moisture was observed at 30 minute intervals.

To compare soil moisture conditions at various locations and to consider antecedent moisture conditions, the change in VWC above the minimum observed VWC for the water year (VWC_{min}) was accumulated for each water year. VWC_{min} was used to account for antecedent moisture conditions and to ensure influence from a series of melt events in a water year were comparable to one another between sensors that may experience varying residual VWC (Fig. 5.2b). Data were analyzed by observing the change above this minimum value and length of

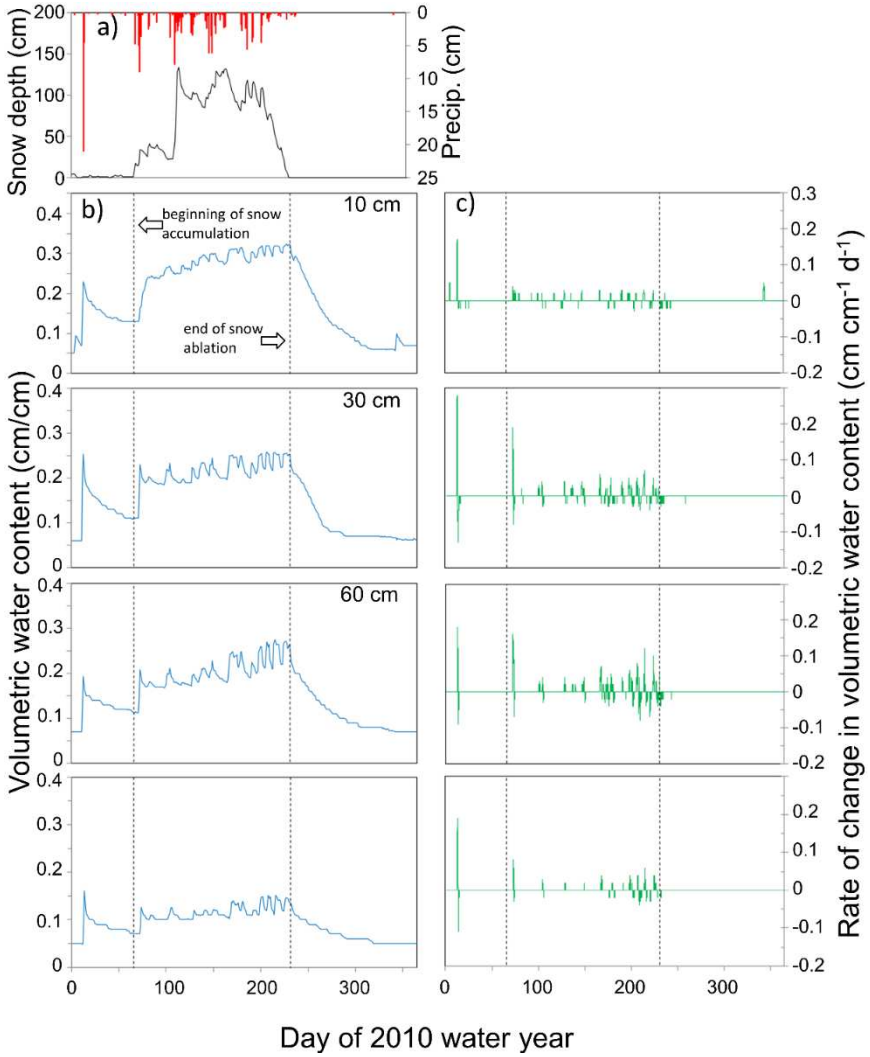

Figure 5.2: 2010 water year data for all sensors located at the upper elevation, flat aspect, *Abies concolor* drip edge displaying a) daily snow depth and precipitation recorded, b) daily volumetric water content, and c) time derivative of volumetric water content. The dashed black lines indicate the beginning of snow accumulation and end of snow ablation.

time these changes remained. This was accomplished through taking the VWC value of a given time step, subtracting the VWC_{min} of that sensor, and multiplying by the 30 minute time step (decimal day). This results in a time series of data with units of percent·days which may be accumulated over a water year to determine the accumulation of the percent·days which is representative of the persistence of soil moisture above the VWC_{min} value for each sensor within the network.

Vertical VWC gradients were computed between sensors for each vertical profile per unit length between the sensors, with positive gradients representing an increase in VWC in the downward direction. For example, if a sensor at 30 cm depth records a higher VWC than the corresponding 10 cm deep sensor, a positive gradient is present. Vertical gradients were qualitatively interpreted to determine depths within individual profiles that tend to retain higher values of VWC beneath a snowpack. These data display the time of year that positive or negative gradients are dominant between two sensors. Additionally, these data show periods of wetting and drying in regions between sensors as gradients increase or decrease in magnitude.

Twenty-four hour rates of change in VWC were calculated for each 30 minute time step throughout the year for all sensors. The magnitudes of the rates of change were analyzed by using a backward looking approach. Each calculation “looked back” a period of 24 hours by subtracting the VWC value observed 24 hours prior resulting in a rate of change in VWC (D_t) with units cm/cm per day. The D_t results within a vertical profile of the top meter of soil can show the timing of soil moisture movement at different depths.

The results from the above methods were additionally analyzed between locations for comparisons of elevation, aspect, and canopy cover. Comparisons were made to identify depths within the top meter of soil at the 27 locations that had a higher persistence of soil moisture, timing of positive vertical gradients, and experienced more high D_t values.

Results

VWC sensors show soil moisture content being primarily driven by snowmelt processes with some influences from rain events early and late in the water year (e.g. UF_acde, Fig. 5.2), as described by *Bales et al*. [*2011*]. From 2003 to 2011, snow at these locations generally began to accumulate in October, peaked in March, and was fully melted by the end of May (Fig. 5.3). For water years 2009, 2010, and 2011 snow accumulation at the upper meteorological station peaked on water year days 155, 164, and 177 (March 5, March 14, and March 27), respectively. The lowest peak SWE of these 3 years was observed in 2009 at the upper meteorological station, with 460 mm whereas peak SWE in 2010 was 860 mm and 2011 had the highest peak SWE of 1140 mm (Fig. 5.4). The last day with snow at the upper meteorological station instruments was water year day 204 (April 23) in 2009, 250 (June 8) in 2010, and 246 (June 4) in 2011. For the lower meteorological station, snow had completely melted by day 202 (April 21) in 2009, 231 (May 20) in 2010, and 235 (May 24) in 2011. Snow depth at the lower meteorological station (SWE data not available) followed a similar pattern to the upper meteorological station with maximum depths of 140 cm (day 140 - Feb 18, 2009), 160 cm (day 114 - Jan. 23, 2010), and 260 cm (day 175 - Mar 25, 2011).

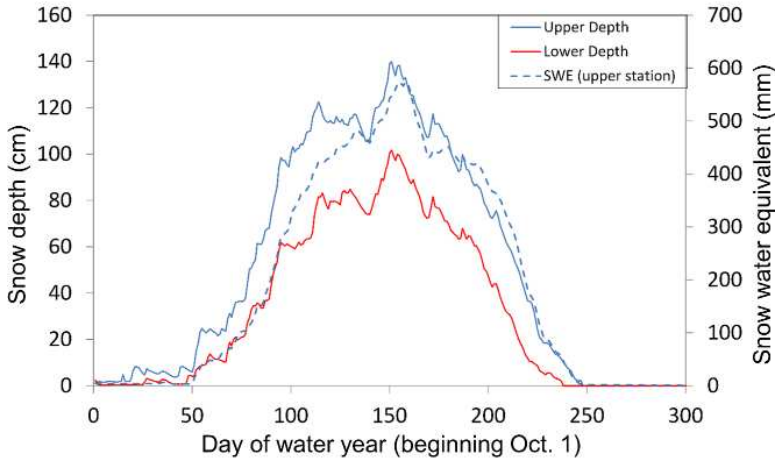

Figure 5.3: Nine year average (2003-2011) of snow depth for both the upper and lower meteorological stations as well as the average snow water equivalent measured at the upper meteorological station.

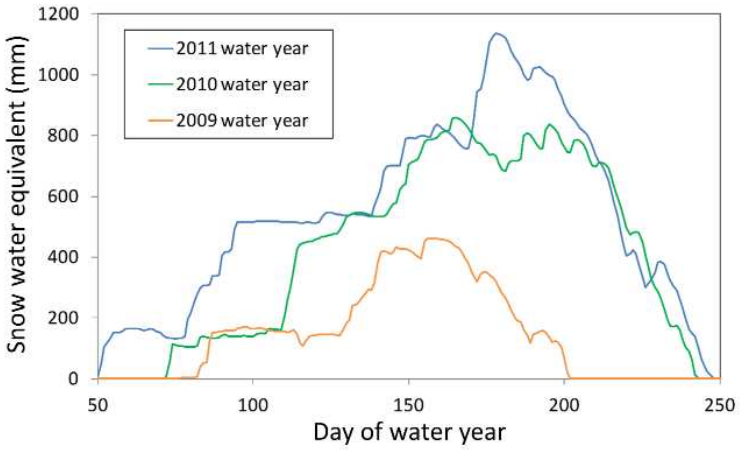

Figure 5.4: Snow water equivalent from the upper elevation meteorological station for the 2009, 2010, and 2011 water years.

The persistence of soil moisture over each water year developed S-shaped curves for each sensor, displaying little to no increase for the first and last days of each water year (Fig. 5.5). Most elevations, aspects, and depths remained relatively consistent with patterns of magnitude for total accumulated persistence of soil moisture for each water year. The UF cluster at 60 cm depth (Fig. 5.5) showed the same pattern of locations from highest to lowest accumulated values each year, this order being (in decreasing order) ppuc, ppde, open, acde, and acuc. On average 62% of the accumulated persistence of soil moisture occurred beneath a snowpack.

The highest values of these accumulated soil moisture persistence data were often found at 10 cm depth; this is the depth that is impacted the most from snowmelt infiltration, as per *Blankenship et al*. [*2014*]. However, this is not always the case and some locations show 30 cm, 60 cm, or 90 cm depths experiencing the highest value within a vertical profile (Fig. 5.6). The greatest variability among the three years studied was seen in the lower elevations with the LS cluster showing more than the LN (Fig. 5.6). At the upper elevation sites, low variability among the three years studied is observed for all sensors.

The main differences between clusters for the ac data were observed under canopy with the lowest soil moisture persistence occurring at the UN and UF clusters at all depths (Fig. 5.6).

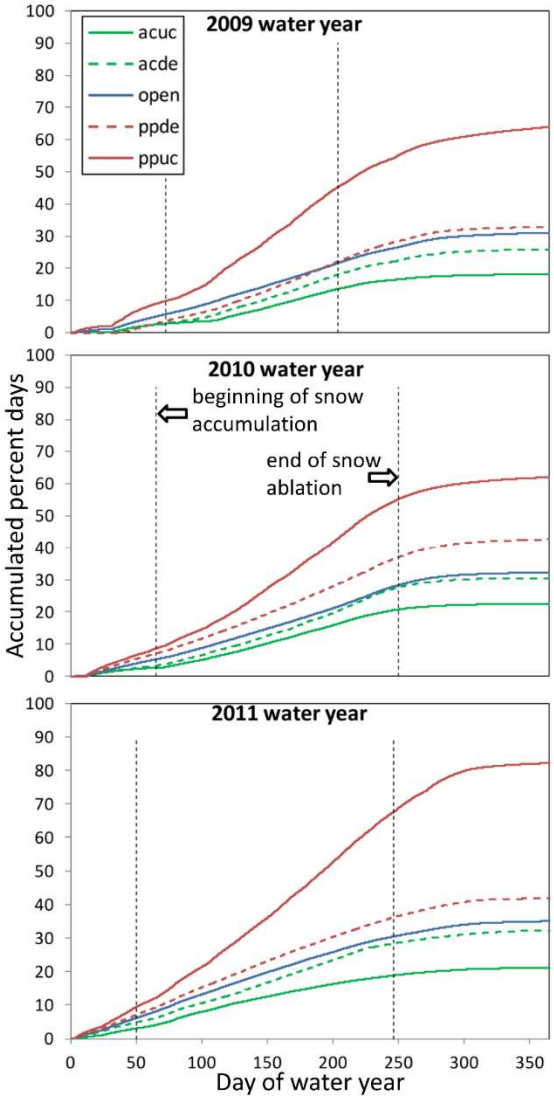

Figure 5.5: The accumulation of soil moisture persistence shown for all locations at the upper elevation, flat aspect, and 60 cm depth for the 2009, 2010, and 2011 water years. Sensors shown are *Abies concolor* (ac) and *Pinus ponderosa* (pp) both under canopy (uc) and at the drip edge (de) as well as the open canopy sensor. The black dashed lines indicate the beginning of snow accumulation and end of snow ablation for each of the three water years based on data from the upper elevation meteorological station.

The UN sensors also displayed lower values for the drip edge of ac at 10 cm depth. The drip edge of the ac at the LN sensors displayed increasing soil moisture persistence with depth. The difference between clusters for the cd trees is primarily seen in the 60 and 90 cm depths with LN and LS locations displaying much higher soil moisture persistence than the UN (Fig. 5.6).

The pp resulted in higher values at the drip edge of the LS cluster relative to the UF with the under canopy instruments showing the inverse relation at 30 cm depth (Fig. 5.6). The LN and LS sensors, in general, display higher values occurring at 60 and 90 cm depths (Fig. 5.6). The pl and qk tree species were only instrumented at UN and US, respectively, so no comparison between aspects and elevations are possible.

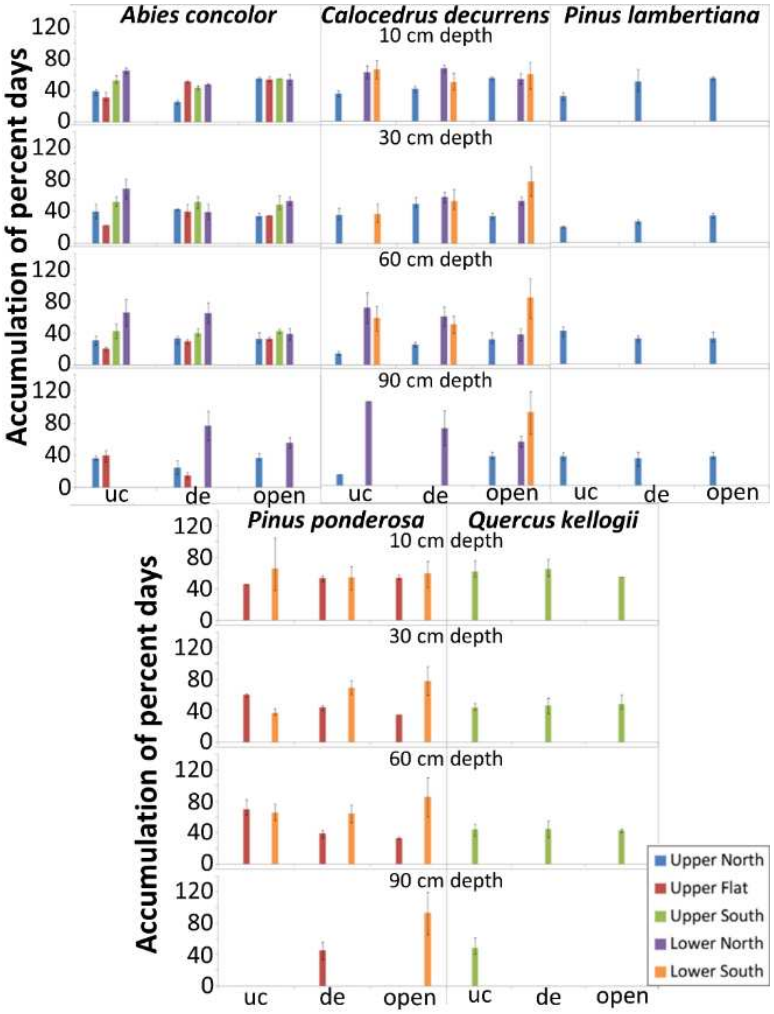

Figure 5.6: Average accumulation of percent days over the 2009, 2010, and 2011 water years for each of the 97 volumetric water content sensors with the total range of variability over the three years shown with the error bars.

Vertical VWC gradients between sensors resulted in most gradients having an asymptotic type of curve later in each water year, many times near a zero gradient (Fig. 5.7). Approximately half of the sensor locations displayed consistent gradients among water years for

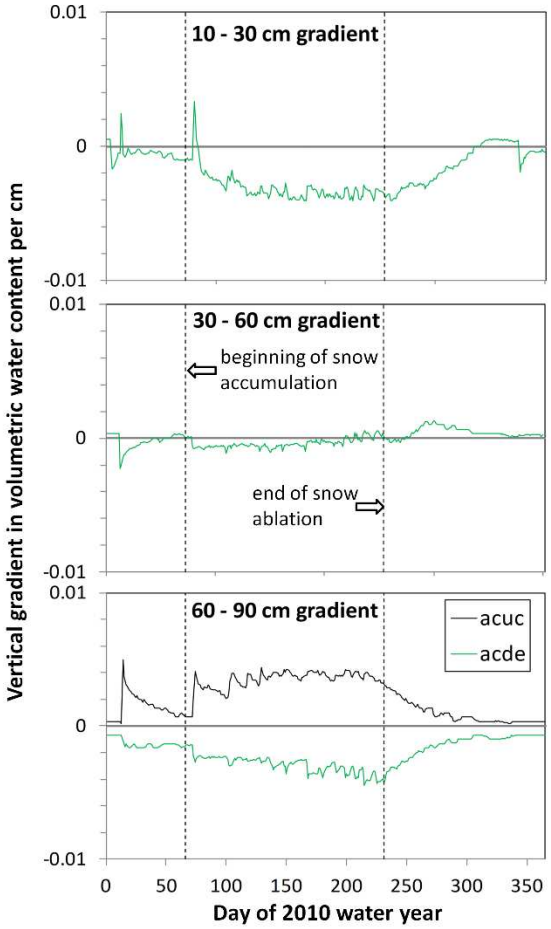

Figure 5.7: Calculated vertical gradients for the 2010 water year measured between the volumetric water content sensors at the upper elevation, flat aspect location for *Abies concolor* (ac) for both under canopy (uc) and the drip edge (de) locations. Only the 60-90 cm gradient was calculated for the under canopy condition due to the 30 cm sensor malfunctioning. The dashed lines indicate the beginning of snow accumulation and the end of snow ablation.

depths that were generally experiencing wetter conditions within each vertical profile. The vertical gradients between most sensors generally remained either positive or negative beneath a snowpack each year, with an occasional brief increase/decrease above or below zero, likely the result of a single pulse of water movement. Often between 10 and 30 cm sensors, the 30 cm was wetter under no snow conditions and drier beneath a snowpack. For example, the vertical VWC gradient between the 10 and 30 cm sensors display a general decreasing pattern with

depth at the UF_ac location (Fig. 5.7). The gradient between the 30 and 60 cm sensors show generally decreasing VWC with depth, but there was a positive gradient with depth during the spring snowmelt. Between the 60 and 90 cm sensors, a consistent gradient direction is displayed with little change where the sensors uc are increasing in VWC with depth and the de sensors are decreasing with depth. The uc sensor at 30 cm depth malfunctioned during the 2010 water year so only the 60-90 cm gradient is shown at this location. However, the opposite direction of gradients between uc and de locations can be seen between the 60 and 90 cm depths.

Although only half of the gradients remained consistent over the three water years, a number of locations developed increasing or decreasing patterns with depth. The UN cluster developed the highest number of locations with depths remaining wetter beneath a snowpack for at least two out of the three years at the locations UN_acde at 30 cm, UN_cdde and UN_cduc at 30 cm, UN_plde and UN_pluc at 60 cm. The US_acde and LS_ppde locations also developed this pattern at 30 cm for two out of the three years. The UN_acuc at 30 cm and UN_pluc at 60 cm sensors were the only ones that displayed a generally wet condition relative to other sensors in the profile beneath a snowpack for all three years observed.

The D_t results display sensor noise, with a rate of change, both positive and negative, of approximately 0.01 cm/cm per day. To analyze only larger water movement events, water pulses causing a rate of change 0.05 cm/cm or greater per day above the normal noise were further analyzed (0.06 cm/cm per day). This filtering of events for all three years resulted in over 1,400 pulse events above the threshold with multiple events having rates of change greater than 0.10 cm/cm per day (Fig. 5.2). The total number of pulse events above the threshold for all 97 sensors was 518, 366, and 531 for water years 2009, 2010, and 2011, respectively. Average number of events for individual sensors per year ranged from one to 18 with a median value of 4.3 (Fig. 5.8). More pulses of water content tended to occur at the 10 cm depth, though not in all

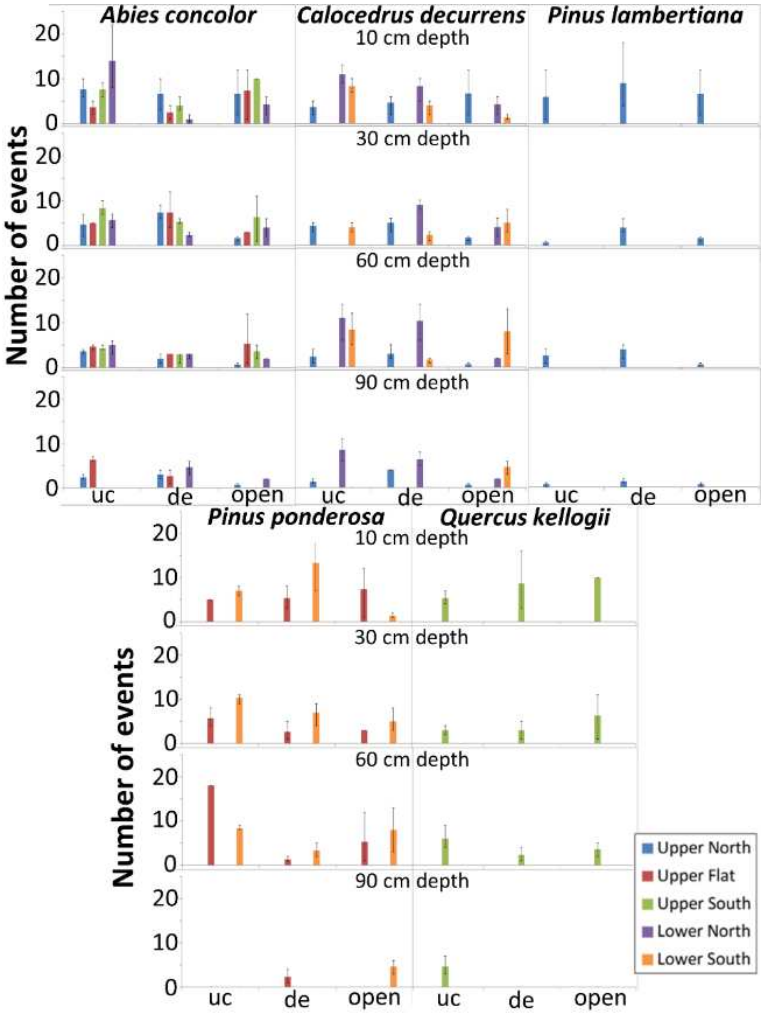

Figure 5.8: The average number of events displaying rates of change in VWC above 0.06 cm/cm per day over the course of the 2009, 2010, and 2011 water years with the total range of variability over the three years indicated by the error bars.

profiles (Fig. 5.8). Most pulse increases in VWC had a subsequent decrease of a similar amount, but with various temporal lags (Fig. 5.2).

The LN and LS sensors both showed a greater number of D_t events, including those that reached 60 cm depth. The lower elevation sensors averaged 6.0 D_t events per year and the upper sensors averaged 4.7 with standard deviations among elevation and aspect clusters ranging from 2.5 to 3.0 for upper elevation sites and 2.9 to 3.2 for lower elevation sites. The open canopy sensors generally showed fewer large wetting events with depth for all elevations

and aspects, with the UN location showing the lowest number in sensors deeper than 10 cm. The UN cluster also displayed similar number of pulse events at the drip edge and under canopy conditions. A similar result is observed at the UF sensors with the exception of the ppuc sensor at 60 cm that regularly experienced the highest number of pulses compared to all other nearby sensors (Fig. 5.8). The US cluster resulted in fewer pulse events with depth for all canopy types other than the qkuc location that generally resulted in more events at 60 and 90 cm depth relative to the 30 cm sensor. The LN locations generally saw more pulse events uc when compared to de sensors, particularly at the ac tree. This pattern is also observed at the LS cluster, with the exception of the ppde at 10 cm.

Discussion

Results of this study display the high variability in wetting and drying magnitudes that occur in a mixed conifer forest throughout a catchment and at the sub-hillslope scale. More wetting pulses reach deeper sensors at the lower elevations along with more variability between sensors. The under canopy and drip edge location differences, highlighted at the lower elevation sites, are likely due to the known higher ablation rates in open areas [*Musselman et al., 2008*]. In addition, microtopographical variability has been observed to induce localized snowmelt infiltration caused by meter-scale runoff and run-on during the snowmelt season in this CZO [*Bales et al., 2011*]. Stemflow is also known to occur during rain events causing concentrated infiltration under tree canopies [*Liang et al., 2007*]. It is also possible that melting snow within the canopy produces a similar effect which could introduce more pulse infiltration events in under canopy conditions than expected [*Levia and Underwood, 2004*]. Soil moisture patterns have been attributed to variations in soil properties, topography, and snow distribution with the interactions between variables controlling the moisture distribution [*Williams et al., 2009*]. The known variability inherent within a snowpack [*Fassnacht et al., 2009*], ablation rates in forested areas [*Musselman et al., 2008*] forms variable infiltration within the top meter of soil, introducing complex soil moisture distribution within a subalpine mixed conifer forest.

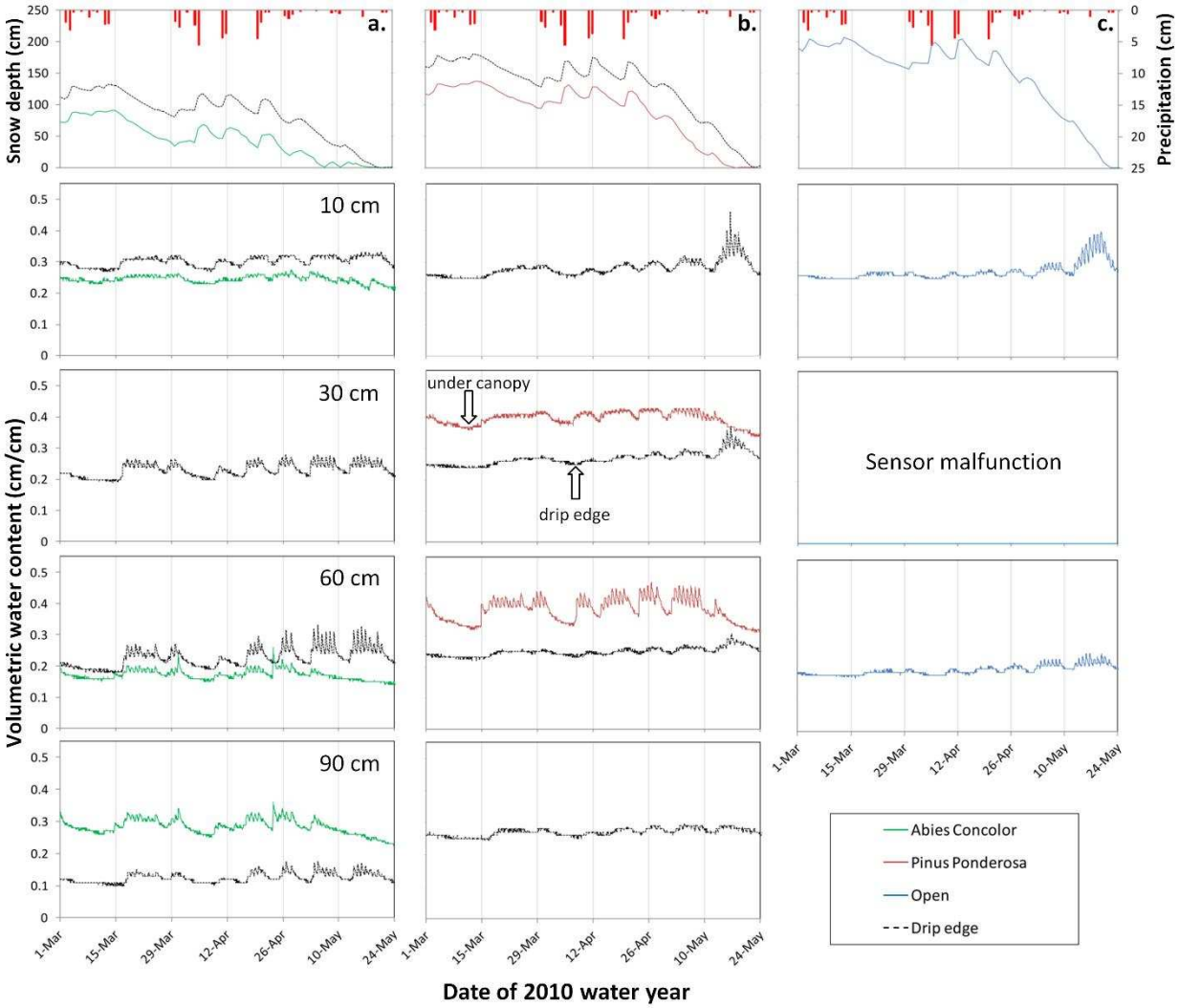

Figure 5.9: Volumetric water content for the 2010 spring snowmelt (days 151 through 235 of the water year) at the upper elevation, flat aspect for a) *Abies concolor,* b) *Pinus ponderosa*, and c) open canopy. The solid color lines indicate under canopy conditions whereas the black dotted lines indicate sensors beneath the drip edges. The solid red bars display daily precipitation.

It is also possible that lateral flow paths develop within the top meter of soil. *Iwata et al*. [*2011*] observed similar lateral flow impacting the results of infiltration experiments at the plot scale. These flow paths could be developing in profiles that showed little to no attenuation of moisture pulses with depth (Fig. 5.9). If shallow soil has a higher VWC, a vertical pulse of water movement would show a greater change in the deeper sensor; though if the shallow soil is at a lower VWC and the deeper sensor exhibits a greater influence from the pulse of water movement, it is possible this is from lateral movement of soil moisture. These potential lateral influences could be a result of either movement across the soil-bedrock interface or dispersion

of meltwater from a nearby location melting at a greater rate. However, water potential measurements are necessary to properly assess this process in order to calculate fluxes in multiple directions.

The variability in soil moisture wetting and drying dynamics also has implications in the groundwater recharge of a catchment. The data show that large wetting pulses followed by multiple diurnal pulses are not reaching 60 and 90 cm depth at all locations (Fig. 5.9). For example, at the UF cluster in 2010, sensors with open canopy conditions resulted in fewer pulses of soil moisture increases at 60 cm depth compared to other nearby sensors at this depth. The ppuc condition likely resulted in more groundwater recharge than the ppde and open canopy conditions. This is additionally supported by the ppuc location showing higher persistence of soil moisture each year (Fig. 5.5). A location that tends to remain wetter for longer periods will conduct soil moisture more efficiently due to the differences in soil moisture storage deficits. The inverse is likely true for the acuc and acde locations with the acde sensors resulting in more pulses of increased VWC (Fig. 5.8) in addition to a greater persistence of soil moisture (Fig. 5.6). This displays the variability of recharge in a mixed conifer forest indicating that a uniform, one-dimensional approach to soil moisture movement beneath a seasonally persistent snowpack is insufficient to appropriately represent existing dynamics. Groundwater recharge simulations that assume uniform snowmelt and a one-dimensional process [*e.g*. *Flint et al., 2008*] will likely over or underestimate recharge depending on the location and depth of instrumentation. Instrumentation under a canopy may underestimate the SWE for the area due to canopy interception and instrumentation with open canopy conditions may overestimate SWE for a forested area [*Musselman et al., 2008*]. Results from this study suggests that VWC sensors under the canopy in a mixed conifer forest may overestimate the number of wetting events from snowmelt that recharge groundwater and open canopy sensors may underestimate the number of wetting events.

In order to account for this meter-scale variability, multiple sensor locations should be utilized in order to quantify the variability of infiltration during snowmelt. Results from this study indicate that patterns may vary depending upon the antecedent moisture conditions, snow depth, and amount of snowmelt per event. Some sensor locations resulted in similar numbers of wetting and drying events each year while other locations and depths had high variability over the three years observed (Fig. 5.6). Hydrologic modeling efforts that attempt to include this variability will need to quantify each of these variabilities for the site of interest from long term datasets, such as those currently being developed within the CZO network.

With projected changes to precipitation patterns and duration of snowcover in mountainous regions [*Adam et al., 2009*], knowledge of the variable wetting and drying of soil moisture will be important. Climate change implications from snow and soil moisture interactions have suggested earlier peak soil moisture in areas such as the western United States including the Sierra Nevada [*Harpold et al., 2014*]. These three years of study show a low, normal, and high snowpack with wetting and drying variability among elevation, aspect, and canopy conditions developing each year. A better understanding of the distribution of soil moisture within a watershed could be vital in predicting consequences of a changing climate for these types of environments and the response that may occur in plant production, groundwater recharge, and streamflow.

Conclusions

Considering the persistence of soil moisture in addition to the vertical gradients between sensors assists in identifying regions of varying wetting and drying dynamics. Observing the rates of change in VWC data and observing the larger pulse events along with the vertical gradient in VWC within a vertical profile offers insight into whether snowmelt may be recharging groundwater at a particular location and the variability that this recharge may be occurring across a catchment. Results from this study indicate that the wetting and drying dynamics within

the top meter of soil in a mixed conifer forest is highly variable at the catchment and sub-hillslope (meter) scale.

Differences in elevation, aspect, and canopy cover impact the processes that distribute soil moisture within the shallow subsurface beneath a snowpack. The 97 sensors resulted in over 1,400 pulse events above a rate of change in VWC of 0.06 cm/cm per day with many above 0.10 cm/cm per day. Average numbers of pulse events per year ranged from 1 to 18 with a median of 4.3 for all sensors was observed with sensors at 10 cm depth having more events than deeper sensors. The lower elevation sensors averaged 6.0 D_t events per year and the upper sensors averaged 4.7 with standard deviations among elevation and aspect clusters ranging from 2.5 to 3.0 for upper elevation sites and 2.9 to 3.2 for lower elevation sites. Lower elevation sensors showed slightly more VWC increases reach 60 cm deep sensors and the UN cluster resulted in the fewest. A general pattern for canopy conditions was not observed to produce more VWC increases at depths. Even at the same elevation and aspect cluster, the drip edge of one tree may result in more VWC pulses at any particular depth than under the canopy whereas a nearby tree of a different species displayed the opposite results.

The variability in the wetting and drying dynamics in the top meter of soil may be the result of lateral flowpaths above and below the soil surface developing from non-uniform meltrates and layered characteristics of a snowpack. However, additional data are necessary to confirm and quantify this. The variable wetting and drying dynamics observed in this study indicate that groundwater recharge could vary between tree species and canopy conditions. Further investigation of these moisture distribution processes is necessary to improve the understanding of mountainous systems and the potential impact of a changing climate on groundwater recharge, plant production, and streamflow response.

REFERENCES

Adam, J.C., A.F. Hamlet, and D.P. Lettenmaier (2009), Implications of global climate change for snowmelt hydrology in the twenty-first century, *Hydrological Processes* 23, 962–972, DOI: 10.1002/hyp.7201.

Bales, R.C., N.P. Molotch, T.H. Painter, M.D. Dettinger, R. Rice, and J. Dozier (2006), Mountain hydrology of the western United States, Water Resources Research 42(8), W08432, Doi:10.1029/2005WR004387

Bales, R.C., J. Hopmans, A.T. O'Geen, M. Meadows, P.C. Hartsough, P. Kirchner, C.T. Hunsaker, and D. Beaudette (2011), Soil Moisture Response to Snowmelt and Rainfall in a Sierra Nevada Mixed-Conifer Forest, *Vadose Zone J*., 10, 786-799.

Bales, R.C., M. Meadows, and X. Meng (2013), CZO Dataset: Providence, Lower and Upper Met, North, South, and Flat aspect - Soil Moisture, Soil Temperature, Snow Depth, Air Temperature (2008-2013), Retrieved 03 Jul 2014, from http://criticalzone.org/sierra/data/dataset/2530/, 2595, 2598, 2597, 2596.

Blankinship, J.C., Meadows, R.G. Lucas, and S.C. Hart (2014), Snowmelt timing alters shallow but not deep soil moisture in the Sierra Nevada, *Water Resour. Res.,* 50, 1448-1456, doi:10.1002/2013WR014541.

Fassnacht, S.R., M. Skordahl, and S. Simonson (2008), Variability and Consistency in Select Colorado Snowcourses, *Proceedings of the International Snow Science Workshop*, p964-966, Whistler BC, September 21-27 2008.

Fassnacht, S.R., Williams, and M.V. Corrao (2009), Changes in the surface roughness of snow from millimetre to metre scales, *Ecological Complexity*, 6(3), 221-229. doi, 10.1016/j.ecocom.2009.05.003.

Flint, A.L., L.E. Flint, and M.D. Dettinger (2008), Modeling soil moisture processes and recharge under a melting snowpack, *Vadose Zone J.,* 7 (1), 350-357, doi:10.2136/vzj2006.0135.

Ghasemizade, M., and M. Schirmer (2013), Subsurface flow contribution in the hydrological cycle: lessons learned and challenges ahead—a review, *Environ. Earth Sci.,* 69, 707-718, doi: 10.1007/sl2665-013-2329-8.

Harpold, A.A., N.P. Molotch, K.N. Muselman, R.C. Bales, P.B. Kirchner, M. Litvak, and P.D. Brooks (2014), Soil moisture response to snowmelt timing in mixed-conifer subalpine forests, *Hydrological Processes,* DOI: 10.1002/hyp.10400.

Hinckley, E.S., B.A. Ebel, R.T. Barnes, R.S. Anderson, Williams, and S.P. Anderson (2014), Aspect control of water movement on hillslopes near the rain-snow transition of the Colorado Front Range, *Hydrol. Process.* 28, 74-85, DOI: 10.1002/hyp.9549.

Hunsaker, C.T. (2011), CZO Dataset: Meteorological stations, Providence, Upper and Lower - Meteorology (2002-2011), Retrieved 03 Jul 2014, from http://criticalzone.org/sierra/data/dataset/2406/ and 2529.

Hunsaker, C.T., T.W. Whitaker, and R.C. Bales (2012), Snowmelt runoff and water yield along elevation and temperature gradients in Californias Southern Sierra Nevada, *J. of the Amer. Water Resour. Assoc.,* 1-12: p. 667-678.

Iwata, Y., M. Nemoto, S. Hasegawa, Y. Yanai, K. Kuwao, and T. Hirota (2011), Influence of rain, air temperature, and snow cover on subsequent spring-snowmelt infiltration into thin frozen soil layer in northern Japan, *J. of Hydrology,* 401, 165-176.

Kampf, S., J. Markus, J. Heath, and C. Moore (2014), Snowmelt runoff and soil moisture dynamics on steep subalpine hillslopes, *Hydrol. Process*., doi:10.1002/hyp.10179.

Levia, D.F. & S.J. Underwood (2004), Snowmelt induced stemflow in northern hardwood forests: a theoretical explanation on the causation of a neglected hydrological process, *Advances in Water Resources,* 27: 121-128.

Liang, W.L., K.I. Kosugi, and T. Mizuyama (2007), Heterogeneous soil water dynamics around a tree growing on a steep hillslope, *Vadose Zone J.,* 6:879–889. doi:10.2136/vzj2007.0029

Musselman, K.N., N.P. Molotch, and P.D. Brooks (2008), Effects of vegetation on snow accumulation and ablation in a mid-latitude sub-alpine forest, *Hydrol. Process.,* 22, 2767-2776, DOI: 10.1002/hyp.7050.

Sexstone, G.A. and S.R. Fassnacht (2014), What drives basin scale spatial variability of snowpack properties in northern Colorado, *The Cryosphere*, 8, 329-344, Doi: 10.5194/tc-8-329-2014.

Williams , J.P. McNamara, and D.G. Chandler (2009), Controls on the temporal and spatial variability of soil moisture in a mountainous landscape: the signature of snow and complex terrain, *Hydrology and Earth System Sciences* 13: 1325–1336, DOI: 10.5194/hess-13-1325-2009.

Winter, T.C. (2007), Role of ground water in generating streamflow in headwater areas and in maintaining base flow, *J. Amer. Water Resour. Assoc.,* 43(1):15-2.

CHAPTER 6: CONCLUSIONS

Summary of Findings

The preceding chapters investigated multiple components of the physical processes that occur during snowmelt and control the fate of snowmelt in spring. Insights were provided into the flow paths that develop during this time of year and how snowmelt water distributes throughout complex subalpine terrain. Estimates of the water balance for management and assessment of ecosystem dynamics will benefit from considering the diurnal patterns of snowmelt determined in chapter 2, the potential for hydraulic barriers to form in layered snowpacks from chapter 3, the pattern of water distribution in a small headwater catchment in chapter 4, and the variability of wetting and drying of the top meter of soil beneath a melting snowpack from chapter 5.

The methods presented in chapter 2 were able to capture the diurnal pattern of snowmelt outflow from a snowpack in the Colorado Front Range using only three years of hourly SWE data. The diurnal pattern of snowmelt was fit by a modified gamma distribution function showing the fast increase in the meltwater outflow followed by a longer recession. Hourly SWE data has some inherent errors that are unavoidable when snowmelt rates were computed using snow pillow data, however the addition of soil moisture data is beneficial in confirming the pattern observed from SWE data and could be used for correcting the timing of snowmelt outflow from a snowpack. The presented methods can be used to parameterize a design (sub-daily) snowmelt event that is comparable to the SCS rainfall distribution curve for design purposes.

Many previous hydrological modeling efforts incorporate a temperature index modeling scheme [*Jost et al., 2012; Tobin et al., 2013*]. Though these methods have shown improvements upon previous snow runoff models when including radiation data, they require additional data collection and calibration. With the demonstrated diurnal pattern of snowmelt

outflow from a snowpack (Chapter 2), sub-daily time varying melt factors could be modified from a simple sinusoidal curve to a simple gamma FDM function shown in chapter 2. This would allow a simpler method for estimating snowmelt outflow and save computational expense for complex, larger systems. Additionally, groundwater recharge studies [*Flint et al., 2008*] could utilize the shown FDM to drive sub-surface gradients for unsaturated flow investigations.

The modeling exercises presented in chapter 3 demonstrated the range of diversion lengths for meltwater within a snowpack for a range of densities and grain sizes. Highly stratified snowpacks as observed in the north aspect snow pit data used for this chapter formed the most hydraulic barriers to vertically infiltrating meltwater at normal melt rates determined in chapter 2. Capillary barriers formed only on the north aspect slope with diversion lengths ranging from 1.0 m to ≥25 m. Permeability barriers were observed in the south and flat aspect snowpack simulations with diversion lengths from 2.5 m to 9.5 m. The simulations in this chapter display the large potential for percolating water to move laterally within a snowpack. Highly stratified snowpacks such as the north aspect snow pit in chapter 3 produce higher potential for lateral diversion of percolating melt water, though these capillary barriers are less persistent temporally and only important at the daily or weekly time scale prior to metamorphism and possibly becoming permeability barriers. Permeability barriers between snowpack layers are likely more temporally persistent and thus important at the monthly or seasonal melt timescale. These results have strong implications on the distribution of water within a layered snowpack during the transition period from winter to spring, though further studies are necessary to verify large capillary diversion lengths in layered snowpacks in the field.

The results of chapter 3 show the ability to simulate preferential flow paths that are known to occur within a snowpack at the scale of simulations [*Colbeck, 1991; Williams et al., 2009a; Williams et al., 2009b; Eiriksson et al., 2013*]. Previous simulations of water flow through a layered snowpack have been limited to one-dimension (vertical) and thus were unable to capture the lateral flow of water downslope [*Wever et al., 2014*]. With the advancement of

capabilities being made for the parameterization of hydraulic properties for snow [*Yamaguchi et al., 2010; Hirashima et al., 2010; Calonne et al., 2012*] future simulations will be able to better represent the flow of water through a snowpack and hydraulic barriers that form to estimate the distribution of flux across the SSI.

The spatio-temporal patterns of SWE and VWC in chapter 4 demonstrate the variability of water movement in a subalpine headwater catchment with a deep seasonally persistent snowpack during spring melt. Previous investigations have been limited to lower elevation sites for a single year of observations [*Williams et al., 2009a*] or an alpine setting with two years of data [*Litaor et al., 2008*]. Field observations were made at the DL study site for greater than normal, approximately normal, and less than normal snow seasons. The static control that was shown to be the most influential on VWC was the hill slope aspect similar to other studies [*Williams et al., 2009a; Hinckley et al., 2014*]. Dynamic controls showed stronger influence, particularly previous soil moisture measurements showing locations that were wet relative to other locations tend to remain wetter beneath a snowpack similar to other investigations in Idaho conducted by *Williams et al.* [*2009a*]. Bulk SWE and soil moisture variability in space and time during spring snowmelt and the range of meteorological forcing conditions including rain-on-snow events in 2015 showed evidence of meltwater flowing above the SSI on the north aspect hillslope and to a lesser extent at the base of the north aspect hillslope on a relatively flat aspect. The base of the north aspect hillslope resulted in the convergence of flow paths, both above and below the SSI, causing the water table to rise above the soil surface and into the snowpack. This event displays the potential for a snowpack in a catchment to increase the water storage capacity of a location by as much as 270 mm of water that would otherwise directly runoff. The south aspect hillslope did not display evidence of water flow through the snowpack above the SSI. The differences in flow path development on the two opposite facing hillslopes is due to characteristics of each slope's soil, slope angle, snowpack, and snowmelt rates as a result of meteorological forcing variability producing a permeability barrier on the

north aspect hillslope at the SSI. These controls on the flow path development is reflected in the SWE and VWC observations based on north, south, and flat aspects in addition to the VWC measurements at the base of hill slopes relative to flat and sloped areas. Results from chapter 4 show that the snow acts as an extension of the vadose zone during spring snowmelt.

The observations of the vadose zone in chapter 5 using a network of soil moisture sensors showed that considering the persistence of soil moisture in addition to the vertical gradients between sensors assists in identifying regions of varying wetting and drying dynamics. Observing the rates of change in VWC data and the larger pulse events along with the vertical gradient in VWC within a vertical profile offers insight into whether snowmelt is recharging groundwater at a particular location and the variability that this recharge occurs across a catchment or hillslope. Results from this chapter indicate that the wetting and drying dynamics within the top meter of soil in a mixed conifer forest is highly variable at the catchment and sub-hillslope (meter) scale. This is comparable to the known melt rate differences based on canopy cover [*Musselman et al., 2008*], microtopographical variability [*Bales et al.,* 2011], stemflow [*Liang et al., 2007*], and influences of hydraulic barriers between snow layers that are sloped (Chapter 3) as a result of canopy interception. Differences in elevation, aspect, and canopy cover impact the processes that distribute soil moisture in the shallow subsurface beneath a snowpack. The 97 sensors analyzed in chapter 5 resulted in over 1,400 pulse events above a rate of change in VWC of 0.06 cm/cm per day with many above 0.10 cm/cm per day. Average numbers of pulse events per year ranged from 1 to 18 with a median of 4.3 for all sensors was observed with sensors at 10 cm depth having more events than deeper sensors. The lower elevation sensors averaged 6.0 D_t events per year and the upper sensors averaged 4.7 with standard deviations among elevation and aspect clusters ranging from 2.5 to 3.0 for upper elevation sites and 2.9 to 3.2 for lower elevation sites. Lower elevation sensors showed slightly more VWC increases reach 60 cm deep sensors and the UN cluster resulted in the fewest. The elevation influences are reflective of known climatological differences between different

elevations and the effects on snow [*Fassnacht and Derry, 2010; Sextone and Fassnacht, 2014*]. A general pattern for canopy conditions was not observed to produce more VWC increases at depths. Even at the same elevation and aspect cluster, the drip edge of one tree may result in more VWC pulses at any particular depth than under the canopy whereas a nearby tree of a different species displayed the opposite results.

The variability in the wetting and drying dynamics in the top meter of soil shown in chapter 5 will also be influenced by lateral flow paths developing above the ground surface in addition to non-uniform melt rates as discussed in chapters 2, 3, and 4. Even in a relatively flat topographic region, the variable depth that is created by canopy interception will result in a sloping snow surface and snow layer interfaces that can create hydraulic barriers and divert vertically percolating meltwater. The variable wetting and drying dynamics observed in chapter 5 indicate that groundwater recharge will vary between tree species, canopy conditions, slope, and aspect. Further investigation of these moisture distribution processes is necessary to improve the understanding of mountainous systems and the potential impact of a changing climate on groundwater recharge, plant production, and streamflow response.

The findings of this dissertation show the complex movement of liquid water during snowmelt in complex terrain. During spring, snowmelt rates will fluctuate diurnally driving variably saturated flow with unsteady conditions. The layered nature of a snowpack will create hydraulic barriers to vertically percolating water with a range of diversion lengths depending on the snowpack characteristics and melt rate that will temporally vary. These physical processes can be seen reflected in SWE and shallow soil moisture in complex subalpine terrain where snowpack properties and melt rates change based on differing meteorological forcing conditions for opposing slope aspects. Topographic influences at multiple scales will also affect the flow paths that develop as diversion lengths are a function of slope angle. The distribution of meltwater across a landscape above the SSI will ultimately drive variable wetting and drying of

the vadose zone with implications towards streamflow generation, groundwater recharge, and plant production.

Future Work & Applications

When comparing the sub-daily melt pattern determined in chapter 2 to the SCS rainfall curve, each have a different shape and would be applied to different antecedent soil moisture conditions of systems providing unique runoff processes that could be important for design purposes. The method presented in chapter 2 can also be used to provide a representation of snowmelt outflow for groundwater recharge or general hydrological modeling that is less computationally expensive than energy balance calculations, though further testing is necessary. The methods presented in this chapter are derived from publically available data sources across the western United States. Expansion of these methods may include regions other than the Colorado Rocky Mountains, as well as for rain-on-snow events that are important to other areas of the western U.S. Additionally, scaling the diurnal melt pattern up from point measurements to the catchment scale will be needed. A south aspect slope will have a longer melt duration and higher melt rates relative to the flat aspect of SNOTEL snow pillows and a north aspect will have shorter duration and lesser melt rates. A mosaic approach to determine the subdaily melt pattern of a catchment to include variations such as aspect and vegetative cover will improve upon the methods presented in chapter 2. However, general investigations of snowmelt and runoff processes may still benefit from application of the methods presented with consideration of implications from using single point measurements.

Future studies modeling the flow of water through a layered snowpack will benefit from incorporating temporally varying hydraulic properties of snow layers to improve upon the investigations in chapter 3. In addition to the temporal variability of the hydraulic parameters of snow layers, the spatial variability of melt should also be incorporated in future numerical investigations to determine the impact of these variations. Field investigations that utilize tracer experiments to quantify the diversion lengths as well as the total flux of water diverted will assist

in determining the effective properties of snow layers at the hillslope scale to expand upon the laboratory scale investigations currently used. The natural heterogeneity will likely impact the larger scale effective properties and will be necessary for consideration in future modeling efforts. Results from simulations in chapter 3 and future expansion upon the work will be important for incorporating the variable input of snowmelt water to the ground surface and improving estimates of spatial variability of groundwater recharge, plant production, and watershed and hillslope scale stream connectivity.

The future field investigations mentioned above will additionally expand on the findings in chapter 4. The formation of a permeability barrier at the SSI will be dependent upon parameters of both the snow and soil. Results from chapter 4 show that the snow acts as an extension of the vadose zone during spring snowmelt and future investigations will benefit from studying both the snow and soil rather than one or the other as is the case in many current approaches including simulations in chapter 3. Field investigations will need to incorporate varying slopes, aspects and elevation ranges along with complimentary laboratory investigations with ranging slopes and melt rates to determine the influences of each of these static and dynamic parameters. It will also be important to consider the changing climate of headwater catchments that alters the meteorological forcing conditions and thus change dynamic parameters such as the snow stratigraphy and melt rate. Future investigations will need to incorporate a combination of field investigations, laboratory experiments, and numerical simulations of variably saturated flow representing both the soil and snow together to improve hydrologic modeling of processes such as groundwater recharge, streamflow generation, and floods during snowmelt.

Projects that study the manner that water flows through a layered snowpack in the future will benefit from full utilization of current groundwater strategies including tracer studies and geophysical surveys. New methods that have been developed in recent years will allow surveys of liquid water content and estimates of water flux through non-destructive means. This will

greatly improve studies by expanding datasets from discrete locations and times to time-series and spatial surveys. It is also important to consider the scaling of processes from the laboratory scale parameter development and the single-point measurement location. This is an area of research that is still being developed and will advance with the advancement of new technology and methods.

Certainly the advances in technology and capability of institutions to install large networks of sensors as utilized in chapter 5 will also benefit future investigations. In chapter 5, I used a network of volumetric water content sensors, but future investigations will certainly benefit from large spatial networks of tensiometers for observations of water potential and quantifications of the spatial variability of flux rates. Networks such as the Critical Zone Observatories will certainly be beneficial in providing continuous long-term datasets for investigations of processes such as groundwater recharge, stream connectivity and flow generation. The establishment of spatial networks such as these in addition to advancements in remote sensing will assist future studies in moving beyond single point measurements and one-dimensional approaches.

The applications of results from this dissertation include modeling, remote sensing, and water balance calculations. Modeling efforts will benefit from a stronger conceptual model of the physical processes that occur during spring snowmelt. Remote sensing observations often need to make a number of assumptions concerning the snowpack and distribution of meltwater within it. The presence of liquid water within a snowpack will alter the albedo of the snowpack and will vary spatially from the movement of water across layer interfaces as well as temporally from the diurnal cycle of melting, percolation, and release of melt water. Furthermore, the movement of water within a catchment will non-uniformly distribute SWE across a landscape and estimates from light detecting and ranging that assume uniform density distributions for SWE calculations will be improved by consideration of the movement of water within the snowpack.

Results of this dissertation display that the snowpack acts as an extension of the vadose zone during spring snowmelt and that one-dimensional assumptions are not appropriate in complex terrain (Fig. 4.8). The distribution of water within the snowpack based on slope, aspect, and soil parameters will be important for consideration when developing a hydrological model. Variable input of snowmelt water to the soil surface will create varying hydraulic gradients that drive groundwater recharge and streamflow connectivity. As shown in this dissertation, water movement across the SSI can be highly variable and the hydraulic gradients can be extended beyond the limits provided by soils through the presence of a snowpack. Consideration of the snowpack and soil together will improve hydrological studies occurring during spring snowmelt for modeling investigations of streamflow, groundwater recharge, and evapotranspiration.

REFERENCES

Bales, R. C., J. W. Hopmans, A. T. O'Geen, M. Meadows, P. C. Hartsough, P. Kirchner, C. T. Hunsaker, and D. Beaudette (2011), Soil Moisture Response to Snowmelt and Rainfall in a Sierra Nevada Mixed-Conifer Forest, Vadose Zone Journal, 10(3), 786, doi: 10.2136/vzj2011.0001.

Calonne, N., C. Geindreau, F. Flin, S. Morin, B. Lesaffre, S. Rolland du Roscoat, and P. Charrier (2012), 3-D image-based numerical computations of snow permeability: links to specific surface area, density, and microstructural anisotropy, The Cryosphere, 6(5), 939-951, doi: 10.5194/tc-6-939-2012.

Colbeck, S. C. (1991), The layered character of snow covers, Reviews of Geophysics, 29(1), 81-96.

Eiriksson, D., M. Whitson, C. H. Luce, H. P. Marshall, J. Bradford, S. G. Benner, T. Black, H. Hetrick, and J. P. McNamara (2013), An evaluation of the hydrologic relevance of lateral flow in snow at hillslope and catchment scales, Hydrological Processes, 27(5), 640-654, doi: 10.1002/hyp.9666.

Fassnacht, S.R., and J.E. Derry (2010), Defining similar regions of snow in the Colorado River Basin using self-organizing maps, Water Resour. Res., 46, W04507, doi:10.1029/2009WR007835.

Flint, A. L., L. E. Flint, and M. D. Dettinger (2008), Modeling Soil Moisture Processes and Recharge under a Melting Snowpack, Vadose Zone Journal, 7(1), 350, doi: 10.2136/vzj2006.0135.

Hinckley, E.-L. S., B. A. Ebel, R. T. Barnes, R. S. Anderson, M. W. Williams, and S. P. Anderson (2014), Aspect control of water movement on hillslopes near the rain-snow transition of the Colorado Front Range, Hydrological Processes, 28(1), 74-85, doi: 10.1002/hyp.9549.

Hirashima, H., S. Yamaguchi, A. Sato, and M. Lehning (2010), Numerical modeling of liquid water movement through layered snow based on new measurements of the water retention curve, Cold Regions Science and Technologh, 64, 94-103, doi: 10.1016/j.coldregions.2010.09.003.

Jost, G., R. Moore, R. Smith, and D. Gluns (2012), Distributed temperature-index snowmelt modelling for forested catchments, Journal of Hydrology, 420, 87-101, doi: 10.1016/j.jhydrol.2011.11.045.

Liang, W.L., K.I. Kosugi, and T. Mizuyama (2007), Heterogeneous soil water dynamics around a tree growing on a steep hillslope, *Vadose Zone J.,* 6:879–889. doi:10.2136/vzj2007.0029

Litaor, M. I., M. Williams, and T. R. Seastedt (2008), Topographic controls on snow distribution, soil moisture, and species diversity of herbaceous alpine vegetation, Niwot Ridge, Colorado, Journal of Geophysical Research, 113(G2), doi: 10.1029/2007jg000419.

Musselman, K. N., N. P. Molotch, and P. D. Brooks (2008), Effects of vegetation on snow accumulation and ablation in a mid-latitude sub-alpine forest, Hydrological Processes, 22(15), 2767-2776, doi: 10.1002/hyp.7050.

Sexstone, G. A., and S. R. Fassnacht (2014), What drives basin scale spatial variability of snowpack properties in northern Colorado?, The Cryosphere, 8(2), 329-344, doi: 10.5194/tc-8-329-2014.

Tobin, C., B. Schaefli, L. Nicotina, S. Simoni, G. Barrenetxea, R. Smith, M. Parlange, and A. Rinaldo (2013), Improving the degree-day method for sub-daily melt simulations with physically-based diurnal variations, Advances in Water Resources, 55, 149-164, doi: 10.1016/j.advwatres.2012.08.008.

Wever, N., C. Fierz, C. Mitterer, H. Hirashima, and M. Lehning (2014), Solving Richards Equation for snow improves snowpack meltwater runoff estimations in detailed multi-layer snowpack model, The Cryosphere, 8(1), 257-274, doi: 10.5194/tc-8-257-2014.

Williams, C. J., J. P. McNamara, and D. G. Chandler (2009a), Controls on the temporal and spatial variability of soil moisture in a mountainous landscape: the signature of snow and complex terrain, Hydrology and Earth System Sciences, 13, 1325-1336.

Williams, M. W., C. Seibold, and K. Chowanski (2009b), Storage and release of solutes from a subalpine seasonal snowpack: soil and stream water response, Niwot Ridge, Colorado, Biogeochemistry, 95(1), 77-94, doi: 10.1007/s10533-009-9288-x.

Yamaguchi, S., T. Katsushima, A. Sato, and T. Kumakura (2010), Water retention curve of snow with different grain sizes, Cold Regions Science and Technology, 64(2), 87-93, doi: 10.1016/j.coldregions.2010.05.008.

APPENDIX A1: SUPPLEMENTARY MATERIAL FOR DIURNAL PATTERN OF SNOWMELT

MATLAB Script for Threshold Processing

```
% This script smooths the hourly SWE SNOTEL data using a threshold method.
% NRCS QC'd daily data are used to set upper and lower thresholds.  When an hourly
% reading is outside of the thresholds, this value is replaced by the
% previous hourly measurement.
% written by Ryan Webb based on Avanzi (2014).

n = length(dailySWE);
dailySWE(n+1,1) = 0;
processed = zeros(n,1);

j = 0;

for i = 1:n
    upper = max(dailySWE(i,1), dailySWE(i+1,1));
    lower = min(dailySWE(i,1), dailySWE(i+1,1));
    for k = (24*j+1) : (24*j+24)
        if (hourlySWE(k,1) > upper)
            processed(k,1) = processed(k-1,1);
        elseif (hourlySWE(k,1) < lower)
            processed(k,1) = processed(k-1,1);
        else
            processed(k,1) = hourlySWE(k,1);
        end
```

```
    end
    j = j+1;
end

for i = 2:n-1
    if (processed(i,1) > processed(i-1,1)) && (processed(i,1) > processed(i+1,1))
        processed(i,1) = processed(i-1,1);
    elseif (processed(i,1) < processed(i-1,1)) && (processed(i,1) < processed(i+1,1))
        processed(i,1) = processed(i-1,1);
    else
        processed(i,1) = processed(i,1);
    end
end

plot(processed);
```

Sixth Order FDM Function Comparison

Comparison of the SNOTEL composite data for the five stations used to develop the FDM function are further used for comparison against the sixth order fit FDM function for individual hours FDM as well as cumulative FDM over a 24 hour period (Fig. A.1.1).

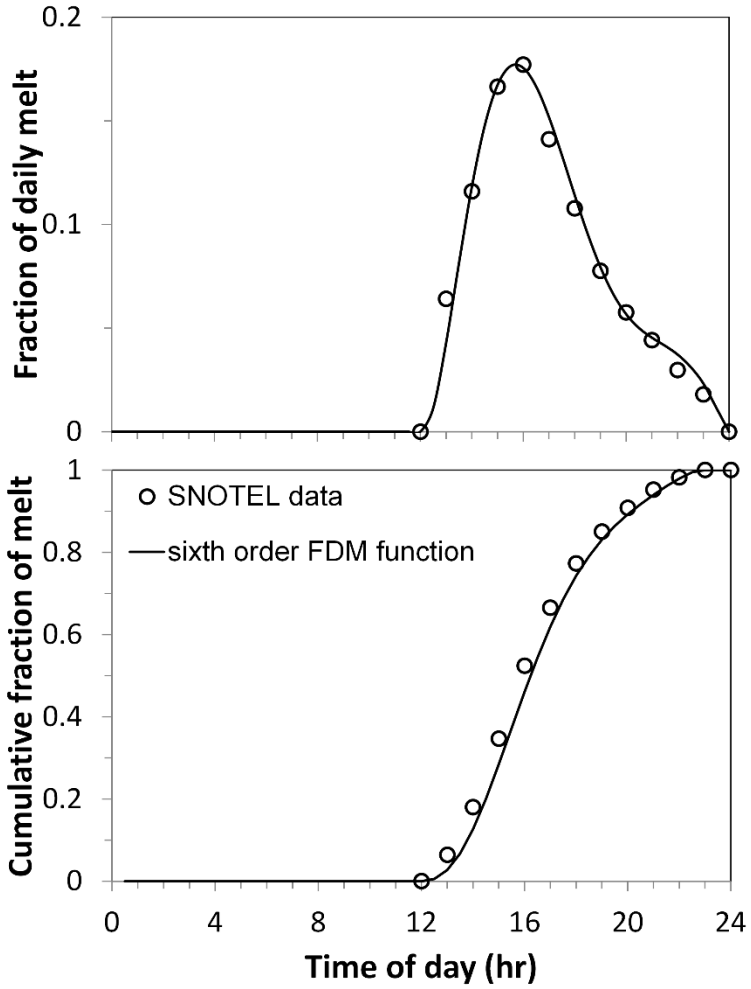

Figure A.1.1: Comparison of the fraction of daily melt (FDM) sixth order function to the SNOTEL data points for the five stations used to develop the function. Comparisons are for hourly FDM (top) as well as cumulative FDM (bottom).

APPENDIX A2: SUPPLEMENTARY MATERIAL FOR SIMULATING WATER FLOW THROUGH A LAYERED SNOWPACK

Hydraulic Properties of Snow Layers

The tables of snow pit and calculated hydraulic properties are on the following pages.

Table A.2.1: South aspect snow pit data and computed hydraulic properties.

RSSP12	South														
	Top (cm)	Avg. (cm)	Bottom (cm)	Depth (m)	Cumulative Depth (m)	Density (kg/m^3)	crystal diam. (mm)	Ksat (m/s)	Abs. Perm. (m^2)	alpha	1/P0	n	m	Theta S	Theta R
layer 1	162	157	152	0.1	0.1	67	1.0	1.71839	3.14E-07	16.5	1.68E-03	7.25	0.86	0.926936	0.02
layer 2	152	149.5	147	0.05	0.15	140.5	1.0	0.660927	1.21E-07	16.5	1.68E-03	7.25	0.86	0.846783	0.02
layer 3	147	144.5	142	0.05	0.2	140.5	0.7	0.323854	5.92E-08	12.12	1.24E-03	9.23	0.89	0.846783	0.02
layer 4	142	138.5	135	0.07	0.27	268.5	0.7	0.061331	1.12E-08	12.12	1.24E-03	9.23	0.89	0.707197	0.02
layer 5	135	133.5	132	0.03	0.3	268.5	1.0	0.125166	2.29E-08	16.5	1.68E-03	7.25	0.86	0.707197	0.02
layer 6	132	127	122	0.1	0.4	355	1.0	0.040656	7.43E-09	16.5	1.68E-03	7.25	0.86	0.612868	0.02
layer 7	122	117	112	0.1	0.5	404.5	1.0	0.021363	3.9E-09	16.5	1.68E-03	7.25	0.86	0.558888	0.02
layer 8	112	107	102	0.1	0.6	458	1.0	0.010656	1.95E-09	16.5	1.68E-03	7.25	0.86	0.500545	0.02
layer 9	102	100.5	99	0.03	0.63	461	1.0	0.010249	1.87E-09	16.5	1.68E-03	7.25	0.86	0.497274	0.02
layer 10	99	95.5	92	0.07	0.7	461	0.7	0.005022	9.17E-10	12.12	1.24E-03	9.23	0.89	0.497274	0.02
layer 11	92	87	82	0.1	0.8	394.5	0.7	0.011921	2.18E-09	12.12	1.24E-03	9.23	0.89	0.569793	0.02
layer 12	82	77	72	0.1	0.9	413.5	0.7	0.009312	1.7E-09	12.12	1.24E-03	9.23	0.89	0.549073	0.02
layer 13	72	67	62	0.1	1	338	0.7	0.024848	4.54E-09	12.12	1.24E-03	9.23	0.89	0.631407	0.02
layer 14	62	57	52	0.1	1.1	329	0.7	0.027933	5.1E-09	12.12	1.24E-03	9.23	0.89	0.641221	0.02
layer 15	52	47	42	0.1	1.2	350.5	0.7	0.021122	3.86E-09	12.12	1.24E-03	9.23	0.89	0.617775	0.02
layer 16	42	37	32	0.1	1.3	373.5	0.7	0.015663	2.86E-09	12.12	1.24E-03	9.23	0.89	0.592694	0.02
layer 17	32	29.5	27	0.05	1.35	380.5	0.7	0.0143	2.61E-09	12.12	1.24E-03	9.23	0.89	0.58506	0.02
layer 18	27	24.5	22	0.05	1.4	380.5	1.2	0.038597	7.05E-09	18.69	1.91E-03	6.44	0.84	0.58506	0.02
layer 19	22	17	12	0.1	1.5	342.5	1.2	0.063255	1.16E-08	18.69	1.91E-03	6.44	0.84	0.626499	0.02
layer 20	12	6	0	0.12	1.62	353	1.2	0.055184	1.01E-08	18.69	1.91E-03	6.44	0.84	0.615049	0.02

Table A2.2: Flat Aspect snow pit data and computed hydraulic properties.

RSSP04	Flat														
	Top (cm)	**Avg. (cm)**	**Bottom (cm)**	**Depth (m)**	**Cumulative Depth (m)**	**Density (kg/m3)**	**crystal diam. (mm)**	**Ksat (m/s)**	**Abs. Perm. (m^2)**	**alpha**	**1/P0**	**n**	**m**	**Theta S**	**Theta R**
layer 1	188	183	178	0.1	0.1	61	0.9	1.50481	2.75E-07	15.04	1.53E-03	7.85	0.87	0.93	0.02
layer 2	178	173	168	0.1	0.2	147.5	0.9	0.488785	8.93E-08	15.04	1.53E-03	7.85	0.87	0.84	0.02
layer 3	168	165.5	163	0.05	0.25	204.5	0.9	0.232973	4.26E-08	15.04	1.53E-03	7.85	0.87	0.78	0.02
layer 4	163	160.5	158	0.05	0.3	204.5	0.5	0.071905	1.31E-08	9.2	9.38E-04	10.90	0.91	0.78	0.02
layer 5	158	153	148	0.1	0.4	300.5	0.5	0.020642	3.77E-09	9.2	9.38E-04	10.90	0.91	0.67	0.02
layer 6	148	143	138	0.1	0.5	325	0.5	0.015012	2.74E-09	9.2	9.38E-04	10.90	0.91	0.65	0.02
layer 7	138	134	130	0.08	0.58	359.5	0.5	0.009586	1.75E-09	9.2	9.38E-04	10.90	0.91	0.61	0.02
layer 8	130	129	128	0.02	0.6	359.5	0.7	0.016201	2.96E-09	11.39	1.16E-03	9.62	0.90	0.61	0.02
layer 9	128	123	118	0.1	0.7	412.5	0.7	0.008134	1.49E-09	11.39	1.16E-03	9.62	0.90	0.55	0.02
layer 10	118	113	108	0.1	0.8	432	0.7	0.006313	1.15E-09	11.39	1.16E-03	9.62	0.90	0.53	0.02
layer 11	108	103	98	0.1	0.9	413	0.7	0.008081	1.48E-09	11.39	1.16E-03	9.62	0.90	0.55	0.02
layer 12	98	93	88	0.1	1	420	0.7	0.007379	1.35E-09	11.39	1.16E-03	9.62	0.90	0.54	0.02
layer 13	88	83	78	0.1	1.1	349	0.7	0.018571	3.39E-09	11.39	1.16E-03	9.62	0.90	0.62	0.02
layer 14	78	73	68	0.1	1.2	359	0.7	0.016307	2.98E-09	11.39	1.16E-03	9.62	0.90	0.61	0.02
layer 15	68	63	58	0.1	1.3	364.5	0.7	0.015181	2.77E-09	11.39	1.16E-03	9.62	0.90	0.60	0.02
layer 16	58	53	48	0.1	1.4	391	0.7	0.010757	1.97E-09	11.39	1.16E-03	9.62	0.90	0.57	0.02
layer 17	48	43	38	0.1	1.5	397	0.7	0.00995	1.82E-09	11.39	1.16E-03	9.62	0.90	0.57	0.02
layer 18	38	36.5	35	0.03	1.53	414.5	0.7	0.007925	1.45E-09	11.39	1.16E-03	9.62	0.90	0.55	0.02
layer 19	35	31.5	28	0.07	1.6	414.5	1.1	0.020681	3.78E-09	17.23	1.76E-03	6.97	0.86	0.55	0.02
layer 20	28	23	18	0.1	1.7	356	1.1	0.044244	8.08E-09	17.23	1.76E-03	6.97	0.86	0.61	0.02
layer 21	18	13	8	0.1	1.8	371	1.1	0.036406	6.65E-09	17.23	1.76E-03	6.97	0.86	0.60	0.02
layer 22	8	4	0	0.08	1.88	371	1.1	0.036406	6.65E-09	17.23	1.76E-03	6.97	0.86	0.60	0.02

Table A2.3: North Aspect snow pit data and computed hydraulic properties.

RSSP01	North														
	Top (cm)	Avg. (cm)	Bottom (cm)	Depth (m)	Cumulative Depth (m)	Density (kg/m^3)	crystal diam. (mm)	Ksat (m/s)	Abs. Perm. (m^2)	alpha (1/m)	1/P0	n	m	Theta S	Theta R
layer 1	230	225	220	0.1	0.1	48.5	0.3	0.196704	3.59E-08	6.28	6.40E-04	12.90	0.92	0.94711	0.02
layer 2	220	215	210	0.1	0.2	131	0.3	0.067303	1.23E-08	6.28	6.40E-04	12.90	0.92	0.85714	0.02
layer 3	210	205	200	0.1	0.3	164	0.3	0.043825	8.01E-09	6.28	6.40E-04	12.90	0.92	0.82116	0.02
layer 4	200	195	190	0.1	0.4	202	0.4	0.04754	8.68E-09	7.74	7.89E-04	11.85	0.92	0.77972	0.02
layer 5	190	188	186	0.04	0.44	236	1.0	0.190975	3.49E-08	16.5	1.68E-03	7.25	0.86	0.74264	0.02
layer 6	186	183	180	0.06	0.5	236	0.3	0.017188	3.14E-09	6.28	6.40E-04	12.90	0.92	0.74264	0.02
layer 7	180	177.5	175	0.05	0.55	234.5	1.5	0.438155	8E-08	23.8	2.43E-03	4.94	0.80	0.74427	0.02
layer 8	175	172.5	170	0.05	0.6	234.5	0.2	0.007789	1.42E-09	4.82	4.91E-04	14.04	0.93	0.74427	0.02
layer 9	170	165	160	0.1	0.7	250.5	0.2	0.006327	1.16E-09	4.82	4.91E-04	14.04	0.93	0.72683	0.02
layer 10	160	155	150	0.1	0.8	274	0.2	0.004661	8.51E-10	4.82	4.91E-04	14.04	0.93	0.7012	0.02
layer 11	150	145	140	0.1	0.9	319	0.2	0.002597	4.74E-10	4.82	4.91E-04	14.04	0.93	0.65213	0.02
layer 12	140	135	130	0.1	1	318.5	0.2	0.002614	4.77E-10	4.82	4.91E-04	14.04	0.93	0.65267	0.02
layer 13	130	125	120	0.1	1.1	308.5	0.2	0.002977	5.44E-10	4.82	4.91E-04	14.04	0.93	0.66358	0.02
layer 14	120	116.5	113	0.07	1.17	318.5	0.2	0.002614	4.77E-10	4.82	4.91E-04	14.04	0.93	0.65267	0.02
layer 15	113	111.5	110	0.03	1.2	318.5	0.3	0.005881	1.07E-09	6.28	6.40E-04	12.90	0.92	0.65267	0.02
layer 16	110	105	100	0.1	1.3	321	0.3	0.005693	1.04E-09	6.28	6.40E-04	12.90	0.92	0.64995	0.02
layer 17	100	95	90	0.1	1.4	340.5	0.3	0.004418	8.07E-10	6.28	6.40E-04	12.90	0.92	0.62868	0.02
layer 18	90	85	80	0.1	1.5	343.5	0.3	0.004249	7.76E-10	6.28	6.40E-04	12.90	0.92	0.62541	0.02
layer 19	80	75	70	0.1	1.6	362.5	0.3	0.003319	6.06E-10	6.28	6.40E-04	12.90	0.92	0.60469	0.02
layer 20	70	65	60	0.1	1.7	378.5	0.3	0.002696	4.92E-10	6.28	6.40E-04	12.90	0.92	0.58724	0.02
layer 21	60	55.5	51	0.09	1.79	389.5	0.3	0.002337	4.27E-10	6.28	6.40E-04	12.90	0.92	0.57525	0.02
layer 22	51	49.5	48	0.03	1.82	356.5	1	0.039871	7.28E-09	16.5	1.68E-03	7.25	0.86	0.61123	0.02
layer 23	48	46	44	0.04	1.86	356.5	0.8	0.025517	4.66E-09	13.58	1.38E-03	8.51	0.88	0.61123	0.02
layer 24	44	42	40	0.04	1.9	356.5	1	0.039871	7.28E-09	16.5	1.68E-03	7.25	0.86	0.61123	0.02
layer 25	40	35	30	0.1	2	321	1	0.063253	1.16E-08	16.5	1.68E-03	7.25	0.86	0.64995	0.02
layer 26	30	25	20	0.1	2.1	349	1	0.043954	8.03E-09	16.5	1.68E-03	7.25	0.86	0.61941	0.02
layer 27	10	5	0	0.1	2.2	359.5	1	0.038346	7E-09	16.5	1.68E-03	7.25	0.86	0.60796	0.02

TOUGH2 Output Files

The following documents are TOUGH2 output files for the EOS9 module that include the input parameters for the 15 total simulations. Included are three simulation files, one for each aspect (south, flat, and north) at a generation rate of 1.0 mm/hr. These output files are for example only and thus shortened to show parameters that may be important for reproduction of work, but unnecessary data such as intermittent time step results have been omitted.

South Aspect – 1.0 mm/hr

```
  TOUGH2 IS A PROGRAM FOR MULTIPHASE MULTICOMPONENT FLOW IN PERMEABLE
MEDIA, INCLUDING HEAT FLOW.
         IT IS A MEMBER OF THE MULKOM FAMILY OF CODES, DEVELOPED BY
KARSTEN PRUESS AT LAWRENCE BERKELEY NATIONAL LABORATORY.

                                    COPYRIGHT (C) 1999, THE REGENTS OF
THE UNIVERSITY OF CALIFORNIA.


********************************************************************
**********
                          *********  THIS IS TOUGH2 RUN NO.    1
CALLED BY iTOUGH2 RUN NO.    1  *********
                          ************  iTOUGH2 V6.9 (OCTOBER, 2014)
FOR LINUX, S. FINSTERLE  ************
                          ********************      EQUATION OF STATE
MODULE:  9       ******************
                          ********************    TODAY'S DATE:   10-
Jun-15  09:50     ******************

********************************************************************
**********


================================================================
============================================================

 UNIX COMMAND LINE: ./itough2 -tough2 South_input_1_mm_hr.txt 9
 PROBLEM TITLE    :  *RE South Aspect Snow Pit Simulation


================================================================
============================================================

 PARAMETERS FOR FLEXIBLE DIMENSIONING OF MAJOR ARRAYS (SEE FILE
maxsize.inc) ARE SUMMARIZED AT THE END.
```

```
================================================================================
================================================================

 ====================================
           MESH IS 2-D YZ
 ------------------------------------
 COORD.         MINIMUM         MAXIMUM
 ------------------------------------
   Y        0.25000E+00     0.24750E+02
   Z       -0.29205E+01    -0.15150E-01
 ====================================
 ALL NCON =  41728 CONNECTIONS READ FROM FILE *MESH* REFERENCE KNOWN
ELEMENTS



********************************************************************************
************************************************************
 *                              EOS9: EQUATION OF STATE FOR
SATURATED/UNSATURATED FLOW (RICHARDS EQUATION)
*

********************************************************************************
************************************************************


    OPTIONS SELECTED ARE: (NK,NEQ,NPH,NB) = (1,1,1, 6)

                          NK  =  1   - NUMBER OF FLUID COMPONENTS
                          NEQ =  1   - NUMBER OF EQUATIONS PER GRID
BLOCK
                          NPH =  1   - NUMBER OF PHASES THAT CAN BE
PRESENT
                          NB  =  6   - NUMBER OF SECONDARY PARAMETERS
(OTHER THAN COMPONENT MASS FRACTIONS)


    ONLY AVAILABLE OPTION IS: (NK,NEQ,NPH,NB) = (1,1,1,6)


********************************************************************************
************************************************************

 REFERENCE CONDITIONS
 --------------------

 GAS PRESSURE             = 0.101250E+06 PA
 TEMPERATURE              = 0.500000E+01 DEG-C
 SATURATED VAPOR PRESSURE = 0.871835E+03 PA
 WATER DENSITY            = 0.100002E+04 KG/M^3
 WATER VISCOSITY          = 0.150116E-02 PA-S
```

```
 WATER COMPRESSIBILITY    = 0.485869E-09 1/PA


 THE PRIMARY VARIABLE X1 IS PRESSURE FOR (X1.GE.0.101250E+06); IT IS
LIQUID SATURATION FOR (X1.LT. 1.)


************************************************************************
************************************************************

 ********** VOLUME- AND MASS-BALANCES
************************************************************************
**********************

 ********** [KCYC,ITER] = [   0,  0] *****
THE TIME IS  0.00000E+00 SECONDS, OR  0.00000E+00 DAYS


 PHASE VOLUMES IN PLACE
 GAS  0.47797E+02 M**3;   LIQUID  0.30388E+01 M**3

 LIQUID MASS IN PLACE  0.30389E+04 KG


************************************************************************
************************************************************



 MESH HAS 21100 ELEMENTS ( 21100 ACTIVE) AND 41728 CONNECTIONS
(INTERFACES) BETWEEN THEM
 GENER HAS   50 SINKS/SOURCES

************************************************************************
************************************************************
 *
*
 *                                        M A T R I X   S O L V E R
*
 *
*

************************************************************************
************************************************************

    THE SOLVER IS DETERMINED FROM MOP(21)

    THE SOLUTION METHOD INDICATOR MATSLV =  3
         MATSLV = 1: MATB - (PROPRIETARY - MAY NOT BE AVAILABLE)
         MATSLV = 2: DSLUBC - BI-CONJUGATE GRADIENT SOLVER
                                        INCOMPLETE LU FACTORIZATION
PRECONDITIONING
```

```
         MATSLV = 3: DSLUCS - LANCZOS-TYPE CONJUGATE GRADIENT SQUARED
SOLVER
                                          INCOMPLETE LU FACTORIZATION
PRECONDITIONING
         MATSLV = 4: DSLUGM - GENERALIZED MINIMUM RESIDUAL CONJUGATE
GRADIENT SOLVER
                                          INCOMPLETE LU FACTORIZATION
PRECONDITIONING
         MATSLV = 5: DLUSTB - STABILIZED BI-CONJUGATE GRADIENT SOLVER
                                          INCOMPLETE LU FACTORIZATION
PRECONDITIONING
         MATSLV = 6: LUBAND - DIRECT SOLVER USING LU DECOMPOSITION

    RITMAX: MAXIMUM # OF CG ITERATIONS AS FRACTION OF THE TOTAL NUMBER
OF EQUATIONS           =  1.00000E-01
         (0.0 < RITMAX <= 1.0,   DEFAULT = 0.1)
    CLOSUR: CONVERGENCE CRITERION FOR THE CG ITERATIONS
=  1.00000E-06
         (1.0E-12 <= CLOSUR <= 1.0E-6,  DEFAULT = 1.0E-6)
    NMAXIT: MAXIMUM # OF CG ITERATIONS - NOT TO EXCEED THE TOTAL
NUMBER OF EQUATIONS NELA*NEQ =  2110
         (20 < NMAXIT <= NREDM)

 !!!!! NEQ=1; DO NOT PERFORM ANY MATRIX PREPROCESSING

    THE MATRIX Z-PREPROCESSING SYSTEM IS ZPROCS = Z0

         ZPROCS = Z0: NO Z-PREPROCESSING; DEFAULT FOR NEQ = 1 AND FOR
MATSLV = 6
         ZPROCS = Z1: REPLACEMENT OF ZEROS ON THE MAIN-DIAGONAL BY A
SMALL NUMBER;
                       DEFAULT FOR NEQ > 1 AND FOR 2 < MATSLV < 6
         ZPROCS = Z2: LINEAR COMBINATION Of EQUATIONS IN EACH ELEMENT
TO PRODUCE NON-ZERO MAIN DIAGONAL ENTRIES
         ZPROCS = Z3: NORMALIZATION OF EQUATIONS, FOLLOWED BY Z2
         ZPROCS = Z4: SAME AS IN OPROCS = O4


    THE MATRIX O-PREPROCESSING SYSTEM IS OPROCS = O0

         OPROCS = O0: NO O-PREPROCESSING; DEFAULT (AND ONLY OPTION FOR
NEQ=1)
         OPROCS = O1: ELIMINATION OF LOWER HALF OF THE MAIN-DIAGONAL
SUBMATRIX WITH CENTER PIVOTING
         OPROCS = O2: O1+ELIMINATION OF UPPER HALF OF THE MAIN-
DIAGONAL SUBMATRIX WITH CENTER PIVOTING
         OPROCS = O3: O2+NORMALIZATION - RESULTS IN UNIT MAIN-DIAGONAL
SUBMATRICES
         OPROCS = O4: PRE-PROCESSING WHICH RESULTS IN UNIT MAIN-
DIAGONAL SUBMATRICES WITHOUT CENTER PIVOTING
```

```
 VALUE OF INCREMENT FACTOR FOR NUMERICAL DERIVATIVES:    1.05367E-08
1
     TOUGH2 INPUT DATA

     PROBLEM TITLE: *RE South Aspect Snow Pit Simulation


********************************************************************************
**********************************************

********************************************************************************
**********************************************

     PROBLEM SPECIFICATIONS

     NOITE  KDATA    MCYC   MSEC          MCYPR  MOP-
123456789012345678901234
         5      2  999999      0           9999
100000100001000300003000

            DIFF0           TEXP             BE             ZA
      0.00000E+00    0.00000E+00    0.00000E+00    0.00000E+00

           TSTART          TIMAX         DELTEN         DELTMX
ELST             GF          REDLT          SCALE
      0.00000E+00    0.86400E+05    0.10000E+01    0.36000E+04
0.98066E+01    0.40000E+01    0.10000E+01

      A CONSTANT TIME STEP OF DELTEN IS PRESCRIBED

              RE1            RE2              U            WUP
WNR           DFAC            FOR          AMRES
      0.10000E-04    0.10000E+01    0.10000E+00    0.10000E+01
0.10000E+01    0.10537E-07    0.10000E+01    0.10000E+06

           DEP(1)         DEP(2)
      0.00000E+00

********************************************************************************
**********************************************

     ROCK PROPERTIES

     ------------------------------------------------------------------
---------------------------------------- LAY01 --
     DOMAIN     MAT        DENSITY        POROSITY   HEAT COND. WET
HEAT CAP.      COMPRESS.    EXPANSIVITY
        1      LAY01     0.6700E+02     0.9300E+00     0.2000E+01
0.1000E+04     0.0000E+00     0.0000E+00

            PERM1          PERM2          PERM3      HEAT COND. DRY
TORTUOSITY    KLINKENBERG
```

```
          0.3140E-06     0.3140E-06     0.3140E-06     0.2000E+01
0.0000E+00     0.0000E+00

     REL. PERM.  IRP          RP(1)       RP(2)       RP(3)
RP(4)
                   7     0.8600E+00  0.2000E-01  0.9300E+00  0.1000E-
01
     CAP. PRES.  ICP          CP(1)       CP(2)       CP(3)
CP(4)       CP(5)
                   7     0.8600E+00  0.1000E-01  0.1680E-02
0.1000E+06  0.9300E+00

     ------------------------------------------------------------------
---------------------------------------- LAY02 --
     DOMAIN     MAT        DENSITY        POROSITY   HEAT COND. WET
HEAT CAP.      COMPRESS.    EXPANSIVITY
        2      LAY02     0.1405E+03     0.8500E+00     0.2000E+01
0.1000E+04     0.0000E+00     0.0000E+00

            PERM1          PERM2          PERM3      HEAT COND. DRY
TORTUOSITY    KLINKENBERG
          0.1210E-06     0.1210E-06     0.1210E+01     0.2000E+01
0.0000E+00     0.0000E+00

     REL. PERM.  IRP          RP(1)       RP(2)       RP(3)
RP(4)
                   7     0.8600E+00  0.2000E-01  0.8500E+00  0.1000E-
01
     CAP. PRES.  ICP          CP(1)       CP(2)       CP(3)
CP(4)       CP(5)
                   7     0.8600E+00  0.1000E-01  0.1680E-02
0.1000E+06  0.8500E+00

     ------------------------------------------------------------------
---------------------------------------- LAY03 --
     DOMAIN     MAT        DENSITY        POROSITY   HEAT COND. WET
HEAT CAP.      COMPRESS.    EXPANSIVITY
        3      LAY03     0.1405E+03     0.8500E+00     0.2000E+01
0.1000E+04     0.0000E+00     0.0000E+00

            PERM1          PERM2          PERM3      HEAT COND. DRY
TORTUOSITY    KLINKENBERG
          0.5920E-07     0.5920E-07     0.5920E-07     0.2000E+01
0.0000E+00     0.0000E+00

     REL. PERM.  IRP          RP(1)       RP(2)       RP(3)
RP(4)
                   7     0.8900E+00  0.2000E-01  0.8500E+00  0.1000E-
01
     CAP. PRES.  ICP          CP(1)       CP(2)       CP(3)
CP(4)       CP(5)
```

```
                  7     0.8900E+00  0.1000E-01  0.1240E-02
0.1000E+06  0.8500E+00

     ------------------------------------------------------------------
---------------------------------------- LAY04 --
     DOMAIN     MAT        DENSITY        POROSITY   HEAT COND. WET
HEAT CAP.      COMPRESS.    EXPANSIVITY
        4      LAY04     0.2685E+03     0.7100E+00     0.2000E+01
0.1000E+04     0.0000E+00     0.0000E+00

            PERM1          PERM2          PERM3      HEAT COND. DRY
TORTUOSITY    KLINKENBERG
          0.1120E-07     0.1120E-07     0.1120E-07     0.2000E+01
0.0000E+00     0.0000E+00

     REL. PERM.  IRP          RP(1)       RP(2)       RP(3)
RP(4)
                  7     0.8900E+00  0.2000E-01  0.7100E+00  0.1000E-
01
     CAP. PRES.  ICP          CP(1)       CP(2)       CP(3)
CP(4)       CP(5)
                  7     0.8900E+00  0.1000E-01  0.1240E-02
0.1000E+06  0.7100E+00

     ------------------------------------------------------------------
---------------------------------------- LAY05 --
     DOMAIN     MAT        DENSITY        POROSITY   HEAT COND. WET
HEAT CAP.      COMPRESS.    EXPANSIVITY
        5      LAY05     0.2685E+03     0.7100E+00     0.2000E+01
0.1000E+04     0.0000E+00     0.0000E+00

            PERM1          PERM2          PERM3      HEAT COND. DRY
TORTUOSITY    KLINKENBERG
          0.2290E-07     0.2290E-07     0.2290E-07     0.2000E+01
0.0000E+00     0.0000E+00

     REL. PERM.  IRP          RP(1)       RP(2)       RP(3)
RP(4)
                  7     0.8600E+00  0.2000E-01  0.7100E+00  0.1000E-
01
     CAP. PRES.  ICP          CP(1)       CP(2)       CP(3)
CP(4)       CP(5)
                  7     0.8600E+00  0.1000E-01  0.1680E-02
0.1000E+06  0.7100E+00

     ------------------------------------------------------------------
---------------------------------------- LAY06 --
     DOMAIN     MAT        DENSITY        POROSITY   HEAT COND. WET
HEAT CAP.      COMPRESS.    EXPANSIVITY
        6      LAY06     0.3550E+03     0.6100E+00     0.2000E+01
0.1000E+04     0.0000E+00     0.0000E+00
```

```
            PERM1          PERM2          PERM3      HEAT COND. DRY
TORTUOSITY    KLINKENBERG
          0.7430E-08     0.7430E-08     0.7430E-08     0.2000E+01
0.0000E+00     0.0000E+00

     REL. PERM.  IRP          RP(1)       RP(2)       RP(3)
RP(4)
                   7     0.8600E+00  0.2000E-01  0.6100E+00  0.1000E-
01
     CAP. PRES.  ICP          CP(1)       CP(2)       CP(3)
CP(4)       CP(5)
                   7     0.8600E+00  0.1000E-01  0.1680E-02
0.1000E+06  0.6100E+00

     ------------------------------------------------------------------
---------------------------------------- LAY07 --
     DOMAIN     MAT        DENSITY        POROSITY   HEAT COND. WET
HEAT CAP.      COMPRESS.    EXPANSIVITY
        7      LAY07     0.4045E+03     0.5600E+00     0.2000E+01
0.1000E+04     0.0000E+00     0.0000E+00

            PERM1          PERM2          PERM3      HEAT COND. DRY
TORTUOSITY    KLINKENBERG
          0.3900E-08     0.3900E-08     0.3900E-08     0.2000E+01
0.0000E+00     0.0000E+00

     REL. PERM.  IRP          RP(1)       RP(2)       RP(3)
RP(4)
                   7     0.8600E+00  0.2000E-01  0.5600E+00  0.1000E-
01
     CAP. PRES.  ICP          CP(1)       CP(2)       CP(3)
CP(4)       CP(5)
                   7     0.8600E+00  0.1000E-01  0.1680E-02
0.1000E+06  0.5600E+00

     ------------------------------------------------------------------
---------------------------------------- LAY08 --
     DOMAIN     MAT        DENSITY        POROSITY   HEAT COND. WET
HEAT CAP.      COMPRESS.    EXPANSIVITY
        8      LAY08     0.4580E+03     0.5000E+00     0.2000E+01
0.1000E+04     0.0000E+00     0.0000E+00

            PERM1          PERM2          PERM3      HEAT COND. DRY
TORTUOSITY    KLINKENBERG
          0.1950E-08     0.1950E-08     0.1950E-08     0.2000E+01
0.0000E+00     0.0000E+00

     REL. PERM.  IRP          RP(1)       RP(2)       RP(3)
RP(4)
                   7     0.8600E+00  0.2000E-01  0.5000E+00  0.1000E-
01
```

```
     CAP. PRES.  ICP          CP(1)       CP(2)       CP(3)
CP(4)       CP(5)
                   7     0.8600E+00  0.1000E-01  0.1680E-02
0.1000E+06  0.5000E+00

     ------------------------------------------------------------------
---------------------------------------- LAY09 --
     DOMAIN     MAT        DENSITY        POROSITY   HEAT COND. WET
HEAT CAP.      COMPRESS.    EXPANSIVITY
        9      LAY09     0.4610E+03     0.5000E+00     0.2000E+01
0.1000E+04     0.0000E+00     0.0000E+00

            PERM1          PERM2          PERM3      HEAT COND. DRY
TORTUOSITY    KLINKENBERG
          0.1870E-08     0.1870E-08     0.1870E-08     0.2000E+01
0.0000E+00     0.0000E+00

     REL. PERM.  IRP          RP(1)       RP(2)       RP(3)
RP(4)
                   7     0.8600E+00  0.2000E-01  0.5000E+00  0.1000E-
01
     CAP. PRES.  ICP          CP(1)       CP(2)       CP(3)
CP(4)       CP(5)
                   7     0.8600E+00  0.1000E-01  0.1680E-02
0.1000E+06  0.5000E+00

     ------------------------------------------------------------------
---------------------------------------- LAY10 --
     DOMAIN     MAT        DENSITY        POROSITY   HEAT COND. WET
HEAT CAP.      COMPRESS.    EXPANSIVITY
       10      LAY10     0.4610E+03     0.5000E+00     0.2000E+01
0.1000E+04     0.0000E+00     0.0000E+00

            PERM1          PERM2          PERM3      HEAT COND. DRY
TORTUOSITY    KLINKENBERG
          0.9170E-09     0.9170E-09     0.9170E-09     0.2000E+01
0.0000E+00     0.0000E+00

     REL. PERM.  IRP          RP(1)       RP(2)       RP(3)
RP(4)
                   7     0.8900E+00  0.2000E-01  0.5000E+00  0.1000E-
01
     CAP. PRES.  ICP          CP(1)       CP(2)       CP(3)
CP(4)       CP(5)
                   7     0.8900E+00  0.1000E-01  0.1240E-02
0.1000E+06  0.5000E+00

     ------------------------------------------------------------------
---------------------------------------- LAY11 --
     DOMAIN     MAT        DENSITY        POROSITY   HEAT COND. WET
HEAT CAP.      COMPRESS.    EXPANSIVITY
```

```
       11      LAY11     0.3945E+03     0.5700E+00     0.2000E+01
0.1000E+04     0.0000E+00     0.0000E+00

            PERM1          PERM2          PERM3      HEAT COND. DRY
TORTUOSITY    KLINKENBERG
          0.2180E-08     0.2180E-08     0.2180E-08     0.2000E+01
0.0000E+00     0.0000E+00

     REL. PERM.  IRP          RP(1)       RP(2)       RP(3)
RP(4)
                  7     0.8900E+00  0.2000E-01  0.5700E+00  0.1000E-
01
     CAP. PRES.  ICP          CP(1)       CP(2)       CP(3)
CP(4)       CP(5)
                  7     0.8900E+00  0.1000E-01  0.1240E-02
0.1000E+06  0.5700E+00

     ------------------------------------------------------------------
---------------------------------------- LAY12 --
     DOMAIN     MAT        DENSITY        POROSITY   HEAT COND. WET
HEAT CAP.      COMPRESS.    EXPANSIVITY
       12      LAY12     0.4135E+03     0.5500E+00     0.2000E+01
0.1000E+04     0.0000E+00     0.0000E+00

            PERM1          PERM2          PERM3      HEAT COND. DRY
TORTUOSITY    KLINKENBERG
          0.1700E-08     0.1700E-08     0.1700E-08     0.2000E+01
0.0000E+00     0.0000E+00

     REL. PERM.  IRP          RP(1)       RP(2)       RP(3)
RP(4)
                  7     0.8900E+00  0.2000E-01  0.5500E+00  0.1000E-
01
     CAP. PRES.  ICP          CP(1)       CP(2)       CP(3)
CP(4)       CP(5)
                  7     0.8900E+00  0.1000E-01  0.1240E-02
0.1000E+06  0.5500E+00

     ------------------------------------------------------------------
---------------------------------------- LAY13 --
     DOMAIN     MAT        DENSITY        POROSITY   HEAT COND. WET
HEAT CAP.      COMPRESS.    EXPANSIVITY
       13      LAY13     0.3380E+03     0.6300E+00     0.2000E+01
0.1000E+04     0.0000E+00     0.0000E+00

            PERM1          PERM2          PERM3      HEAT COND. DRY
TORTUOSITY    KLINKENBERG
          0.4540E-08     0.4540E-08     0.4540E-08     0.2000E+01
0.0000E+00     0.0000E+00

     REL. PERM.  IRP          RP(1)       RP(2)       RP(3)
RP(4)
```

```
                  7     0.8900E+00  0.2000E-01  0.6300E+00  0.1000E-
01
     CAP. PRES.  ICP          CP(1)       CP(2)       CP(3)
CP(4)       CP(5)
                  7     0.8900E+00  0.1000E-01  0.1240E-02
0.1000E+06  0.6300E+00

     ------------------------------------------------------------------
---------------------------------------- LAY14 --
     DOMAIN     MAT        DENSITY        POROSITY   HEAT COND. WET
HEAT CAP.      COMPRESS.    EXPANSIVITY
       14      LAY14     0.3290E+03     0.6400E+00     0.2000E+01
0.1000E+04     0.0000E+00     0.0000E+00

            PERM1          PERM2          PERM3      HEAT COND. DRY
TORTUOSITY    KLINKENBERG
          0.5100E-08     0.5100E-08     0.5100E-08     0.2000E+01
0.0000E+00     0.0000E+00

     REL. PERM.  IRP          RP(1)       RP(2)       RP(3)
RP(4)
                  7     0.8900E+00  0.2000E-01  0.6400E+00  0.1000E-
01
     CAP. PRES.  ICP          CP(1)       CP(2)       CP(3)
CP(4)       CP(5)
                  7     0.8900E+00  0.1000E-01  0.1240E-02
0.1000E+06  0.6400E+00

     ------------------------------------------------------------------
---------------------------------------- LAY15 --
     DOMAIN     MAT        DENSITY        POROSITY   HEAT COND. WET
HEAT CAP.      COMPRESS.    EXPANSIVITY
       15      LAY15     0.3505E+03     0.6200E+00     0.2000E+01
0.1000E+04     0.0000E+00     0.0000E+00

            PERM1          PERM2          PERM3      HEAT COND. DRY
TORTUOSITY    KLINKENBERG
          0.3860E-08     0.3860E-08     0.3860E-08     0.2000E+01
0.0000E+00     0.0000E+00

     REL. PERM.  IRP          RP(1)       RP(2)       RP(3)
RP(4)
                  7     0.8900E+00  0.2000E-01  0.6200E+00  0.1000E-
01
     CAP. PRES.  ICP          CP(1)       CP(2)       CP(3)
CP(4)       CP(5)
                  7     0.8900E+00  0.1000E-01  0.1240E-02
0.1000E+06  0.6200E+00

     ------------------------------------------------------------------
---------------------------------------- LAY16 --
```

```
     DOMAIN     MAT        DENSITY        POROSITY   HEAT COND. WET
HEAT CAP.      COMPRESS.    EXPANSIVITY
       16      LAY16     0.3735E+03     0.5900E+00     0.2000E+01
0.1000E+04     0.0000E+00     0.0000E+00

            PERM1          PERM2          PERM3      HEAT COND. DRY
TORTUOSITY    KLINKENBERG
          0.2860E-08     0.2860E-08     0.2860E-08     0.2000E+01
0.0000E+00     0.0000E+00

     REL. PERM.  IRP          RP(1)       RP(2)       RP(3)
RP(4)
                  7     0.8900E+00  0.2000E-01  0.5900E+00  0.1000E-
01
     CAP. PRES.  ICP          CP(1)       CP(2)       CP(3)
CP(4)       CP(5)
                  7     0.8900E+00  0.1000E-01  0.1240E-02
0.1000E+06  0.5900E+00

     ------------------------------------------------------------------
---------------------------------------- LAY17 --
     DOMAIN     MAT        DENSITY        POROSITY   HEAT COND. WET
HEAT CAP.      COMPRESS.    EXPANSIVITY
       17      LAY17     0.3805E+03     0.5900E+00     0.2000E+01
0.1000E+04     0.0000E+00     0.0000E+00

            PERM1          PERM2          PERM3      HEAT COND. DRY
TORTUOSITY    KLINKENBERG
          0.2610E-08     0.2610E-08     0.2610E-08     0.2000E+01
0.0000E+00     0.0000E+00

     REL. PERM.  IRP          RP(1)       RP(2)       RP(3)
RP(4)
                  7     0.8900E+00  0.2000E-01  0.5900E+00  0.1000E-
01
     CAP. PRES.  ICP          CP(1)       CP(2)       CP(3)
CP(4)       CP(5)
                  7     0.8900E+00  0.1000E-01  0.1240E-02
0.1000E+06  0.5900E+00

     ------------------------------------------------------------------
---------------------------------------- LAY18 --
     DOMAIN     MAT        DENSITY        POROSITY   HEAT COND. WET
HEAT CAP.      COMPRESS.    EXPANSIVITY
       18      LAY18     0.3805E+03     0.5900E+00     0.2000E+01
0.1000E+04     0.0000E+00     0.0000E+00

            PERM1          PERM2          PERM3      HEAT COND. DRY
TORTUOSITY    KLINKENBERG
          0.7050E-08     0.7050E-08     0.7050E-08     0.2000E+01
0.0000E+00     0.0000E+00
```

```
     REL. PERM.  IRP          RP(1)       RP(2)       RP(3)
RP(4)
                   7     0.8400E+00  0.2000E-01  0.5900E+00  0.1000E-
01
     CAP. PRES.  ICP          CP(1)       CP(2)       CP(3)
CP(4)       CP(5)
                   7     0.8400E+00  0.1000E-01  0.1910E-02
0.1000E+06  0.5900E+00

     ------------------------------------------------------------------
------------------------------------------ LAY19 --
     DOMAIN     MAT        DENSITY        POROSITY   HEAT COND. WET
HEAT CAP.      COMPRESS.    EXPANSIVITY
       19      LAY19     0.3425E+03     0.6300E+00     0.2000E+01
0.1000E+04     0.0000E+00     0.0000E+00

            PERM1          PERM2          PERM3      HEAT COND. DRY
TORTUOSITY    KLINKENBERG
          0.1160E-07     0.1160E-07     0.1160E-07     0.2000E+01
0.0000E+00     0.0000E+00

     REL. PERM.  IRP          RP(1)       RP(2)       RP(3)
RP(4)
                   7     0.8400E+00  0.2000E-01  0.6300E+00  0.1000E-
01
     CAP. PRES.  ICP          CP(1)       CP(2)       CP(3)
CP(4)       CP(5)
                   7     0.8400E+00  0.1000E-01  0.1910E-02
0.1000E+06  0.6300E+00

     ------------------------------------------------------------------
------------------------------------------ LAY20 --
     DOMAIN     MAT        DENSITY        POROSITY   HEAT COND. WET
HEAT CAP.      COMPRESS.    EXPANSIVITY
       20      LAY20     0.3530E+03     0.6200E+00     0.2000E+01
0.1000E+04     0.0000E+00     0.0000E+00

            PERM1          PERM2          PERM3      HEAT COND. DRY
TORTUOSITY    KLINKENBERG
          0.1010E-07     0.1010E-07     0.1010E-07     0.2000E+01
0.0000E+00     0.0000E+00

     REL. PERM.  IRP          RP(1)       RP(2)       RP(3)
RP(4)
                   7     0.8400E+00  0.2000E-01  0.6200E+00  0.1000E-
01
     CAP. PRES.  ICP          CP(1)       CP(2)       CP(3)
CP(4)       CP(5)
                   7     0.8400E+00  0.1000E-01  0.1910E-02
0.1000E+06  0.6200E+00
```

```
     ------------------------------------------------------------------
---------------------------------------- GRND  --
     DOMAIN     MAT        DENSITY        POROSITY   HEAT COND. WET
HEAT CAP.      COMPRESS.    EXPANSIVITY
       21      GRND      0.8800E+03     0.6700E+00     0.2000E+01
0.1000E+04     0.0000E+00     0.0000E+00

            PERM1          PERM2          PERM3      HEAT COND. DRY
TORTUOSITY    KLINKENBERG
          0.4480E-09     0.4480E-09     0.4480E-09     0.2000E+01
0.0000E+00     0.0000E+00

     REL. PERM.  IRP          RP(1)       RP(2)       RP(3)
RP(4)
                   7     0.8600E+00  0.1000E-01  0.6700E+00  0.1000E-
01
     CAP. PRES.  ICP          CP(1)       CP(2)       CP(3)
CP(4)       CP(5)
                   7     0.8600E+00  0.9000E-02  0.7650E-05
0.1000E+06  0.6700E+00

     ------------------------------------------------------------------
---------------------------------------- REFCO --
     DOMAIN     MAT        DENSITY        POROSITY   HEAT COND. WET
HEAT CAP.      COMPRESS.    EXPANSIVITY
       22      REFCO     0.1012E+06     0.5000E+01     0.0000E+00
0.0000E+00     0.0000E+00     0.0000E+00

            PERM1          PERM2          PERM3      HEAT COND. DRY
TORTUOSITY    KLINKENBERG
          0.0000E+00     0.0000E+00     0.0000E+00     0.0000E+00
0.0000E+00     0.0000E+00

     REL. PERM.  IRP
                   5
     CAP. PRES.  ICP          CP(1)       CP(2)       CP(3)
                   1     0.0000E+00  0.0000E+00  0.1000E+01


*********************************************************************
*******************************************

     END OF INPUT DATA


*********************************************************************
*******************************************

*********************************************************************
*******************************************
```

```
 END OF TOUGH2 INPUT JOB --- ELAPSED TIME =     1.660 SECONDS


..............  TIME STEP SIZE UNCHANGED            --> NEXT DELTEX =
1.280000E+02
 ...ITERATING...  AT [ 1628, 1] --- DELTEX = 1.280000E+02   MAX. RES.
= 5.275373E-02  AT ELEMENT Ga101  EQUATION   1
 ...ITERATING...  AT [ 1628, 2] --- DELTEX = 1.280000E+02   MAX. RES.
= 3.288413E-02  AT ELEMENT Ga101  EQUATION   1
 ...ITERATING...  AT [ 1628, 3] --- DELTEX = 1.280000E+02   MAX. RES.
= 8.515200E-04  AT ELEMENT Ga101  EQUATION   1
 GZ101( 1628,4) ST =  8.6353E+04 DT =  1.2800E+02 DX1=  1.9842E-05
DX2=  0.0000E+00 T =   5.000 P =   101250. S =  2.0068E-02

 -------------- REDUCE TIME STEP BY FACTOR OF    0.37 --> NEXT DELTEX
= 4.687500E+01
 ...ITERATING...  AT [ 1629, 1] --- DELTEX = 4.687500E+01   MAX. RES.
= 4.339327E-02  AT ELEMENT Ga101  EQUATION   1
 ...ITERATING...  AT [ 1629, 2] --- DELTEX = 4.687500E+01   MAX. RES.
= 5.034545E-04  AT ELEMENT Gb101  EQUATION   1
 Ga101( 1629,3) ST =  8.6400E+04 DT =  4.6875E+01 DX1=  6.5349E-04
DX2=  0.0000E+00 T =   5.000 P =   101250. S =  1.3025E-02

 CPU-TIME SINCE LAST OUTPUT:  2929.39 SEC;  TOTAL CPU-TIME:  2929.39
SEC;  SIMULATION TIME:          86400.00 SEC;  TIME STEPS: 1629


 *RE South Aspect Snow Pit Simulation

          OUTPUT DATA AFTER ( 1629, 3)-2-TIME STEPS
THE TIME IS  0.10000E+01 DAYS


@@@@@@@@@@@@@@@@@@@@@@@@@@@@@@@@@@@@@@@@@@@@@@@@@@@@@@@@@@@@@@@@@@@@@@@@@@@@
@@@@@@@@@@@@@@@@@@@@@@@@@@@@@@@@@@@@@@@@@@@@@@@@@@@@@@@@@@@@

  TOTAL TIME     KCYC   ITER  ITERC   KON        DX1M
MAX. RES.      NER    KER        DELTEX
  0.86400E+05   1629      3   7495     2       0.65349E-03
0.48619E-06     402     1       0.46875E+02

@@@@@@@@@@@@@@@@@@@@@@@@@@@@@@@@@@@@@@@@@@@@@@@@@@@@@@@@@@@@@@@@@@@@@@@@@@@@
@@@@@@@@@@@@@@@@@@@@@@@@@@@@@@@@@@@@@@@@@@@@@@@@@@@@@@@@@@@@


 ********** VOLUME- AND MASS-BALANCES
**********************************************************************
**********************

 ********** [KCYC,ITER] = [1629,  3] *****
THE TIME IS  0.86400E+05 SECONDS, OR  0.10000E+01 DAYS
```

```
 PHASE VOLUMES IN PLACE
 GAS  0.48504E+02 M**3;   LIQUID  0.23317E+01 M**3

 LIQUID MASS IN PLACE  0.23318E+04 KG


**********************************************************************
**********************************************************

 WRITE FILE *SAVE* AFTER  1629 TIME STEPS  ---  THE TIME IS
0.864000E+05 SECONDS


======================================================================
============================================================
      ARRAY DIMENSIONS (SEE FILE maxsize.inc)
 ----------------------------------------------------------------------
------------------------------------------------------------
      MAXEL     =  100000      Maximum number of elements
      MAXCON    =  400000      Maximum number of connections
      MAXK      =       3      Maximum number of components
      MAXEQ     =       4      Maximum number of equations
      MAXPH     =       2      Maximum number of phases
      MAXB      =       8      Maximum number of phase-dependent
secondary variables
      MAXSS     =     900      Maximum number of sinks/sources
      MAVTAB    =     100      Maximum average number of table entries
per sink/source
      MAXROC    =     200      Maximum number of rock types
      MAXTSP    =       5      Maximum number of specified time steps,
divided by eight
      MAXLAY    =      10      Maximum number of reservoir layers for
wells on deliverability
      MXRPCP    =      14      Maximum number of parameters for
relative permeability and capillary pressure functions
      MXPCTB    =       5      Maximum number of points in table for
ECM capillary pressure
      MXTBC     =       5      Maximum number of elements with time
vs. boundary condition
      MXTBCT    =     600      Maximum number of time vs. pressure
data
      MAXTIM    =    1000      Maximum number of calibration times
      MAXN      =      50      Maximum number of parameters to be
estimated
      MAXO      =     200      Maximum number of datasets
      MAXM      =    1400      Maximum number of calibration points
      MAXPD     =    1000      Maximum number of paired data
      MAXR      =     200      Maximum number of elements or indices
of each parameter or observation
```

```
      MAXBRK    =      20      Maximum number of points in time at
which SAVE file is written for restart
      MAXEBRK   =      50      Maximum number of elements with new
initial conditions after restart
      MAXCOEFF  =       5      Maximum number of coefficients for data
modeling functions
      MAXXGR    =       3      Dimension of third index of array
XGUESSR
      MTYPE     =      31      Number of observation types
      MPFMT     =       5      Number of plot file formats
 ------------------------------------------------------------------
-----------------------------------------------------------


 ------------------------------------------------------------------
-----------------------------------------------------------
      PROGRAM  VERSION   DATE                    COMMENT
 ------------------------------------------------------------------
-----------------------------------------------------------
      iTOUGH2            Current version       iTOUGH2 V6.9 (OCTOBER,
2014)
 ------------------------------------------------------------------
-----------------------------------------------------------



==================================================================
===========================================================

 ---   105th iTOUGH2 run stopped fatally       on 10-Jun-15  10:39 ---
CPU time used =    2930.09 sec.

@@@@@@@@@@@@@@@@@@@@@@@@@@@@@@@@@@@@@@@@@@@@@@@@@@@@@@@@@@@@@@@@@@@@@@@@
@@@@@@@@@@@@@@@@@@@@@@@@@@@@@@@@@@@@@@@@@@@@@@@@@@

  END OF TOUGH2 SIMULATION JOB --- ELAPSED TIME =     2930.09 SEC
```

Flat Aspect – 1.0 mm/hr

```
TOUGH2 IS A PROGRAM FOR MULTIPHASE MULTICOMPONENT FLOW IN PERMEABLE
MEDIA, INCLUDING HEAT FLOW.
         IT IS A MEMBER OF THE MULKOM FAMILY OF CODES, DEVELOPED BY
KARSTEN PRUESS AT LAWRENCE BERKELEY NATIONAL LABORATORY.

                                    COPYRIGHT (C) 1999, THE REGENTS OF
THE UNIVERSITY OF CALIFORNIA.

**********************************************************************
**********
```

```
                          *********  THIS IS TOUGH2 RUN NO.    1
CALLED BY iTOUGH2 RUN NO.    1  *********
                          ************  iTOUGH2 V6.9 (OCTOBER, 2014)
FOR LINUX, S. FINSTERLE  ************
                          ********************      EQUATION OF STATE
MODULE:  9       *******************
                          ********************    TODAY'S DATE:    9-
Jun-15  15:22     *******************

*******************************************************************
**********


================================================================
================================================================

 UNIX COMMAND LINE: ./itough2 -tough2 Flat_input_1_mm_hr.txt 9
 PROBLEM TITLE    :  *RE Spring Creek Flat Aspect Snow Pit 04


================================================================
================================================================

 PARAMETERS FOR FLEXIBLE DIMENSIONING OF MAJOR ARRAYS (SEE FILE
maxsize.inc) ARE SUMMARIZED AT THE END.


================================================================
================================================================


 ===================================
           MESH IS 2-D YZ
 -----------------------------------
 COORD.         MINIMUM        MAXIMUM
 -----------------------------------
   Y        0.25000E+00    0.24750E+02
   Z       -0.36158E+01   -0.15150E-01
 ===================================
 ALL NCON =  46282 CONNECTIONS READ FROM FILE *MESH* REFERENCE KNOWN
ELEMENTS



*******************************************************************
**********************************************************
 *                            EOS9: EQUATION OF STATE FOR
SATURATED/UNSATURATED FLOW (RICHARDS EQUATION)
*

*******************************************************************
**********************************************************
```

```
    OPTIONS SELECTED ARE: (NK,NEQ,NPH,NB) = (1,1,1, 6)

                          NK  =  1   - NUMBER OF FLUID COMPONENTS
                          NEQ =  1   - NUMBER OF EQUATIONS PER GRID
BLOCK
                          NPH =  1   - NUMBER OF PHASES THAT CAN BE
PRESENT
                          NB  =  6   - NUMBER OF SECONDARY PARAMETERS
(OTHER THAN COMPONENT MASS FRACTIONS)


    ONLY AVAILABLE OPTION IS: (NK,NEQ,NPH,NB) = (1,1,1,6)


*****************************************************************
************************************************************

 REFERENCE CONDITIONS
 --------------------

 GAS PRESSURE             = 0.101250E+06 PA
 TEMPERATURE              = 0.500000E+01 DEG-C
 SATURATED VAPOR PRESSURE = 0.871835E+03 PA
 WATER DENSITY            = 0.100002E+04 KG/M^3
 WATER VISCOSITY          = 0.150116E-02 PA-S
 WATER COMPRESSIBILITY    = 0.485869E-09 1/PA


 THE PRIMARY VARIABLE X1 IS PRESSURE FOR (X1.GE.0.101250E+06); IT IS
LIQUID SATURATION FOR (X1.LT. 1.)


*****************************************************************
************************************************************

 ********** VOLUME- AND MASS-BALANCES
*****************************************************************
**********************

 ********** [KCYC,ITER] = [   0,  0] *****
THE TIME IS  0.00000E+00 SECONDS, OR  0.00000E+00 DAYS


 PHASE VOLUMES IN PLACE
 GAS  0.59421E+02 M**3;   LIQUID  0.39668E+01 M**3

 LIQUID MASS IN PLACE  0.39668E+04 KG


*****************************************************************
************************************************************
```

```
 MESH HAS 23400 ELEMENTS ( 23400 ACTIVE) AND 46282 CONNECTIONS
(INTERFACES) BETWEEN THEM
 GENER HAS   50 SINKS/SOURCES

*********************************************************************
************************************************************
 *
*
 *                                        M A T R I X   S O L V E R
*
 *
*

*********************************************************************
************************************************************

    THE SOLVER IS DETERMINED FROM MOP(21)

    THE SOLUTION METHOD INDICATOR MATSLV =  3
         MATSLV = 1: MATB - (PROPRIETARY - MAY NOT BE AVAILABLE)
         MATSLV = 2: DSLUBC - BI-CONJUGATE GRADIENT SOLVER
                                          INCOMPLETE LU FACTORIZATION
PRECONDITIONING
         MATSLV = 3: DSLUCS - LANCZOS-TYPE CONJUGATE GRADIENT SQUARED
SOLVER
                                          INCOMPLETE LU FACTORIZATION
PRECONDITIONING
         MATSLV = 4: DSLUGM - GENERALIZED MINIMUM RESIDUAL CONJUGATE
GRADIENT SOLVER
                                          INCOMPLETE LU FACTORIZATION
PRECONDITIONING
         MATSLV = 5: DLUSTB - STABILIZED BI-CONJUGATE GRADIENT SOLVER
                                          INCOMPLETE LU FACTORIZATION
PRECONDITIONING
         MATSLV = 6: LUBAND - DIRECT SOLVER USING LU DECOMPOSITION

    RITMAX: MAXIMUM # OF CG ITERATIONS AS FRACTION OF THE TOTAL NUMBER
OF EQUATIONS           =  1.00000E-01
         (0.0 < RITMAX <= 1.0,   DEFAULT = 0.1)
    CLOSUR: CONVERGENCE CRITERION FOR THE CG ITERATIONS
=  1.00000E-06
         (1.0E-12 <= CLOSUR <= 1.0E-6,  DEFAULT = 1.0E-6)
    NMAXIT: MAXIMUM # OF CG ITERATIONS - NOT TO EXCEED THE TOTAL
NUMBER OF EQUATIONS NELA*NEQ =  2340
         (20 < NMAXIT <= NREDM)

 !!!!! NEQ=1; DO NOT PERFORM ANY MATRIX PREPROCESSING

    THE MATRIX Z-PREPROCESSING SYSTEM IS ZPROCS = Z0

         ZPROCS = Z0: NO Z-PREPROCESSING; DEFAULT FOR NEQ = 1 AND FOR
MATSLV = 6
```

```
         ZPROCS = Z1: REPLACEMENT OF ZEROS ON THE MAIN-DIAGONAL BY A
SMALL NUMBER;
                        DEFAULT FOR NEQ > 1 AND FOR 2 < MATSLV < 6
         ZPROCS = Z2: LINEAR COMBINATION Of EQUATIONS IN EACH ELEMENT
TO PRODUCE NON-ZERO MAIN DIAGONAL ENTRIES
         ZPROCS = Z3: NORMALIZATION OF EQUATIONS, FOLLOWED BY Z2
         ZPROCS = Z4: SAME AS IN OPROCS = O4


    THE MATRIX O-PREPROCESSING SYSTEM IS OPROCS = O0

         OPROCS = O0: NO O-PREPROCESSING; DEFAULT (AND ONLY OPTION FOR
NEQ=1)
         OPROCS = O1: ELIMINATION OF LOWER HALF OF THE MAIN-DIAGONAL
SUBMATRIX WITH CENTER PIVOTING
         OPROCS = O2: O1+ELIMINATION OF UPPER HALF OF THE MAIN-
DIAGONAL SUBMATRIX WITH CENTER PIVOTING
         OPROCS = O3: O2+NORMALIZATION - RESULTS IN UNIT MAIN-DIAGONAL
SUBMATRICES
         OPROCS = O4: PRE-PROCESSING WHICH RESULTS IN UNIT MAIN-
DIAGONAL SUBMATRICES WITHOUT CENTER PIVOTING


 VALUE OF INCREMENT FACTOR FOR NUMERICAL DERIVATIVES:    1.05367E-08
1
     TOUGH2 INPUT DATA

     PROBLEM TITLE: *RE Spring Creek Flat Aspect Snow Pit 04


********************************************************************
*********************************************

********************************************************************
*********************************************

     PROBLEM SPECIFICATIONS

     NOITE  KDATA    MCYC   MSEC          MCYPR  MOP-
123456789012345678901234
         5      2    2000      0           2000
100000100001000300003000

            DIFF0           TEXP             BE             ZA
      0.00000E+00    0.00000E+00    0.00000E+00    0.00000E+00

           TSTART          TIMAX         DELTEN         DELTMX
ELST             GF          REDLT          SCALE
      0.00000E+00    0.86400E+05    0.10000E+01    0.36000E+04
0.98066E+01    0.40000E+01    0.10000E+01
      A CONSTANT TIME STEP OF DELTEN IS PRESCRIBED
```

```
              RE1             RE2               U             WUP
WNR           DFAC             FOR           AMRES
      0.10000E-04    0.10000E+01    0.10000E+00    0.10000E+01
0.10000E+01    0.10537E-07    0.10000E+01    0.10000E+06

           DEP(1)         DEP(2)
      0.00000E+00

*************************************************************************
*****************************************

     ROCK PROPERTIES

     ------------------------------------------------------------------
---------------------------------------- LAY01 --
     DOMAIN     MAT         DENSITY         POROSITY   HEAT COND. WET
HEAT CAP.      COMPRESS.    EXPANSIVITY
        1      LAY01     0.6100E-02     0.9300E+00     0.2000E+01
0.1000E+04     0.0000E+00     0.0000E+00

            PERM1           PERM2           PERM3      HEAT COND. DRY
TORTUOSITY    KLINKENBERG
          0.2750E-06     0.2750E-06     0.2750E-06     0.2000E+01
0.0000E+00     0.0000E+00

     REL. PERM.  IRP          RP(1)       RP(2)       RP(3)
RP(4)
                  7     0.8700E+00  0.2000E-01  0.9300E+00  0.1000E-
01
     CAP. PRES.  ICP          CP(1)       CP(2)       CP(3)
CP(4)       CP(5)
                  7     0.8700E+00  0.1000E-01  0.1530E-02
0.1000E+06  0.9300E+00

     ------------------------------------------------------------------
---------------------------------------- LAY02 --
     DOMAIN     MAT         DENSITY         POROSITY   HEAT COND. WET
HEAT CAP.      COMPRESS.    EXPANSIVITY
        2      LAY02     0.1475E+03     0.8400E+00     0.2000E+01
0.1000E+04     0.0000E+00     0.0000E+00

            PERM1           PERM2           PERM3      HEAT COND. DRY
TORTUOSITY    KLINKENBERG
          0.8930E-07     0.8930E-07     0.8930E-07     0.2000E+01
0.0000E+00     0.0000E+00

     REL. PERM.  IRP          RP(1)       RP(2)       RP(3)
RP(4)
                  7     0.8700E+00  0.2000E-01  0.8400E+00  0.1000E-
01
    CAP. PRES.  ICP          CP(1)       CP(2)       CP(3)       CP(4)
CP(5)
```

```
                  7     0.8700E+00  0.1000E-01  0.1530E-02
0.1000E+06  0.8400E+00

     ------------------------------------------------------------------
---------------------------------------- LAY03 --
     DOMAIN     MAT        DENSITY        POROSITY   HEAT COND. WET
HEAT CAP.      COMPRESS.    EXPANSIVITY
        3      LAY03     0.2045E+03     0.7800E+00     0.2000E+01
0.1000E+04     0.0000E+00     0.0000E+00

            PERM1          PERM2          PERM3      HEAT COND. DRY
TORTUOSITY    KLINKENBERG
          0.4260E-07     0.4260E-07     0.4260E-07     0.2000E+01
0.0000E+00     0.0000E+00

     REL. PERM.  IRP          RP(1)       RP(2)       RP(3)
RP(4)
                  7     0.8700E+00  0.2000E-01  0.7800E+00  0.1000E-
01
     CAP. PRES.  ICP          CP(1)       CP(2)       CP(3)
CP(4)       CP(5)
                  7     0.8700E+00  0.1000E-01  0.1530E-02
0.1000E+06  0.7800E+00

     ------------------------------------------------------------------
---------------------------------------- LAY04 --
     DOMAIN     MAT        DENSITY        POROSITY   HEAT COND. WET
HEAT CAP.      COMPRESS.    EXPANSIVITY
        4      LAY04     0.2045E+03     0.7800E+00     0.2000E+01
0.1000E+04     0.0000E+00     0.0000E+00

            PERM1          PERM2          PERM3      HEAT COND. DRY
TORTUOSITY    KLINKENBERG
          0.1310E-07     0.1310E-07     0.1310E-07     0.2000E+01
0.0000E+00     0.0000E+00

     REL. PERM.  IRP          RP(1)       RP(2)       RP(3)
RP(4)
                  7     0.9100E+00  0.2000E-01  0.7800E+00  0.1000E-
01
     CAP. PRES.  ICP          CP(1)       CP(2)       CP(3)
CP(4)       CP(5)
                  7     0.9100E+00  0.1000E-01  0.9380E-03
0.1000E+06  0.7800E+00

     ------------------------------------------------------------------
---------------------------------------- LAY05 --
     DOMAIN     MAT        DENSITY        POROSITY   HEAT COND. WET
HEAT CAP.      COMPRESS.    EXPANSIVITY
        5      LAY05     0.3005E+03     0.6700E+00     0.2000E+01
0.1000E+04     0.0000E+00     0.0000E+00
```

```
           PERM1          PERM2          PERM3      HEAT COND. DRY
TORTUOSITY    KLINKENBERG
          0.3770E-08     0.3770E-08     0.3770E-08     0.2000E+01
0.0000E+00     0.0000E+00

     REL. PERM.  IRP          RP(1)       RP(2)       RP(3)
RP(4)
                  7     0.9100E+00  0.2000E-01  0.6700E+00  0.1000E-
01
     CAP. PRES.  ICP          CP(1)       CP(2)       CP(3)
CP(4)       CP(5)
                  7     0.9100E+00  0.1000E-01  0.9380E-03
0.1000E+06  0.6700E+00

     ------------------------------------------------------------
------------------------------------------ LAY06 --
     DOMAIN     MAT        DENSITY        POROSITY   HEAT COND. WET
HEAT CAP.      COMPRESS.    EXPANSIVITY
        6      LAY06     0.3250E+03     0.6500E+00     0.2000E+01
0.1000E+04     0.0000E+00     0.0000E+00

           PERM1          PERM2          PERM3      HEAT COND. DRY
TORTUOSITY    KLINKENBERG
          0.2740E-08     0.2740E-08     0.2740E-08     0.2000E+01
0.0000E+00     0.0000E+00

     REL. PERM.  IRP          RP(1)       RP(2)       RP(3)
RP(4)
                  7     0.9100E+00  0.2000E-01  0.6500E+00  0.1000E-
01
     CAP. PRES.  ICP          CP(1)       CP(2)       CP(3)
CP(4)       CP(5)
                  7     0.9100E+00  0.1000E-01  0.9380E-03
0.1000E+06  0.6500E+00

     ------------------------------------------------------------
------------------------------------------ LAY07 --
     DOMAIN     MAT        DENSITY        POROSITY   HEAT COND. WET
HEAT CAP.      COMPRESS.    EXPANSIVITY
        7      LAY07     0.3595E+03     0.6100E+00     0.2000E+01
0.1000E+04     0.0000E+00     0.0000E+00

           PERM1          PERM2          PERM3      HEAT COND. DRY
TORTUOSITY    KLINKENBERG
          0.1750E-08     0.1750E-08     0.1750E-08     0.2000E+01
0.0000E+00     0.0000E+00

     REL. PERM.  IRP          RP(1)       RP(2)       RP(3)
RP(4)
                  7     0.9100E+00  0.2000E-01  0.6100E+00  0.1000E-
01
```

```
     CAP. PRES.  ICP          CP(1)       CP(2)       CP(3)
CP(4)       CP(5)
                   7     0.9100E+00  0.1000E-01  0.9380E-03
0.1000E+06  0.6100E+00

     ------------------------------------------------------------------
---------------------------------------- LAY08 --
     DOMAIN     MAT        DENSITY        POROSITY   HEAT COND. WET
HEAT CAP.      COMPRESS.    EXPANSIVITY
        8      LAY08     0.3595E+03     0.6100E+00     0.2000E+01
0.1000E+04     0.0000E+00     0.0000E+00

            PERM1          PERM2          PERM3      HEAT COND. DRY
TORTUOSITY    KLINKENBERG
          0.2960E-08     0.2960E-08     0.2960E-08     0.2000E+01
0.0000E+00     0.0000E+00

     REL. PERM.  IRP          RP(1)       RP(2)       RP(3)
RP(4)
                   7     0.9000E+00  0.2000E-01  0.6100E+00  0.1000E-
01
     CAP. PRES.  ICP          CP(1)       CP(2)       CP(3)
CP(4)       CP(5)
                   7     0.9000E+00  0.1000E-01  0.1160E-02
0.1000E+06  0.6100E+00

     ------------------------------------------------------------------
---------------------------------------- LAY09 --
     DOMAIN     MAT        DENSITY        POROSITY   HEAT COND. WET
HEAT CAP.      COMPRESS.    EXPANSIVITY
        9      LAY09     0.4125E+03     0.5500E+00     0.2000E+01
0.1000E+04     0.0000E+00     0.0000E+00

            PERM1          PERM2          PERM3      HEAT COND. DRY
TORTUOSITY    KLINKENBERG
          0.1490E-08     0.1490E-08     0.1490E-08     0.2000E+01
0.0000E+00     0.0000E+00

     REL. PERM.  IRP          RP(1)       RP(2)       RP(3)
RP(4)
                   7     0.9000E+00  0.2000E-01  0.5500E+00  0.1000E-
01
     CAP. PRES.  ICP          CP(1)       CP(2)       CP(3)
CP(4)       CP(5)
                   7     0.9000E+00  0.1000E-01  0.1160E-02
0.1000E+06  0.5500E+00

     ------------------------------------------------------------------
---------------------------------------- LAY10 --
     DOMAIN     MAT        DENSITY        POROSITY   HEAT COND. WET
HEAT CAP.      COMPRESS.    EXPANSIVITY
```

```
       10      LAY10     0.4320E+03     0.5300E+00     0.2000E+01
0.1000E+04     0.0000E+00     0.0000E+00

            PERM1          PERM2          PERM3      HEAT COND. DRY
TORTUOSITY    KLINKENBERG
          0.1150E-08     0.1150E-08     0.1150E-08     0.2000E+01
0.0000E+00     0.0000E+00

     REL. PERM.  IRP          RP(1)       RP(2)       RP(3)
RP(4)
                   7     0.9000E+00  0.2000E-01  0.5300E+00  0.1000E-
01
     CAP. PRES.  ICP          CP(1)       CP(2)       CP(3)
CP(4)       CP(5)
                   7     0.9000E+00  0.1000E-01  0.1160E-02
0.1000E+06  0.5300E+00

     ------------------------------------------------------------------
------------------------------------------ LAY11 --
     DOMAIN     MAT        DENSITY        POROSITY   HEAT COND. WET
HEAT CAP.      COMPRESS.    EXPANSIVITY
       11      LAY11     0.4130E+03     0.5500E+00     0.2000E+01
0.1000E+04     0.0000E+00     0.0000E+00

            PERM1          PERM2          PERM3      HEAT COND. DRY
TORTUOSITY    KLINKENBERG
          0.1480E-08     0.1480E-08     0.1480E-08     0.2000E+01
0.0000E+00     0.0000E+00

     REL. PERM.  IRP          RP(1)       RP(2)       RP(3)
RP(4)
                   7     0.9000E+00  0.2000E-01  0.5500E+00  0.1000E-
01
     CAP. PRES.  ICP          CP(1)       CP(2)       CP(3)
CP(4)       CP(5)
                   7     0.9000E+00  0.1000E-01  0.1160E-02
0.1000E+06  0.5500E+00

     ------------------------------------------------------------------
------------------------------------------ LAY12 --
     DOMAIN     MAT        DENSITY        POROSITY   HEAT COND. WET
HEAT CAP.      COMPRESS.    EXPANSIVITY
       12      LAY12     0.4200E+03     0.5400E+00     0.2000E+01
0.1000E+04     0.0000E+00     0.0000E+00

            PERM1          PERM2          PERM3      HEAT COND. DRY
TORTUOSITY    KLINKENBERG
          0.1350E-08     0.1350E-08     0.1350E-08     0.2000E+01
0.0000E+00     0.0000E+00

     REL. PERM.  IRP          RP(1)       RP(2)       RP(3)
RP(4)
```

```
                  7     0.9000E+00  0.2000E-01  0.5400E+00  0.1000E-
01
     CAP. PRES.  ICP          CP(1)       CP(2)       CP(3)
CP(4)       CP(5)
                  7     0.9000E+00  0.1000E-01  0.1160E-02
0.1000E+06  0.5400E+00

     ------------------------------------------------------------------
---------------------------------------- LAY13 --
     DOMAIN     MAT        DENSITY        POROSITY   HEAT COND. WET
HEAT CAP.      COMPRESS.    EXPANSIVITY
       13      LAY13     0.3490E+03     0.6200E+00     0.2000E+01
0.1000E+04     0.0000E+00     0.0000E+00

            PERM1          PERM2          PERM3      HEAT COND. DRY
TORTUOSITY    KLINKENBERG
          0.3390E-08     0.3390E-08     0.3390E-08     0.2000E+01
0.0000E+00     0.0000E+00

     REL. PERM.  IRP          RP(1)       RP(2)       RP(3)
RP(4)
                  7     0.9000E+00  0.2000E-01  0.6200E+00  0.1000E-
01
     CAP. PRES.  ICP          CP(1)       CP(2)       CP(3)
CP(4)       CP(5)
                  7     0.9000E+00  0.1000E-01  0.1160E-02
0.1000E+06  0.6200E+00

     ------------------------------------------------------------------
---------------------------------------- LAY14 --
     DOMAIN     MAT        DENSITY        POROSITY   HEAT COND. WET
HEAT CAP.      COMPRESS.    EXPANSIVITY
       14      LAY14     0.3590E+03     0.6100E+00     0.2000E+01
0.1000E+04     0.0000E+00     0.0000E+00

            PERM1          PERM2          PERM3      HEAT COND. DRY
TORTUOSITY    KLINKENBERG
          0.2980E-08     0.2980E-08     0.2980E-08     0.2000E+01
0.0000E+00     0.0000E+00

     REL. PERM.  IRP          RP(1)       RP(2)       RP(3)
RP(4)
                  7     0.9000E+00  0.2000E-01  0.6100E+00  0.1000E-
01
     CAP. PRES.  ICP          CP(1)       CP(2)       CP(3)
CP(4)       CP(5)
                  7     0.9000E+00  0.1000E-01  0.1160E-02
0.1000E+06  0.6100E+00

     ------------------------------------------------------------------
---------------------------------------- LAY15 --
```

```
     DOMAIN     MAT        DENSITY        POROSITY   HEAT COND. WET
HEAT CAP.      COMPRESS.    EXPANSIVITY
       15      LAY15     0.3645E+03     0.6000E+00     0.2000E+01
0.1000E+04     0.0000E+00     0.0000E+00

            PERM1          PERM2          PERM3      HEAT COND. DRY
TORTUOSITY    KLINKENBERG
          0.2770E-08     0.2770E-08     0.2770E-08     0.2000E+01
0.0000E+00     0.0000E+00

     REL. PERM.  IRP          RP(1)       RP(2)       RP(3)
RP(4)
                  7     0.9000E+00  0.2000E-01  0.6000E+00  0.1000E-
01
     CAP. PRES.  ICP          CP(1)       CP(2)       CP(3)
CP(4)       CP(5)
                  7     0.9000E+00  0.1000E-01  0.1160E-02
0.1000E+06  0.6000E+00

     ------------------------------------------------------------------
---------------------------------------- LAY16 --
     DOMAIN     MAT        DENSITY        POROSITY   HEAT COND. WET
HEAT CAP.      COMPRESS.    EXPANSIVITY
       16      LAY16     0.3910E+03     0.5700E+00     0.2000E+01
0.1000E+04     0.0000E+00     0.0000E+00

            PERM1          PERM2          PERM3      HEAT COND. DRY
TORTUOSITY    KLINKENBERG
          0.1970E-08     0.1970E-08     0.1970E-08     0.2000E+01
0.0000E+00     0.0000E+00

     REL. PERM.  IRP          RP(1)       RP(2)       RP(3)
RP(4)
                  7     0.9000E+00  0.2000E-01  0.5700E+00  0.1000E-
01
     CAP. PRES.  ICP          CP(1)       CP(2)       CP(3)
CP(4)       CP(5)
                  7     0.9000E+00  0.1000E-01  0.1160E-02
0.1000E+06  0.5700E+00

     ------------------------------------------------------------------
---------------------------------------- LAY17 --
     DOMAIN     MAT        DENSITY        POROSITY   HEAT COND. WET
HEAT CAP.      COMPRESS.    EXPANSIVITY
       17      LAY17     0.3970E+03     0.5700E+00     0.2000E+01
0.1000E+04     0.0000E+00     0.0000E+00

            PERM1          PERM2          PERM3      HEAT COND. DRY
TORTUOSITY    KLINKENBERG
          0.1820E-08     0.1820E-08     0.1820E-08     0.2000E+01
0.0000E+00     0.0000E+00
```

```
     REL. PERM.  IRP          RP(1)       RP(2)       RP(3)
RP(4)
                   7     0.9000E+00  0.2000E-01  0.5700E+00  0.1000E-
01
     CAP. PRES.  ICP          CP(1)       CP(2)       CP(3)
CP(4)       CP(5)
                   7     0.9000E+00  0.1000E-01  0.1160E-02
0.1000E+06  0.5700E+00

     ------------------------------------------------------------------
------------------------------------------ LAY18 --
     DOMAIN     MAT        DENSITY        POROSITY   HEAT COND. WET
HEAT CAP.      COMPRESS.    EXPANSIVITY
       18      LAY18     0.4145E+03     0.5500E+00     0.2000E+01
0.1000E+04     0.0000E+00     0.0000E+00

            PERM1          PERM2          PERM3      HEAT COND. DRY
TORTUOSITY    KLINKENBERG
          0.1450E-08     0.1450E-08     0.1450E-08     0.2000E+01
0.0000E+00     0.0000E+00

     REL. PERM.  IRP          RP(1)       RP(2)       RP(3)
RP(4)
                   7     0.9000E+00  0.2000E-01  0.5500E+00  0.1000E-
01
     CAP. PRES.  ICP          CP(1)       CP(2)       CP(3)
CP(4)       CP(5)
                   7     0.9000E+00  0.1000E-01  0.1160E-02
0.1000E+06  0.5500E+00

     ------------------------------------------------------------------
------------------------------------------ LAY19 --
     DOMAIN     MAT        DENSITY        POROSITY   HEAT COND. WET
HEAT CAP.      COMPRESS.    EXPANSIVITY
       19      LAY19     0.4145E+03     0.5500E+00     0.2000E+01
0.1000E+04     0.0000E+00     0.0000E+00

            PERM1          PERM2          PERM3      HEAT COND. DRY
TORTUOSITY    KLINKENBERG
          0.3780E-08     0.3780E-08     0.3780E-08     0.2000E+01
0.0000E+00     0.0000E+00

     REL. PERM.  IRP          RP(1)       RP(2)       RP(3)
RP(4)
                   7     0.8600E+00  0.2000E-01  0.5500E+00  0.1000E-
01
     CAP. PRES.  ICP          CP(1)       CP(2)       CP(3)
CP(4)       CP(5)
                   7     0.8600E+00  0.1000E-01  0.1760E-02
0.1000E+06  0.5500E+00
```

```
     ------------------------------------------------------------------
---------------------------------------- LAY20 --
     DOMAIN     MAT        DENSITY        POROSITY   HEAT COND. WET
HEAT CAP.      COMPRESS.    EXPANSIVITY
       20      LAY20     0.3560E+03     0.6100E+00     0.2000E+01
0.1000E+04     0.0000E+00     0.0000E+00

            PERM1          PERM2          PERM3      HEAT COND. DRY
TORTUOSITY    KLINKENBERG
          0.8080E-08     0.8080E-08     0.8080E-08     0.2000E+01
0.0000E+00     0.0000E+00

     REL. PERM.  IRP          RP(1)       RP(2)       RP(3)
RP(4)
                  7     0.8600E+00  0.2000E-01  0.6100E+00  0.1000E-
01
     CAP. PRES.  ICP          CP(1)       CP(2)       CP(3)
CP(4)       CP(5)
                  7     0.8600E+00  0.1000E-01  0.1760E-02
0.1000E+06  0.6100E+00

     ------------------------------------------------------------------
---------------------------------------- LAY21 --
     DOMAIN     MAT        DENSITY        POROSITY   HEAT COND. WET
HEAT CAP.      COMPRESS.    EXPANSIVITY
       21      LAY21     0.3710E+03     0.6000E+00     0.2000E+01
0.1000E+04     0.0000E+00     0.0000E+00

            PERM1          PERM2          PERM3      HEAT COND. DRY
TORTUOSITY    KLINKENBERG
          0.6650E-08     0.6650E-08     0.6650E-08     0.2000E+01
0.0000E+00     0.0000E+00

     REL. PERM.  IRP          RP(1)       RP(2)       RP(3)
RP(4)
                  7     0.8600E+00  0.2000E-01  0.6000E+00  0.1000E-
01
     CAP. PRES.  ICP          CP(1)       CP(2)       CP(3)
CP(4)       CP(5)
                  7     0.8600E+00  0.1000E-01  0.1760E-02
0.1000E+06  0.6000E+00

     ------------------------------------------------------------------
---------------------------------------- LAY22 --
     DOMAIN     MAT        DENSITY        POROSITY   HEAT COND. WET
HEAT CAP.      COMPRESS.    EXPANSIVITY
       22      LAY22     0.3710E+03     0.6000E+00     0.2000E+01
0.1000E+04     0.0000E+00     0.0000E+00

            PERM1          PERM2          PERM3      HEAT COND. DRY
TORTUOSITY    KLINKENBERG
```

```
          0.6650E-08     0.6650E-08     0.6650E-08     0.2000E+01
0.0000E+00     0.0000E+00

     REL. PERM.  IRP          RP(1)       RP(2)       RP(3)
RP(4)
                   7     0.8600E+00  0.2000E-01  0.6000E+00  0.1000E-
01
     CAP. PRES.  ICP          CP(1)       CP(2)       CP(3)
CP(4)       CP(5)
                   7     0.8600E+00  0.1000E-01  0.1760E-02
0.1000E+06  0.6000E+00

     ------------------------------------------------------------------
---------------------------------------- GRND  --
     DOMAIN     MAT        DENSITY        POROSITY   HEAT COND. WET
HEAT CAP.      COMPRESS.    EXPANSIVITY
       23      GRND      0.8800E+03     0.6700E+00     0.2000E+01
0.1000E+04     0.0000E+00     0.0000E+00

            PERM1          PERM2          PERM3      HEAT COND. DRY
TORTUOSITY    KLINKENBERG
          0.4480E-09     0.4480E-09     0.4480E-09     0.2000E+01
0.0000E+00     0.0000E+00

     REL. PERM.  IRP          RP(1)       RP(2)       RP(3)
RP(4)
                   7     0.8600E+00  0.1000E-01  0.6700E+00  0.1000E-
01
     CAP. PRES.  ICP          CP(1)       CP(2)       CP(3)
CP(4)       CP(5)
                   7     0.8600E+00  0.9000E-02  0.7650E-05
0.1000E+06  0.6700E+00

     ------------------------------------------------------------------
---------------------------------------- REFCO --
     DOMAIN     MAT        DENSITY        POROSITY   HEAT COND. WET
HEAT CAP.      COMPRESS.    EXPANSIVITY
       24      REFCO     0.1012E+06     0.5000E+01     0.0000E+00
0.0000E+00     0.0000E+00     0.0000E+00

            PERM1          PERM2          PERM3      HEAT COND. DRY
TORTUOSITY    KLINKENBERG
          0.0000E+00     0.0000E+00     0.0000E+00     0.0000E+00
0.0000E+00     0.0000E+00

     REL. PERM.  IRP
                   5
     CAP. PRES.  ICP          CP(1)       CP(2)       CP(3)
                   1     0.0000E+00  0.0000E+00  0.1000E+01
**********************************************************************
******************************************
```

```
     END OF INPUT DATA

********************************************************************************
*********************************************

********************************************************************************
*********************************************


 END OF TOUGH2 INPUT JOB --- ELAPSED TIME =     1.240 SECONDS


********************************************************************************
************************************************************
.............  TIME STEP SIZE UNCHANGED             --> NEXT DELTEX =
3.600000E+03
 ...ITERATING...  AT [ 1489, 1] --- DELTEX = 3.600000E+03   MAX. RES.
= 1.106702E-01  AT ELEMENT HY101  EQUATION   1
 ...ITERATING...  AT [ 1489, 2] --- DELTEX = 3.600000E+03   MAX. RES.
= 6.346599E-03  AT ELEMENT HY101  EQUATION   1
 ...ITERATING...  AT [ 1489, 3] --- DELTEX = 3.600000E+03   MAX. RES.
= 1.498638E-05  AT ELEMENT HY101  EQUATION   1
 Fxo 1( 1489,4) ST =  8.5947E+04 DT =  3.6000E+03 DX1= -1.4614E-15
DX2=  0.0000E+00 T =   5.000 P =   101250. S =  3.3437E-02

 -------------- REDUCE TIME STEP BY FACTOR OF    0.13 --> NEXT DELTEX
= 4.530000E+02
 ...ITERATING...  AT [ 1490, 1] --- DELTEX = 4.530000E+02   MAX. RES.
= 1.240108E-02  AT ELEMENT HZ101  EQUATION   1
 ...ITERATING...  AT [ 1490, 2] --- DELTEX = 4.530000E+02   MAX. RES.
= 1.119599E-05  AT ELEMENT Ha101  EQUATION   1
 FxG 1( 1490,3) ST =  8.6400E+04 DT =  4.5300E+02 DX1=  6.8317E-16
DX2=  0.0000E+00 T =   5.000 P =   101250. S =  3.0463E-02

 CPU-TIME SINCE LAST OUTPUT:   355.55 SEC;  TOTAL CPU-TIME:   355.55
SEC;  SIMULATION TIME:          86400.00 SEC;  TIME STEPS: 1490


 *RE Spring Creek Flat Aspect Snow Pit 04

          OUTPUT DATA AFTER ( 1490, 3)-2-TIME STEPS
THE TIME IS  0.10000E+01 DAYS


@@@@@@@@@@@@@@@@@@@@@@@@@@@@@@@@@@@@@@@@@@@@@@@@@@@@@@@@@@@@@@@@@@@@@@@@@@@@
@@@@@@@@@@@@@@@@@@@@@@@@@@@@@@@@@@@@@@@@@@@@@@@@@@@@@@@@@@@@@@@@

  TOTAL TIME     KCYC   ITER  ITERC   KON        DX1M
MAX. RES.      NER    KER        DELTEX
  0.86400E+05   1490      3   6690     2       0.50651E-03
0.47325E-07    7384     1       0.45300E+03
```

```
@@@@@@@@@@@@@@@@@@@@@@@@@@@@@@@@@@@@@@@@@@@@@@@@@@@@@@@@@@@@@@@@@@@@@@

@@@@@@@@@@@@@@@@@@@@@@@@@@@@@@@@@@@@@@@@@@@@@@@@@@@@@@@@@@@@@

********** VOLUME- AND MASS-BALANCES
**********************************************************************
**********************

 ********** [KCYC,ITER] = [1490,  3] *****
THE TIME IS  0.86400E+05 SECONDS, OR  0.10000E+01 DAYS


 PHASE VOLUMES IN PLACE
 GAS  0.59581E+02 M**3;   LIQUID  0.38067E+01 M**3

 LIQUID MASS IN PLACE  0.38067E+04 KG


**********************************************************************
***********************************************************



 WRITE FILE *SAVE* AFTER  1490 TIME STEPS  ---  THE TIME IS
0.864000E+05 SECONDS
======================================================================
============================================================
      ARRAY DIMENSIONS (SEE FILE maxsize.inc)
 ---------------------------------------------------------------------
-------------------------------------------------------------
      MAXEL     =  100000      Maximum number of elements
      MAXCON    =  400000      Maximum number of connections
      MAXK      =       3      Maximum number of components
      MAXEQ     =       4      Maximum number of equations
      MAXPH     =       2      Maximum number of phases
      MAXB      =       8      Maximum number of phase-dependent
secondary variables
      MAXSS     =     900      Maximum number of sinks/sources
      MAVTAB    =     100      Maximum average number of table entries
per sink/source
      MAXROC    =     200      Maximum number of rock types
      MAXTSP    =       5      Maximum number of specified time steps,
divided by eight
      MAXLAY    =      10      Maximum number of reservoir layers for
wells on deliverability
      MXRPCP    =      14      Maximum number of parameters for
relative permeability and capillary pressure functions
      MXPCTB    =       5      Maximum number of points in table for
ECM capillary pressure
      MXTBC     =       5      Maximum number of elements with time
vs. boundary condition
```

```
      MXTBCT    =     600      Maximum number of time vs. pressure
data
      MAXTIM    =    1000      Maximum number of calibration times
      MAXN      =      50      Maximum number of parameters to be
estimated
      MAXO      =     200      Maximum number of datasets
      MAXM      =    1400      Maximum number of calibration points
      MAXPD     =    1000      Maximum number of paired data
      MAXR      =     200      Maximum number of elements or indices
of each parameter or observation
      MAXBRK    =      20      Maximum number of points in time at
which SAVE file is written for restart
      MAXEBRK   =      50      Maximum number of elements with new
initial conditions after restart
      MAXCOEFF  =       5      Maximum number of coefficients for data
modeling functions
      MAXXGR    =       3      Dimension of third index of array
XGUESSR
      MTYPE     =      31      Number of observation types
      MPFMT     =       5      Number of plot file formats
 ------------------------------------------------------------------------
------------------------------------------------------------


 ------------------------------------------------------------------------
------------------------------------------------------------
      PROGRAM  VERSION   DATE                  COMMENT
 ------------------------------------------------------------------------
------------------------------------------------------------
      iTOUGH2            Current version       iTOUGH2 V6.9 (OCTOBER,
2014)
 ------------------------------------------------------------------------
------------------------------------------------------------


========================================================================
============================================================

 ---   100th iTOUGH2 run stopped fatally       on  9-Jun-15  15:28 ---
CPU time used =     356.42 sec.

@@@@@@@@@@@@@@@@@@@@@@@@@@@@@@@@@@@@@@@@@@@@@@@@@@@@@@@@@@@@@@@@@@@@@@@@@@@@
@@@@@@@@@@@@@@@@@@@@@@@@@@@@@@@@@@@@@@@@@@@@@@@@@@@@@@@@

  END OF TOUGH2 SIMULATION JOB --- ELAPSED TIME =      356.42 SEC
```

North Aspect – 1.0 mm/hr

The north aspect simulations had difficulty converging and thus produced rather large output files. The following is for a single simulation for a 1.0 second simulation using the output of the original north aspect simulation as input to reduce file size.

```
TOUGH2 IS A PROGRAM FOR MULTIPHASE MULTICOMPONENT FLOW IN PERMEABLE
MEDIA, INCLUDING HEAT FLOW.
         IT IS A MEMBER OF THE MULKOM FAMILY OF CODES, DEVELOPED BY
KARSTEN PRUESS AT LAWRENCE BERKELEY NATIONAL LABORATORY.

                                    COPYRIGHT (C) 1999, THE REGENTS OF
THE UNIVERSITY OF CALIFORNIA.


******************************************************************
**********
                          *********  THIS IS TOUGH2 RUN NO.    1
CALLED BY iTOUGH2 RUN NO.    1  *********
                          ************  iTOUGH2 V6.9 (OCTOBER, 2014)
FOR LINUX, S. FINSTERLE  ************
                          ********************      EQUATION OF STATE
MODULE:  9       ******************
                          ********************    TODAY'S DATE:   12-
Jun-15  08:32     ******************

******************************************************************
**********


================================================================
============================================================

 UNIX COMMAND LINE: ./itough2 -tough2 North_input_1_mm_hr.txt 9
 PROBLEM TITLE    :  *North Aspect RE ISA snow pit 01


================================================================
============================================================

 PARAMETERS FOR FLEXIBLE DIMENSIONING OF MAJOR ARRAYS (SEE FILE
maxsize.inc) ARE SUMMARIZED AT THE END.


================================================================
============================================================
```

```
 ====================================
           MESH IS 2-D YZ
 ------------------------------------
 COORD.         MINIMUM         MAXIMUM
 ------------------------------------
   Y        0.25000E+00     0.24750E+02
   Z       -0.35038E+01    -0.15150E-01
 ====================================
 ALL NCON =  55687 CONNECTIONS READ FROM FILE *MESH* REFERENCE KNOWN
ELEMENTS



*********************************************************************
************************************************************
 *                              EOS9: EQUATION OF STATE FOR
SATURATED/UNSATURATED FLOW (RICHARDS EQUATION)
*

*********************************************************************
************************************************************


    OPTIONS SELECTED ARE: (NK,NEQ,NPH,NB) = (1,1,1, 6)

                          NK  =  1   - NUMBER OF FLUID COMPONENTS
                          NEQ =  1   - NUMBER OF EQUATIONS PER GRID
BLOCK
                          NPH =  1   - NUMBER OF PHASES THAT CAN BE
PRESENT
                          NB  =  6   - NUMBER OF SECONDARY PARAMETERS
(OTHER THAN COMPONENT MASS FRACTIONS)


    ONLY AVAILABLE OPTION IS: (NK,NEQ,NPH,NB) = (1,1,1,6)


*********************************************************************
************************************************************

 REFERENCE CONDITIONS
 --------------------

 GAS PRESSURE             = 0.101250E+06 PA
 TEMPERATURE              = 0.500000E+01 DEG-C
 SATURATED VAPOR PRESSURE = 0.871835E+03 PA
 WATER DENSITY            = 0.100002E+04 KG/M^3
 WATER VISCOSITY          = 0.150116E-02 PA-S
 WATER COMPRESSIBILITY    = 0.485869E-09 1/PA
```

```
 THE PRIMARY VARIABLE X1 IS PRESSURE FOR (X1.GE.0.101250E+06); IT IS
LIQUID SATURATION FOR (X1.LT. 1.)


************************************************************************
************************************************************

 ********** VOLUME- AND MASS-BALANCES
************************************************************************
**********************

 ********** [KCYC,ITER] = [   0,  0] *****
THE TIME IS  0.00000E+00 SECONDS, OR  0.00000E+00 DAYS


 PHASE VOLUMES IN PLACE
 GAS  0.59791E+02 M**3;   LIQUID  0.32893E+01 M**3

 LIQUID MASS IN PLACE  0.32893E+04 KG


************************************************************************
************************************************************



 MESH HAS 28150 ELEMENTS ( 28150 ACTIVE) AND 55687 CONNECTIONS
(INTERFACES) BETWEEN THEM
 GENER HAS   50 SINKS/SOURCES

************************************************************************
************************************************************
 *
*
 *                                        M A T R I X   S O L V E R
*
 *
*

************************************************************************
************************************************************

    THE SOLVER IS DETERMINED FROM MOP(21)

    THE SOLUTION METHOD INDICATOR MATSLV =  3
         MATSLV = 1: MATB - (PROPRIETARY - MAY NOT BE AVAILABLE)
         MATSLV = 2: DSLUBC - BI-CONJUGATE GRADIENT SOLVER
                                          INCOMPLETE LU FACTORIZATION
PRECONDITIONING
         MATSLV = 3: DSLUCS - LANCZOS-TYPE CONJUGATE GRADIENT SQUARED
SOLVER
```

```
                                          INCOMPLETE LU FACTORIZATION
PRECONDITIONING
         MATSLV = 4: DSLUGM - GENERALIZED MINIMUM RESIDUAL CONJUGATE
GRADIENT SOLVER
                                          INCOMPLETE LU FACTORIZATION
PRECONDITIONING
         MATSLV = 5: DLUSTB - STABILIZED BI-CONJUGATE GRADIENT SOLVER
                                          INCOMPLETE LU FACTORIZATION
PRECONDITIONING
         MATSLV = 6: LUBAND - DIRECT SOLVER USING LU DECOMPOSITION

    RITMAX: MAXIMUM # OF CG ITERATIONS AS FRACTION OF THE TOTAL NUMBER
OF EQUATIONS           =  1.00000E-01
         (0.0 < RITMAX <= 1.0,   DEFAULT = 0.1)
    CLOSUR: CONVERGENCE CRITERION FOR THE CG ITERATIONS
=  1.00000E-06
         (1.0E-12 <= CLOSUR <= 1.0E-6,  DEFAULT = 1.0E-6)
    NMAXIT: MAXIMUM # OF CG ITERATIONS - NOT TO EXCEED THE TOTAL
NUMBER OF EQUATIONS NELA*NEQ =  2815
         (20 < NMAXIT <= NREDM)

 !!!!! NEQ=1; DO NOT PERFORM ANY MATRIX PREPROCESSING

    THE MATRIX Z-PREPROCESSING SYSTEM IS ZPROCS = Z0

         ZPROCS = Z0: NO Z-PREPROCESSING; DEFAULT FOR NEQ = 1 AND FOR
MATSLV = 6
         ZPROCS = Z1: REPLACEMENT OF ZEROS ON THE MAIN-DIAGONAL BY A
SMALL NUMBER;
                       DEFAULT FOR NEQ > 1 AND FOR 2 < MATSLV < 6
         ZPROCS = Z2: LINEAR COMBINATION Of EQUATIONS IN EACH ELEMENT
TO PRODUCE NON-ZERO MAIN DIAGONAL ENTRIES
         ZPROCS = Z3: NORMALIZATION OF EQUATIONS, FOLLOWED BY Z2
         ZPROCS = Z4: SAME AS IN OPROCS = O4


    THE MATRIX O-PREPROCESSING SYSTEM IS OPROCS = O0

         OPROCS = O0: NO O-PREPROCESSING; DEFAULT (AND ONLY OPTION FOR
NEQ=1)
         OPROCS = O1: ELIMINATION OF LOWER HALF OF THE MAIN-DIAGONAL
SUBMATRIX WITH CENTER PIVOTING
         OPROCS = O2: O1+ELIMINATION OF UPPER HALF OF THE MAIN-
DIAGONAL SUBMATRIX WITH CENTER PIVOTING
         OPROCS = O3: O2+NORMALIZATION - RESULTS IN UNIT MAIN-DIAGONAL
SUBMATRICES
         OPROCS = O4: PRE-PROCESSING WHICH RESULTS IN UNIT MAIN-
DIAGONAL SUBMATRICES WITHOUT CENTER PIVOTING


 VALUE OF INCREMENT FACTOR FOR NUMERICAL DERIVATIVES:    1.05367E-08
1
```

```
     TOUGH2 INPUT DATA

     PROBLEM TITLE: *North Aspect RE ISA snow pit 01


*******************************************************************************
*********************************************

*******************************************************************************
*********************************************

     PROBLEM SPECIFICATIONS

     NOITE  KDATA    MCYC   MSEC          MCYPR  MOP-
12345678901234567890123456789012345678901234
         5      2  999999      0           9999
10000010000100030000300000

            DIFF0           TEXP             BE             ZA
      0.00000E+00    0.00000E+00    0.00000E+00    0.00000E+00

           TSTART          TIMAX         DELTEN         DELTMX
ELST             GF          REDLT          SCALE
      0.00000E+00    0.86400E+05    0.10000E+01    0.36000E+04
0.98066E+01    0.40000E+01    0.10000E+01

      A CONSTANT TIME STEP OF DELTEN IS PRESCRIBED
              RE1            RE2              U            WUP
WNR           DFAC            FOR          AMRES
      0.10000E-04    0.10000E+01    0.10000E+00    0.10000E+01
0.10000E+01    0.10537E-07    0.10000E+01    0.10000E+06

           DEP(1)         DEP(2)
      0.00000E+00

*******************************************************************************
*********************************************

     ROCK PROPERTIES

     ------------------------------------------------------------------
---------------------------------------- LAY01 --
     DOMAIN     MAT        DENSITY        POROSITY   HEAT COND. WET
HEAT CAP.      COMPRESS.    EXPANSIVITY
        1      LAY01     0.4850E+02     0.9500E+00     0.2000E+01
0.1000E+04     0.0000E+00     0.0000E+00

            PERM1          PERM2          PERM3      HEAT COND. DRY
TORTUOSITY    KLINKENBERG
          0.3590E-07     0.3590E-07     0.3590E-07     0.2000E+01
0.0000E+00     0.0000E+00
```

```
     REL. PERM.  IRP          RP(1)       RP(2)       RP(3)
RP(4)
                   7     0.9200E+00  0.2000E-01  0.9500E+00  0.1000E-
01
     CAP. PRES.  ICP          CP(1)       CP(2)       CP(3)
CP(4)       CP(5)
                   7     0.9200E+00  0.1000E-01  0.6400E-03
0.1000E+06  0.9500E+00

     ------------------------------------------------------------------
------------------------------------------ LAY02 --
     DOMAIN     MAT        DENSITY        POROSITY   HEAT COND. WET
HEAT CAP.      COMPRESS.    EXPANSIVITY
        2      LAY02     0.1310E+03     0.8600E+00     0.2000E+01
0.1000E+04     0.0000E+00     0.0000E+00

            PERM1          PERM2          PERM3      HEAT COND. DRY
TORTUOSITY    KLINKENBERG
          0.1230E-07     0.1230E-07     0.1230E-07     0.2000E+01
0.0000E+00     0.0000E+00

     REL. PERM.  IRP          RP(1)       RP(2)       RP(3)
RP(4)
                   7     0.9200E+00  0.2000E-01  0.8600E+00  0.1000E-
01
     CAP. PRES.  ICP          CP(1)       CP(2)       CP(3)
CP(4)       CP(5)
                   7     0.9200E+00  0.1000E-01  0.6400E-03
0.1000E+06  0.8600E+00

     ------------------------------------------------------------------
------------------------------------------ LAY03 --
     DOMAIN     MAT        DENSITY        POROSITY   HEAT COND. WET
HEAT CAP.      COMPRESS.    EXPANSIVITY
        3      LAY03     0.1640E+03     0.8200E+00     0.2000E+01
0.1000E+04     0.0000E+00     0.0000E+00

            PERM1          PERM2          PERM3      HEAT COND. DRY
TORTUOSITY    KLINKENBERG
          0.8010E-08     0.8010E-08     0.8010E-08     0.2000E+01
0.0000E+00     0.0000E+00

     REL. PERM.  IRP          RP(1)       RP(2)       RP(3)
RP(4)
                   7     0.9200E+00  0.2000E-01  0.8200E+00  0.1000E-
01
     CAP. PRES.  ICP          CP(1)       CP(2)       CP(3)
CP(4)       CP(5)
                   7     0.9200E+00  0.1000E-01  0.6400E-03
0.1000E+06  0.8200E+00
```

```
     ------------------------------------------------------------------
---------------------------------------- LAY04 --
     DOMAIN     MAT        DENSITY        POROSITY   HEAT COND. WET
HEAT CAP.      COMPRESS.    EXPANSIVITY
        4      LAY04     0.2020E+03     0.7800E+00     0.2000E+01
0.1000E+04     0.0000E+00     0.0000E+00

            PERM1          PERM2          PERM3      HEAT COND. DRY
TORTUOSITY    KLINKENBERG
          0.8680E-08     0.8680E-08     0.8680E-08     0.2000E+01
0.0000E+00     0.0000E+00

     REL. PERM.  IRP          RP(1)       RP(2)       RP(3)
RP(4)
                  7     0.9200E+00  0.2000E-01  0.7800E+00  0.1000E-
01
     CAP. PRES.  ICP          CP(1)       CP(2)       CP(3)
CP(4)       CP(5)
                  7     0.9200E+00  0.1000E-01  0.7890E-03
0.1000E+06  0.7800E+00

     ------------------------------------------------------------------
---------------------------------------- LAY05 --
     DOMAIN     MAT        DENSITY        POROSITY   HEAT COND. WET
HEAT CAP.      COMPRESS.    EXPANSIVITY
        5      LAY05     0.2360E-01     0.7400E+00     0.2000E+01
0.1000E+04     0.0000E+00     0.0000E+00

            PERM1          PERM2          PERM3      HEAT COND. DRY
TORTUOSITY    KLINKENBERG
          0.3490E-07     0.3490E-07     0.3490E-07     0.2000E+01
0.0000E+00     0.0000E+00

     REL. PERM.  IRP          RP(1)       RP(2)       RP(3)
RP(4)
                  7     0.8600E+00  0.2000E-01  0.7400E+00  0.1000E-
01
     CAP. PRES.  ICP          CP(1)       CP(2)       CP(3)
CP(4)       CP(5)
                  7     0.8600E+00  0.1000E-01  0.1680E-02
0.1000E+06  0.7400E+00

     ------------------------------------------------------------------
---------------------------------------- LAY06 --
     DOMAIN     MAT        DENSITY        POROSITY   HEAT COND. WET
HEAT CAP.      COMPRESS.    EXPANSIVITY
        6      LAY06     0.2360E+03     0.7400E+00     0.2000E+01
0.1000E+04     0.0000E+00     0.0000E+00

            PERM1          PERM2          PERM3      HEAT COND. DRY
TORTUOSITY    KLINKENBERG
```

```
          0.3140E-08     0.3140E-08     0.3140E-08     0.2000E+01
0.0000E+00     0.0000E+00

     REL. PERM.  IRP          RP(1)       RP(2)       RP(3)
RP(4)
                   7     0.9200E+00  0.2000E-01  0.7400E+00  0.1000E-
01
     CAP. PRES.  ICP          CP(1)       CP(2)       CP(3)
CP(4)       CP(5)
                   7     0.9200E+00  0.1000E-01  0.6400E-03
0.1000E+06  0.7400E+00

     ------------------------------------------------------------------
---------------------------------------- LAY07 --
     DOMAIN     MAT        DENSITY        POROSITY   HEAT COND. WET
HEAT CAP.      COMPRESS.    EXPANSIVITY
        7      LAY07     0.2345E+03     0.7400E+00     0.2000E+01
0.1000E+04     0.0000E+00     0.0000E+00

            PERM1          PERM2          PERM3      HEAT COND. DRY
TORTUOSITY    KLINKENBERG
          0.8000E-07     0.8000E-07     0.8000E-07     0.2000E+01
0.0000E+00     0.0000E+00

     REL. PERM.  IRP          RP(1)       RP(2)       RP(3)
RP(4)
                   7     0.8000E+00  0.2000E-01  0.7400E+00  0.1000E-
01
     CAP. PRES.  ICP          CP(1)       CP(2)       CP(3)
CP(4)       CP(5)
                   7     0.8000E+00  0.1000E-01  0.2430E-02
0.1000E+06  0.7400E+00

     ------------------------------------------------------------------
---------------------------------------- LAY08 --
     DOMAIN     MAT        DENSITY        POROSITY   HEAT COND. WET
HEAT CAP.      COMPRESS.    EXPANSIVITY
        8      LAY08     0.2345E+03     0.7400E+00     0.2000E+01
0.1000E+04     0.0000E+00     0.0000E+00

            PERM1          PERM2          PERM3      HEAT COND. DRY
TORTUOSITY    KLINKENBERG
          0.1420E-08     0.1420E-08     0.1420E-08     0.2000E+01
0.0000E+00     0.0000E+00

     REL. PERM.  IRP          RP(1)       RP(2)       RP(3)
RP(4)
                   7     0.9300E+00  0.2000E-01  0.7400E+00  0.1000E-
01
     CAP. PRES.  ICP          CP(1)       CP(2)       CP(3)
CP(4)       CP(5)
```

```
                  7     0.9300E+00  0.1000E-01  0.4910E-03
0.1000E+06  0.7400E+00

     ------------------------------------------------------------------
---------------------------------------- LAY09 --
     DOMAIN     MAT        DENSITY        POROSITY   HEAT COND. WET
HEAT CAP.      COMPRESS.    EXPANSIVITY
        9      LAY09     0.2502E+03     0.7300E+00     0.2000E+01
0.1000E+04     0.0000E+00     0.0000E+00

            PERM1          PERM2          PERM3      HEAT COND. DRY
TORTUOSITY    KLINKENBERG
          0.1160E-08     0.1160E-08     0.1160E-08     0.2000E+01
0.0000E+00     0.0000E+00

     REL. PERM.  IRP          RP(1)       RP(2)       RP(3)
RP(4)
                  7     0.9300E+00  0.2000E-01  0.7300E+00  0.1000E-
01
     CAP. PRES.  ICP          CP(1)       CP(2)       CP(3)
CP(4)       CP(5)
                  7     0.9300E+00  0.1000E-01  0.4910E-03
0.1000E+06  0.7300E+00

     ------------------------------------------------------------------
---------------------------------------- LAY10 --
     DOMAIN     MAT        DENSITY        POROSITY   HEAT COND. WET
HEAT CAP.      COMPRESS.    EXPANSIVITY
       10      LAY10     0.2740E+03     0.7000E+00     0.2000E+01
0.1000E+04     0.0000E+00     0.0000E+00

            PERM1          PERM2          PERM3      HEAT COND. DRY
TORTUOSITY    KLINKENBERG
          0.8510E-09     0.8510E-09     0.8510E-09     0.2000E+01
0.0000E+00     0.0000E+00

     REL. PERM.  IRP          RP(1)       RP(2)       RP(3)
RP(4)
                  7     0.9300E+00  0.2000E-01  0.7000E+00  0.1000E-
01
     CAP. PRES.  ICP          CP(1)       CP(2)       CP(3)
CP(4)       CP(5)
                  7     0.9300E+00  0.1000E-01  0.4910E-03
0.1000E+06  0.7000E+00

     ------------------------------------------------------------------
---------------------------------------- LAY11 --
     DOMAIN     MAT        DENSITY        POROSITY   HEAT COND. WET
HEAT CAP.      COMPRESS.    EXPANSIVITY
       11      LAY11     0.3190E+03     0.6500E+00     0.2000E+01
0.1000E+04     0.0000E+00     0.0000E+00
```

```
            PERM1          PERM2          PERM3      HEAT COND. DRY
TORTUOSITY    KLINKENBERG
          0.4740E-09     0.4740E-09     0.4740E-09     0.2000E+01
0.0000E+00     0.0000E+00

     REL. PERM.  IRP          RP(1)       RP(2)       RP(3)
RP(4)
                   7     0.9300E+00  0.2000E-01  0.6500E+00  0.1000E-
01
     CAP. PRES.  ICP          CP(1)       CP(2)       CP(3)
CP(4)       CP(5)
                   7     0.9300E+00  0.1000E-01  0.4910E-03
0.1000E+06  0.6500E+00

     ------------------------------------------------------------------
---------------------------------------- LAY12 --
     DOMAIN     MAT        DENSITY        POROSITY   HEAT COND. WET
HEAT CAP.      COMPRESS.    EXPANSIVITY
       12      LAY12     0.3185E+03     0.6500E+00     0.2000E+01
0.1000E+04     0.0000E+00     0.0000E+00

            PERM1          PERM2          PERM3      HEAT COND. DRY
TORTUOSITY    KLINKENBERG
          0.4770E-09     0.4770E-09     0.4770E-09     0.2000E+01
0.0000E+00     0.0000E+00

     REL. PERM.  IRP          RP(1)       RP(2)       RP(3)
RP(4)
                   7     0.9300E+00  0.2000E-01  0.6500E+00  0.1000E-
01
     CAP. PRES.  ICP          CP(1)       CP(2)       CP(3)
CP(4)       CP(5)
                   7     0.9300E+00  0.1000E-01  0.4910E-03
0.1000E+06  0.6500E+00

     ------------------------------------------------------------------
---------------------------------------- LAY13 --
     DOMAIN     MAT        DENSITY        POROSITY   HEAT COND. WET
HEAT CAP.      COMPRESS.    EXPANSIVITY
       13      LAY13     0.3085E+03     0.6600E+00     0.2000E+01
0.1000E+04     0.0000E+00     0.0000E+00

            PERM1          PERM2          PERM3      HEAT COND. DRY
TORTUOSITY    KLINKENBERG
          0.5440E-09     0.5440E-09     0.5440E-09     0.2000E+01
0.0000E+00     0.0000E+00

     REL. PERM.  IRP          RP(1)       RP(2)       RP(3)
RP(4)
                   7     0.9300E+00  0.2000E-01  0.6600E+00  0.1000E-
01
```

```
     CAP. PRES.  ICP          CP(1)       CP(2)       CP(3)
CP(4)       CP(5)
                   7     0.9300E+00  0.1000E-01  0.4910E-03
0.1000E+06  0.6600E+00

     ------------------------------------------------------------------
---------------------------------------- LAY14 --
     DOMAIN     MAT        DENSITY        POROSITY   HEAT COND. WET
HEAT CAP.      COMPRESS.    EXPANSIVITY
       14      LAY14     0.3185E+03     0.6500E+00     0.2000E+01
0.1000E+04     0.0000E+00     0.0000E+00

            PERM1          PERM2          PERM3      HEAT COND. DRY
TORTUOSITY    KLINKENBERG
          0.4770E-09     0.4770E-09     0.4770E-09     0.2000E+01
0.0000E+00     0.0000E+00

     REL. PERM.  IRP          RP(1)       RP(2)       RP(3)
RP(4)
                   7     0.9300E+00  0.2000E-01  0.6500E+00  0.1000E-
01
     CAP. PRES.  ICP          CP(1)       CP(2)       CP(3)
CP(4)       CP(5)
                   7     0.9300E+00  0.1000E-01  0.4910E-03
0.1000E+06  0.6500E+00

     ------------------------------------------------------------------
---------------------------------------- LAY15 --
     DOMAIN     MAT        DENSITY        POROSITY   HEAT COND. WET
HEAT CAP.      COMPRESS.    EXPANSIVITY
       15      LAY15     0.3185E+03     0.6500E+00     0.2000E+01
0.1000E+04     0.0000E+00     0.0000E+00

            PERM1          PERM2          PERM3      HEAT COND. DRY
TORTUOSITY    KLINKENBERG
          0.1070E-08     0.1070E-08     0.1070E-08     0.2000E+01
0.0000E+00     0.0000E+00

     REL. PERM.  IRP          RP(1)       RP(2)       RP(3)
RP(4)
                   7     0.9200E+00  0.2000E-01  0.6500E+00  0.1000E-
01
     CAP. PRES.  ICP          CP(1)       CP(2)       CP(3)
CP(4)       CP(5)
                   7     0.9200E+00  0.1000E-01  0.6400E-03
0.1000E+06  0.6500E+00

     ------------------------------------------------------------------
---------------------------------------- LAY16 --
     DOMAIN     MAT        DENSITY        POROSITY   HEAT COND. WET
HEAT CAP.      COMPRESS.    EXPANSIVITY
```

```
       16      LAY16     0.3210E+03     0.6500E+00     0.2000E+01
0.1000E+04     0.0000E+00     0.0000E+00

            PERM1          PERM2          PERM3      HEAT COND. DRY
TORTUOSITY    KLINKENBERG
          0.1040E-08     0.1040E-08     0.1040E-08     0.2000E+01
0.0000E+00     0.0000E+00

     REL. PERM.  IRP          RP(1)       RP(2)       RP(3)
RP(4)
                   7     0.9200E+00  0.2000E-01  0.6500E+00  0.1000E-
01
     CAP. PRES.  ICP          CP(1)       CP(2)       CP(3)
CP(4)       CP(5)
                   7     0.9200E+00  0.1000E-01  0.6400E-03
0.1000E+06  0.6500E+00

     ------------------------------------------------------------------
------------------------------------------ LAY17 --
     DOMAIN     MAT        DENSITY        POROSITY   HEAT COND. WET
HEAT CAP.      COMPRESS.    EXPANSIVITY
       17      LAY17     0.3405E+03     0.6300E+00     0.2000E+01
0.1000E+04     0.0000E+00     0.0000E+00

            PERM1          PERM2          PERM3      HEAT COND. DRY
TORTUOSITY    KLINKENBERG
          0.8070E-09     0.8070E-09     0.8070E-09     0.2000E+01
0.0000E+00     0.0000E+00

     REL. PERM.  IRP          RP(1)       RP(2)       RP(3)
RP(4)
                   7     0.9200E+00  0.2000E-01  0.6300E+00  0.1000E-
01
     CAP. PRES.  ICP          CP(1)       CP(2)       CP(3)
CP(4)       CP(5)
                   7     0.9200E+00  0.1000E-01  0.6400E-03
0.1000E+06  0.6300E+00

     ------------------------------------------------------------------
------------------------------------------ LAY18 --
     DOMAIN     MAT        DENSITY        POROSITY   HEAT COND. WET
HEAT CAP.      COMPRESS.    EXPANSIVITY
       18      LAY18     0.3435E+03     0.6300E+00     0.2000E+01
0.1000E+04     0.0000E+00     0.0000E+00

            PERM1          PERM2          PERM3      HEAT COND. DRY
TORTUOSITY    KLINKENBERG
          0.7760E-09     0.7760E-09     0.7760E-09     0.2000E+01
0.0000E+00     0.0000E+00

     REL. PERM.  IRP          RP(1)       RP(2)       RP(3)
RP(4)
```

```
                  7     0.9200E+00  0.2000E-01  0.6300E+00  0.1000E-
01
     CAP. PRES.  ICP          CP(1)       CP(2)       CP(3)
CP(4)       CP(5)
                  7     0.9200E+00  0.1000E-01  0.6400E-03
0.1000E+06  0.6300E+00

     ------------------------------------------------------------------
---------------------------------------- LAY19 --
     DOMAIN     MAT        DENSITY        POROSITY   HEAT COND. WET
HEAT CAP.      COMPRESS.    EXPANSIVITY
       19      LAY19     0.3625E+03     0.6000E+00     0.2000E+01
0.1000E+04     0.0000E+00     0.0000E+00

            PERM1          PERM2          PERM3      HEAT COND. DRY
TORTUOSITY    KLINKENBERG
          0.6060E-09     0.6060E-09     0.6060E-09     0.2000E+01
0.0000E+00     0.0000E+00

     REL. PERM.  IRP          RP(1)       RP(2)       RP(3)
RP(4)
                  7     0.9200E+00  0.2000E-01  0.6000E+00  0.1000E-
01
     CAP. PRES.  ICP          CP(1)       CP(2)       CP(3)
CP(4)       CP(5)
                  7     0.9200E+00  0.1000E-01  0.6400E-03
0.1000E+06  0.6000E+00

     ------------------------------------------------------------------
---------------------------------------- LAY20 --
     DOMAIN     MAT        DENSITY        POROSITY   HEAT COND. WET
HEAT CAP.      COMPRESS.    EXPANSIVITY
       20      LAY20     0.3785E+03     0.5800E+00     0.2000E+01
0.1000E+04     0.0000E+00     0.0000E+00

            PERM1          PERM2          PERM3      HEAT COND. DRY
TORTUOSITY    KLINKENBERG
          0.4920E-09     0.4920E-09     0.4920E-09     0.2000E+01
0.0000E+00     0.0000E+00

     REL. PERM.  IRP          RP(1)       RP(2)       RP(3)
RP(4)
                  7     0.9200E+00  0.2000E-01  0.5800E+00  0.1000E-
01
     CAP. PRES.  ICP          CP(1)       CP(2)       CP(3)
CP(4)       CP(5)
                  7     0.9200E+00  0.1000E-01  0.6400E-03
0.1000E+06  0.5800E+00

     ------------------------------------------------------------------
---------------------------------------- LAY21 --
```

```
     DOMAIN     MAT        DENSITY        POROSITY   HEAT COND. WET
HEAT CAP.      COMPRESS.    EXPANSIVITY
       21      LAY21     0.3895E+03     0.5800E+00     0.2000E+01
0.1000E+04     0.0000E+00     0.0000E+00

            PERM1          PERM2          PERM3      HEAT COND. DRY
TORTUOSITY    KLINKENBERG
          0.4270E-09     0.4270E-09     0.4270E-09     0.2000E+01
0.0000E+00     0.0000E+00

     REL. PERM.  IRP          RP(1)       RP(2)       RP(3)
RP(4)
                  7     0.9200E+00  0.2000E-01  0.5800E+00  0.1000E-
01
     CAP. PRES.  ICP          CP(1)       CP(2)       CP(3)
CP(4)       CP(5)
                  7     0.9200E+00  0.1000E-01  0.6400E-03
0.1000E+06  0.5800E+00

     ------------------------------------------------------------------
---------------------------------------- LAY22 --
     DOMAIN     MAT        DENSITY        POROSITY   HEAT COND. WET
HEAT CAP.      COMPRESS.    EXPANSIVITY
       22      LAY22     0.3565E+03     0.6100E+00     0.2000E+01
0.1000E+04     0.0000E+00     0.0000E+00

            PERM1          PERM2          PERM3      HEAT COND. DRY
TORTUOSITY    KLINKENBERG
          0.7280E-08     0.7280E-08     0.7280E-08     0.2000E+01
0.0000E+00     0.0000E+00

     REL. PERM.  IRP          RP(1)       RP(2)       RP(3)
RP(4)
                  7     0.8600E+00  0.2000E-01  0.6100E+00  0.1000E-
01
     CAP. PRES.  ICP          CP(1)       CP(2)       CP(3)
CP(4)       CP(5)
                  7     0.8600E+00  0.1000E-01  0.1680E-02
0.1000E+06  0.6100E+00

     ------------------------------------------------------------------
---------------------------------------- LAY23 --
     DOMAIN     MAT        DENSITY        POROSITY   HEAT COND. WET
HEAT CAP.      COMPRESS.    EXPANSIVITY
       23      LAY23     0.3565E+03     0.6100E+00     0.2000E+01
0.1000E+04     0.0000E+00     0.0000E+00

            PERM1          PERM2          PERM3      HEAT COND. DRY
TORTUOSITY    KLINKENBERG
          0.6600E-09     0.4660E-08     0.4660E-08     0.2000E+01
0.0000E+00     0.0000E+00
```

```
     REL. PERM.  IRP          RP(1)       RP(2)       RP(3)
RP(4)
                   7     0.8800E+00  0.2000E-01  0.6100E+00  0.1000E-
01
     CAP. PRES.  ICP          CP(1)       CP(2)       CP(3)
CP(4)       CP(5)
                   7     0.8800E+00  0.1000E-01  0.1380E-02
0.1000E+06  0.6100E+00

     ------------------------------------------------------------------
---------------------------------------- LAY24 --
     DOMAIN     MAT        DENSITY        POROSITY   HEAT COND. WET
HEAT CAP.      COMPRESS.    EXPANSIVITY
       24      LAY24     0.3565E+03     0.6100E+00     0.2000E+01
0.1000E+04     0.0000E+00     0.0000E+00

            PERM1          PERM2          PERM3      HEAT COND. DRY
TORTUOSITY    KLINKENBERG
          0.7280E-08     0.7280E-08     0.7280E-08     0.2000E+01
0.0000E+00     0.0000E+00

     REL. PERM.  IRP          RP(1)       RP(2)       RP(3)
RP(4)
                   7     0.8600E+00  0.2000E-01  0.6100E+00  0.1000E-
01
     CAP. PRES.  ICP          CP(1)       CP(2)       CP(3)
CP(4)       CP(5)
                   7     0.8600E+00  0.1000E-01  0.1680E-02
0.1000E+06  0.6100E+00

     ------------------------------------------------------------------
---------------------------------------- LAY25 --
     DOMAIN     MAT        DENSITY        POROSITY   HEAT COND. WET
HEAT CAP.      COMPRESS.    EXPANSIVITY
       25      LAY25     0.3210E+03     0.6500E+00     0.2000E+01
0.1000E+04     0.0000E+00     0.0000E+00

            PERM1          PERM2          PERM3      HEAT COND. DRY
TORTUOSITY    KLINKENBERG
          0.1160E-07     0.1160E-07     0.1160E-07     0.2000E+01
0.0000E+00     0.0000E+00

     REL. PERM.  IRP          RP(1)       RP(2)       RP(3)
RP(4)
                   7     0.8600E+00  0.2000E-01  0.6500E+00  0.1000E-
01
     CAP. PRES.  ICP          CP(1)       CP(2)       CP(3)
CP(4)       CP(5)
                   7     0.8600E+00  0.1000E-01  0.1680E-02
0.1000E+06  0.6500E+00
```

```
     ------------------------------------------------------------------
---------------------------------------- LAY26 --
     DOMAIN     MAT        DENSITY        POROSITY   HEAT COND. WET
HEAT CAP.      COMPRESS.    EXPANSIVITY
       26      LAY26     0.3490E+03     0.6200E+00     0.2000E+01
0.1000E+04     0.0000E+00     0.0000E+00

            PERM1          PERM2          PERM3      HEAT COND. DRY
TORTUOSITY    KLINKENBERG
          0.8030E-08     0.8030E-08     0.8030E-08     0.2000E+01
0.0000E+00     0.0000E+00

     REL. PERM.  IRP          RP(1)       RP(2)       RP(3)
RP(4)
                  7     0.8600E+00  0.2000E-01  0.6200E+00  0.1000E-
01
     CAP. PRES.  ICP          CP(1)       CP(2)       CP(3)
CP(4)       CP(5)
                  7     0.8600E+00  0.1000E-01  0.1680E-02
0.1000E+06  0.6200E+00

     ------------------------------------------------------------------
---------------------------------------- LAY27 --
     DOMAIN     MAT        DENSITY        POROSITY   HEAT COND. WET
HEAT CAP.      COMPRESS.    EXPANSIVITY
       27      LAY27     0.3595E+03     0.6100E+00     0.2000E+01
0.1000E+04     0.0000E+00     0.0000E+00

            PERM1          PERM2          PERM3      HEAT COND. DRY
TORTUOSITY    KLINKENBERG
          0.7000E-08     0.7000E-08     0.7000E-08     0.2000E+01
0.0000E+00     0.0000E+00

     REL. PERM.  IRP          RP(1)       RP(2)       RP(3)
RP(4)
                  7     0.8600E+00  0.2000E-01  0.6100E+00  0.1000E-
01
     CAP. PRES.  ICP          CP(1)       CP(2)       CP(3)
CP(4)       CP(5)
                  7     0.8600E+00  0.1000E-01  0.1680E-02
0.1000E+06  0.6100E+00

     ------------------------------------------------------------------
---------------------------------------- GRND  --
     DOMAIN     MAT        DENSITY        POROSITY   HEAT COND. WET
HEAT CAP.      COMPRESS.    EXPANSIVITY
       28      GRND      0.8800E+03     0.6700E+00     0.2000E+01
0.1000E+04     0.0000E+00     0.0000E+00

            PERM1          PERM2          PERM3      HEAT COND. DRY
TORTUOSITY    KLINKENBERG
```

```
          0.4480E-09     0.4480E-09     0.4480E-09     0.2000E+01
0.0000E+00     0.0000E+00

     REL. PERM.  IRP          RP(1)       RP(2)       RP(3)
RP(4)
                   7     0.8600E+00  0.1000E-01  0.6700E+00  0.1000E-
01
     CAP. PRES.  ICP          CP(1)       CP(2)       CP(3)
CP(4)       CP(5)
                   7     0.8600E+00  0.9000E-02  0.7650E-05
0.1000E+06  0.6700E+00

     ------------------------------------------------------------------
---------------------------------------- REFCO --
     DOMAIN     MAT        DENSITY        POROSITY   HEAT COND. WET
HEAT CAP.      COMPRESS.    EXPANSIVITY
       29      REFCO     0.1012E+06     0.5000E+01     0.0000E+00
0.0000E+00     0.0000E+00     0.0000E+00

            PERM1          PERM2          PERM3      HEAT COND. DRY
TORTUOSITY    KLINKENBERG
          0.0000E+00     0.0000E+00     0.0000E+00     0.0000E+00
0.0000E+00     0.0000E+00

     REL. PERM.  IRP
                   5
     CAP. PRES.  ICP          CP(1)       CP(2)       CP(3)
                   1     0.0000E+00  0.0000E+00  0.1000E+01
**********************************************************************
*********************************************

     END OF INPUT DATA


**********************************************************************
*********************************************

**********************************************************************
*********************************************


 END OF TOUGH2 INPUT JOB --- ELAPSED TIME =     1.995 SECONDS

.............  TIME STEP SIZE UNCHANGED             --> NEXT DELTEX =
2.500000E-01
 ...ITERATING...  AT [    3, 1] --- DELTEX = 2.500000E-01   MAX. RES.
= 1.524934E-03  AT ELEMENT ADo 1  EQUATION   1
 ...ITERATING...  AT [    3, 2] --- DELTEX = 2.500000E-01   MAX. RES.
= 1.434219E-01  AT ELEMENT AEo 1  EQUATION   1
 ...ITERATING...  AT [    3, 3] --- DELTEX = 2.500000E-01   MAX. RES.
= 1.989900E-05  AT ELEMENT AEo 1  EQUATION   1
```

```
 ADo 1(    3,4) ST =  7.5000E-01 DT =  2.5000E-01 DX1= -6.7968E-05
DX2=  0.0000E+00 T =   5.000 P =   101250. S =  4.6569E-02

 ..............  TIME STEP SIZE UNCHANGED            --> NEXT DELTEX
= 2.500000E-01
 ...ITERATING...  AT [    4, 1] --- DELTEX = 2.500000E-01   MAX. RES.
= 1.460710E-03  AT ELEMENT ADo 1  EQUATION   1
 ...ITERATING...  AT [    4, 2] --- DELTEX = 2.500000E-01   MAX. RES.
= 1.393950E-01  AT ELEMENT AEo 1  EQUATION   1
 ...ITERATING...  AT [    4, 3] --- DELTEX = 2.500000E-01   MAX. RES.
= 2.665686E-05  AT ELEMENT AEo 1  EQUATION   1
 ADo 1(    4,4) ST =  1.0000E+00 DT =  2.5000E-01 DX1= -6.4460E-05
DX2=  0.0000E+00 T =   5.000 P =   101250. S =  4.6505E-02

 CPU-TIME SINCE LAST OUTPUT:    29.49 SEC;  TOTAL CPU-TIME:    29.49
SEC;  SIMULATION TIME            1.00 SEC;  TIME STEPS:    4


 *North Aspect RE ISA snow pit 01

          OUTPUT DATA AFTER (    4, 4)-2-TIME STEPS
THE TIME IS  0.11574E-04 DAYS


@@@@@@@@@@@@@@@@@@@@@@@@@@@@@@@@@@@@@@@@@@@@@@@@@@@@@@@@@@@@@@@@@@@@@@@@@@@@
@@@@@@@@@@@@@@@@@@@@@@@@@@@@@@@@@@@@@@@@@@@@@@@@@@@@@@@@@@@@

  TOTAL TIME     KCYC   ITER  ITERC   KON        DX1M
MAX. RES.      NER    KER        DELTEX
  0.10000E+01      4      4     20     2       0.64460E-04
0.17238E-05    ****     1       0.25000E+00
********** VOLUME- AND MASS-BALANCES
**************************************************************************
**********************

 ********** [KCYC,ITER] = [   4,  4] *****
THE TIME IS  0.10000E+01 SECONDS, OR  0.11574E-04 DAYS


 PHASE VOLUMES IN PLACE
 GAS  0.61750E+02 M**3;   LIQUID  0.13309E+01 M**3

 LIQUID MASS IN PLACE  0.13309E+04 KG


**************************************************************************
************************************************************


 WRITE FILE *SAVE* AFTER     4 TIME STEPS  ---  THE TIME IS
0.100000E+01 SECONDS
```

```
================================================================================
================================================================
      ARRAY DIMENSIONS (SEE FILE maxsize.inc)
 ---------------------------------------------------------------------
-------------------------------------------------------------
      MAXEL     =  100000      Maximum number of elements
      MAXCON    =  400000      Maximum number of connections
      MAXK      =       3      Maximum number of components
      MAXEQ     =       4      Maximum number of equations
      MAXPH     =       2      Maximum number of phases
      MAXB      =       8      Maximum number of phase-dependent
secondary variables
      MAXSS     =     900      Maximum number of sinks/sources
      MAVTAB    =     100      Maximum average number of table entries
per sink/source
      MAXROC    =     200      Maximum number of rock types
      MAXTSP    =       5      Maximum number of specified time steps,
divided by eight
      MAXLAY    =      10      Maximum number of reservoir layers for
wells on deliverability
      MXRPCP    =      14      Maximum number of parameters for
relative permeability and capillary pressure functions
      MXPCTB    =       5      Maximum number of points in table for
ECM capillary pressure
      MXTBC     =       5      Maximum number of elements with time
vs. boundary condition
      MXTBCT    =     600      Maximum number of time vs. pressure
data
      MAXTIM    =    1000      Maximum number of calibration times
      MAXN      =      50      Maximum number of parameters to be
estimated
      MAXO      =     200      Maximum number of datasets
      MAXM      =    1400      Maximum number of calibration points
      MAXPD     =    1000      Maximum number of paired data
      MAXR      =     200      Maximum number of elements or indices
of each parameter or observation
      MAXBRK    =      20      Maximum number of points in time at
which SAVE file is written for restart
      MAXEBRK   =      50      Maximum number of elements with new
initial conditions after restart
      MAXCOEFF  =       5      Maximum number of coefficients for data
modeling functions
      MAXXGR    =       3      Dimension of third index of array
XGUESSR
      MTYPE     =      31      Number of observation types
      MPFMT     =       5      Number of plot file formats
 ---------------------------------------------------------------------
-------------------------------------------------------------


 ---------------------------------------------------------------------
-------------------------------------------------------------
```

```
      PROGRAM  VERSION   DATE                    COMMENT
 ------------------------------------------------------------------------
------------------------------------------------------------
      iTOUGH2            Current version       iTOUGH2 V6.9 (OCTOBER,
2014)
 ------------------------------------------------------------------------
------------------------------------------------------------



========================================================================
============================================================

 ---   113rd iTOUGH2 run stopped fatally       on 21-Jun-15  09:55 ---
CPU time used =      31.40 sec.

@@@@@@@@@@@@@@@@@@@@@@@@@@@@@@@@@@@@@@@@@@@@@@@@@@@@@@@@@@@@@@@@@@@@@@@@@@@@
@@@@@@@@@@@@@@@@@@@@@@@@@@@@@@@@@@@@@@@@@@@@@@@@@@@@@@@@

  END OF TOUGH2 SIMULATION JOB --- ELAPSED TIME =       31.40 SEC
```

APPENDIX A3: SUPPLEMENTARY MATERIAL FOR PATTERN ANALYSIS AT DRY LAKE FIELD SITE

Snow Pit Data

The following figures display bar graphs of the individual snow pits that were returned to for each survey period followed by scatter plots that show data for all locations surveyed for 2013 and 2015 (2014 is shown in Fig. 4.6), whether locations that were returned to or not.

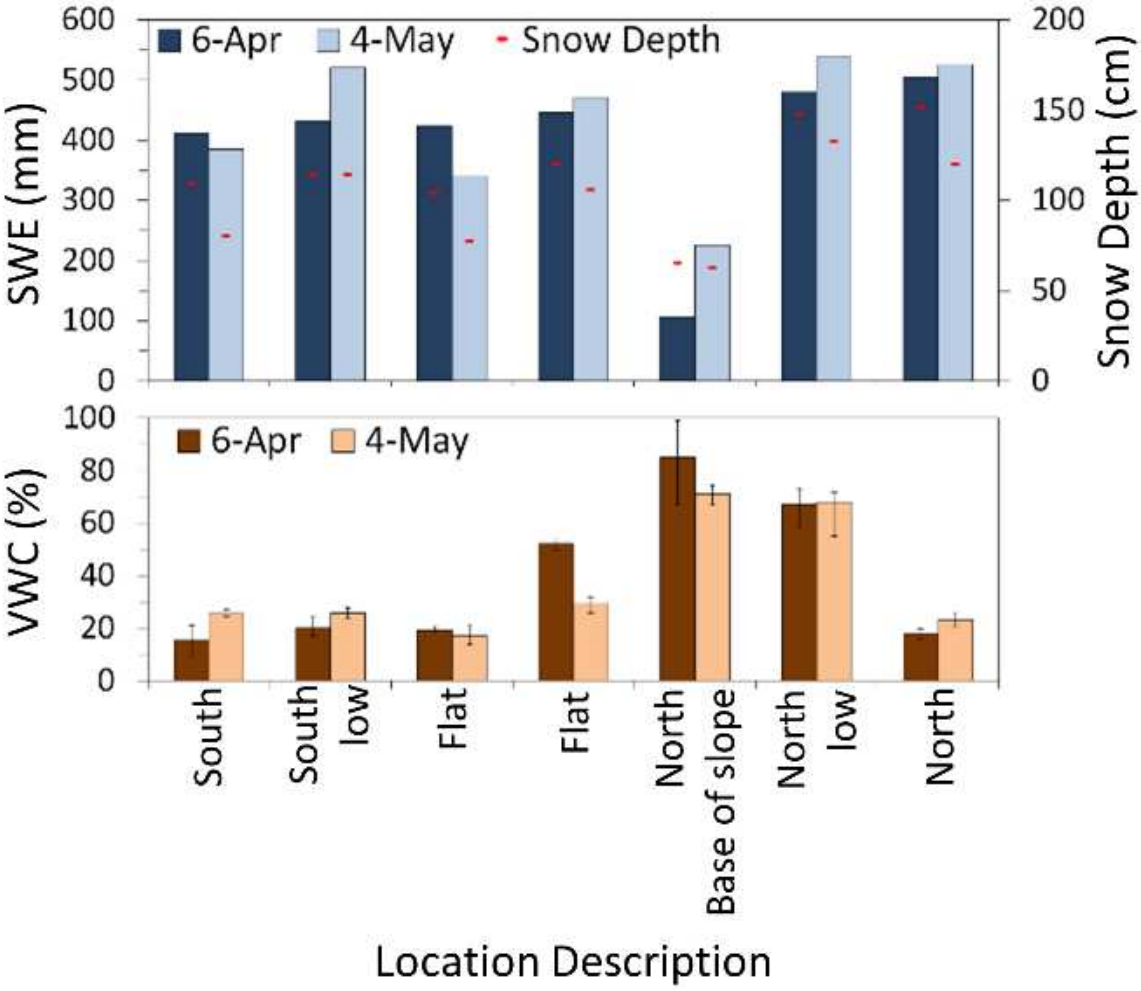

Figure A.3.1. Snow water equivalent (SWE), snow depth, and soil volumetric water content (VWC) as measured at the Dry Lake study site in 2013.

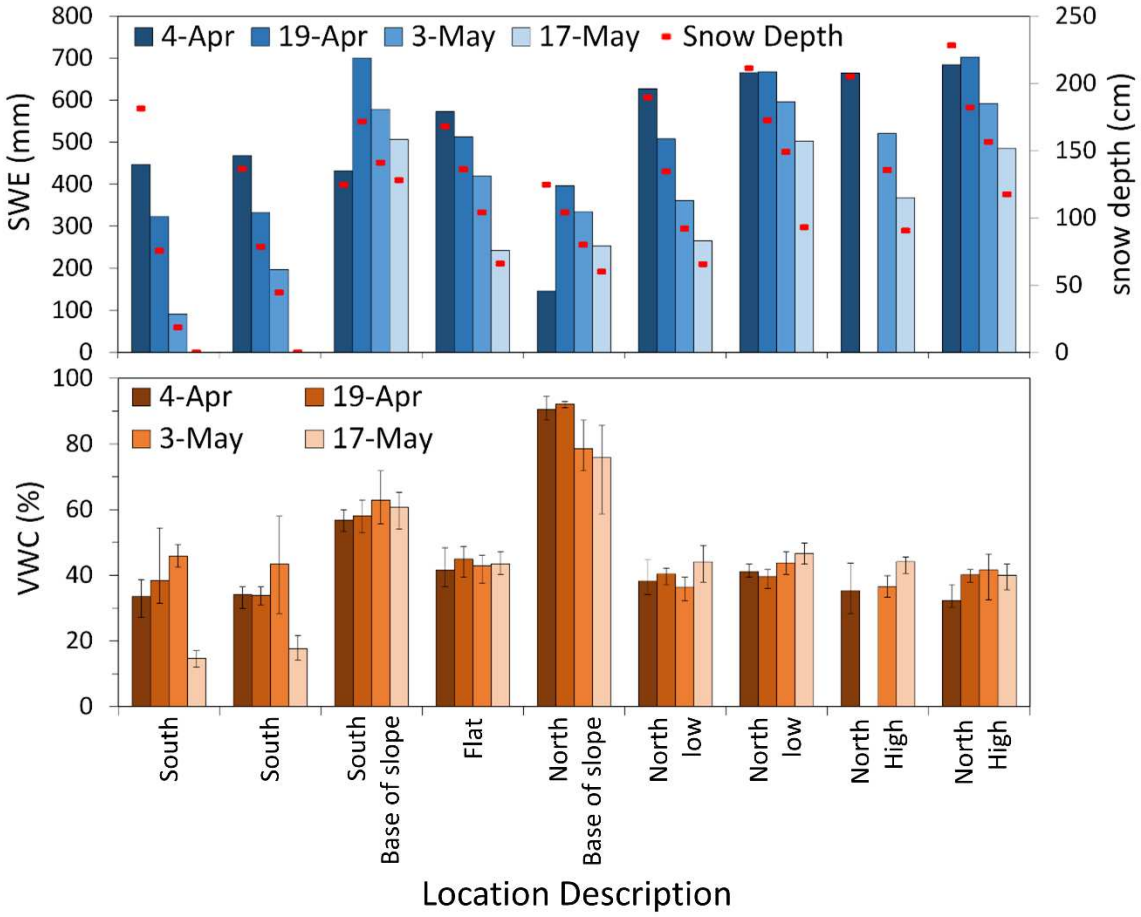

Figure A.3.2. Snow water equivalent (SWE), snow depth, and soil volumetric water content (VWC) as measured at the Dry Lake study site in 2014.

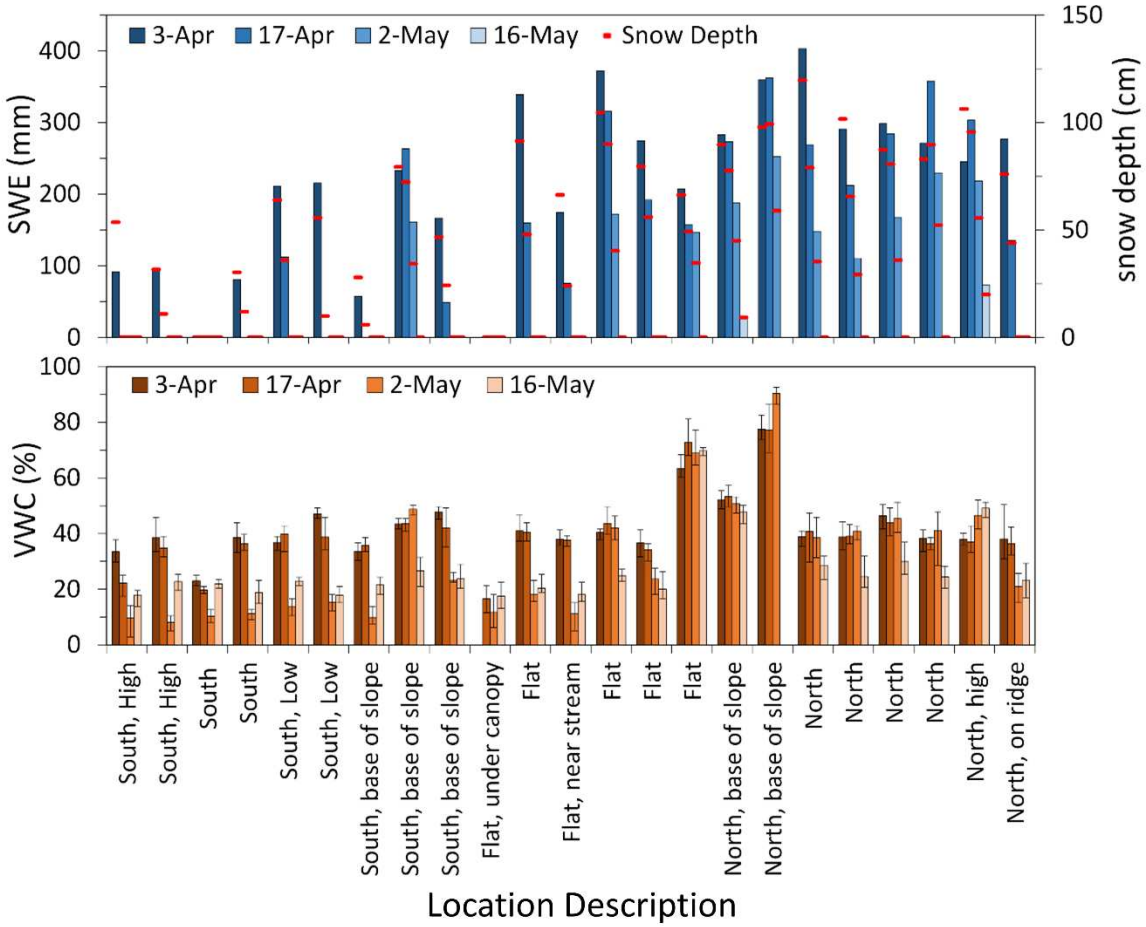

Figure A.3.3. Snow water equivalent (SWE), snow depth, and soil volumetric water content (VWC) as measured at the Dry Lake study site in 2015.

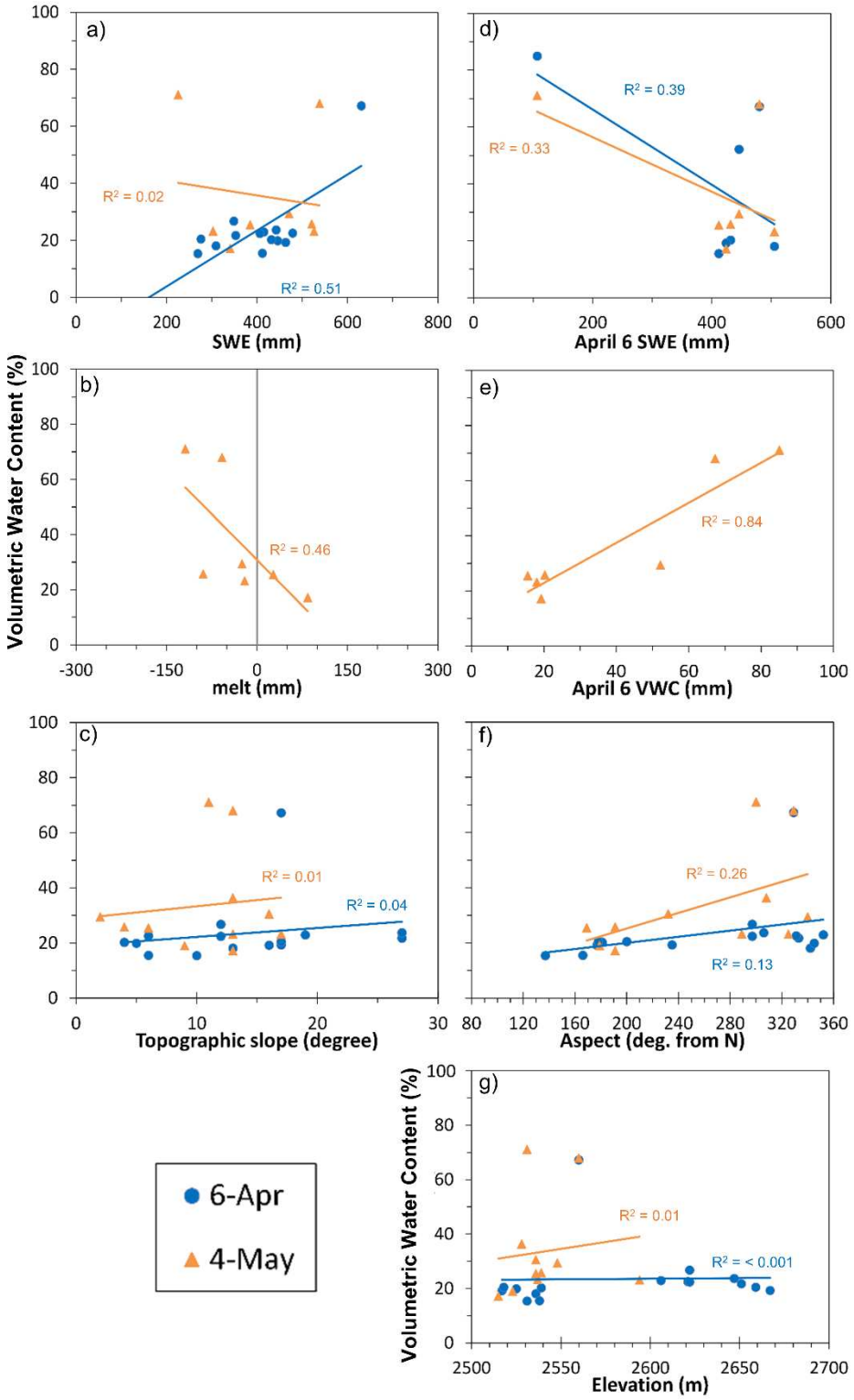

Figure A.3.4: Pattern analysis of the 2013 volumetric water content (VWC) surveys with R^2 (squared pearson r values from table 4.1) values shown for dynamic controls of a) snow water equivalent (SWE), b) change in SWE between surveys, c) topographic slope, d) April 4, 2014 SWE value, and e) April 4, 2014 VWC value, f) aspect, and g) elevation.

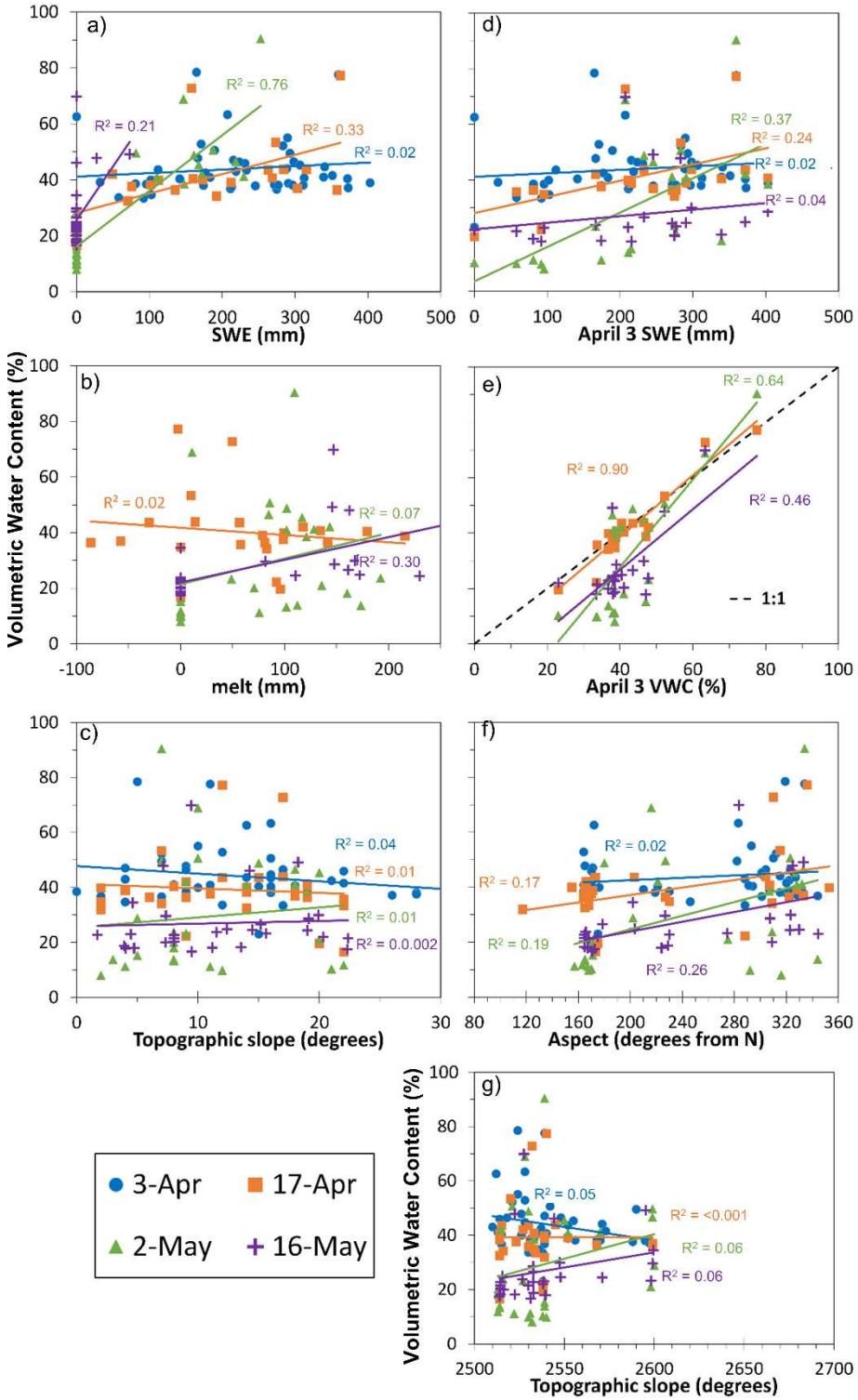

Figure A.3.5: Pattern analysis of the 2014 volumetric water content (VWC) surveys with R^2 (squared pearson r values from table 4.1) values shown for dynamic controls of a) snow water equivalent (SWE), b) change in SWE between surveys, c) topographic slope, d) April 4, 2014 SWE value, and e) April 4, 2014 VWC value, f) aspect, and g) elevation.

Soil Samples and Profile

The figure is the sieve analysis of soil samples taken during a the summer of 2013(Fig. A.3.6). The dimensions of the volumetric samples are 10.2 cm long with a 4.9 cm diameter.

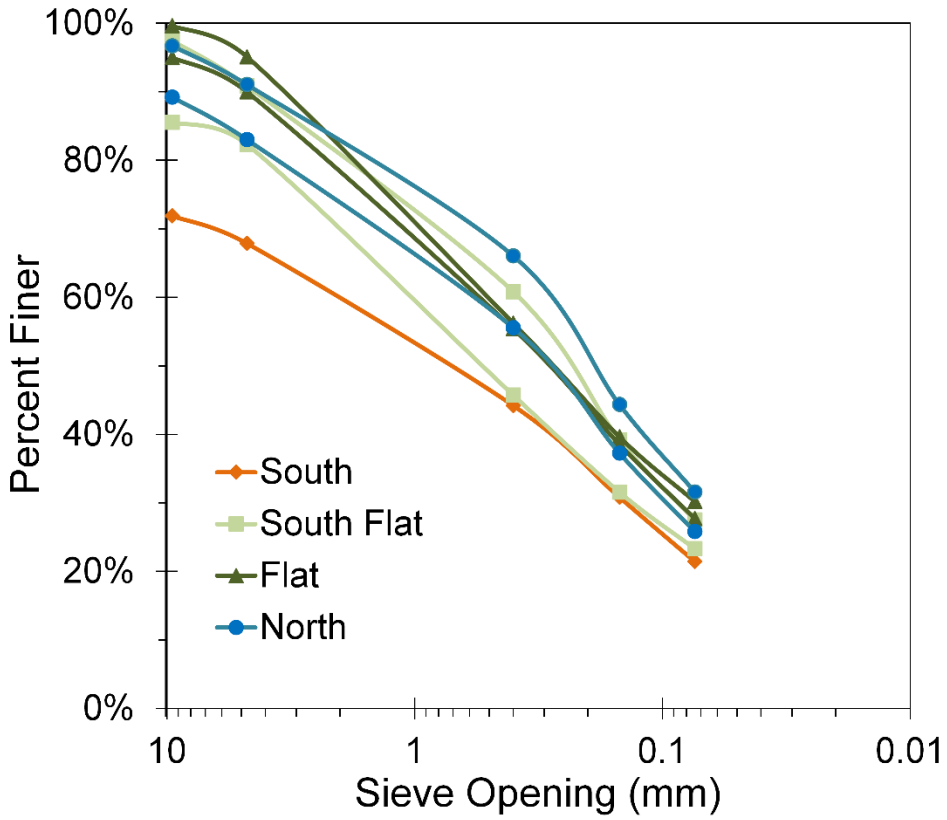

Figure A.3.6: Sieve analysis results of 200 cm^3 samples with aspect of sample locations shown.

The following table is qualitative assessment of the soil profile observed during the investigations into the depth of bedrock using a one meter hand auger (Table A.3.1). The observations were made on August 8 and 9, 2015. Two boreholes were made at each location, one meter apart.

Table A.3.1: Qualitative soil profile observations made during hang auger investigations.

			Borehole 1, H1								Borehole 2, H2					
Easting	**Northing**	**Surface**	**depth (cm)**	**comment**	**depth (cm)**	**comment**	**depth (cm)**	**comment**	**depth (cm)**	**comment**	**H2 (cm)**	**comment**	**depth (cm)**	**comment**	**depth (cm)**	**comment**
349424	4488349	Loam	15	rock							18	sandy	38	rock		
349394	4488367	sandy loam	15	rock							10	rock				
349376	4488398	sandy loam	28	rock							32	rock				
349358	4488419	cobbly sand	28	rock							19	rock				
349341	4488437	Loam	25	rock							23	rock				
349332	4488467	sandy loam	17	rock							19	rock				
349312	4488509	duff	10	clayey loam	43	rock					10	clayey loam	43	clay	48	rock
349288	4488549	duff/loam	23	sandy clay	42	sandy	47	rock			28	rock				
349187	4488633	loam	13	rock							11	rock				
349187	4488611	gravelly sandy loam	20	rock							25	rock				
349193	4488581	loam	54	rock							58	rock				
349199	4488555	loam	90	very sandy loam	97	clayey loam	> 100	never hit rock								
349206	4488539	loam w/ duff	45	clayey loam	62	sandy	65 rock				48	rock				
349409	4488592	loam w/ organic	35	rock							45	sandy	53	rock		
349403	4488599	black organic	20	black clay	40	tan clay	65	sandy clay	70	rock	20	gray clay	40	sandy clay	55	rock
349366	4488637	loam	45	clay	75	rock					45	clay	82	rock		

TDR Comparison to Volumetric Samples

The following figure was used to correct the field readings of the TDR probe using 55 volumetric samples 4.9 cm long and 3.2 cm in diameter (39.4 cc) co-located with field readings (Fig. A.3.7). All samples were taken beneath a snowpack in non-frozen soils that were assumed to have a temperature near 0°C.

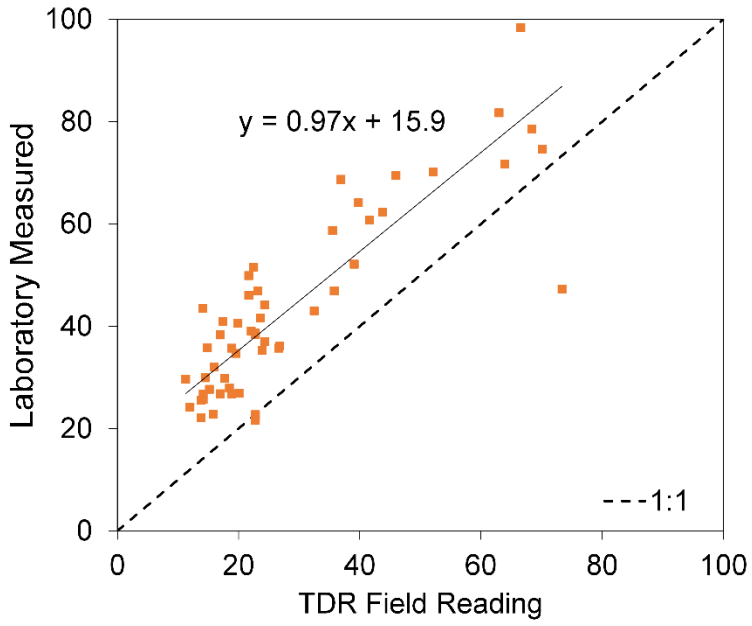

Figure A.3.7: Comparison of TDR probe readings in the field at Dry Lake study site beneath a snowpack and measured volumetric water content (VWC) in the laboratory. The equation shown was used to correct field readings.

APPENDIX A4: SUPPLEMENTARY MATERIAL FOR WETTING AND DRYING VARIABILITY OF THE SHALLOW SUBSURFACE BENEATH A SNOWPACK IN CALIFORNIA'S SOUTHERN SIERRA NEVADA

License Permissions from the Vadose Zone Journal

ACSESS-Alliance of Crop, Soil, and Environmental Science Societies LICENSE TERMS AND CONDITIONS

Apr 20, 2016

This is a License Agreement between Ryan Webb ("You") and ACSESS-Alliance of Crop, Soil, and Environmental Science Societies ("ACSESS-Alliance of Crop, Soil, and Environmental Science Societies") provided by Copyright Clearance Center ("CCC"). The license consists of your order details, the terms and conditions provided by ACSESS-Alliance of Crop, Soil, and Environmental Science Societies, and the payment terms and conditions.

All payments must be made in full to CCC. For payment instructions, please see information listed at the bottom of this form.

License Number	3853150366713
License date	Apr 20, 2016
Licensed content publisher	ACSESS-Alliance of Crop, Soil, and Environmental Science Societies
Licensed content publication	Vadose Zone Journal
Licensed content title	Wetting and Drying Variability of the Shallow Subsurface Beneath a Snowpack in California's Southern Sierra Nevada
Licensed copyright line	Copyright ©2015 by the Soil Science Society of America, Inc.
Licensed content author	Ryan W. Webb, Steven R. Fassnacht, andMichael N. Gooseff
Licensed content date	Aug 1, 2015
Volume number	14
Issue number	8
Type of Use	Thesis/Dissertation
Requestor type	Author of requested content
Format	Electronic
Portion	chapter/article
Rights for	Main product
Creation of copies for the disabled	no
With minor editing privileges	no
For distribution to	United States
In the following language(s)	Original language of publication
With incidental promotional use	no
The lifetime unit quantity of new product	0 to 499
The requesting person/organization is:	Ryan W. Webb
Order reference number	None

MATLAB Script for Calculating Time Derivative and Soil Moisture Persistence

```
% This script is manipulating CZO data from the Providence Met Clusters

% to observe various time derivatives and accumulative water*days for 30 minute
data.


function [time_derivative,accumulative] = derivatives(filename)  %input matrix to be
analyzed here.

processing = (filename);


n = length(processing(:,1));

m = length(processing(1,:));


%creating decimal day for water year

firstday = min(processing(:,1));


decday = zeros(n,1);

New_Matrix = zeros(n,1);

time_step = processing(2,1)-processing(1,1);


for i = 1:n;

   decday(i,1) = processing(i,1) - firstday;

   New_Matrix(i,1) = decday (i,1);

end


%computing time derivative of columns (change per day)

time_derivative = New_Matrix;


for j = 2:m;

   for i = 1:n-48;
```

```
        time_derivative(i,j) = (processing(i+48,j)-processing(i,j))/(48*time_step); % per
day
    end
end

%integrating above "flatline" of each dataset (or accumulative, measure in unit*days)
accumulative = New_Matrix;

for j = 2:m;
    flat = min(processing(:,j));
    accumulative(1,j) = (processing(1,j)-flat)*time_step;
    for i = 2:n;
        accumulative(i,j) = (processing(i,j)-flat)*time_step + accumulative(i-1,j);
    end
end

end
```

MATLAB Script for Calculating Vertical Gradients Between Sensors

```
% This script is to take vertical gradients for the Upper Flat Met station
% data in Providence Creek CZO, water years 2009-2011, VWC and soil Temp 30
% minute data.

function [vert_grad] = UF_vertical_gradients_09_thru_11(filename)
processing = (filename);

n = length(processing(:,1));
m = length(processing(1,:));
```

```
%creating decimal day for water year
firstday = min(processing(:,1));

decday = zeros(n,1);

for i = 1:n;
   decday(i,1) = processing(i,1) - firstday;
end

%computing time derivative of columns (change per day)

vert_grad= zeros(n,m);

for i = 1:n;
   vert_grad(i,1) = decday(i,1);
end

for j = 2:m;
   for i = 1:n;
      if (j <= 6);
         vert_grad(i,j) = (processing(i,j+5)-processing(i,j))/20;  %VWC gradient from
10 - 30 cm
      elseif ((j > 6) && (j <= 11));
         vert_grad(i,j) = (processing(i,j+5)-processing(i,j))/30;  %VWC gradient from
30 - 60 cm
      elseif ((j > 12) && (j <= 15));
         vert_grad(i,j) = (processing(i,j+4)-processing(i,j))/30;  %VWC gradient from
60-90 cm
      elseif ((j > 19) && (j <= 24));
```

```
        vert_grad(i,j) = (processing(i,j+5)-processing(i,j))/20;  %Temp gradient from
10 - 30 cm

    elseif ((j > 24) && (j <= 29));

        vert_grad(i,j) = (processing(i,j+5)-processing(i,j))/30;  %Temp gradient from
30 - 60 cm

    elseif ((j > 30) && (j <= 33));

        vert_grad(i,j) = (processing(i,j+4)-processing(i,j))/30;  %Temp gradient from
60 - 90 cm

    else

        vert_grad(i,j) = NaN;

    end

  end

end




end
```